ABSTRACT

Paleopedology of Paleo-wetland and Barite-bearing, Hydric Paleosols in the Morrison Formation (Upper Jurassic-Lower Cretaceous), North Central Wyoming, USA: A Multianalytical Approach

Debra S. Jennings, Ph.D.

Supervisor: Steven G. Driese, Ph.D.

Whereas lakes and wetlands are very sensitive to changes in climate, high-resolution data in these archives are lost unless it is possible to differentiate these deposits from other "floodplain" deposits. Synthesis of micromorphological and geochemical data with facies relationships is critical to accurate interpretations of ancient wetland-lacustrine deposits. A proposed hydrogeomorphological classification and appropriate genetic terminology that is useful in the rock record is presented. Eight Morrison Formation subenvironments, including barite-bearing paleosols, within lacustrine depositional successions from north central Wyoming were delineated using micromorphology and geochemistry, combined with facies relationships. The distribution of wetland pedotypes indicates that evapotranspiration remained high, suggesting that a stable, semi-arid to arid climate dominated in this area throughout Morrison time. This study also characterizes the micromorphology, elemental trends, and stable isotope geochemistry of sulfates in a barite-bearing Morrison paleosols and a modern analog soil (Lufkin Series) using optical microscopy, XRD, ICP-MS, and stable S and O isotope

data. Data indicate that barium-rich parent material provides adequate barium for barite precipitation. Barium is mobilized and concentrated in Btg horizons ~100-160 cm below the surface. The presence of humic acids in profiles lower on the landscape prevents barite precipitation and drives the precipitation of gypsum between saturated, anoxic conditions and drier, more oxic conditions. Barite precipitation is a slow, punctuated process that begins first along evacuated macropores and then in the adjacent matrix. The modern analog displays similar catenary relationships, redox features, and micromorphological characteristics compared to the Morrison paleosols, suggesting that similar pedogenic processes led to barite precipitation. Synthesized data reveal that conditions favorable to barite-bearing soil formation are low-gradient basins that have received feldspar-rich sediments (i.e. volcanically influenced basins), soils that developed near salt domes, soils that developed in exposed wetland or lacustrine sediments, and coastal plain deposits. Combined with regional paleosols, barite-bearing paleosols may document temporal changes in drainage, surface stability, and accommodation consistent with sequence boundaries/maximum flooding surfaces, and climate changes.

Paleopedology of Paleo-wetland and Barite-bearing, Hydric Paleosols in the Morrison Formation (Upper Jurassic-Lower Cretaceous), North Central Wyoming USA: A Multianalytical Aproach

by

Debra Sue Jennings, M.S.

A Dissertation

Department of Geology

Stacy C. Atchley, Ph.D., Chairperson

Submitted to the Graduate Faculty of
Baylor University in Partial Fulfillment of the
Requirements for the Degree
of

Doctor of Philosophy

Approved by the Enter Dissertation or Thesis Committee

Steven G. Driese, Ph.D., Chairperson

Stacy C. Atchley, Ph. D.

Stephen I. Dworkin, Ph. D.

Daniel J. Peppe, Ph. D.

Anne E. Rushing, Ph. D.

Accepted by the Graduate School

May 2114

J. Larry Lyon, Ph.D., Dean

Page bearing signatures is kept on file in the Graduate School.

TABLE OF CONTENTS

LIST OF TABLES

LIST OF FIGURES

ACKNOWLEDGMENTS

The study was funded by grants from the Clay Minerals Society, Geological Society of America, and the Baylor University Geology Department. The authors thank Baylor Univ. colleagues (Dr. Steve Dworkin, Dr. Daniel Peppe, and Dr. Stacy Atchley), Dr. Michael Vepraskas (NC State Univ.), ***Sedimentary Geology*** Editor Brian Jones, Dr. William DiMichele, and Dr. Elizabeth Gierlowski-Kordesch, and an annonymous reviewer for their invaluable comments and suggestions on the original manuscripts. I am ever grateful to my advisor, Dr. Steven Driese for his well-timed guidance and patience. Many thanks also go to my dissertation committee for all their comments that greatly improved this work.

I also appreciate the assistance and guidance of Dr. Joe Dixon in the Lufkin soil field area and Dr. Tom Hallmark at Texas A&M University and help with sampling using the Giddings probe. Jamie Applewhite (TAMU), Dr. David Lovelace (UW), Aaron Shunk (BU), and all the undergraduate assistants that provided much appreciated field assistance. Dr. Burkhard Pohl and the Big Horn Basin Foundation allowed open access to outcrops on the Warm Springs Ranch, provided additional photos for the supplementary data, and provided practical support as needed.

DEDICATION

To my Lord and Savior, Jesus Christ who made all things possible and smoothed the path for this adventure and to the many friends and family members that God planted in my life along the way, particularly my friend Judy Kuester, my grandmother, friend David Lovelace, Kim Green, and my ever-growing church family whose support was invaluable as I navigated all the hurdles along the way

CHAPTER ONE

Introduction

The farther back you can look the farther forward you are likely to see.

-- Winston Churchill

Wetland-lacustrine deposits and their associated hydric paleosols are common in the rock record and are particularly sensitive to subtle local and regional changes in climate, hydrodynamics, and biochemical fluctuations (Richardson and Brinson, 2001; Alonso-Zarza, 2003; Cohen, 2003; Greb and others, 2006). The associated hydric and hydromorphic soil profiles, that accumulate in these systems preserve high-resolution paleoclimatic, paleoecological, and paleoenvironmental data (Richardson and Brinson, 2001; Cohen, 2003; Scheiber, 2003; Greb and others, 2006), making them important research components of Earth's Critical Zone (Brantley and others, 2007). As high-resolution sedimentary archives, wetland-lacustrine deposits provide valuable counterparts to coeval well-drained paleosols and have the potential to greatly augment our understanding of the effects of climate change on landscape development and deep-time critical zone research (DTCZ, (*sensu*, Nordt and Driese, 2013). In spite of their potential to enhance paleoclimate and paleoenvironmental studies, wetland-lacustrine systems are often misidentified as floodplain, palustrine, or "pond" deposits, ignored altogether (Soils, 1987), or classified as "undifferentiated" for want of appropriate terminology (i.e., Dunagan and Turner, 2004). Delineating complex wetland-lacustrine deposits requires a multi-analytical approach, using geochemical trends, isotope geochemistry, X-ray diffraction, micromorphology, sedimentology, and facies analyses.

The first part of this research (presented in Chapter Two establishes a genetic wetland-lacustrine classification scheme and documents landscape evolution over time using an example from the Morrison Formation in north central Wyoming. During the course of this step of the study, several barite-bearing paleosols were discovered and classified. Chapter Two was published in *Sedimentary Geology*.

An additional problem faced by paleopedologists who study hydric paleosols and more problematic paleosols such as barite-bearing paleosols is comparison of ancient soils with modern analogs. Taxonomic uniformitarianism (sensu, Lovely and others, 1998) is fundamental to understanding and accurately interpreting paleopedogenic process and ancient landscape development. One particular limitation to taxonomic uniformitarianism is that it may be difficult to establish that pedogenic processes that occurred in paleosols and soils are truly analogous. However, barite-bearing soils are unique in that the conditions that lead to pedogenic barite precipitation may be documented by micromorphological features and geochemical data, specifically stable isotope geochemistry, which is little-affected by diagenetic overprinting (Lovely and others, 1998; Seal and others, 2000). Chapter Three documents the pedogenic processes that occur in a modern barite-bearing soil (the Lufkin soil series from central Texas). This chapter was published in *Sedimentary Geology*. Chapter Four synthesizes data from Chapter Two and Chapter Three in a taphonomic comparison of barite-bearing soils and paleosols and has been accepted for publication in *Sedimentology*.

CHAPTER TWO

Morrison Formation Paleowetland-Lacustrine Deposits and Associated Barite-bearing Paleosols

This chapter published as: Jennings, D., Lovelace, D., and Driese, S.G., 2011, Differentiating paleowetland subenvironments using a multi-disciplinary approach: An example from the Morrison formation, South Central Wyoming, USA: Sedimentary Geology, v. 238, p. 23-47.

Abstract

Small lakes are excellent records of environmental changes and are sensitive to local climate fluctuations. Large lacustrine systems record larger-scale climate events. Wetland deposits also provide high-resolution paleoclimatic and paleoenvironmental data. Although wetland deposits are typically associated with wet climatic conditions, they actually occur in a wide variety of climates. Whereas lakes and wetlands are very sensitive to changes in climate, high-resolution data in these archives are lost unless it is possible to differentiate these deposits from other "floodplain" deposits. Synthesis of micromorphological and geochemical data with facies relationships is critical to accurate interpretations of ancient wetland-lacustrine deposits. This study illustrates how micromorphology and geochemistry, combined with facies relationships, provide a viable method for differentiating complex, ancient wetland-lacustrine subenvironments. A hydrogeomorphological classification is proposed to provide appropriate genetic terminology that is useful in the rock record. Eight Morrison Formation subenvironments within lacustrine depositional successions from north central Wyoming were delineated using this interdisciplinary approach. Subenvironments include shallow-water wetlands, marsh, lacustrine fringe, and fen basin and fringe deposits. Synthesized data indicate that

an overall basinal infilling succession was punctuated by 3 major lake contraction events, which were followed by extended periods of landscape stability. Initially balance-filled conditions dominated the shallowing-upward lacustrine deposits such that sediment and water supply, and accommodation space were relatively equal. As the lake basin filled, shallower water, underfilled lake conditions prevailed. The distribution of wetland pedotypes indicates that evapotranspiration remained high, suggesting that a stable, semi-arid to arid climate dominated in this area throughout Morrison time. Also supporting a semi-arid to arid climate are more positive carbon isotopes compared to values for disseminated organic material in the surrounding area, abundant barite nodules, gypsum pseudomorphs, and zeolites. Although major fluctuations in lake level may have resulted from punctuated wetter episodes, synthesized data suggest that overall the climate remained relatively arid to semiarid and the lake basin remained closed throughout most of Morrison time. Fluctuations in lake level likely resulted from a significant increase in recharge in the source area, possibly related to volcanic events rather than a change in climate.

Introduction

Wetlands and lacustrine systems occur in a wide variety of modern climate regimes and these types of deposits are common in the rock record (Alonso-Zarza, 2003; Cohen, 2003; Greb and others, 2006). Wetlands and lakes are also present in a wide range of tectonic and hydrologic settings (Cohen, 2003; Alho, 2005; Greb and others, 2006). Because wetland-lacustrine systems form in topographic lows, favorable geochemical conditions, low erosion rates, relatively high sedimentation rates, and high accommodation result in a high preservation potential, particularly in large, low-gradient

depositional basins (Greb and others, 2006). Lakes and associated wetland areas are dynamic systems that are particularly sensitive to subtle local and regional changes in climate, hydrodynamics, and biochemical fluctuations (Richardson and Brinson, 2001; Cohen, 2003). The siliciclastic mud and carbonate deposits, and associated hydric and hydromorphic soil profiles, that accumulate in these systems preserve high-resolution paleoclimatic, paleoecological, and paleoenvironmental data (Richardson and Brinson, 2001; Cohen, 2003; Scheiber, 2003; Greb and others, 2006), making them important research components of Earth's Critical Zone (Brantley and others, 2007). As high-resolution sedimentary archives, wetland-lacustrine deposits are also critical components of climate research because they are valuable counterparts to coeval well-drained paleosols. The key to understanding how climate affects the distribution of ancient wetland-lacustrine systems and their link to terrestrial counterparts is the ability to delineate complex wetland-lacustrine subenvironments and define their relationship with surrounding depositional systems.

Sediments deposited in lakes and surrounding wetlands have distinctive profiles, genetic relationships, and authigenic constituents that are useful for distinguishing subenvironments according to their hydromorphic regime and hydrologic zone (Vepraskas and others, 1992; Richardson and others, 2001; Richardson and Brinson, 2001). However, many ancient wetland deposits often are misidentified, undifferentiated, or understudied in the rock record due to challenging terminology, heterogeneous and laterally variable lithologies, and a paucity of comparative studies (Soils, 1987; Dunagan and Turner, 2004; Greb and others, 2006).

Changes in authigenic mineral compositions and redoximorphic characteristics useful for defining subtle differences in hydrology and climatic influences are often only discernable at microscopic levels (Vepraskas and others, 1992). Subtle geochemical indicators, such as reducible elements and isotopic signatures, also contribute lines of independent data that, when combined with micromorphological data, help to demarcate facies that developed in the primary depositional system and under original climatic conditions from late diagenetic influences. This study seeks to: (1) illustrate the use of micromorphological and geochemical characteristics of hydric and hydromorphic paleosols associated with documented lacustrine deposits to delineate paleowetland sub-environments, and then (2) assess the overall climate signature based on one ancient example from the Upper Jurassic-Lower Cretaceous Morrison Formation in north-central Wyoming, USA.

Apparent contradictory sedimentary, geochemical, and paleontological data from Morrison deposits have resulted in conflicting Late Jurassic paleoenvironmental and paleoclimatic interpretations. Paleobotanical data suggest that the climate during the latest Jurassic was humid and wet based on localized data (Tidwell, 1990; Ash, 1994), but lithologic data and climatic models indicate a drier, more temperate climate (Demko and Parrish, 1998). Parrish et al. (2004) proposed a change from a humid to a semi-arid climate from the Kimmeridgian to the Tithonian, and Hasiotis (2004) interpreted a more tropical wet-dry climate based on hydrological changes indicated by trace fossils. Dunagan and Turner (2004) suggested that in the latest Jurassic the climate began to cool and become wetter. Late Jurassic paleoclimatic and paleoenvironmental interpretations remain a point of contention largely because they are based on localized data that

correspond to microenvironments rather than data directly related to regional climate. Although broad paleoclimatic and paleoecological interpretations have been proposed (i.e., Turner and Peterson, 2004), no significant latitudinal climatic variation as is observed in similarly sized modern basins (Alho, 2005) has been documented across the Morrison basin. Although paleobotanical and paleoichnological data has been documented across the Morrison basin, most data have been evaluated on a local scale independent of the larger surrounding landscape. Basin-scale distributions of paleobotanical data have been based on widely separated data that may not be coeval. These disparities are compounded by the lack of reliable chronostratigraphic controls, viable methods to differentiate wetland-lacustrine deposits, and useful terminology. A major problem that complicates correlating coeval deposits across the Morrison Basin and refining paleoclimate interpretations is the lack of reliable stratigraphic markers (Turner and Fishman, 1998). Although a "clay change" has been proposed as a stratigraphic marker, clay phase variations related to environmental conditions (i.e., Turner and Fishman, 1991; Trujillo, 2003; Jennings and Hasiotis, 2006a) have brought in to question the usefulness of clay mineralogy as a tool to recognize isochronous surfaces in Morrison deposits. However, major climate fluctuations may serve as a more reliable tool in terrestrial deposits. This study illustrates how the synthesis of micromorphological and geochemical data allow for the differentiation of wetland classes from lacustrine and “floodplain” deposits and emphasizes the importance of using a hydrogeomorphological classification scheme in paleowetland studies to document major climate fluctuations useful in correlating terrestrial deposits.

Defining Lacustrine and Wetland Settings in the Rock Record

In spite of their potential to enhance paleoclimate and paleoenvironmental studies, wetland-lacustrine systems are often misidentified as floodplain, palustrine, or "pond" deposits, ignored altogether (Soils, 1987), or classified as "undifferentiated" for want of appropriate terminology (i.e., Dunagan and Turner, 2004). Consequently, it is essential to first define terminology that is useful in differentiating lacustrine deposits from wetland deposits in the rock record.

Lacustrine deposits, by definition, are sediments that were deposited in bodies of standing water that were totally surrounded by terrestrial deposits (Cohen, 2003). Many factors determine the geological features of lacustrine deposits. These factors include, but are not restricted to: a) the dominant type of sediment the lake received; b) physical conditions that existed within the lake; (i.e. depth, temperature, degree of interaction with surficial water and ground water, mixing within the water column, and climate conditions); c) water chemistry; and d) biota that lived in or near the lake (Cohen, 2003).

Lacustrine deposits are commonly interpreted based on the presence of laminated, organic-rich, deep water deposits, carbonates, authigenic mineral assemblages, trace fossils, and invertebrate biota (i.e., Meyers and Ishiwatari, 1993; Liuqi and others, 1997; Buatois and Mangano, 1998; Dunagan, 2000; Hay and Kyser, 2001; Freytet and Verrecchia, 2002; Cohen, 2003; Schnurrenberger and others, 2003). Lakes exhibit a wide range of characteristics that are dependent on whether the lake is a relatively open or closed system, the dominant climate, underlying bedrock, and location on the landscape (Carroll and Bohacs, 1999; Cohen, 2003; Liutkus and others, 2005). Abrupt facies changes and compositional diversity that may be observed over short vertical and lateral distances, and a wide range of physico-chemical variability may be used to distinguish

lacustrine deposits from their marine counterparts (Cohen, 2003; Schnurrenberger and others, 2003). Facies models and lateral facies relationships document large-scale changes within the lake system over time and microfacies are useful for documenting the short-term processes that were dominant in the original system (Cohen, 2003).

According to the National Soil Conservation Service, a soil is a "natural body comprised of solids (minerals and organic matter), liquid, and gases that occurs on the land surface, occupies space, and is characterized by one or both of the following: 1) horizons, or layers, that are distinguishable from the initial material as a result of additions, losses, transfers, and transformations of energy and matter, or 2) the ability to support rooted plants in a natural environment (NRCS, 2010) ". A wetland-lacustrine fringe where previously submerged sediments may dry out, be colonized by plants, and become pedogenically modified meet the definition of a soil. By definition (*stricto senso*), pedogenically modified lacustrine sediments, no matter how poorly developed, must be classified as soils. Only those sedimentary characteristics (micro- and macro-scale) that support deposition in a standing body of water and permanently saturated conditions in a terrestrial setting with no subsequent pedogenesis define lacustrine deposits. Consequently, for the purpose of this study, lacustrine deposits are defined as those deposits that exhibit evidence of limnic processes and that exhibit no pedogenic features that would suggest subsequent pedogenesis.

The term "pond" is an expression that describes an inland body of water, either man-made or natural, that is smaller than a lake. Although in modern environmental studies this may be a useful term, the size of the original body of water is so seldom documentable in the rock record that it is unlikely that it could be interpreted with any

degree of accuracy. In addition, the term itself is so subjective as to render it inappropriate for sedimentological studies. Using the term "undifferentiated" is also not useful if the intent is to delineate sub-environments within a lacustrine-wetland depositional system and document the effects of extrinsic factors such as climate on the system. We suggest that it is more appropriate to classify transitional, less definitive deposits using a more descriptive, hydrogeomorphological approach and relating them to laterally adjacent deposits that display more definitive hydrological and depositional characteristics (sensu, Schnurrenberger and others, 2003).

The National Technical Committee for Hydric Soils (NTCHS) defines a hydric soil as a soil that "formed under conditions of saturation, flooding, or ponding long enough during the growing season to develop anaerobic conditions in the 'upper part ' (NRCS, 2010)." Unlike lakes, wetlands may be subjected to variable saturation conditions. The main difference between lacustrine deposits and wetland deposits is the development of hydric soils that support vegetation and display definite soil horizons and pedogenic features specific to soil formation processes (Mausbach and Parker, 2001; Tiner, 2003).

Hydric soils are generally classified based on hydrology (discharge vs. recharge, duration of saturation), geomorphic setting (position on the landscape and relationship to adjacent deposits), and origin of water (limnogenous, meteoric, telluric, or marine), water chemistry, and the dominant sediment type (organic or mineral) (Tiner, 2003; NRCS, 2010). Although most hydric paleosols that have been documented are organic (e.g., PaleoHistosols and coals), non-peat producing, mineral-rich hydric soils are also abundant in the rock record and are a critical component in paleowetland studies (Greb

and others, 2006). According to the NRCS, a histosol is a soil that forms in organic soil materials. The general rule is that a soil is classified as a Histosol if half or more of the upper 80 cm is organic. Organic soil materials have organic-carbon contents (by weight) of 12 to 18 percent or more, depending on the clay content of the soil. Organic-rich horizons may be fibric (slightly decayed organic material), hemic (moderately decomposed organic material), or sapric (well-decomposed organic material). Consequently, the definition of PaleoHistosols may be expanded to include coals and horizonated more mineral-rich organic deposits that reflect very different wetland environments (NRCS, 2010).

Wetland environments are defined in many ways, depending on the purpose of any particular study. Although there are many wetland classification systems that define wetland terms, most are designed for use in modern systems where direct observations of climate and ecological data are possible (Tiner, 1999). Classification of ancient wetland subenvironments requires a hierarchical scheme that is dependent on genetic relationships and allow for more descriptive characterizations and comparison with modern wetland systems. The main characteristics that are most likely to be preserved in the rock record include soil type (organic or mineral), water source (as evidenced by lateral facies relationships and inferred from geochemical and mineralogic data), water chemistry (documented by stable isotope geochemistry and authigenic minerals), dominant vegetation (from fossil data), and dominant hydrodynamics (inferred from lateral facies relationships). We suggest a practical, genetic hydrogeomorphological classification scheme, (sensu, Warner and Rubec, 1997; Collins and Kuehl, 2001; Richardson and Brinson, 2001), that is designed strictly for paleowetland classification and

predominantly based on wetland features and characteristics that are preserved in the rock record or inferred by mineralogy, micromorphology, and geochemistry of the sediments (Table 2.1).

In general, organic soils may be subdivided into discharge hydric soils (e.g., fens) that receive most or all of their water and nutrients from groundwater and hydric soils (e.g., swamp, bogs) whose water supply comes mainly from precipitation and streams (Collins and Kuehl, 2001). Fens may accumulate laminated, decomposed peat or fine-grained plant remains in clay-rich sediments with a thick underclay. Because water moves slowly through the system, nutrients increase in abundance basinward. Outwash sands may occur at the wetland fringe and the thickness of organic-rich deposits thicken basinward with a total peat thickness reaching to more than 4 meters (Warner and Rubec, 1997; Collins and Kuehl, 2001). Bogs develop in higher areas relative to the surrounding terrain. Nutrient-poor, meteoric water infiltrates the bog, leading to more acidic conditions that allow the preservation of peat and woody material. Swamps are typically associated with tidal systems, inland salt lakes, and riparian systems. Compared to fens, swamps are much more acidic and discharge dominated. Typically swamps are not as wet as bogs, fens, and marshes and are acidic and nutrient-rich. Thick accumulations of woody material and peat (coal in the rock record) characterize swamp deposits (Warner and Rubec, 1997; Collins and Kuehl, 2001).

Non-peat producing, mineral soils that fringe wetlands may receive water both from groundwater discharge and from overland flow from higher areas adjacent to the associated lake or wetland. Fringing wetlands may include palustrine zones (lacustrine fringe), shallow-water marshes, vernal pools, and playas (Richardson and others, 2001).

Marshes are epiaquatic, shallow water bodies that experience frequent water level fluctuations. Although macerated organic matter may be disseminated throughout the soil matrix, no significant accumulation of organic material occurs due to high rates of decomposition during drier times (Warner and Rubec, 1997). Shallow water wetlands commonly occur in transitional zones between permanently saturated areas (e.g., lakes, riverine wetlands, large depressional wetlands) and seasonally wet areas. Shallow water wetland settings may be briefly subject to limnic processes, but a frequently fluctuating water table may result in occasional drying in the upper part of the soil. Hydrologically, shallow water wetlands are surficially separated from other water bodies, and remain connected through groundwater. Consequently, they may retain lacustrine, organic marl or peat and may also accumulate evaporites. Nutrient fluxes in this dynamic setting may result in shallow water profiles that are calcareous near the wetland fringe due to evaporative capillary rise (Warner and Rubec, 1997; Richardson and others, 2001; Richardson and Brinson, 2001). Much like the term "pond," the term "mire" has become ill-defined and has been used with such variation in the literature, we suggest that it is not useful in ancient wetland studies.

Geologic Setting

During the Late Jurassic-Early Cretaceous, the Morrison depositional basin lay midway between a subduction zone to the west and the retreating marine coastline to the northeast (Lawton, 1994b) and spanned more than 1,555,693 km^2 (Fig. 1). Significant amounts of volcanic debris and ash were transported from the Transcontinental Arc and uplands in the back arc region eastward and northeastward across the Western Interior

Table 2.1. Genetic wetland classification scheme.

Hydrogeomorphic Classification	Wetland Subclass	Soil Type		Water Source				Water Chemistry		Dominant Vegetation Type		Dominant Hydrodynamics	Characteristics
		Organic	Mineral	Groundwater	Limnogenous	Meteoric	Marine	Minerotrophic	Ombrotrophic	Woody	Herbaceous		
	Bogs	X				X			acidic	shrubs, moss, lichens		water table at or slightly below the surface and raised above the surrounding terrain; recharge dominated	accumulation of peat / woody fragments; raised surface relative to surrounding terrain; high water table, acidic conditions
Stratigraphic Slope	Fens	X		X					neutral to alkaline	trees, shrubs near wetland fringe	ferns, floating hydrophytes	Surface level with the water table, with slow water flow on the surface and through the subsurface	accumulation of decomposed peat / fine-grained plant remains; level surface relative to surrounding terrain; fluctuating water table; accumulation of ions and nutrients basinward; outwash sands at fringe; >4m of peat basinward; accumulation of ions, nutrients, and thick underclay basinward
Topographic Slope, Lacustrine Fringe	Marshes		X	X	X	X	X	X	acidic to neutral	reeds, floating hydrophytes		Epiaquatic; Shallow surface water which fluctuates dramatically; slow moving water during wet times	shallow water, frequent water level fluctuation; little accumulation of organic material due to high rates of decomposition

Table continued

Hydrogeomorphic Classification	Wetland Subclass	Soil Type		Water Source				Water Chemistry		Dominant Vegetation Type		Dominant Hydrodynamics	Characteristics
		Organic	Mineral	Groundwater	Limnogenous	Meteoric	Marine	Minerotrophic	Ombrotrophic	Woody	Herbaceous		
Estuarine Fringe, Lacustrine Fringe, Riverine Wetlands	Swamps	X	X			X	X		acidic	trees, shrubs,		water table at or near the surface, discharge dominated	thick accumulation of woody material and peat; associated with tidal systems, inland salt lakes, riparian systems; not as wet as bogs, fens, and marshes; common wet mineral rises and raised peat plateaus; nutrient rich
Flats, Lacustrine Fringe, Riverine Wetlands, Depressional	Shallow Water		X	X	X	X	X	X	acidic to alkaline	sparse vegetation, may include charophytes		Transitional between permanently saturated areas and seasonally wet; free surface water up to 2m deep; subject to limnic processes; fluctuating water table; surficially separated from other water bodies, but groundwater hydrologically connected	shallow water / occasionally dry, nutrient fluxes; usually contain limnic peat and marl; in semi-arid to arid settings may accumulate evaporites; usually associated with lacustrine, fluvial, and tidal systems ; calcareous at fringe due to evaporative capillary rise;

during retroarc magmatic events (Suttner, 1969; Santos and Peterson, 1986; Johnson, 1991; Peterson, 1994; DeCelles, 2004; Turner and Peterson, 2004). Volcanic activity began earlier on the Colorado Plateau and progressed to the north as the Cordilleran Belt and foreland basin developed together, and the continent moved into a higher latitude (Brenner and Peterson, 1994; DeCelles, 2004). Increased sedimentation from plinian eruptions and uplift along the Andean-type magmatic arc increased siliciclastic input exponentially. East-northeast flowing rivers transported volcanically derived sediments across the alluvial plain from the western highlands as the back bulge migrated to the east (DeCelles, 2004). Subsequent thrust faulting and folding contributed to continued lacustrine development in semi-isolated to isolated basins throughout the Western Interior (Dunagan, 2000). Geochemically unstable rhyolitic-dacitic volcanic ash altered to smectite-rich sediments in lacustrine and wetland environments that developed in the foreland and back-bulge basins (Brenner and Peterson, 1994; Christiansen and others, 1994; DeCelles, 2004). In spite of evidence of widespread wetland-lacustrine systems throughout the Morrison Basin (e.g., Tanner, 1968; Lockley and others, 1986; Turner and Fishman, 1991; Dunagan, 2000; Dunagan and Turner, 2004; Kirkland, 2006), these complex wetland- palustrine-lacustrine deposits and their associated wetland paleosols remain largely undifferentiated and poorly understood (Dunagan and Turner, 2004). The study area is located on the Warm Springs Ranch and adjacent BLM lands near Thermopolis, Wyoming, at the southeastern most corner of the Bighorn Basin (Fig. 2.1). The Warm Springs Ranch covers an area of more than 45 km^2 located 1.5 km southeast of Thermopolis. Most of the outcrop area is highly eroded and littered with conglomerate

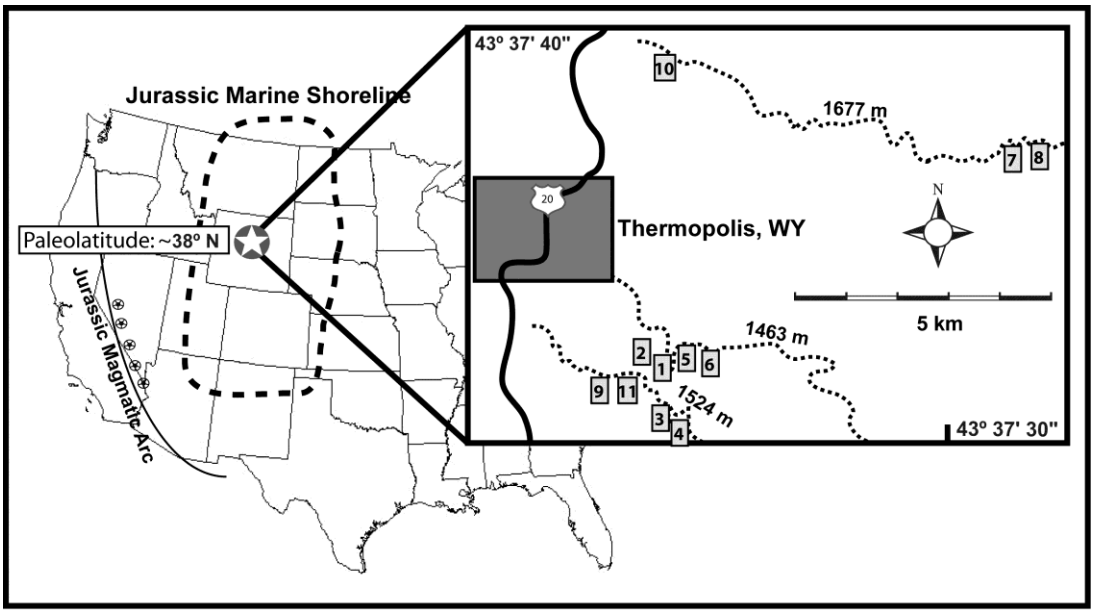

Figure 2. 1. Study area map and relative position in the Morrison depositional basin. Dashed lines on the study area map represent contour lines of uppermost elevation of Morrison outcrop in the study area. Stratigraphic sections were measured along 3 transects. The study area is situated in approximately the center of the Morrison depositional basin (dashed lines on regional map).

and sandstone boulders from the overlying Cloverly Formation; however, gullies along three east-west trending, south-facing exposures and road cuts near recently excavated dinosaur quarries allow access to relatively open slopes.

During Morrison time, the study area was situated 200-300 km south of the paleo-shoreline and 150-200 km west of the magmatic arc (Fig. 2.1). The estimated paleolatitude of this area is ~38°N (Peterson, 1988; DeCelles, 2004; Turner and Peterson, 2004).

Methods

Stratigraphic Sections

Eleven detailed stratigraphic sections were measured and described from freshly excavated trenches of outcrops (Fig. 2.2 A). Sedimentary descriptions include unit thickness, sedimentary structures, pedogenic features, grain size, fossils, and color.

Colors were described using a Munsell rock-color chart. Rock samples were collected from each unit for geochemical analyses and thin sections.

Packages of rocks with pedogenic features such as horizons, biogenic structures, nodules, and exposure features were classified into pedotypes. Type sections of pedotypes with distinctive macro- and micromorphological characteristics were described in more detail (Fig. 2.2 B). Pedotypes were then interpreted based on a generic wetland classification scheme (Table 2.1). Pedotype descriptions and wetland generic classification are summarized in Table 2.2.

Microscopy and Mineralogy

Individual rock samples were analyzed with powder X-ray diffraction (XRD) to identify authigenic mineral compositions. Six random-mount samples were analyzed to determine the mineralogy of nodules and other distinct authigenic minerals. The < 0.5 μm size fraction was chosen to limit the detrital clay mineral component. Clays from ten samples were separated by standard centrifugation methods. Samples were then saturated with 10% KCl and MgCl (Moore and Reynolds, 1997), mounted on glass slides using Drever's Millipore method (1973), and glycolated for two days. Eighht samples were heated at 300ºC for 1 hour to differentiate clays with 14Å peaks. Mounted clay samples and randomly oriented powdered samples of minerals were analyzed on a SCINTAG XDS 2000 with CuK α radiation. Scans were evaluated with methods described in Moore and Reynolds (1997). Data from this new sample set was combined with previously published data (Jennings and Hasiotis, 2006a).

One hundred thirty-nine thin sections were examined for sedimentary and pedogenic microfabric, microfossils, and other mineralogical constituents representative

of depositional environments. Color images of stratigraphic sections, microscopy, and interpretive figures are available as online supplemental information.

Images of gold-coated rock chips from representative lithofacies, nodules, and carbonates were taken with a Leo 1550 field-emission scanning-electron microscope (SEM) at Baylor University to compare subtle mineral relationships and morphologies.

Geochemistry

Stable isotope analysis was conducted on 27 barite nodules and 32 carbonate samples collected from lacustrine deposits and paleosols in the study area. Values of $\delta^{34}S$ were measured for SO_2 gas in a continuous-flow gas-ratio mass spectrometer (ThermoQuest Finnigan Delta PlusXL) at the University of Northern Arizona. Precision is estimated to be ± 0.15‰ or better, based on repeated internal standards. Values of $\delta^{18}O_{SO4}$ for sulfate were measured on a continuous-flow gas-ratio mass spectrometer (ThermoQuest Finnigan Delta PlusXL). Standardization is based on international standard OGS-1. Precision is estimated to be ± 0.3 ‰ or better, based on repeated internal standards. Values for $\delta^{18}O_{SO4}$ were reported relative to VSMOW (Vienna Standard Mean Ocean Water) and $\delta^{34}S$ values were reported relative to VCDT (troilite of the Canyon Diablo iron meteorite).

The $\delta^{13}C$ and $\delta^{18}O_{CaCO3}$ analyses were carried out by gas bench online on a Finnigan Delta Plus XP continuous-flow mass spectrometer at the University of Wyoming. Six standards were used. An overall precision of 0.06 ‰ for $\delta^{18}O_{CaCO3}$ and of 0.03 ‰ for $\delta^{13}C$ is estimated based on repeated standards. Values are reported relative to V-PDB.

Reducible Fe, Mn, and Al analyses were performed at the USDA-NRCS National Soil Survey Laboratory in Lincoln, Nebraska using methods described in Jackson et al. (Jackson and others, 1986b). Citrate-dithionite-bicarbonate extractable elemental data are reported in ppm.

Stratigraphy

The Morrison Formation, in the study area, is bounded by the Upper Jurassic Sundance Formation and the chert pebble conglomerate of the Lower Cretaceous Cloverly Formation (Douglass, 1984; Carson, 1998; Trujillo, 2003). Overall, there is a sharp contact between the glauconitic sandstone of the Sundance Formation and quartz-rich basal sandstone of Morrison Formation (Fig. 2.3). However, in the northernmost transect, exposures of the Sundance-Morrison contact are limited.

Stratigraphic sections in the area generally measure 50-60 m thick and are composed of heterolithic sandstone, siltstone, mudstone, claystone, and shale. Lithologies above the basal sandstone are laterally variable over short distances and difficult to trace for more than 10s of meters. In section 6 fluvial deposits of the Cloverly Formation cut down and removed the upper half of the Morrison Formation. Sections 7 and 8 are largely composed of stacked mudstone units of varying character, which overly thick, off-white (N8) sandstone units. The top 20 m of complete sections are devoid of significant sandstone units throughout the area. The distribution of pedotypes (sensu, Behrensmeyer and others, 1989) relative to lacustrine deposits is represented in the generalized stratigraphic sections in Figure 2.2 A.

Table 2.2. Pedotype descriptions.

Pedotype	Pedogenic features	Micromorphology	Geochemistry	Hydromorphic classification
A	BW/Bt/Btk/Btg/By /Cyg/Cg profile; reddish brown; Gypsum pseudomorphs; diffuse root mottles; argillaceous, quartz sandstone parent material	mm-scale, clay-filled rhizoliths; burrows; hematite nodules;	illite; low reducible Al, Mn, Fe; avg. $\delta^{13}C$ = -6.7‰ ; avg. $\delta^{18}O$ = -9.6‰	distal floodplain paleosol
B	BW/Bg/Btg/Btk/Bg/Cg profile; reddish brown; krotovina; diffuse black or pinkish gray mottles; hematite-rich matrix; oolitic skeletal grainstone parent material	weathered ooids; burrows; mineralized fecal pellets	illite; relatively low reducible Al, Mn, Fe with highest Al and Fe in Bg/Cg horizon ; avg. $\delta^{13}C$ = -1.8‰ ; avg. $\delta^{18}O$ = -10.2‰	lacustrine plain
C	Bg/Btg/Btkg/B/Cg profile; greenish gray; slickensides along micrite-filled mudcracks; carbonate nodules; burrows; bone fragments; lacustrine shale parent material	bifurcate rhizoliths/burrows; brecciated bone fragments	vermiculite/illite; low reducible Al, Fe; moderate reducible Mn; avg. $\delta^{13}C$ = -5.3‰ ; avg. $\delta^{18}O$ = -10.4‰	shallow water lacustrine fringe

Table continued

Pedotype	Pedogenic features	Micromorphology	Geochemistry	Hydromorphic classification
D	BW/Bt/B/C profile; grayish black; slickensides in BW horizon; carbonate nodules; micrite-coated tree trunks; macerated organic matter; dinosaur bones with exposure features; scattered, small barite nodules; bioturbated lacustrine limestone parent material	clay-filled burrows in silty matrix; Fe-Mn masses with diffuse, irregular boundaries; macerated organic matter	illite; moderate reducible Al, Mn, Fe (higher than Pedotypes A, B, C); avg. $\delta^{13}C$ = -7.5‰ ; avg. $\delta^{18}O$ = -11.0‰; avg. $\delta^{34}S$ = +18.3‰ ; avg. $\delta^{18}O$ = +15.6‰	marsh
E	Bg/Btk/Btg/Bg/2Bg/B/C profile; grayish purple to greenish gray; barite nodules in Btg horizon; abundant mottles; scattered slickensides in uppermost horizon; decimeter-scale carbonate steinkerns; clusters of carbonate nodules; Pedotype D and parent material	silicified parenchyma; reworked clay skins; matrix inclusions and bacterial filaments in barite nodules	illite/smectite; low reducible Al, Mn, Fe; avg. $\delta^{13}C$ = -7.5‰ ; avg. $\delta^{18}O$ = -11.1‰; avg. $\delta^{34}S$ = +14.4‰ ; avg. $\delta^{18}O$ = +14.6‰	upland sulfate soil

Table continued

Pedotype	Pedogenic features	Micromorphology	Geochemistry	Hydromorphic classification
F	Stacked Btg/Bg horizons; greenish gray; barite nodules in uppermost Btg horizon; Fe-Mn nodules; mottles; barite-filled rhizoliths in B/C horizon; greenish black, quartz-cemented, lacustrine shoreline sands parent material	pyrite in parent material; Fe-coated barite rhizoliths; leached macropores; Fe-Mn masses with irregular boundaries; cross-striated fabric; matrix inclusions and Fe-Mn in barite nodules; granular structure with dogtooth calcite fracture fill	illite/smectite; high reducible Al; low reducible Mn, Fe; avg. $\delta^{34}S$ = +13.9‰ ; avg. $\delta^{18}O$ = +13.7‰	upland sulfate soil between Pedotype E and Pedotype D
G	Cg/B/Cg/Btkg/Btg/ Bg profile; greenish gray; abundant mottles; clay-filled burrows and calcite-filled rhizoliths; centimeter-scale Fe=Mn nodules; shallow water, lacustrine muds parent material	Fe-Mn lined burrows; small micritic carbonate nodules; abundant mineralized fecal pellets; scattered, macerated organic matter	illite/smectite; avg. $\delta^{13}C$ = -3.7‰ ; avg. $\delta^{18}O$ = -9.76‰	shallow water lacustrine fringe
H	Cg/Oa/Oi to Btg/Oa/Oi profile; abundant, fibric to sapric organic material; zeolites in northeast; burrows in north west; Pedotype E, F, G parent material	Silt-filled burrows; pelleted fabric; zeolites and illite; charcoal in sandstone lenses; abundant volcanic rock fragments and K-feldspar; Fe-Mn coated burrows; sapric organic matter	illite in shale; smectite in sandier profiles; extremely high reducible Fe, Mn and moderate reducible Al in Btg horizons; abundant zeolites	fen (fringe to basin)

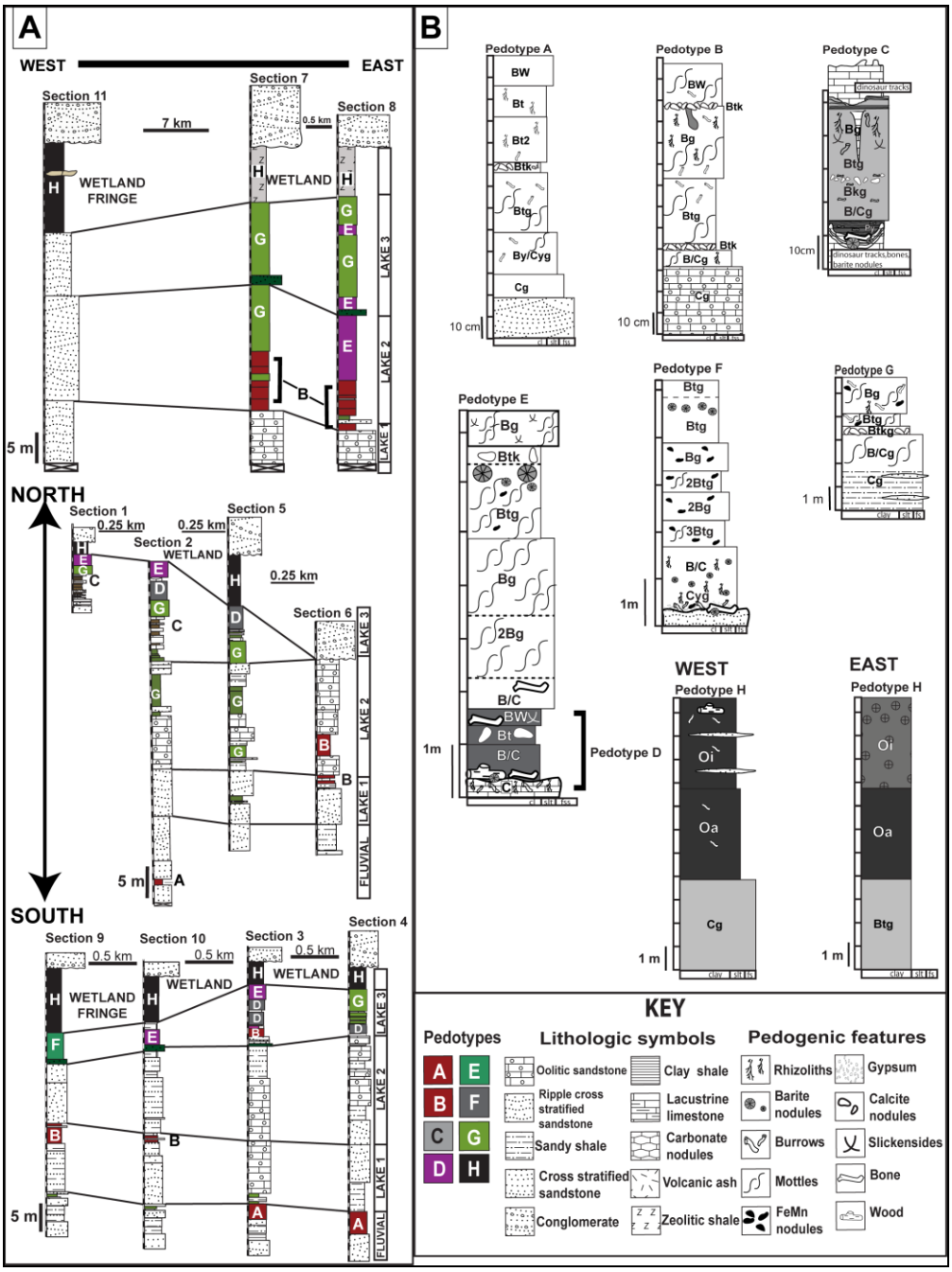

Figure 2. 2. Stratigraphic sections with relative positions of pedotypes. Three genetic lacustrine sequences and associated paleosols are separated by sharp lithological changes that represent a boundaries between flooding surfaces and the underlying lowstand deposits. B) Representative pedotype profiles. See discussion in text for details.

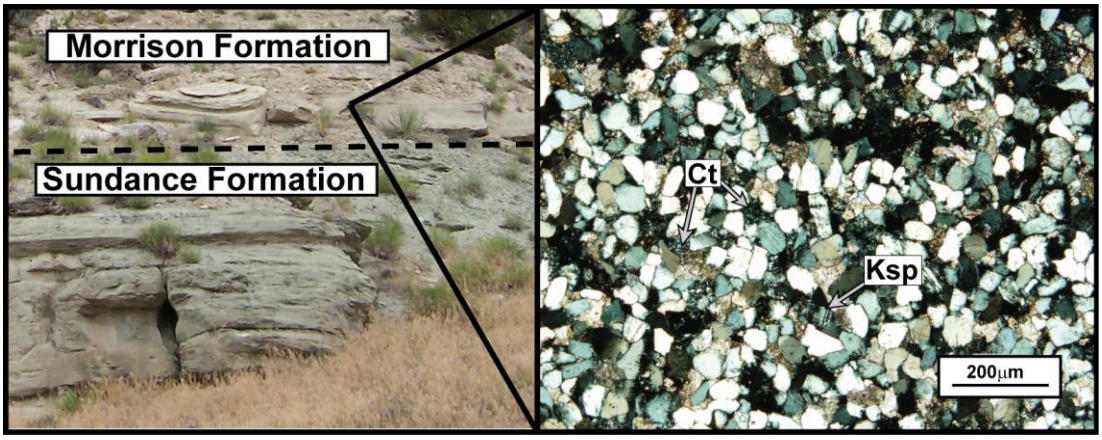

Figure 2. 3. Representative photo of area outcrop. The base of the Morrison Formation in the study area (where exposed) is marked by a sharp lithological contact between the glauconitic sandstone of the Sundance formation and a quartz-rich, well-sorted, fine-grained, calcite-cemented sandstone of the Morrison . Micrograph (inset) taken under cross-polarized light (XPL). Scattered chert (Ct) and potassium feldspar grains (Ksp) are also present in the basal Morrison sandstone.

Sedimentology

Although Morrison deposits in the study area have historically been interpreted as fluvial deposits, abundant lacustrine units were recently documented based on paleontological, geochemical, and micromorphological data (Jennings, 2005; Jennings and Hasiotis, 2006b; Jennings and others, 2006). Additional sedimentary and micromorphological data provided evidence that led to: (1) the differentiation of lacustrine subenvironments and the fluvially derived basal sandstone nits, and (2) refinement of previously published data (i.e., Jennings, 2005; Jennings and Hasiotis, 2006b; Jennings and others, 2006; Takehito and others, 2006).The basal Morrison sandstone is composed of thinly bedded, planar to cross-laminated, tabular sandstones that fine-upward and grade into overlying greenish-gray (5GY4/1) shale or shaly siltstone. Small asymmetrical ripples occur at the tops of the thin beds.

Micrographs reveal that the basal sandstone is a very fine-grained, moderately sorted, rounded to subrounded, calcite-cemented, argillaceous, quartz sandstone (inset, Fig. 2.3). Chert and feldspar grains are minor components. In most sections, the basal sandstone is the parent material for an overlying red paleosol (Pedotype A). Small crossbeds, ripple cross laminations, and fining up sequences of the basal sandstone support an interpretation of vertically accreting channel and point bar deposits (Boggs, 1995; Collinson, 1996; Walker and Cant, 19984).

Above the basal sandstone, three discrete packages of rocks are documented in the upper 40 meters of most sections (see Fig. 2.2). Each package or sequence (*sensu*, Bohacs and others, 2000) is defined by major lithological changes, which represent disconformable contacts between exposure surfaces and flooding surfaces at the base of the overlying deposits. Although sandstone dominates section 10 in the northwest portion of the study area, the majority of the sandstone is concentrated in the lower 40 m of the remaining measured sections. In sandstone dominated sequences, package boundaries are documented by a sharp to erosional contact.

The lowest sequence is composed of: (1) thin, off-white (N8) cross-laminated to laminated oolitic sandstone beds, (2) thick, massive to thinly bedded, off-white (N8), oolitic sandstone, (3) light greenish-gray (5GY7/1) shaly siltstone, and (4) light olive-gray (5Y6/4), trough cross-bedded sandstone units that contain ooids and skeletal fragments (see appendix for additional images). Dark greenish-gray (10 4/1) mudstone and claystone intraclasts occur in the base of off-white sandstone units bounded by thin mudstone packages in the lower parts of sections 3, 4, and 6. Large dinosaur tracks are documented in this interval (Jennings et al., 2006b). Although Jennings et al. (2006)

initially interpreted these deposits as laterally restricted, petrographic evidence from laterally adjacent sandstones in the field area indicates that this interval is laterally continuous for more than 8 kilometers.

Thin sections reveal that sandstones in the lowest sequence range from well-sorted, quartz-rich sandstone in the west to oolitic skeletal grainstones in the east. Quartz, potassium feldspar, chert, volcanic rock fragments, reworked ooids, and skeletal fragments (bivalve and gastropod) are the predominant framework grains in these deposits (Fig. 2.4, Lake 1, A-D). Although these sandstone units were initially interpreted as point-bar and crevasse splay deposits (Jennings and others, 2006), the distribution of lateral facies relationships, well-preserved ooids, and skeletal fragments indicate that these deposits instead represent nearshore to offshore sands that accumulated in a high-energy, bench-type carbonate lake margin similar to those documented in the Pliocene Glenns Ferry Formation (Swirydczuk and Wilkinson, 1979). Similar deposits have also been documented in a Triassic oolitic lake sequence in southeast England (Milroy and Wright, 2000) and lacustrine sediments in other parts of the Morrison basin (Lockley and others, 1986; Dunagan and Turner, 2004). The middle lacustrine sequence (Fig. 2.4, Lake 2, A-D) contains the thickest sandstone units in the study area. Off-white (N8), sheet sandstones that measure 10 m or more thick are separated by cm-scale, silty sandstone beds. The sheet sandstones are characterized by large-scale cross-stratified, oolitic sands that dip 15 °NE(see Appendix for additional images). Small, theropod dinosaur trackways are abundant on bedding plane surfaces with asymmetrical to translational ripples(Jennings and others, 2006).

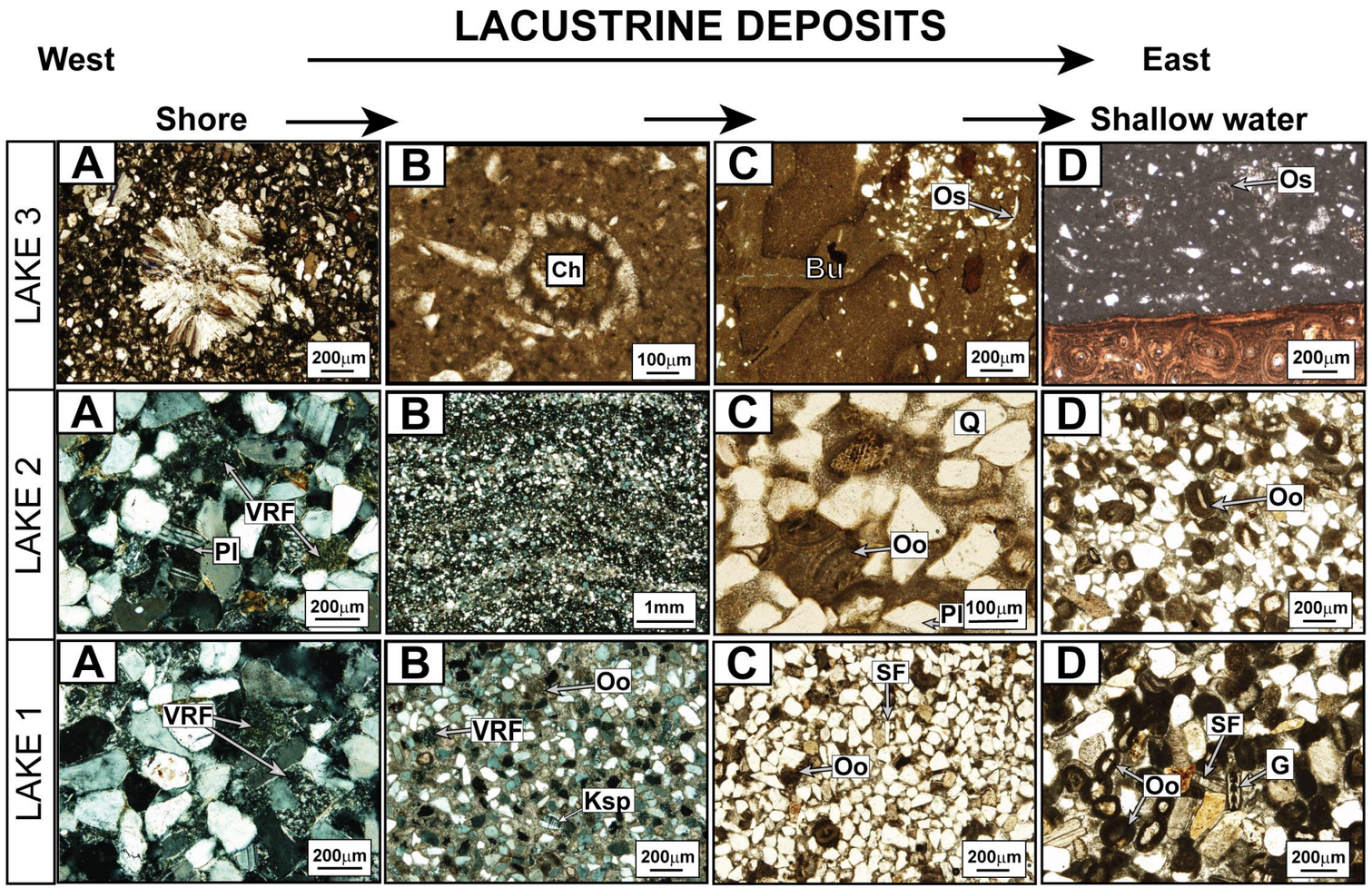

Figure 2. 4 Lacustrine microfacies. Cross-polarized light (XPL); plane-polarized light (PPL). Lake 1. A) Volcanic rock fragments (VRF), feldspar, and subrounded to subangular quartz grains are closely packed (XPL). B) Matrix supported quartz and potassium feldspar (Ksp) grains, reworked ooids (Oo), and volcanic rock fragments (VRF) are common in off shore deposits (XPL). C) Wave reworked skeletal fragments (SF) and ooids (Oo) are scattered throughout fine-grained sandstone (PPL). D) Shallow water oolitic grainstone (PPL) contains abundant skeletal fragments (SF), gastropod shells (G), and ooids (Oo). Lake 2. A) Plagioclase (Pl) and volcanic rock fragments (VRF) are more abundant in this interval (XPL). B) Symmetrical ripples in near shore quartz-cemented sandstone (XPL). C) Reworked oolitic lithoclasts (Oo), quartz (Q), and plagioclase (Pl) are the most abundant framework grains in offshore sandstone (PPL). D) Shallow-water deposits contain grain-supported abundant ooids (Oo), skeletal fragments, gastropods, and detrital grains (PPL). Lake 3. A) Length-slow quartz after gypsum in siliceous, fine-grained sandstone (XPL). B) Charophytes (Ch) are abundant in near shore mud (PPL). C) Burrowed (Bu) limey mud with ostracode (Os) fragments (PPL). (D) Silty, shallow water, micritic limestone contains well-preserved dinosaur bone (bottom) and ostracode (OS) fragments (PPL).

Photomicrographs indicate that sandstone units in the south and east are oolitic grainstones with scattered skeletal fragments (Fig. 2.4, Lake 2, D). In sections 9, 10, and 11 the sandstone is more thinly bedded and is composed of oolitic lithoclasts, scattered skeletal fragments, quartz sand, and feldspar grains (Fig. 2.4, Lake 2, C). Small ripples in sandstones in the westernmost part of the study area exhibit microscale, fining-upward sequences and small symmetrical ripples (Fig. 2.4, Lake 2, B). Photomicrographs reveal that sandstones in the western sections contain plagioclase, quartz, and volcanic rock fragments (Fig. 2.4, Lake 2, A) and that the sandstones in the middle sequence contain more volcaniclastic grains than those in the lower sequence. Facies in this sequence are also interpreted as nearshore to offshore lacustrine deposits that accumulated in a large, high-energy, high gradient, carbonate lake (Swirydczuk and Wilkinson, 1979). During lake lowstand events, oolitic sands on the bench platform were exposed, allowing dinosaurs to traverse the area (Jennings et al., 2006b).

A 2-3 m thick, pale yellow (5Y 7/3), quartz-rich sandstone and a greenish-gray (5GY 5/1), shaly siltstone are present at the top of multistory, sheet sandstone units in section 3. A similar yellow sandstone unit occurs approximately 24 m above the basal sandstone in sections 2 and 4. This sandstone unit is laterally restricted to less than 500 m along the outcrop face and displays a lenticular geometry. Abundant dinosaur tracks, disarticulated dinosaur bones, and plant debris (see Appendix for additional images), and large lithoclasts have been documented in exposure surfaces in a similar interval in section 2 (Jennings and others, 2006). The limited lateral extent, large lithoclasts, and abundant disarticulated plant and dinosaur material suggest that this is a crevasse splay

deposit that sourced from a stream that fed out into the lake basin during a lake contraction event.

The base of the third sequence is characterized by a greenish-black (5G 2.5/2) to greenish-gray (10Y 2.5/1), quartz-cemented, argillaceous sandstone. Thin sections and XRD data reveal that this unit contains length slow quartz pseudomorphs after gypsum, clinoptilolite, and quartz sand grains in a clay-rich matrix (Fig. 2.4, Lake 3, A). Overlying deposits are interbedded limestone and mudstone (see Appendix for additional images). Charophytes, ostracodes, and microburrows are common in these deposits (Fig. 2.4, Lake 3, B, C). Silty, micritic limestone units generally are dinoturbated (*sensu*, Lockley, 1986) and commonly contain well-preserved, articulated dinosaur bones with associated barite nodules (Jennings, 2004a; Jennings and Hasiotis, 2006b; Jennings and others, 2006). Micrographs of these limestones reveal that gypsum pseudomorphs and ostracode fragments are also present (Fig. 2.4, Lake 3 D).

The $\delta^{13}C$ values of the carbonates in this sequence range from -5.4 to -6.56 ‰ and $\delta^{18}O$ values range from -10.25 to -10.6 ‰ (Fig. 2.5). The $\delta^{13}C$ values for bioturbated units range from -6.64 to -6.74 ‰ and $\delta^{18}O$ ranges from -8.97 to -9.61 ‰ (Fig. 2.5). Synthesized carbonate isotope data from the study area are shown in Figure 2.5. Barite $\delta^{18}O$ values range from +10.2 to +17.7‰. $\delta^{34}S$ values range from+5.4 to +20.7‰. Both oxygen and sulfur isotopes are more enriched in the heavy isotope towards the outside edge of large barite nodules. Although carbonate precipitation may occur in the central, deep portion of a lake (Kelts and Hsu, 1978; Cohen, 2003), carbonate muds that exhibit subtle facies changes associated with lake water depth most often occur in lakes with low gradients and low energy conditions (Cohen, 2003). This sequence is interpreted as

shallow water carbonate lake deposits that accumulated in a relatively closed lake basin. The presence of pseudomorphs after gypsum suggest that evapotranspiration was high.

The presence of barite nodules around dinosaur bones indicates that barite precipitated at a redox boundary below the sediment water interface (Breheret and Brumsack, 2000). Stable isotope data from barite nodules indicate that the initial source of sulfate was the oxidation of thiol from decaying dinosaur flesh in shallow alkaline water (Jennings, 2005; Jennings and Hasiotis, 2006b). Subsequent anoxic conditions resulted in bacterial sulfate reduction and subsequent enrichment of heavy oxygen and sulfur isotopes (Seal and others, 2000).

Pedotypes

Eight pedotypes are represented in the study area. Composite paleosols, 1.0 to 1.5 meters thick, are limited to Pedotype A and Pedotype C. Cumulative paleosols are characterized by thick sequences of stacked paleosols that vary in thickness from 2-10 m. Particularly thick, cumulative paleosol sequences occur in sections 7 and 8.

Pedotype A. Description: Pedotype A is a well-developed paleosol that occurs only above the basal sandstone in sections 2, 3, and 4. In general it is 50-130 cm thick and displays seven horizons with gradational contacts. See supplementary data for additional images.

A gray (5Y5/1), massive, argillaceous siltstone Bw horizon commonly occurs at the top of this pedotype (Fig. 2.6 A). Red mudstone Bt2 horizons are composed of silty clay to claystone with a color range of dark reddish-brown to reddish brown (2.5YR3/3 to 5YR4/3). Abundant, sub-millimeter-scale hematite nodules and calcite-filled rhizoliths

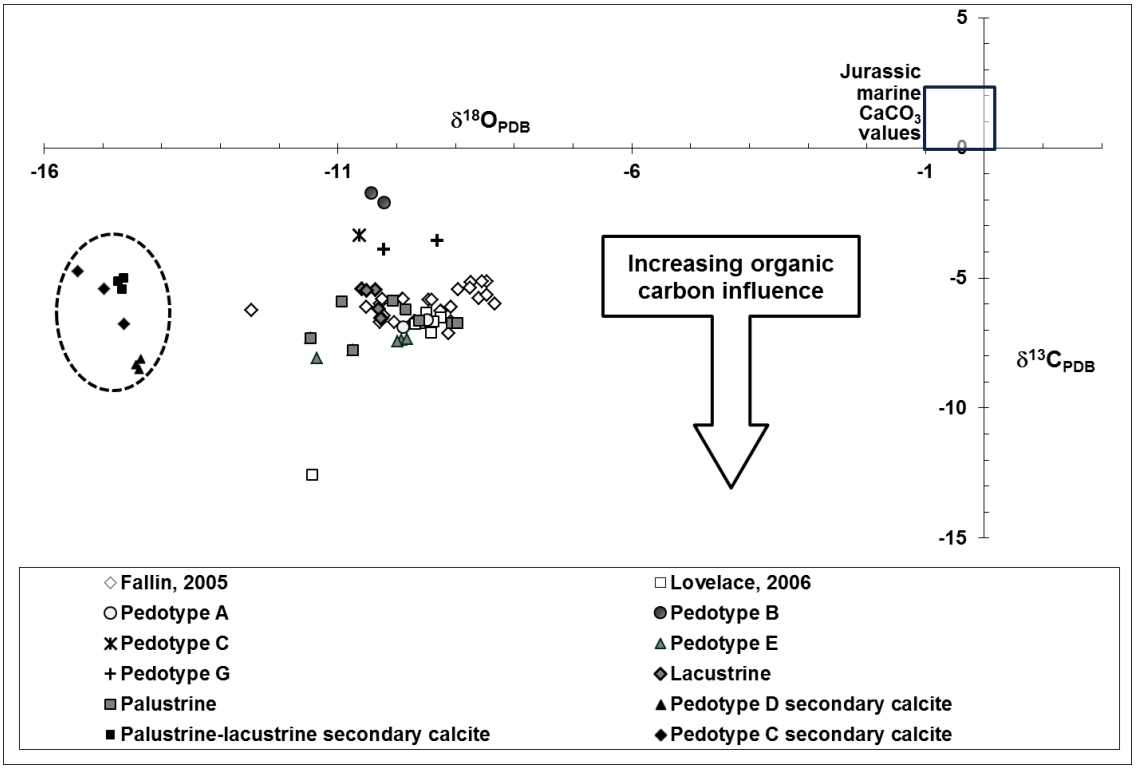

Figure 2.5. Stable carbon and oxygen isotopic composition of carbonate minerals. Overall, carbon and oxygen isotopes from paleosols and lacustrine carbonates in the study area display a narrow range of values and are very similar to other studies in the northern part of the Morrison depositional basin (Fallin, 2005; Lovelace, 2006). Pedotypes B, C, and G display more positive $\delta^{13}C$ values, suggesting increased influence from atmospheric CO_2 and evaporative stress. Palustrine-lacustrine limestones and pedogenic carbonate from Pedotype E display $\delta^{18}O$ values with more variability than from other deposits in the study area. Data from secondary carbonates in barite nodules are more enriched with respect to $\delta^{18}O$ and $\delta^{13}C$ values (circled).

(Fig. 2.6 B) characterize the Bt2 horizon. A dark brown (10YR3/3) Bt1 horizon has diffuse root mottles and becomes moregray upsection. A gleyed Btg horizon also contains olive gray (5Y4/2) mottles and significantly more clay than the underlying horizons. SEM images reveal that well-preserved, μm-scale, clay-filled rhizoliths with root hairs are present (Fig.2.6 C). A thin horizon composed of micritic calcite nodules (Btk) contains mm-scale rhizoliths (Fig. 2.6 D). The By/Cyg horizon exhibits olive gray (5Y 4/2) mottles and clay-filled burrows in a greenish gray (10Y 5/1) matrix. Micrographs reveal that the By/Cyg horizon contains abundant calcite pseudomorphs

after gypsum (Fig. 2.6 E). The fabric displayed in this horizon is eogypsic (Stoops and Poch, 1994). Pseudomorphs are loose, coarse- to fine-grained, sand-sized, lenticular crystals that occur in clay-filled biogenic structures and the matrix. Gypsum pseudomorphs generally comprise less than 10 percent of the non-matrix constituents in a thin section. The parent material is a calcite-cemented, fine-grained, quartz-rich, argillaceous sandstone (Fig. 2.6 F). A gradational boundary is present between the gleyed (10Y 5/1), silty mudstone Cg-horizon and the basal sandstone unit.

Carbon isotope values from pedogenic carbonate in Pedotype A average -6.7 ‰ and oxygen isotope values average -9.64 ‰ (Fig. 2.5). The clay assemblage in this pedotype is predominantly illite with minor chlorite and may be related to iron-rich clays inherited from the parent material (Jennings and Hasiotis, 2006a). Aluminum, iron, and manganese reduced by citrate-dithionate bicarbonate in the Bw horizons and Bt2 horizons average 80.5, 387.0, and 2.4 ppm respectively (Table 2.3).

Interpretation*:* Pedotype A is interpreted as a well-developed paleosol that initially developed in a floodplain distal from a channel (Kraus, 1999b). The presence of pedogenic carbonate and gypsum pseudomorphs suggests that this pedotype was subjected to high evaporative stress. The eogypsic fabric (*sensu*, Stoops and Poch, 1994) in this paleosol indicates that there was not enough gypsum in the soil profile to affect plant growth. Compared to other pedotypes in the area, low reducible element values in Pedotype A indicate that reducible elements were either leached from the profile or oxidized. The lowest percentages of reducible iron are documented in Bt2 horizons compared to Bw horizons, suggesting that translocation of iron was limited in this pedotype.

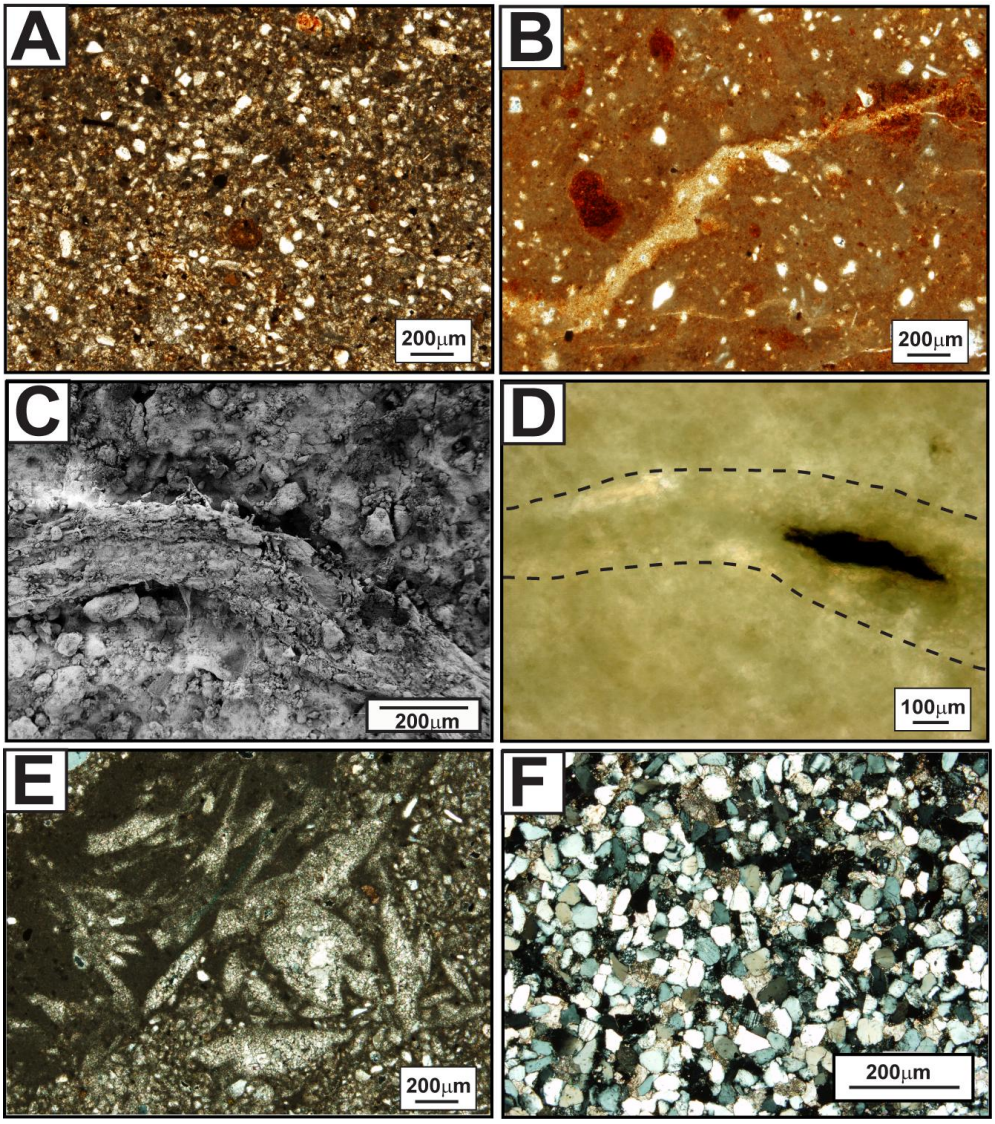

Figure 2.6. Pedotype A microfacies. A) The Bw horizon is a silty mudstone with abundant mineralized fecal pellets (small opaque grains), hematite nodules, and organic matter (PPL). B) Calcite-filled root pores and hematite nodules are common in the silty claystone matrix (PPL). C) SEM image of the Bt2 horizon displays the micro-scale, clay-filled root pores. D) Dashed lines outline a rhizolith in micritic pedogenic carbonate (PPL). E) By/Cyg horizons contain calcite pseudomorphs after gypsum (XPL). F) Parent material for Pedotype A is a quartz-rich, calcite-cemented, fine-grained sandstone (XPL).

Pedotype B. Description: In sections 6, 7, and 8, Pedotype B occurs in stacked successions with olive mudstone or greenish-gray mudstone and scattered thin carbonate horizons (Fig. 2.2 A). A representative cumulative profile is illustrated in Figure 2.2 B. Silty Bw horizons contain millimeter-scale, clay-filled, meniscate backfilled burrows (Fig. 2.7 A). Photomicrographs reveal that degraded skeletal fragments and abundant,

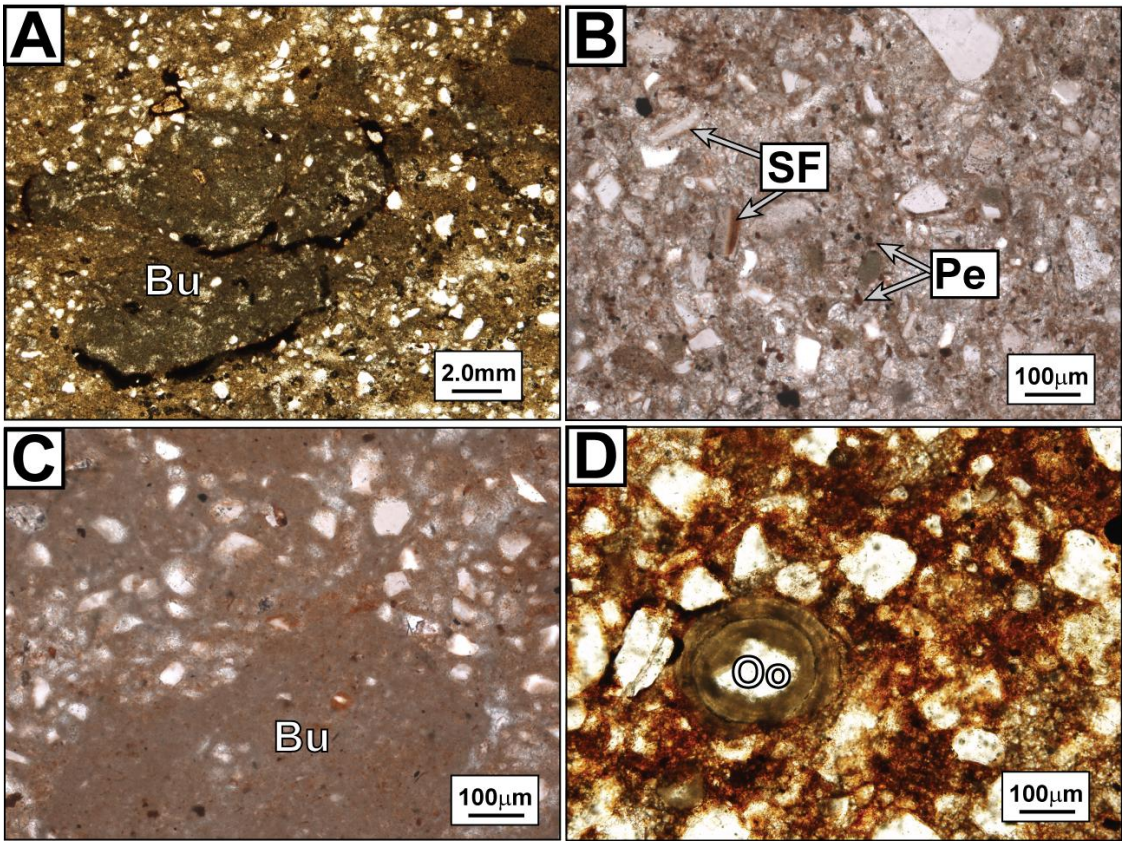

Figure 2.7. Pedotype B microfacies. A) Bw horizons contain reduced clay-filled burrows (Bu) and possible mineralized fecal pellets (opaque grains), (PPL). B) B/Cg horizons are gleyed and contain skeletal fragments (SF), similarly sized peloids (Pe), and quartz grains (white), (PPL). C) Btg horizons contain pinkish gray, clay-filled burrows (Bu), (PPL). D) Weathered ooids (Oo) and quartz grains are common constituents in the B/C horizons. The matrix is hematite-rich (PPL).
Table 2.3. Reducible elements.

similarly sized peloids are present in Bg horizons (Fig. 2.7 B). Carbonate-filled macropores are common in Btg horizons (Fig. 2.7 C). Paleosols that occur lower in the section exhibit a thin Btk horizon. Greenish-gray (5Y6/2) Btg horizons have rare black (N2) or pinkish-gray mottling (7.5YR7/2). Mottles are irregular to elongate in shape and display diffuse boundaries with the matrix.

Bg horizons in the northern portion of the study area commonly contain cm-scale, regularly spaced, discrete, elongate red mudstone-filled voids that are compositionally similar to overlying reddish-brown (2.5YR4/3) Bt horizons. The mudstone within the structure is lighter in color with pale leached edges. Scattered mottles occur along the

edge of one side toward the base and 30 to 40 cm of greenish gray clay-rich mudstone surrounds the structures. No organic matter is associated with the structures; however, calcite- and clay-filled rhizoliths are present in the adjacent matrix. Reddish-brown (5YR4/3) B/C horizons contain weathered ooids and a hematite-rich matrix (Fig. 2.7 D).

The parent material for Pedotype B is oolitic skeletal grainstone (Fig. 2.4, Lake 1 D and Lake 2 D). Olive-gray (5Y5/2) siltstone Cg horizons have brown to light olive-gray mottles (5Y6/3-5Y6/2) and display a gradational contact with the underlying off-white (N8), fine-grained, oolitic sandstone. Carbon isotope values from pedogenic carbonate in Pedotype B range from -1.73‰ to -2.1‰ and oxygen isotope values range from -10.22‰ to -10.44‰ PDB (Fig. 2.5). Reducible aluminum, iron, and manganese measured from the Btg horizon and Bg horizon average 792.0, 219.5, and 4.75 ppm respectively (Table 2.3), with the highest concentrations of reducible iron and aluminum in the Bg horizon. The clay assemblage in this pedotype is dominated by illite with minor amounts of chlorite.

Interpretation: Although Pedotype B has a very similar profile compared with Pedotype A, the characteristic that defines these two pedotypes is parent material. Pedotype B is interpreted as a moderately well-developed paleosol that developed in nearshore oolitic sands that were exposed during lake lowstand. Rhizoliths, mottles, and abundant peloids indicate that this part of the study area was vegetated and supported soil fauna. Nodular micritic calcite accumulated as Btk horizons in well-drained soils adjacent to a carbonate lake as a result of translocation of Ca-rich material down through the soil, with freshwater recharge at the capillary fringe during times of increased evapotranspiration (Wright and others, 1991). Calcareous lacustrine parent material and

increased evapotranspiration during lowstand resulted in pedogenic carbonate that is enriched in ^{13}C.

Redoximorphic features resulted from associated short-term fluctuations in hydrology related to changes in lake level. Reduced iron-rich horizons are associated with reduced pedogenically modified lacustrine deposits. High water-tables resulted in reduced, gleyed horizons lower in the profile (Kraus, 1999b). Decreased sedimentation rates between intermittent lake fluctuation events resulted in paleosol development in shoreward sediments between infrequent flooding events. Upper horizons remained primarily dry after fast infiltration of surface water. Manganese and iron were translocated to lower horizons in soils adjacent to the lake that were saturated long enough to become anoxic during lake highstand and subsequently reprecipitated along pore linings when the soil was better-drained during lake lowstand (Vepraskas, 2001). Gleyed, olive-gray mottles resulted from top-down infiltration of water along macropores in upper horizons (Pipujol and Buurman, 1994)) during lake expansion events.

Reddish-brown mudstone structures in Bg horizons are interpreted as krotovina. Krotovina are defined as abandoned animal burrows or other voids infilled with material from overlying horizons in a soil (NRCS, 2010). Overlying gleyed, clay-rich mudstone suggests that the cavity was infilled after the lower horizon was gleyed. The occurrence of fossorial mammals of this age has been reported from Upper Jurassic deposits in Colorado (Luo and Wible, 2005). Modern monotremes and multituburculates inhabit burrows that are similarly shaped on floodplains (Platt and others, 2004). Although the lack of preserved organic material may indicate that these krotovina may be infilled mammal burrows, the presence of rhizoliths in the horizon adjacent to the structures

Table 2.3. Pedotype descriptions

Pedotype	Al_{CDB}	Fe_{CDB}	Mn_{CDB}	Horizon
A	89.0	516.0	3.2	Bt
	72.0	258.0	1.5	Bt2
Average	80.5	387.0	2.4	
B	684.0	117.0	7.4	BW
	900.0	322.0	2.1	B/Cg
Average	792.0	219.5	4.8	
C	84.0	457.0	3.2	Bg
D	167.0	1660.0	9.0	Bt_{BaSO4}
	1180.0	388.0	4.2	Bt
	52.0	100.0	0.6	B/C
Average	466.3	716.0	4.6	
E	87.0	62.0	0.5	Btg_{BaSO4}
	100.0	85.0	1.2	Btk
	302.0	107.0	0.8	Bt
	116.0	102.0	1.0	Bg
Average	151.3	89.0	0.9	
F	41.0	20.0	1.9	Btg_{BaSO4}
	1722.0	177.0	2.2	Bg
	2310.0	3.0	2.8	2Btg
	115.0	147.0	10.0	B/C_{BaSO4}
Average	1047.0	86.8	4.2	
H	436.0	6458.0	16.9	Btg

suggest that they may have instead been root throw cavities (root ball cavities usually left after a tree topples over or the root ball decays due to waterlogging).

Pedotype C. *Description:* Pedotype C is most abundant in the uppermost part of the formation and is commonly interbedded with well-indurated, light gray (N7), micritic lacustrine limestones associated with the third lacustrine sequence (see pedotype profile

in Fig. 2.2 A). These paleosols are located 12-15 m from the contact with the Cloverly Formation in the southern part of the study area.

Horizon colors vary between dark greenish-gray to greenish-gray (5GY5/1, 10GY5/1, and 5GY6/1). Profile thickness varies between 0.5-1.0 m in lower units to 1.0-5.0 m thick in upperunits. Mudcracks filled with micritic carbonate and coarser-grained mudstone extends down 10-20 cm from the top of Bg horizons (Fig. 2.8 A). Slickensides occur along mudcracks and within the matrix of more clay-rich Bg horizons. Carbonate nodules in the Bkg horizons occur either as fine-grained masses with indistinct boundaries with the matrix or as oval to rounded, nodular masses with sharp contacts with the surrounding matrix. Poorly preserved bone fragments are scattered throughout the Bkg horizons and are commonly coated with micritic carbonate. Bone fragments are brecciated and poorly preserved (Fig. 2.8 C). Carbon isotope values from these nodules average -5.34‰ and oxygen isotope values average -10.37‰ PDB (Fig. 2.5).

Clay-filled burrows and rhizoliths are abundant in some horizons with leached matrix (Fig. 2.8 D). Bg horizons commonly contain ~20% silt, whereas B/Cg, Btg, and Btk horizons are much more clay-rich (Fig. 2.8 B-D).

Well-preserved dinosaur specimens with associated barite nodules are also abundant in the limestone units (Jennings and Hasiotis, 2006b). Greenish-gray mudstone is preferentially compacted around the nodules and micrographs reveal that they commonly contain matrix inclusions (Fig. 2.8 E), indicating that barite precipitated during early burial. Larger nodules display tension cracking in the center of the nodules that resulted from volume reduction during burial. Fractures that are filled with barite and dogtooth calcite (Fig. 2.8 E) terminate within the nodule below an outer layer of fine-

grained barite crystals that also contain matrix inclusions. Thin sections reveal that the micritic carbonate units contain calcite pseudomorphs after gypsum and well-preserved dinosaur bone (Fig. 2.8 F). Micritic limestone and overlying grayish black (N2) claystone units have yielded conchostracans and ostracodes, suggesting that the parent material for this pedotype is lacustrine shale that overlies lacustrine limestone units (Jennings, 2005; Jennings and Hasiotis, 2006b). No evidence of subaerial exposure is observed in these limestone units (Jennings and Hasiotis, 2006b).

Carbon isotope values from the secondary calcite in these nodules average -5.21‰ and oxygen isotope values average -14.69‰ PDB (Fig. 2.5). Sulfur isotope values from the barite nodules range from +6.2 to +16.2‰ and average +9.96‰ CDT, and oxygen isotope values range from +10.8‰ to +14.9‰ (Fig. 2.9). In general, all $\delta^{34}S$ values consistently average +7.7‰ CDT in the central portions of the nodules. The $\delta^{18}O$ values average +12.39‰ CDT. Both oxygen and sulfur isotopes are more enriched in the heavy isotope towards the outside edge of large barite nodules. Overlying thin lacustrine black shale contains bone fragments that have been partially pyritized.

Aluminum, iron, and manganese reduced by citrate-dithionate bicarbonate in the Bg horizons and Btg horizons average 84.0, 457.0, and 3.2 ppm respectively (Table 2.3). XRD analyses reveal that the dominant clay phase present in this pedotype is Ca-Mg smectite (Jennings and Hasiotis, 2006a). Kirkland, 1998; Schudack and others, 1998). During times of highest lake levels, organic-rich laminated clay was deposited, burying remains of dinosaurs that died in the shallow water (Jennings and Hasiotis, 2006b).

The fine-grained, interlocking crystals and matrix inclusions in the lacustrine barite nodules indicate that they precipitated during early burial prior to lithification.

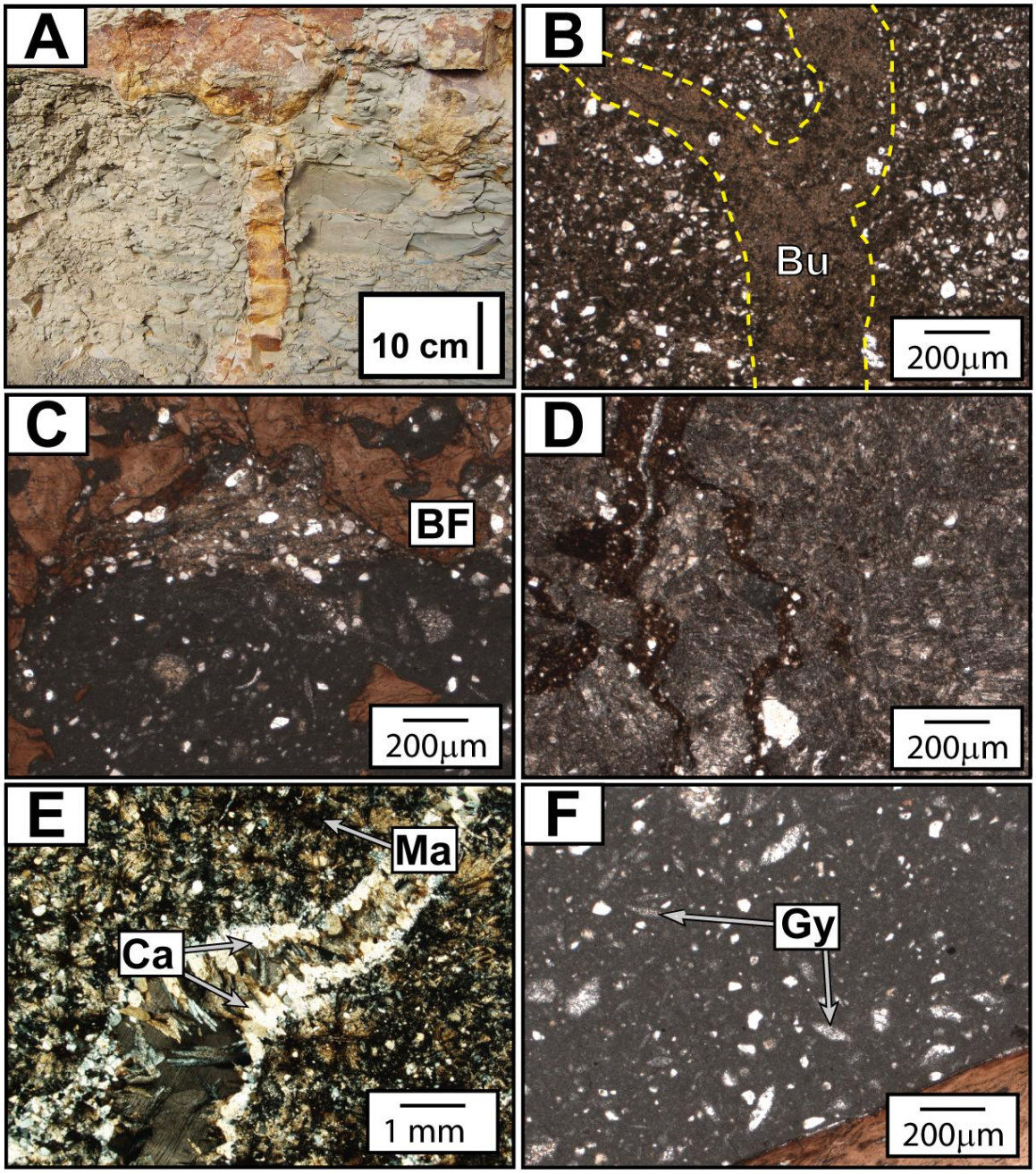

Figure 2.8. Pedotype C microfacies. A) Near vertical mudcracks are filled with micritic calcite. B) Dashed lines highlight a clay-filled burrow (Bu) in a gleyed, silty mudstone (PPL). C) Brecciated dinosaur bone (BF) preserved in a micritic carbonate nodule (PPL). D) Dark, bifurcate macropores are present in the clay-rich matrix (PPL). E) Barite nodules contain matrix inclusions (Ma) and dogtooth calcite (Ca), (XPL). Fractures are limited to the center of the nodules and are commonly filled with coarser-grained barite (brown to gray bladed crystals). F) Micritic lacustrine limestone contains well-preserved dinosaur bone and scattered calcite pseudomorphs after gypsum (Gy), (PPL).

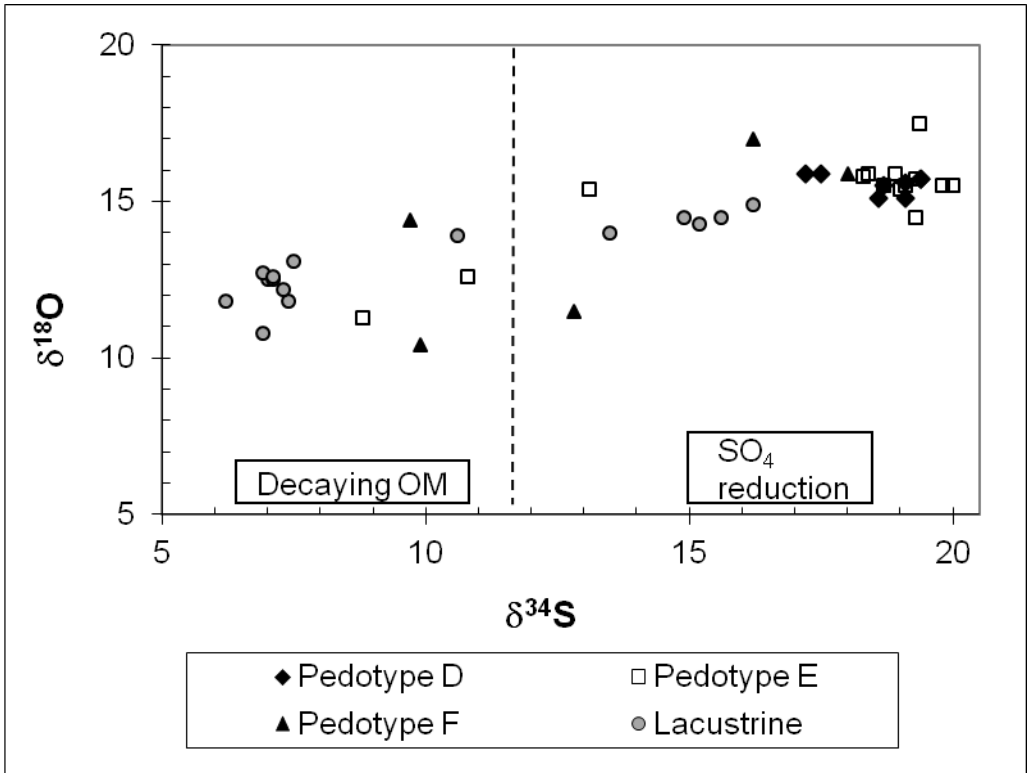

Figure 2.9. Barite isotopes. Low $\delta^{34}S$ values indicate that the source of sulfur was decaying organic material. Subsequent sulfate reduction results in fractionation of sulfur and oxygen isotopes, leading to $\delta^{34}S$ values that are more positive (right side of graph). Barite isotopes from pedogenic nodules have distinctly different isotopic signatures than coeval marine evaporites (large circle).

Sulfur isotopes from lacustrine barite nodules suggest that the initial source of sulfur was sulfides released from dinosaur carcasses during the decay process (Jennings and Hasiotis, 2006b). Oxidation of decaying organic matter created anoxic conditions favorable for microbially mediated barite precipitation during burial at a redox boundary within the lake sediments. In a relatively closed, anoxic system, $\delta^{18}O_{SO4}$ and $\delta^{34}S_{SO4}$ in residual pore fluids at the redox boundary would become enriched with respect to the heavy isotope. $\delta^{34}S$ and $\delta^{18}O$ values increase on the outer portions of the nodules, suggesting subsequent slow rate of sulfate-reduction as sulfate-reducing bacteria flourished in anoxic conditions during a second stage of growth during deeper burial (Seal and others, 2000). Matrix inclusions in outer zones of the nodules indicate that the

second stage of growth in larger nodules also occurred prior to lithification. With increasing burial depth pore fluids evolved isotopically such that dogtooth calcite that precipitated in tension cracks was enriched with respect to ^{18}O (Seal and others, 2000), either due to fractionation from increased temperature and/or infiltration of freshwater rich in dissolved organic carbon during subsequent lake-level expansion events.

The isotopic signature of lacustrine deposits may be quite variable, depending on the balance between carbon sources. Micritic limestone is one of the most reliable and coherent sources of isotopic data, particularly if micromorphology supports that no mixing has occurred from nearshore shell material (Cohen, 2003). However, because ostracode shells and calcite pseudomorphs of gypsum are present, it is likely that the $\delta^{13}C$ values of these limestones indicate that a combination of biogenic and climatic factors contributed to their $\delta^{13}C$ signatures. More positive values from micritic nodules in Pedotype C likely reflect an increased influence from soil-respired CO_2 and higher evaporative stress (Cohen, 2003).

Oxygen isotopes in nearshore lacustrine carbonates reflect the isotopic composition of lake water at the turnaround between lake highstand and the regressive phase. Carbonates that precipitate in closed basins display alternating cycles of $\delta^{18}O$ compositions, with more positive values during drier cycles and more negative values during wetter times. There is little difference between $\delta^{18}O$ and $\delta^{13}C$ of lacustrine and soil carbonates in the study area, suggesting similar source of carbon and similar water composition in and near the lake edge, possibly due to time-averaged groundwater isotopic values.

Higher concentrations of reducible iron compared with Pedotypes A and B, gleyed matrix colors, and indications that sulfate reduction (as indicated by the $\delta^{34}S$ values > +17.0‰ from barite nodules) occurred in underlying lacustrine sediments suggest that this paleosol was predominantly poorly drained and subjected to overall reducing conditions in the lower parts of the profile (Boixadera and others, 2003). Pedogenic carbonate likely precipitated at a slightly more oxic or dysoxic capillary fringe during drier times (Alonzo Zarza and others, 1992).

Pedotype D. *Description:* Pedotype D most commonly occurs in the southern portion of the field area directly above the lacustrine sequence that contains Pedotype C (Fig. 2.2 A). This pedotype commonly displays a gradational boundary with an overlying Pedotype E (see pedotype profile, Fig. 2.2 B).

Massive black to grayish-black (N1/N2) mudstone units that characterize Pedotype D are generally 1.0-2.0 m thick. Nodular, bioturbated limestone (~1 m thick) at the base of this pedotype is interpreted to be the parent material (Fig. 2.2 B). Small, isolated carbonate nodules and centimeter-scale, discrete barite nodules are locally present. Macerated organic material is disseminated throughout the black (N2), silty matrix (Fig. 2.10 A, B). Diffuse concentrations of Fe-Mn oxide with irregular boundaries are present in the uppermost greenish-gray (10Y 5/1) horizons (Fig. 2.10 A). Framework grains are predominantly subangular to subrounded quartz and potassium feldspar.

Clay-filled biogenic structures are present in the upper portion of this pedotype (Fig. 2.10, B). Fragmented and whole ostracode shells are present in carbonate-rich horizons. Slickensides are present along blocky ped surfaces in the uppermost horizons. Although horizonsdisplay little variation in color and textural changes are subtle, thin

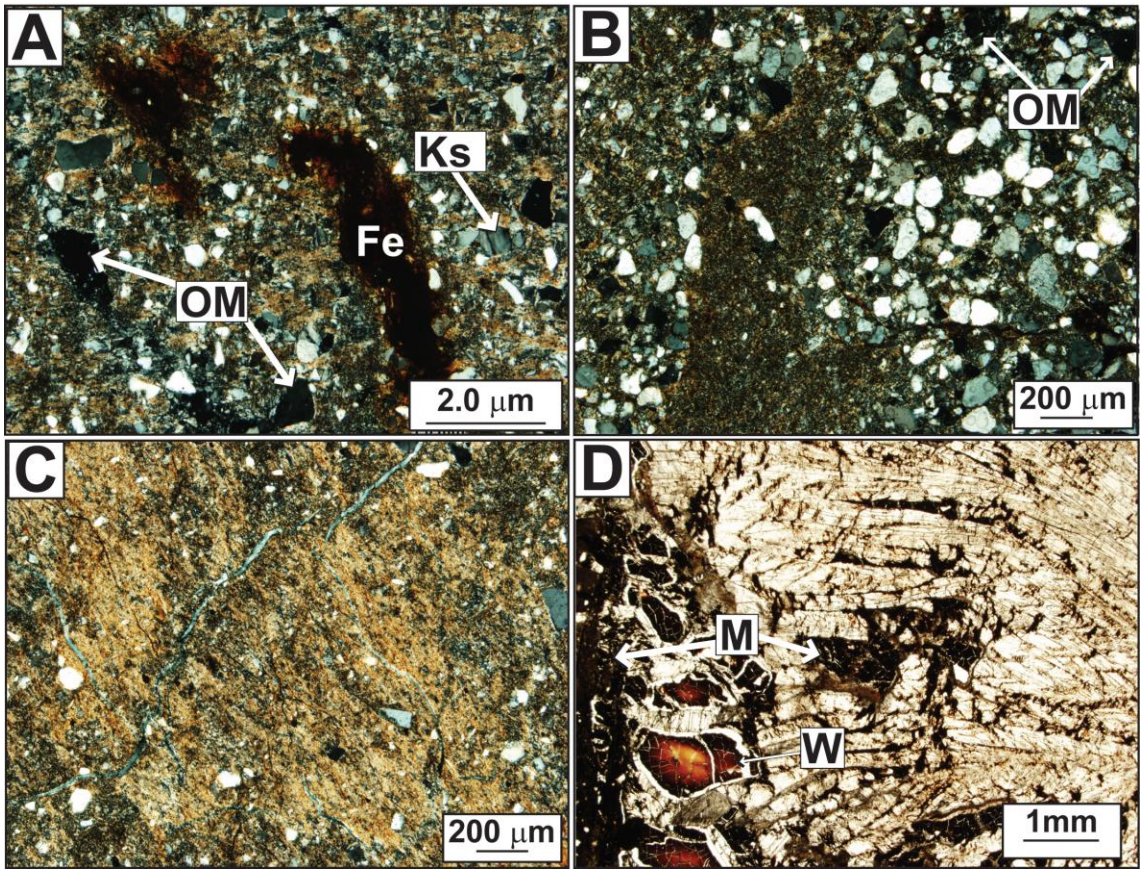

Figure 2.10. Pedotype D microfacies. A) Fe-Mn masses (Fe) have diffuse, irregular boundaries, suggesting that they were not subjected to pedoturbation. Potassium feldspar (Ks) and quartz grains are the predominant non-matrix constituents. Macerated organic matter (OM) is also scattered throughout the matrix (XPL). B) Clay-filled macropores are present in silty horizons. Organic matter (OM) is disseminated throughout the matrix (XPL). C) Clay-rich matrix of a Bt horizon. D) Barite is associated with well-preserved wood (W) in the lower horizons. Matrix inclusions (M) indicate that the barite precipitated before significant burial (PPL).

sections show that Bt horizons contain significantly less silt than bounding horizons (Fig. 2.10 C).

Carbonate-coated, compressed lignite tree trunks over 30cm long with well-preserved bark texture are locally present in the B/C horizon. Cell wall structure is also visible (see Appendix for additional images). Micrographs of tree trunk samples reveal that barite with matrix inclusions and wood fragments are present at the contact between the surrounding matrix and well-preserved woody material (Fig. 2.10 D).

Four articulated and nearly complete, adult *Camarasaurus* skeletons were removed from one of these paleosols and the underlying limestone (Takehito and others, 2006). Rib bones show spiral or helical splitting around the circumference of the shaft along the grain. Calcite mineralization is evident along fractures (Jennings, 2005). Long bones within these sites were preferentially orientated and subhorizontally inclined. Small, light skeletal elements were significantly under-represented (Ikejiri and others, 2006). Stable carbon isotope values from carbonate nodules range from -7.31 to -7.79‰ and oxygen isotope values range from -10.75 to -11.47‰ PDB (Fig. 2.5). Barite $\delta^{34}S$ values range from +17.2 to +19.4‰ CDT and have $\delta^{18}O$ values that range from +15.1 to +15.9‰ (Fig. 2.9). Aluminum, iron, and manganese reduced by citrate-dithionate bicarbonate in the B/C horizons and Bt horizons are significantly higher in this pedotype compared to Pedotypes A, B, and C (Table 2.2). Barite-bearing intervals contain 1660 ppm of reducible iron. Bt horizons without barite contain 1180 ppm of reducible aluminum. XRD patterns indicate primarily illite clay composition for this pedotype.

Interpretations: Pedotype D is interpreted as marsh deposits that developed in depressional, low-lying, lacustrine fringe areas as the lake continued to fill in over time. The presence of both bone and abundant, macerated organic material in the same paleosol suggests fluctuating redox conditions. The presence of large logs indicates that these organic-rich deposits accumulated in low-lying areas that had abundant vegetation and sluggish drainage (Collins and Kuehl, 2001). Groundwater was likely at or above the surface in localized marsh areas for most of the year and reducing conditions dominated this area.

Groundwater movement may cause mineralization of bone, producing the same kind of $CaCO_3$ mineralization in fractures as seen in specimens from section 3 (Irving and others, 1989). Spiral splitting of cortical bone material is indicative of brief subaerial exposure before burial (Behrensmeyer and others, 1989). Limited drying in the uppermost part of the soil profile is also evidenced by slickensides. The orientation of large bones from multiple dinosaurs suggest that the assemblage likely resulted from non-catastrophic, periodic miring of individual dinosaurs in a marshy environment where the surface of the soil may have appeared dry, but the underlying sediments were too saturated to hold the weight of heavy sauropods. The paucity of small elements may be due to post-mortem scavenging (Ikejiri and others, 2006) or weathering of vertebra and crania, 'pumping' to the surface of light, buoyant elements during liquefaction events, or crushing of these elements by mired animals (Wood and others, 2008).

Matrix inclusions in the barite nodules indicate that the barite precipitated prior to significant burial. Sulfur and oxygen isotopes indicate that sulfate reduction occurred lower in the soil profile, however the limited number and size of barite nodules and abundant, macerated organic material in this pedotype suggest that oxidizing conditions rarely occurred enough to allow oxidation of sulfides released during organic matter decay. The presence of humic acids in this soil likely prevented barite precipitation (Smith and others, 2004b).

Carbon isotopes values in this pedotype are more negative than the carbonates from Pedotype C, suggesting that organic carbon was a more significant source of carbon for carbonates in Pedotype D. The presence of both carbonates and macerated organic material in this pedotype indicate that the composition of the pore water fluctuated

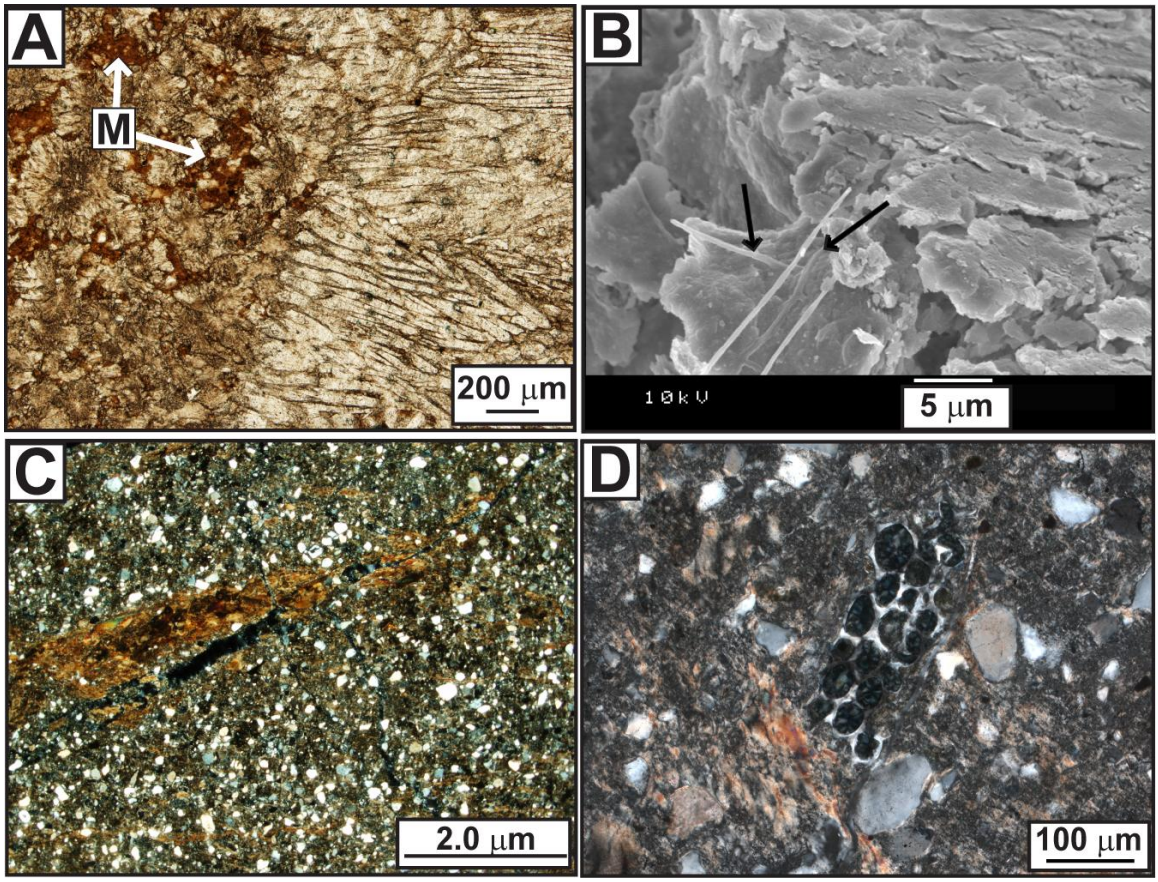

Figure 2.11. Pedotype E microfacies. A) Barite nodules are composed of fine-grained, interlocked crystals (PPL). Crystals are larger near the center of the nodules. Matrix inclusions (M) are abundant. B) SEM image of mineralized bacterial filaments in a pedogenic barite nodule (arrows). C) Siltier Bg horizons contain reworked clay skins (XPL). D) Clay-coated grains are common in buried Bg horizons (XPL). Quartz-filled plant cells and quartz grains are visible in the clay-rich matrix.

between acidic to slightly alkaline in response to seasonal fluctuations in the groundwater table. Oxygen isotopes have similar $\delta^{18}O$ values, indicating that the average oxygen isotopic composition of the water was consistent with values documented in the underlying Pedotype C, inferring overall similar climate conditions.

Pedotype E. Description: In the northern portion of the study area Pedotype E occurs above Pedotype B in the Lake 2 sequence. In the southern portion of the study

area, this pedotype is restricted to the top of the Lake 3 sequence and commonly overlies pedotype D (see Fig. 2.2 A).

Pedotype E varies in thickness from 1-6 m and is composed of stacked B-horizons with mottles and matrixes that vary in color. Slickensides are observed in uppermost silty Bw horizons. Greenish-gray (10Y 5/1), weak red (10R 4/2), and light greenish-gray (10Y 7/1) mottles are abundant. Btk horizons contain decimeter-scale, cone-shaped or ovoid carbonate steinkerns with barite cores and large clusters of cm-scale, micritic carbonate nodules (Jennings, 2005). Illuviated illite-rich clay fills cracks between clusters of carbonate nodules. Depleted zones are common.

Matrix color in Bt horizons varies from grayish-purple to grayish red-purple (5P4/2; 5P6/2; 5RP4/2). Mottles are less abundant in the Bt horizons and usually are greenish-gray (10Y
5/1). Barite nodules that contain abundant matrix inclusions (Fig. 2.11 A) are common in Bt horizons. Although Pedotype E barite nodules vary in size and morphology, decimeter-scale clusters of cm-scale barite nodules are the most common. SEM images reveal that filaments similar to those documented in laboratory studies as a result of bacterial sulfate reduction (Gonzalez-Munoz and others, 2003) are preserved within the barite nodules (Fig. 2.11 B).

Greenish-gray (10Y 5/1) Bg horizons are distinguished by changes in the dominant mottle colors. Bg horizons that underlie barite-bearing horizons are characterized by a silty greenish-gray (10Y 5/1) matrix with dark purple-gray (5P 5/1) mottles. Fragmented clay skins are common in these Bg horizons (Fig. 2.11 C). Lowermost 2Bg horizons contain grayish-green (10Y 4/2) mottles. Unidentifiable, poorly

preserved dinosaur bone is locally present. No cortical bone material is preserved and dissolution features are apparent. Thin-section micrographs reveal clusters of length-slow quartz in a silty matrix (Fig. 2.11 D). The morphology of these features suggests that they are permineralized, parenchyma plant cells. Parent material for this pedotype is pre-existing silty paleosols (usually Pedotype D) and lacustrine deposits.

Stable carbon isotope values from carbonate nodules in Btk horizons range from -7.31 to -7.9‰ and oxygen isotope values range from -10.8 to -11.5‰ (Fig. 2.5). Barite $\delta^{34}S$ values range from +8.8 to +20.0‰ and have $\delta^{18}O$ values that range from +11.3 to +17.5‰ (Fig. 2.9). Aluminum, iron, and manganese reduced by citrate-dithionate bicarbonate in the B/C horizons and Bt horizons average 151.3, 89.0, and 0.9 ppm, respectively (Table 2.3). The highest concentration of reducible aluminum is documented in the Bt horizon below the barite-bearing zone. XRD patterns indicate primarily mixed-layer illite-smectite clay composition for this pedotype (Jennings and Hasiotis, 2006a).

Interpretations: Pedotype E is interpreted as a hydromorphic paleosol that was subjected to seasonal episaturated conditions that lasted long enough for reducing conditions to develop. Fluctuations in the water table allowed the development of slickensides in upper Bg horizons and caused translocation of clays to reduced horizons in higher exposed areas adjacent to the lake. Although purple horizons with gleyed mottles have been interpreted as reduced previously well-drained paleosols that experienced subsequent reducing conditions (Kraus and Gwinn, 1997; Hurt and Carlisle, 2001), the presence of pedogenic barite nodules suggests that seasonal reducing conditions occurred in the Bt horizons of a thick, well-developed, epiaquatic, acid sulfate soil that developed in exposed lacustrine and marsh deposits (i.e., Carson and others,

1982; Darmoody and others, 1989). Although the upper horizons may have commonly experienced dry conditions, gleyed mottles and the paucity of slickensides suggest that epiaquatic conditions limited the shrink-swell capacity of the soil. Reducing conditions likely prevented clay flocculation and allowed clay to migrate down through the soil profile and accumulate in Bt horizon.

Matrix inclusions, fine-grained habit, and the isotopic signature of the barite nodules indicate that they precipitated in the Bt horizons prior to significant burial. The presence of filamentous bacterial fossils similar to those documented in modern laboratory studies (Gonzalez-Munoz and others, 2003) indicates that sulfate-reducing bacteria were present in the soil and that reducing conditions were common in the lower part of the soil profile. Sulfur isotopes indicate that the initial source of sulfur may have been soil organic matter; however, periods of relatively slow sulfate reduction commonly occurred in the soil profile, leading to heavier values of $\delta^{34}S$ and $\delta^{18}O$ compared to lacustrine barite nodules (Seal and others, 2000). Modern barite-bearing soils are typically upland acid-sulfate soils that develop on stable landscapes under relatively arid conditions (Stoops and Zavaleta, 1978; Carson and others, 1982; Darmoody and others, 1989; Sullivan and Koppi, 1995). In these soils, barite precipitation occurs 50 to 150 cm beneath the soil surface.

During brief wet seasons, barite-bearing soils are saturated long enough for reducing conditions to develop for a significant period of time (Carson and others, 1982). Highly reducing conditions that resulted in the mobilization of Fe^{2+} contributed to degradation of bones buried in these units (Behrensmeyer and others, 1989) and the release of barium from clays and feldspar grains (Bjoerlykke and Griffin, 1973; Dalai and

others, 2002; Atun and Bascetin, 2003). Subsequent dry conditions caused oxidation of translocated iron concentrations around roots and pore-linings in the soil (Kraus, 1999a; Vepraskas and Faulkner, 2001). Sulfides released during sulfate reduction also were oxidized, resulting in barite precipitation at a redox boundary in the soil profile. Persistently steady sedimentation rates and a stable landscape contributed to cumulative paleosol development in exposed wetland-lacustrine deposits.

The presence of redoximorphic features, permineralized parenchyma cells, and carbonate steinkerns suggest variable hydrology and epiaquatic conditions during wet seasons for an otherwise well-drained and forested paleosol (Kraus, 1997). Gleyed mottles in the lower horizons suggest a high groundwater table. Surface water gley is more dominant in the upper Bg horizons, which were subsequently submerged, leading to a reduced matrix (Pipujol and Buurman, 1994). Extensive flooding during lake expansion resulted in drowning of waterlogged forested areas adjacent to the permanently saturated areas, leading to calcite precipitation within hollows of rotting trees (Bowen and Bloch, 2002).

Pedotype F. Description: Pedotype F occurs only in section 9 at approximately the same stratigraphic position as Pedotype E (Fig. 2.2 A).

Pedotype F is characterized by 4.0-4.5 m of stacked B-horizons with mottles that developed in greenish-black (5GY 5/1), argillaceous, fine-grained sandstone (Fig. 2.4, Lake 2 B). Poorly preserved dinosaur bones and associated barite nodules are present in the sandstone parent material.

A greenish-gray (10GY 5/1) Btg horizon near the top of this pedotype contains a zone of discrete barite nodules that range in size from 2.0-5.0 cm in diameter. The matrix

of this horizon exhibits cross-striated fabric (Fig. 2.12 A). Barite nodules are finer-grained than other pedogenic barite nodules in the area and contain matrix inclusions and micrometer-scale Fe-Mn masses or oxidized pyrite grains (Fig. 2.12 B).

Dogtooth calcite fills pores between peds. Depleted zones and Fe-Mn nodules with irregular boundaries are common in most Bg, 2Bg and 3Bg horizons (Fig. 2.12 C). Siltier 2Bg horizons exhibit granular microstructure (Fig. 2.12 D). Greenish-gray (5GY 5/1) B/C-horizons are clay-rich and contain mm-scale rhizoliths. Thin sections and XRD data reveal that rhizoliths are infilled with barite and have Fe-Mn coatings (Fig. 2.12 E). Quartz silt inclusions are present in the barite. Many rhizoliths have a Fe-Mn center (Fig. 2.12 E) from which fine-grained barite radiates. Euhedral pyrite grains with diffuse hypocoatings are present in the siliceous parent material (Fig. 2.12 F).

The $\delta^{34}S$ values range from +9.9 to 18.0‰ and $\delta^{18}O$ values range from +10.4 to +17.0‰ (Fig. 2.9). Sulfur and oxygen isotope values are progressively more positive towards the outer rim of the nodules. XRD data indicate that the clay phases present are predominantly mixed-layer illite-smectite. Aluminum, iron, and manganese reduced by citrate-dithionate bicarbonate in this pedotype average 1047.0, 86.8, and 4.2 ppm, respectively (Table 2.3) with the highest concentration of reducible aluminum in the Btg and Bg horizons underlying the barite-bearing horizon. A color change characterizes the contact between the Btg horizon of Pedotype F and the overlying bluish-gray claystone (5B 5/1). A significant change in the concentrations of aluminum, iron, and manganese reduced by citrate- dithionate bicarbonate also occurs at this boundary, suggesting that this is a significant disconformable surface.

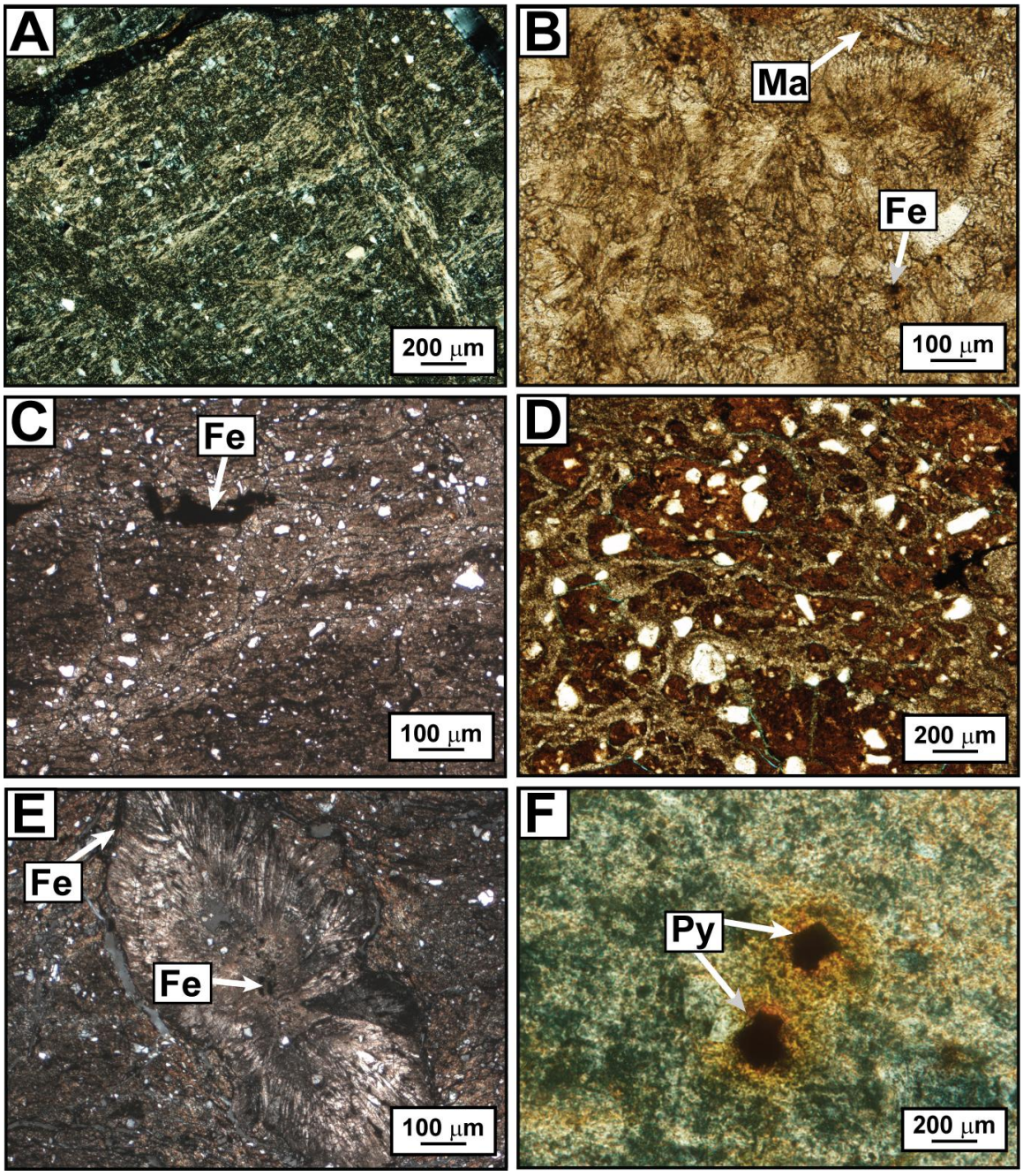

Figure 2.12. Pedotype F microfacies. A) Bisepic plasmic fabric is common in Btg horizons (PPL). B) Very fine-grained barite nodules contain matrix inclusions (Ma) and small Fe-Mn masses (Fe) (XPL). C) Leached zones are abundant in Btg horizons. Silt-sized quartz and potassium feldspar grains are scattered throughout the matrix. Fe-Mn masses (Fe) have irregular boundaries (PPL). D) Buried Bg horizons preserve a granular texture (PPL). E) Small, iron-coated (Fe) barite nodules that precipitated around iron-coated root pores in Btg horizons (PPL). F) Quartz-cemented, lacustrine parent material contains euhedral pyrite grains (Py) with hypocoatings (PPL).

Interpretations: Based on laterally adjacent pedofacies, Pedotype F is interpreted as a gleyed, hydric paleosol that accumulated lower on the topography than Pedotype E and immediately adjacent to the wetland fringe where the water table was at or near the surface most of the time. Assuming that the parent material was not greenish-gray, mottle-free, greenish-gray units and high concentrations of reducible elements, particularly iron, suggest that this pedotype accumulated in poorly drained areas that restricted the movement of elements mobilized under reducing conditions and were seldom dry enough to be oxidized, except within the uppermost part of the soil profile (Vepraskas and Faulkner, 2001). Pyrite with hypocoatings in the parent material suggests that sulfide oxidation in exposed lacustrine deposits occurred in the lower part of the profile. Barite-filled rhizoliths indicate that a redox boundary was present in the B/C horizon. Alternating reducing and oxidizing conditions at the wetland fringe resulted in Fe-Mn hypocoatings on root pores. Granular structure of buried Bg horizons suggests that this horizon may have been inundated after a period of exposure and bioturbation. Dogtooth calcite between granular peds may be meteoric vadose cement. The contact between the uppermost barite- bearing horizon and the overlying gleyed claystone represents a flooding surface that marks the boundary between the Lake 3 sequence and the overlying wetland deposits.

Pedotype G. Description: Pedotype G is present in the eastern portion of the study area. Profiles in the south tend to be much thinner (0.3-1.0 m thick) than profiles preserved in the north (to 2.0-5.0 m thick). This pedotype is limited to intervals interpreted as Lake 2 and Lake 3 sequences (Fig. 2.2 A).

Pedotype G is composed of olive- to olive gray (5Y5/3-5Y5/2) mudstone horizons (Fig. 2.2 B) that are more silt-rich than other pedotypes in the study area. The parent material for this pedotype is a pale olive, calcareous, laminated siltstone with thin siltstone and fine-grained sandstone lenses. Charophyte fragments are common in the parent material (Fig. 2.4, Lake 3 B).

Large Fe-Mn masses with diffuse boundaries and burrows are present in Bg horizons (Fig. 2.13 A). Macerated organic matter, dark greenish-gray (5GY 4/1) mottles, and small Fe-Mn nodules or pellets are common in Btg and Bg horizons (Fig. 2.13 B). Microburrows in Btg horizons are filled with micritic calcite (Fig. 2.13 C).The B/Cg horizon is characterized by an olive gray (5Y 5/2) matrix with light olive- gray (5Y 6/2) mottles. Calcite nodules in the Btkg horizon contain abundant silt and scattered, micrometer-scale, Fe-Mn pellets (Fig. 2.13 D).

XRD patterns document that mixed-layer illite-smectite with minor chlorite are the clay phases present. Smectite peaks do not fully collapse with KCl saturation and do not show a clear chlorite peak at 14.5 Å, indicating the presence of vermiculite layers in the crystal lattice. Stable carbon isotope values from carbonate nodules range from -3.58‰ to -3.91‰ and oxygen isotope values range from -9.31‰ to -10.21‰ (Fig. 2.5).

Interpretation: Based on increased leaching and translocation of iron in reduced horizons as indicated by abundant Fe-Mn nodules, Pedotype G is interpreted as a composite to cumulative, poorly drained, shallow-water wetland paleosol that developed in exposed nearshore lacustrine deposits during lake lowstand. Sandier parent material allowed for better drainage conditions than in other areas near the lacustrine fringe. Cumulative paleosols in sections 7 and 8 likely resulted from a steadier rate of

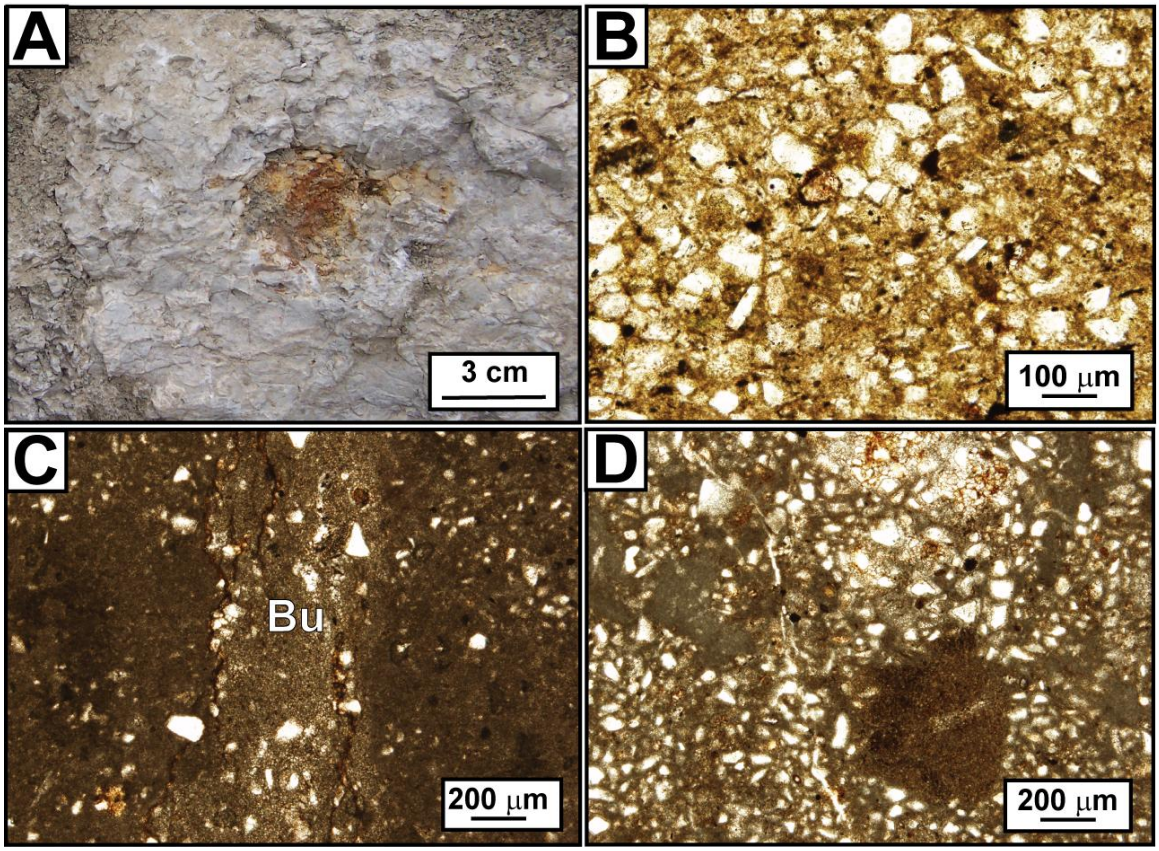

Figure 2.13. Pedotype G microfacies. A) Large iron nodules are present in leached Bg horizons. B) Quartz silt and feldspar grains are the predominant non-matrix constituents in Bg horizons (PPL). Similarly sized, mineralized pellets scattered throughout the matrix are likely mineralized fecal pellets. C) Clay-filled, microburrow (Bu) in Btg horizons have iron-coated walls (PPL). D) Calcite nodules (i.e., lower right) in a silty Bkg horizon (PPL).

sedimentation and a more stable landscape (Kraus, 1999b) than those in the southern portion of the study area, suggesting a slightly higher position on the landscape. Lighter olive gray mottles suggest extended periods of saturated soil conditions thatresulted in leaching of iron along root pores and soil-pore (Vepraskas, 2001). Loss of Fe during reducing conditions prevented clay flocculation, leading to migration of clay and Fe^{2+} from macropores into the matrix (Boixadera and others, 2003). Sediment-water interaction in an already carbonate-rich environment resulted in the precipitation of

carbonate nodules in lower horizons by capillary rise during drier times (Alonso-Zarza, 2003).

Pedotype H. Description: Pedotype H is present at the top of the Morrison in all sections except Section 6 (Fig. 2.2 A). Although the overall profile appears similar in all sections, subtle differences in mineralogy and pedogenic features allow differentiation of the relative hydrogeomorphological conditions across the area (Fig. 2.2 B).

Pedotype H is nearly 12 meters thick and possesses three distinct horizons (see Appendix for additional images). The uppermost Oi horizons in the northwest are bioturbated, organic-rich siltstone units that contain large, lignitic wood fragments and clay-filled burrows (Fig. 2.14 A). Fine-grained sandstone lenses that are present in the northwestern Oi horizon are composed of potassium feldspar, quartz, volcanic rock fragments, and charcoal (Fig. 2.14 B). Smectite is the dominant clay phase present. The middle horizon in this pedotype ranges from an organic-rich silty Bg horizon in the west to, a massive, organic-rich Oa-horizon with a mucky texture (contains between 11 and 18% decomposed organic material). Silty Oa horizons in the northwest contain mm-scale, silt-filled burrows (Fig. 2.14 C).

In the northwest, the basal Cg horizon is composed of well-sorted, fine-grained sandstone. Predominant framework grains are quartz, feldspar, and volcanic rock fragments (Fig. 2.14 D). Many feldspar grains have been replaced by calcite. No primary sedimentary structures or pedogenic features are evident.

Laterally equivalent Oi horizons in the northeast part of the study area are laminated, organic-rich, zeolitic shale (Fig. 2.14 E). Compressed fern pinnae, seeds, macerated, lignitic plant fragments, and leaf fossils are abundant in the horizon. Thin

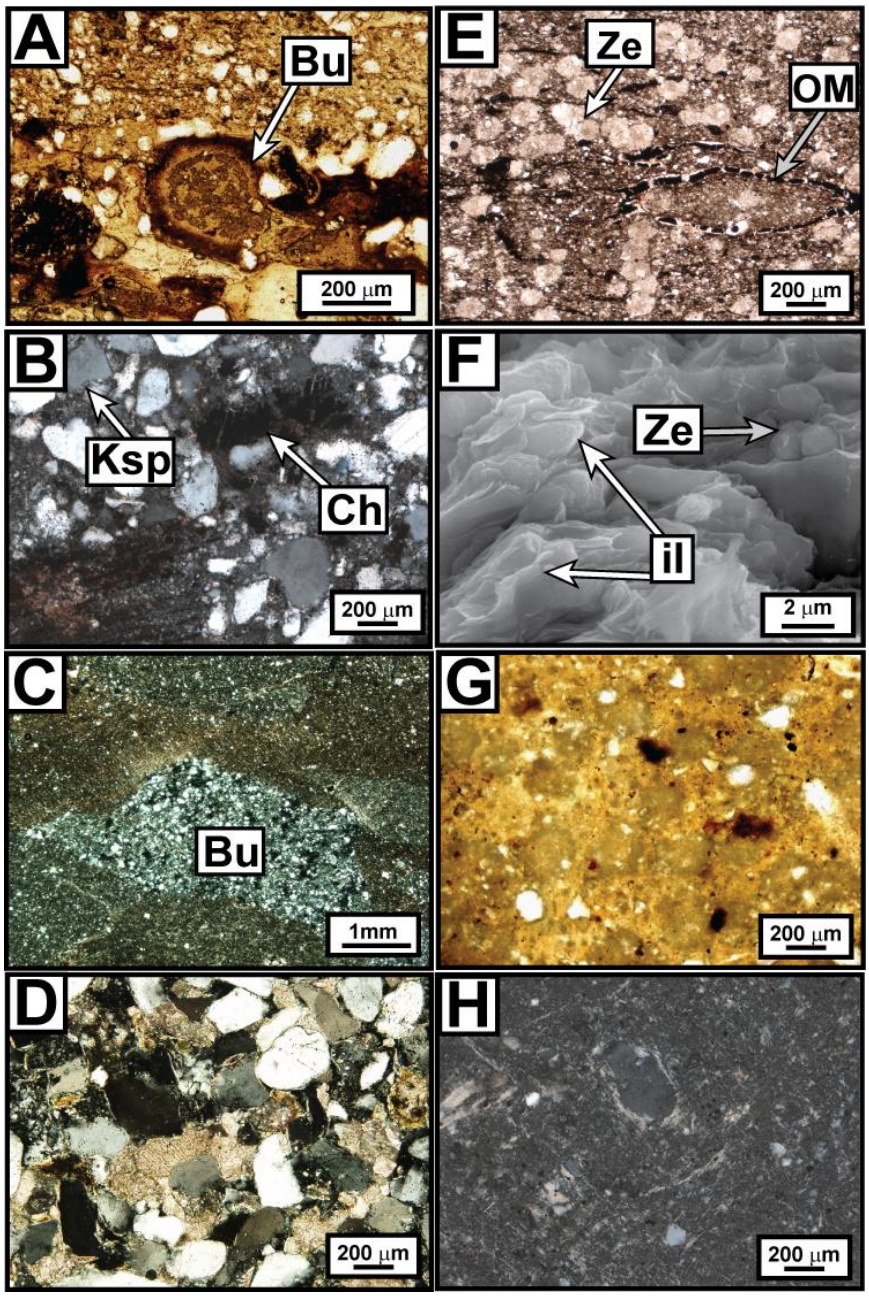

Figure 2.14. Pedotype H microfacies – northwest profiles (A-D); south and east (E-F). A) Burrows (Bu) have iron-coated walls and are infilled with clay (PPL). B) Charcoal (Ch) and potassium feldspar (Ksp) are abundant in thin, discontinuous sandstone lenses (XPL). C) Lower Oa horizons have silt-filled burrows (Bu), (XPL). D) Fine-grained, sand-sized quartz, feldspar grains, and volcanic rock fragments are the most abundant framework grains in calcite-cemented Cg horizons (XPL). E) Oi horizons contain abundant zeolite crystals (Ze) and fine-grained organic matter (OM) in a clay-rich matrix (PPL). F) SEM image of illite (il) and zeolites (Ze) in finer-grained Oi horizons G) Organic matter and pyrite (dark grains) are common in the pelleted matrix of an Oa horizon (PPL). H) Btg horizons in the deeper part of the basin are composed of reduced, iron-rich claystone (XPL).

sections reveal that zeolites are abundant and well distributed throughout the matrix (Fig. 2.14 E). Although organic matter is too abundant in the overlying horizons to allow a good interpretation of clay XRD patterns, scanning electron images reveal that illite is the predominant clay phase present in organic-rich horizons (Fig. 2.14 F). Oa-horizons in the south and east are evidenced by the presence of disseminated, decomposed organic material in hand sample and in photomicrographs (Fig. 2.14 G). These more clay-rich horizons exhibit a pelleted structure and contain abundant, micron-scale, Fe-Mn masses (Fig. 2.14 G).

In the east and south the base of this pedotype is a greenish-gray to bluish-gray (5GY 5/1- 5BG 5/1) Btg horizon that ranges in thickness from 4.0-5.0 meters. The fabric of this horizon is massive (Fig. 2.14 H). Aluminum, iron, and manganese reduced by citrate-dithionate bicarbonate contained in this horizon 436, 6458, and 16.9 ppm, respectively (Table 2.3). The primary clay phase present is illite.

Interpretations: Pedotype H is interpreted as a fen deposit that accumulated during widespread flooding after a long period of landscape stability. Analcime is well documented in organic-rich deposits as a product of altering volcanic ash in low-temperature aqueous environments (Hay, 1970; Renaut, 1993). Highly reactive airfall-ash deposited in water quickly alters to smectite clay and siliceous gel (Chamley, 1989; Hillier, 1995). As alkalinity increases during the alteration process, zeolites form in areas of concentrated ions (Drits and others, 1997; Calvo and others, 1999; Meunier and Velde, 2004). Zeolites in soils may authigenically crystallize during pedogenesis or may be incorporated from zeolite-rich sediments introduced in volcaniclastic parent material (Ming and Dixon, 1988). Pedogenic zeolites occur in saline, alkaline soils of volcanic

origin under alkaline conditions resulting from high evapotranspiration (Ming and Dixon, 1988). Unlike analcime grains in pedotype H, lithogenic zeolites inherited from reworked volcanic parent material tend to be concentrated in upper horizons and show signs of weathering. Conversely zeolites that formed *in situ* would be expected to be euhedral, unabraded, and unfractured , (Ming and Dixon, 1988), similar to those documented in Pedotype H. Abundant analcime and natrolite is well-distributed within laminated, organic rich deposits rather than filling pore space (Ming and Dixon, 1988; Jennings, 2005). No significant amounts of kaolinite or indications of hydrothermal deposits are documented in field area (Owen and others, 1989; Jennings, 2005).

Length-slow quartz is also associated with evaporative conditions in closed, saturated environments (Aoyagi and Kazama, 1980). All-liquid fluid inclusions in these types of length-slow quartz support a low-temperature, shallow burial environment of precipitation (Goldstein and Reynolds, 1994). Radial quartz crystals with matrix inclusions and all-liquid fluid inclusions in upper Morrison Formation units, suggest that silica precipitated out of solution as silica-rich ash altered in water at surface temperatures. As fine-grained, rhyolitic or dacitic ash altered in aqueous Morrison environments, zeolites and quartz precipitated out of porewater similar to deposits in Pleistocene-Holocene systems in Africa (Tiercelin and others, 1987; Ashley and Driese, 2000). Interstitial pore water became more alkaline in lakes and fens with restricted drainage (Hanor, 2000; Jennings, 2005) and excess silica and concentrated ions combined to form early diagenetic zeolites in carbonaceous material accumulating in the fen (Hay, 1970; Taylor and Surdam, 1981; Gottardi and Galli, 1985; Renaut, 1993).The abundance of zeolites and the paucity of plant material and silt- and sand-sized sediments in the Btg

horizons at the base of Pedotype H implies that these environments received little or no overland flow from streams, but rather experienced a rise in the groundwater table.

The paucity of plant material and silt- and sand-sized sediments in the Btg horizons at the base of Pedotype H implies that these environments received little or no overland flow from streams, but rather experienced a rise in the groundwater table. The presence of thick Btg horizons infers the accumulation of an over thickened underclay or seat earth that formed under a long-lived, mineral wetland soil (Richardson and Brinson, 2001). The extremely high concentration of reducible Fe in this horizon indicates that restricted drainage in this wetland allowed reduced iron to accumulate in the base of the wetland soil.

Organic-rich claystone and siltstone horizons are interpreted as Oi horizons similar to hisotsol horizons that have been documented in open parts of fens and associated analcime-rich peat bogs in Africa (Ashley and Driese, 2000) and Minnesota (Collins and Kuehl, 2001). Soil material in which the original plant remains are not recognizable (mucky organic soil material) accumulated in underlying sapric Oa horizons of wetland soils by the decomposition of organic matter and subsequent buildup of organo-mineral complexes. Microscopic rounded masses are interpreted to be fecal pellets of detrital feeding invertebrates and insect larvae (Craft, 2001). In modern hydric soils, similar residual aggregates of organic material, also called organic bodies, have been documented in mucky mineral O horizons (Vepraskas, 2001). Restricted alkaline conditions indicated by illite clays and abundant early authigenic analcime in more basinward deposits suggest that evapotranspiration was a dominant process in this fen,

similar to Quaternary deposits in tropical semi-arid regions (Surdam and Eugster, 1976; Renaut, 1993; Hay and Kyser, 2001).

The accumulation of well-preserved tree trunks in coarser-grained profiles suggests that the water table was at or near the surface at the wetland fringe, resulting in increased acidic conditions in the outwash sands. Shallow, but very poorly drained settings adjacent to vegetated wetland areas allowed organic-rich deposits to accumulate in overlying fibric Oi horizons (Collins and Kuehl, 2001) that were acidic enough to preserve large fragments of wood.

The presence of charcoal in sandstone lenses interbedded with wetland fringe deposits suggests that wetland fires occurred in the area and subsequently led to increased erosion at the wetland fringe. Mineralization of dissolved organic carbon (DOC) resulted as DOC adsorbed onto clays contributed by overland flow during infrequent flooding events, and from alteration of fine-grained volcanic ash (Collins and Kuehl, 2001). Although sandstone lenses containing charcoal indicate that the fen received water from restricted overland flow after wetland fire events, this may not indicate a significant overall change in precipitation. Wetland fires and similar outwash sands are common in arid to semi-arid environments (Scott, 2000). The abundance of ions and nutrients as indicated by the presence of abundant analcime and illite suggest that groundwater was the predominant source of water for this area during the latest Morrison time. It is possible that increased recharge resulting from increased volcanic activity in the source area to the west led to the development of widespread wetlands by a rise in the groundwater table and influx of altered fine-grained sediments into the system without

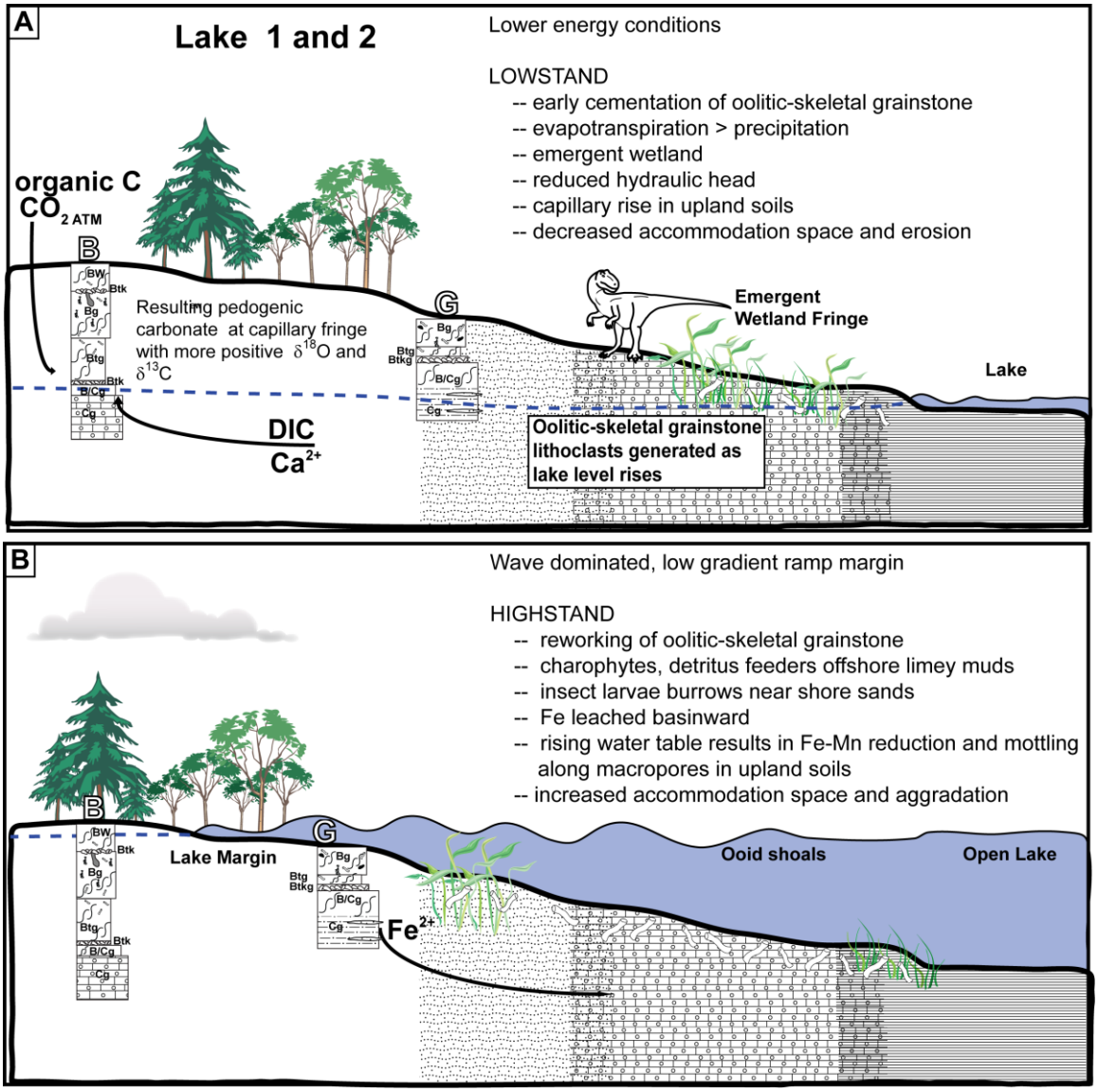

Figure 2.15. Facies model for subenvironments interpreted for Lake 1 and Lake 2. A) During lake lowstand lower energy conditions prevailed. Early cementation of oolitic skeletal grainstone increased the preservation potential of dinosaur tracks. High evapotranspiration resulted in pedogenic carbonate precipitation at the capillary fringe. Emergent shallow water wetlands were present between the lake and better-drained paleosols that developed in exposed oolitic grainstones higher on the topography. B) Increased accommodation and aggradation during lake expansion events, resulted in the accumulation of oolitic shoals on a wave dominated, low gradient ramp margin. Oolitic-skeletal grainstone lithoclasts were generated as lake level rose. Charophytes and detritus feeders populated offshore limey muds. Insect larvae were likely present in near-shore sands. A high water table resulted in Fe-Mn reduction and mottling along macropores in upland soils.

any significant climate change (Kuenzi and others, 1979; Cohen, 2003; Paz and Rossetti, 2005).

Discussion

Fluvial deposits and well-developed floodplain paleosols (Pedotype A) briefly dominated the depositional system in the Big Horn Basin during earliest Morrison time which was subsequently followed by the development of a long-lived carbonate lake system with laterally adjacent poorly drained, wetland soils (Fig. 2.15 A, B), similar to the Great Salt Lake and its precursor Lake Bonneville (Eardley and others, 1957; Eardley and Gvosdetsky, 1960). During the first and second large-scale, lake lowstand events (Lake 1 and Lake 2 sequences), well-developed, well-drained paleosols developed on exposed oolitic shoals and shoreline deposits. Evaporation exceeded precipitation and pedogenic carbonate precipitated at the capillary fringe. Disseminated organic material from nearby Morrison paleosols have average $\delta^{13}C$ values of -26.9‰ (Fallin, 2005). Carbonate isotope data suggest that dissolved inorganic carbon (DIC) from lake carbonates, combined with carbon derived from soil organic matter and atmospheric CO_2, likely contributed to the overall isotopic signature of these carbonates. Low $\delta^{18}O$ values (less than -5.5‰) reflect meteoric values consistent with increased precipitation. More positive $\delta^{13}C$ values documented in the lake carbonates and adjacent wetland carbonates suggest high rates of plant decay and/or increased groundwater flow. Higher averages in $\delta^{18}O$ values and $\delta^{13}C$ occur during dry periods (lake lowstand) when evapotranspiration increased (Liutkus and others, 2005). Evaporative conditions during lake lowstand events also allowed early cementation of oolitic-skeletal grainstones and dinosaur track

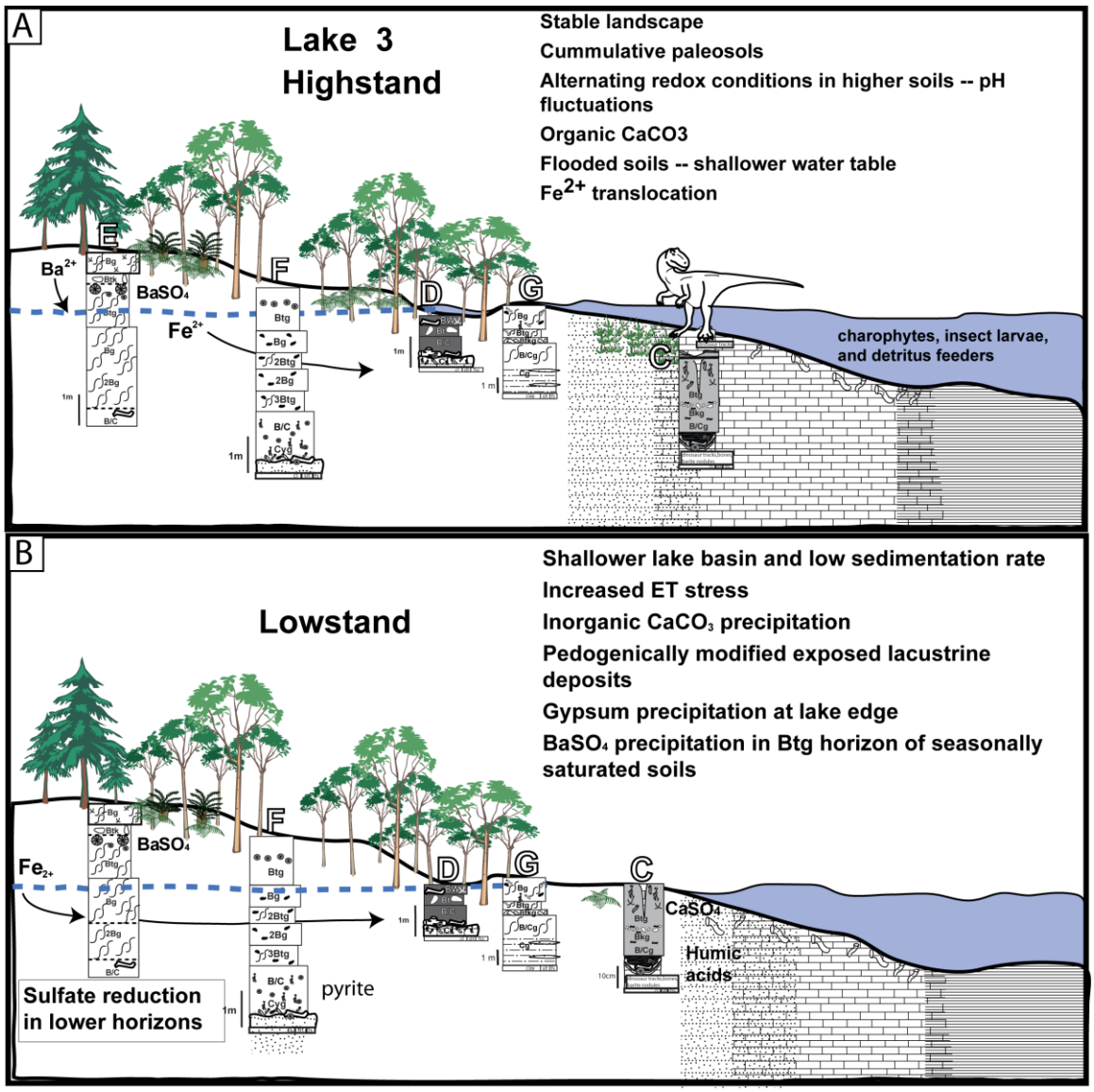

Figure 2.16. Facies model for subenvironments interpreted for Lake 3. A) Shallow carbonate lake basin, low sedimentation rates, and overall landscape stability characterize the highstand deposits in this lacustrine sequence. Frequent lake expansion resulted in rising groundwater table, flooded soils, and widespread reducing conditions. Sulfate reduction in lower part of upland soils released barium from feldspars and clays and mobilized iron. Mobile iron was translocated down gradient to less well-drained soils and wooded marshes. Wooded marshes were present in low-lying areas between the lake proper and upland areas. Iron leached from coarser grained, poorly drained shallow water wetlands was delivered to lake water. B) Exposed lake flats are pedogenically modified during times of lake lowstand. Better-drained upland soils experienced epiaquatic, saturation during wet seasons. During drier times, increased evaporative stress results in the oxidation of sulfides to sulfate and precipitation of barite nodules at a redox boundary in soils adjacent to the lake. Carbonate nodules precipitate above the barite-bearing horizon higher on the topography. Gypsum precipitated at the lake edge and in the lake sediments.

preservation (Jennings and others, 2006). Emergent shallow-water wetlands that developed in exposed offshore, calcareous mud nearer the lacustrine fringe (Pedotype G) were relatively more poorly drained as indicated by comparative higher reducible iron concentrations. Clay migrated into open pores and burrows lower in the soil profile during saturated conditions.

During lake expansion events, cemented oolitic-skeletal grainstones were reworked in shoreline sands (Fig. 2.15 B). A slow rise in water table resulted in Fe-Mn reduction lower in the soil profiles and mottling along macropores in wetland and upland soils. Iron was leached basinward from flooded nearshore sandy paleosols (Fig. 2.15 B). Widespread oolitic-skeletal grainstones indicate that the lake was large enough to generate ooid formation on a wave-dominated, bench platform. Large-scale foresets indicate that mobile oolitic sands formed large benches that prograded basinward. Shallow-water lake and wetland environments supported charophytes, detritus feeders, and insect larvae, resulting in burrowed, limey offshore mud (Jennings, 2004b, 2005).

As the lake basin gradually filled with sediments, succeeding lake deposits (Lake 3) became increasingly finer grained and associated poorly drained wetland paleosols (Pedotypes C, D, E, F, G) became more widespread (Fig. 2.16). The shallowing carbonate lake basin and low siliciclastic input led to carbonate precipitation directly from lake water in shallow-water settings, and gypsum precipitation at the lake edge. Barite nodules precipitated at a redox boundary in shallow-water lake sediments around decayed dinosaur carcasses (Jennings and Hasiotis, 2006b). During lake lowstand events, exposed fine-grained, lacustrine deposits were pedogenically modified (Pedotype C). Large mudcracks, gypsum pseudomorphs, and the

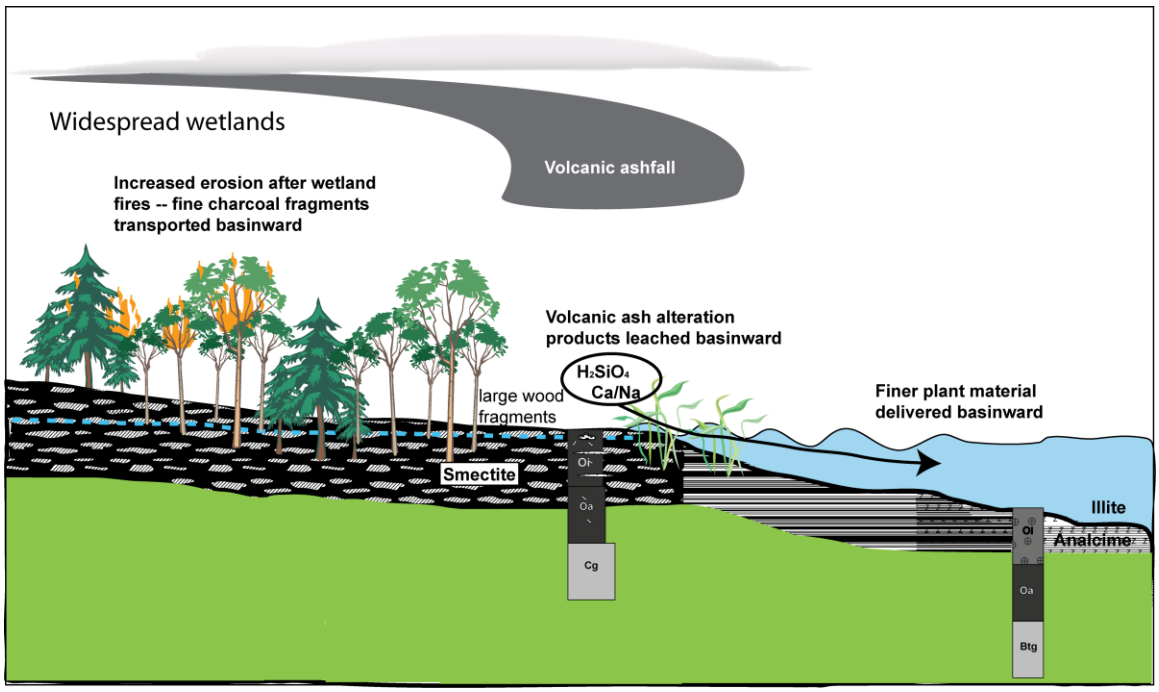

Figure 2.17. Facies model for subenvironments interpreted for widespread wetlands at the top of the Morrison in the study area. Volcaniclastic ash was the predominant sediment delivered to this wetland system. Groundwater was the primary source of water. High concentrations of ions and H_2SiO_4 sourcing from altering volcanic ash were transported basin ward. Coarser-grained, organic-rich deposits accumulated at the fen edge and illitic, analcime-rich sediments accumulated in the wetland basin. Larger woody fragments were preserved at the wetland fringe and finer plant material was transported to deeper water. Wetland fires resulted in increased erosion, incorporating charcoal fragments into sheet wash sands.

precipitation of barite nodules in paleosols adjacent to the lake indicate that evapotranspirative stress continued to be high and bacterial sulfate reduction in anoxic groundwater.

Shallow water wetlands (Pedotypes C, G) developed in areas closer to the lacustrine fringe. Wooded marshes (Pedotype D) were present in depressional areas between the shallow water wetlands and better-drained areas that typically were not submerged during lake expansion events. Groundwater carbonates likely precipitated 2-3 m below the surface. Macerated organic material was preserved in upper, more acidic parts of the profile. In this setting, dinosaur remains would have slowly sank into the

marsh deposits after brief subaerial exposure. Sulfur isotopes from barite nodules in these paleosols indicate that sulfate reduction occurred deep in the profile. However, the paucity of barite nodules suggests oxidizing conditions seldom occurred in more organic-rich soils. The chemistry of slow moving, standing marsh water changed as groundwater fluctuated from neutral to alkaline in response to short-lived lake expansion and contraction events. Rapid fluctuations in lake level, as evidenced by abrupt lithological changes in nearshore deposits, are typical of underfilled lakes and semi-arid to arid climate conditions (Bohacs and others, 2000).

Pedotypes that developed in topographically lower areas (Pedotypes F, G) have the highest reducible iron, manganese, and aluminum compared to pedotypes that developed higher on the landscape (Pedotype E). Modern barite-bearing soils tend to develop on stable, low gradient landscapes and are prone to episaturated and reducing conditions during wet seasons in areas with a seasonally dry climate (i.e., Stoops and Zavaleta, 1978; Darmoody and others, 1989). Saturated and reduced conditions, alternating with dry, oxidizing conditions result in fluctuations in soil chemistry, particularly pH conditions. During saturation Fe^{2+} was translocated down gradient where it was retained in less well-drained soils (Pedotype F).

An abrupt flooding event is represented by widespread fen deposits at the top of the Morrison throughout the study area. Outwash sands at the wetland fringe in the northwest grade laterally to organic-rich, laminated deposits basinward in the south and east. The presence of altered volcaniclastic sand lenses at the wetland fringe, extremely high concentrations of iron in the underclay, and illite and abundant analcime in basinal deposits suggest that drainage remained restricted. Ion- and silica-rich waters from the

alteration of volcanic air fall ash accumulated basinward (Fig. 2.17). Although the abrupt development of widespread wetlands at the top of the Morrison in the field area seems to indicate a change to a wetter climate, the restricted drainage that led to the accumulation of fen deposits suggests that semi-arid conditions may have continued throughout Morrison time.

Wetland fires in semi-arid environments resulted in erosional events, depositing sand lenses at the wetland fringe and transporting finer-grained, plant material basinward. It is likely that fluvial system recovery after major plinian eruptions in the latest Jurassic was similar to that documented in modern systems (Kuenzi and others, 1979).

Conclusions

Whereas lacustrine deposits may be subdivided based on water depth and relative position within the basin (shoreline to deep basin), wetland deposits are typically differentiated by inferred redox conditions related to hydrology and evidence of pedogenic modification. In modern wetland studies it is sometimes possible to document specific soil conditions such as saturation time, chemical conditions, and the types of vegetation that thrive in any given wetland. However, even in modern wetland systems it is necessary to rely on characteristic morphologies and chemical characteristics to demarcate wetland areas (Hurt and Carlisle, 2001). The key to delineating hydric paleosols is the synthesis of hydric soil indicators that are most readily preserved in the rock record, including redox sensitive elements (i.e., Fe^{2+}, Mn^{2+}, SO_4^{2-}, and P), redoximorphic features (i.e., matrix color, mottles, and authigenic minerals), micromorphological characteristics indicative of hydrologic conditions (Vepraskas, 2001), and lateral facies relationships (Richardson and Brinson, 2001).

Although three large-scale climate fluctuations that occurred in the northern Morrison basin were documented in this study, carbonate isotope data display a narrow range $\delta^{18}O$ values, suggesting that under-filled to balance-filled conditions occurred throughout the history of the lake. Lacustrine-wetland carbonate stable isotope values in this study are very similar to others documented in northern Wyoming (Fallin, 2005; Lovelace, 2006) and modern carbonates associated with closed lake basins such as the Great Salt Lake (Pedons, 2002).

Micromorphological and geochemical data from paleoHistosols at the top of the Morrison reveal that it is likely that widespread wetland development in the northern part of the Morrison depositional basin was not the result of major climate change. Rather, volcanic events in the source area likely had a significant impact on the type of sediments supplied to the system, recharge to the groundwater table, and subsequently the chemistry of the groundwater that fed the wetlands and lake (Gran and Montgomery, 2005).

Modern studies indicate that sedimentation rate increases exponentially within a volcanically influenced fluvial system (Smith, 1988; Major and others, 2000; Gran and Montgomery, 2005; Kataoka, 2005). Recovery of the system can be a long-lived process hampered by recurring volcanic events (Gran and Montgomery, 2005). Easily erodible and highly reactive sediments are directed from the de-vegetated source area and through the fluvial system, immediately pushing streams over their capacity. Avulsion rates increase as much as ten-fold as tributaries and main channels *proximal* to the volcanoes are inundated with sediments (Gran and Montgomery, 2005). Tributary streambeds near the source aggrade as much as 4 m/year and drainage is completely restricted within 3-4 years, resulting in flooded drainage areas up to 30 km or more from the source (Kuenzi

and others, 1979; Gran and Montgomery, 2005). Rapid aggradation of the alluvial plain results in a change in avulsion frequency and associated changes in pedogenic development (Gran and Montgomery, 2005). Fluvial and ecological recovery progresses from proximal to distal areas (Gran and Montgomery, 2005). Normal fluvial depositional processes dominate in areas more than 50 km from the volcanic vent (Gran and Montgomery, 2005). At this point on the alluvial plain, climate becomes the most dominant signature as the stream reaches the equilibrium point and the gradient of the alluvial plain decreases in response to extensive aggradation (Blum, 1992; Shanley and McCabe, 1994). It is likely that fluvial system recovery after major plinian eruptions in the latest Jurassic was similar to that documented in modern systems. Although few studies have documented fluvial recovery or alluvial plain development in areas more than 50 km from a volcanic source, it is reasonable to expect that extensive alkaline epiaquatic systems may have developed in distal areas without a significant climatic change because of increased influx of relatively impermeable fine-grained, altered ash and nutrient-rich groundwater (e.g., Kuenzi and others, 1979). It would also be expected that, in this region, coeval deposits would reflect increasing avulsion activity in the west. Deciphering the impact of volcaniclastic events, tectonic activity, and climate across the Morrison basin requires detailed facies analysis and precise mapping of stratal stacking patterns combined with detailed landscape reconstructions (Paz and Rossetti, 2005). Additional comparative studies are necessary to correlate the major climate fluctuations documented in this study with other deposits across the Morrison basin and use them to better define correlative deposits and subsequently evaluate coeval climate variations across the basin.

Only in the last 3 decades have scientists realized the value of wetland studies in Critical Zone research and their impact on our understanding of long-term global climate change and large-scale environmental perturbations. As archives of paleoenvironmental and paleoecological data, wetland paleosols offer an excellent source of information about the impact of climate change on wetlands, how they recover from major environmental disruptions, and how wetland biotas interact with those of surrounding environments. When combined with detailed paleopedological studies of laterally equivalent paleosols they offer the unique potential to document high-resolution paleoclimatic and paleoecological data across a wide area. Differentiating hydrogeomorphological subenvironments within paleowetland-lacustrine systems is vital to the study of ancient terrestrial landscapes and climate, which in turn increase our understanding of the repercussions of anthropogenic and climatic influences on modern wetlands.

REFERENCES

Alho, C.J.R., 2005, The Pantanal, *in* Fraser, L.H., and Keddy, P.A., eds., The World's Largest Wetlands: Ecology and Conservation: Cambridge, Cambridge University Press, p. 203-271.

Alonso-Zarza, A.M., 2003, Palaeoenvironmental significance of palustrine carbonates and calcretes in the geological record: Earth-Science Reviews, v. 60, p. 261-298.

Alonzo Zarza, A.M., Calvo, J.P., and Garcia del Cura, M.A., 1992, Palustrine sedimentation and associated features -- granification and pseudo-microkarst -- in the mIddle MIocene (Intermediate Unit) of the Madrid Basin, Spain: Sedimentary Geology, v. 76, p. 43-61.

Aoyagi, K., and Kazama, T., 1980, Transformational changes of clay minerals, zeolites, and silica during diagenesis: Sedimentology, v. 27, p. 179-188.

Ash, S.R., 1994, First occurrence of *Czekanowskia* (Gymnospermae, Czekanowskiales) in the United States: Review of Palaeobotany and Palynology, v. 81, p. 129-140.

Ashley, G.M., and Driese, S.G., 2000, Paleopedology and paleohydrology of a volcaniclastic paleosol interval: implications for early Pleistocene stratigraphy and paleoclimate record, Olduvai Gorge, Tanzania: Journal of Sedimentary Research, v. 7, no. 5, p. 1065-1080.

Atun, G., and Bascetin, E., 2003, Adsorption of barium on kaolinite, illite, and montmorillonite at various ionic strengths: Radichimica Acta, v. 91, p. 223-228.

Behrensmeyer, A.K., Gordon, K.D., and Yanagi, G.T., 1989, Nonhuman bone modification in Miocene fossils from Pakistan, *in* Bonnichesen, R., and Sorg, M.H., eds., Bone Modification: Orono, Maine, Center for the Study of the First Americans, p. 99-120.

Bjoerlykke, K.O., and Griffin, W.L., 1973, Barium feldspars in Ordovician sediments, Oslo Region, Norway: Journal of Sedimentary Petrology, v. 43, no. 2, p. 461-465.

Blum, M.D., 1992, Modern depositional environments and recent alluvial history of the lower Colorado River, Gulf coastal plain, Texas: Austin, University of Texas at Austin, Dissertation, 304 p.

Boggs, J., Sam, 1995, Principles of Sedimentology and Stratigraphy: Englewood Cliffs, NJ, Prentice Hall, 774 p.

Bohacs, K.M., Carroll, A.R., Neal, J.E., and Mankiewicz, P.J., 2000, Lake-basin type, source potential, and hydrocarbon character: an integrated sequence-stratigraphic-geochemical framework, *in* Gierlowski-Kordesch, E.H., and Kelts, K.R., eds., Lake Basins Through Space and Time: Tulsa, American Association of Petroleum Geologists, p. 3-34.

Boixadera, J., Poch, R.M., Garcia-Gonzalez, M.T., and Vizcayno, C., 2003, Hydromorphic and clay-related processes in soils from the Llanos de Moxos (northern Bolivia): Catena, v. 54, p. 403-424.

Bowen, G.J., and Bloch, J., I., 2002, Petrography and geochemistry of floodplain limestones from the Clarks Fork Basin, Wyoming, U.S.A.: carbonate deposition and fossil accumulation on a Paleocene-Eocene Floodplain: Journal of Sedimentary Research, v. 72, no. 1, p. 46-58.

Brantley, S.L., Goldhaber, M.B., and Ragnarsdottir, K.V., 2007, Crossing disciplines and scales to understand the Critical Zone: Elements, v. 3, p. 307-314.

Breheret, J.G., and Brumsack, H.J., 2000, Barite concretions as evidence of pauses in sedimentation in the Marnes Bleues Formation of the Vocontial Basin (SE France): Sedimentary Geology, v. 130, p. 205-228.

Brenner, R.L., and Peterson, J.A., 1994, Jurassic sedimentary history of the northern portion of the western interior seaway, USA, *in* Caputo, M.V., Peterson, J.A., and Franczyk, K.J., eds., Mesozoic systems of the Rocky Mountain region, p. 217-232.

Buatois, L.A., and Mangano, M.G., 1998, Trace fossil analysis of lacustrine facies and basins: Palaeogeography, Palaeoclimatology, Palaeoecology, v. 140, p. 367-382.

Calvo, J.P., Valleron, M.M., Rodriguez, J.P., Arandia, J.M., and Sanz, M.E., 1999, Authigenic clay minerals in continental evaporitic environments: Special Publications of the International Association of Sedimentologists, v. 27, p. 129-151.

Carroll, A.R., and Bohacs, K.M., 1999, Stratigraphic classification of ancient lakes: balancing tectonic and climatic controls: Geology, v. 27, no. 2, p. 99-102.

Carson, C.D., Fanning, D.S., and Dixon, C.J., 1982, Alfisols and Ultisols with acid sulfate weathering features in Texas, *in* Kittrick, J.A., ed., Acid Sulfate Weathering: Madison, WI, Soil Science Society of America, p. 127-146.

Carson, C.J., 1998, The structural and stratigraphic framework of the Warm Springs Ranch area, Hot Springs County, Wyoming, MS thesis: Oklahoma State University, 90 p.

Chamley, H., 1989, Clay Sedimentology: New York, Springer-Verlag, 623 p.

Christiansen, E.H., Kowallis, B.J., and Barton, M.D., 1994, Temporal and spatial distribution of volcanic ash in Mesozoic rocks of the Western Interior: an alternative record of Mesozoic magmatism, *in* Caputo, M.V., Peterson, J.A., and Franczyk, K.J., eds., Mesozoic Systems of the Rocky Mountain Region, USA: Denver, Rocky Mountain Section SEPM, p. 73-94.

Cohen, A.S., 2003, Paleolimnology: the history and evolution of lake systems: Oxford, Oxford University Press, Inc., 500 p.

Collins, M.E., and Kuehl, R.J., 2001, Organic matter accumulation and organic soils, *in* Richardson, J.L., and Vepraskas, M.J., eds., Wetland Soils: genesis, hydrology, landscapes, and classification: New York, Lewis Publishers, p. 137-162.

Collinson, J.D., 1996, Alluvial sediments, *in* Reading, H.G., ed., Sedimentary Environments: processess, facies, and stratigraphy: London, Blackwell Science, p. 37-82.

Craft, C.B., 2001, Biology of wetland soils, *in* Richardson, J.L., and Vepraskas, M.J., eds., Wetland Soils: genesis, hydrology, landscapes, and classification: New York, Lewis Publishers, p. 107-135.

Dalai, T.K., Krishnaswamie, S., and Sarin, M.M., 2002, Barium in the Uamuna River system in the Himalaya: sources, fluxes, and its behavior during weathering and transport: Geochemistry, Geophysics, Geosystems, v. 3, no. 12, p. 1-23.

Darmoody, R.G., Harding, S.D., and Hassett, J.J., 1989, Barite authigenesis in surficial soils of mid-continental United States, *in* Miles, ed., Rock-Water Interaction: Rotterdam, p. 183-186.

DeCelles, P.G., 2004, Late Jurassic to Eocene evolution of the Cordilleran thrust belt and Foreland basin system, western U.S.A.: American Journal of Science, v. 304, p. 105-168.

Demko, T.M., and Parrish, J.T., 1998, Paleoclimatic setting of the Upper Jurassic Morrison Formation: Modern Geology, v. 22, p. 283-296.

Douglass, D.N., 1984, Stratigraphy and paleomagnetics of the Morrison and Cloverly Formations, Big Horn Basin, Wyoming: Hanover, New Hamshire, MS thesis: Dartmouth College.

Drever, J.I., 1973, The preparation of oriented clay mineral specimens for X-ray diffraction analysis by a filter-membrane peel technique: American Mineralogist, v. 58, p. 553-554.

Drits, V.A., Sakharov, B.A., Lindgreen, H., and Salyn, A., 1997, Sequential structure transformation of illite-smectite-vermiculite during digenesis of Upper Jurassic shales from the North Sea and Denmark: Clay Mineralogy, v. 32, p. 351-371.

Dunagan, S.P., 2000, Lacustrine carbonates of the Morrison Formation (Upper Jurassic, Western Interior), East-central Colorado, U.S.A., *in* Gierlowski-Kordesch, E.H., and Kelts, K.R., eds., Lake Basins Through Space and Time: AAPG Studies in Geology, p. 181-188.

Dunagan, S.P., and Turner, C.E., 2004, Regional paleohydrologic and paleoclimatic setting of wetland/lacustrine depositional systems in the Morrison Formation (Upper Jurassic), Western Interior, USA: Sedimentary Geology, v. 167, p. 269-296.

Eardley, A.J., and Gvosdetsky, V., 1960, Analysis of Peistocene core from Great Salt Lake, Utah: Geological Society of America Bulletin, v. 71, p. 1323-1344.

Eardley, A.J., Gvosdetsky, V., and Marsell, R.E., 1957, Hydrology of Lake Bonneville and sediments and soils of its basin: Geological Society of America Bulletin, v. 68, p. 1141-1201.

Fallin, M.J., 2005, Carbon Isotope Stratigraphy of the Morrison and Cloverly Formations and Assessment of Vertical Color Change in the Morrison Formation, Coyote Basin, Wyoming: Boulder, University of Colorado, M.S. Thesis, 129 p.

Freytet, P., and Verrecchia, E.P., 2002, Lacustrine and palustrine carbonate petrography: an overview: Journal of Paleolimnology, v. 27, no. 221-237.

Goldstein, R.H., and Reynolds, T.J., 1994, Systematics of Fluid Inclusions in Diagenetic Minerals, SEPM Special publication, v. 31, 199 p.

Gonzalez-Munoz, M.T., Fernandez-Luque, B., Martinez-Ruiz, F., Chekroun, K.B., Arias, J.M., Rodriguez-Gallego, M., Martinez-Canamero, M., de Linares, C., and Paytan, A., 2003, Precipitation of barite by *Mycoccus xanthus*: possible implications for the biogeochemical cycle of barium: Applied and Environmental Microbiology, v. September, p. 5722-5725.

Gottardi, G., and Galli, E., 1985, Natural Zeolites: New York, Springer-Verlag, 409 p.

Gran, K.B., and Montgomery, D.R., 2005, Spatial and temporal patterns in fluvial recovery following volcanic eruptions: channel response to basin-wide sediment loading at Mount Pinatubo, Phillipines: Geological Society of America Bulletin, v. 117, no. 1-2, p. 195-211.

Greb, S.F., DiMichele, W.A., and Gastaldo, R.A., 2006, Evolution and importance of wetlands in earth history, *in* Greb, S.F., and DiMichele, W.A., eds., Wetlands Through Time: Boulder, Geological Society of America p. 1-40.

Hanor, J.S., 2000, Barite-celestine geochemistry and environments of formation, *in* Alpers, C.N., Jambor, J.L., and Nordstrom, D.K., eds., Sulfate Minerals: crystallography, geochemistry, and environmental significance: Washington D.C., Mineralogical Society of America, p. 193-275.

Hasiotis, S.T., 2004, Reconnaissance of Upper Jurassic Morrison Formation ichnofossils, Rocky Mountain Region, USA: paleoenvironmental, stratigraphic, and paleoclimatic significance of terrestrial and freshwater ichnocoenoses: Sedimentary Geology, v. 167, p. 177-268.

Hay, R.L., 1970, Silicate reactions in three lithofacies of a semi-arid basin, Olduvai Gorge, Tanzania: Mineralogical Society of America Special Paper, v. 3, p. 237-255.

Hay, R.L., and Kyser, T.K., 2001, Chemical sedimentology and paleoenvironmental history of Lake Olduvai, a Pliocene lake in northern Tanzania: Geological Society of America Bulletin, v. 113, no. 12, p. 1505-1521.

Hillier, S., 1995, Erosion, sedimentation and sedimentary origin of clays, *in* Velde, B., ed., Origin and Mineralogy of Clays: New York, Springer-Verlag, p. 162-219.

Hurt, G.W., and Carlisle, V.W., 2001, Delineating hydric soils, *in* Richardson, J.L., and Vepraskas, M.J., eds., Wetland Soils: genesis, hydrology, landscapes, and classification: New York, Lewis Publishers, p. 183-206.

Ikejiri, T., Watkins, P., and Gray, D., 2006, Stratigraphy, sedimentology, and taphonomy of a sauropod quarry from the Upper Morrison Formation of Thermopolis, central Wyoming: Bulletin - New Mexico Museum of Natural History and Science, v. 36, p. 39-46.

Irving, W.N., Jopling, A.V., and Kritsch-Armstrong, I., 1989, Studies of bone technology and taphonomy, Old Crow Basin, Yukon Territory, *in* Bonnichesen, R., and Sorg, M.H., eds., Bone Modification: Orono, Maine, Center for the Study of the First Americans, p. 347-380.

Jackson, M.L., Lim, C.H., and Zelazny, W., 1986, Oxides, hydroxides, and aluminosilicates, *in* Klute, A., ed., Methods of Soil Analysis, Part 1 -- Agronomy Monograph 9: Madison, Wisconsin, American Society of Agronomy, Inc., p. 101-142.

Jennings, D.S., 2004a, Identification of dinosaur tracks in palustrine-lacustrine deposits of the Morrison Formation; their significance to lacustrine sequence stratigraphy, Annual Meeting Expanded Abstracts - American Association of Petroleum Geologists: United States, American Association of Petroleum Geologists and Society for Sedimentary Geology : Tulsa, OK, United States, v. 13, p. 71.

Jennings, D.S., 2004b, A survey and assessment of lacustrine authigenic minerals from the Morrison Formation, Big Horn Basin, Wyoming, Abstracts with Programs - Geological Society of America: United States, Geological Society of America (GSA) : Boulder, CO, United States, v. 36, p. 472.

Jennings, D.S., 2005, A Paleoenvironmental Analysis of Morrison Formation Deposits, Big Horn Basin, Wyoming: a multivariate approach: Lawrence, University of Kansas, M.S., 110 p.

Jennings, D.S., and Hasiotis, S.T., 2006a, Paleoenvironmental and stratigraphic implications of authigenic clay distributions in Morrison Formation deposits, Bighorn Basin, Wyoming: New Mexico Museum of Natural History Bulletin, v. 36, p. 25-34.

Jennings, D.S., and Hasiotis, S.T., 2006b, Taphonomic Analysis of a Dinosaur Feeding Site Using Geographic Information Systems (GIS), Morrison Formation, Southern Bighorn Basin, Wyoming, USA: Palaios, v. 21, p. In Press.

Jennings, D.S., Platt, B.F., and Hasiotis, S.T., 2006, Distribution of vertebrate trace fossils, Upper Jurassic Morrison Formation, Bighorn Basin, Wyoming, USA: Implications for differentiating paleoecological and preservational bias: New Mexico Museum of Natural History Bulletin, v. 36, p. 183-192.

Johnson, J.S., 1991, Stratigraphy, sedimentology, and depositional environments of the Upper Jurassic Morrison Formation, Colorado front range: Lincoln, Nebraska, Dissertation: University of Nebraska.

Kataoka, K., 2005, Distal fluvial-lacustrine volcaniclastic resedimentation in response to an explosive silicic eruption: the Pliocene Mushono tephra bed, central Japan: Geological Society of America Bulletin, v. 117, no. 1-2, p. 3-17.

Kelts, K., and Hsu, K.J., 1978, Freshwater carbonate sedimentation, *in* Lerman, A., ed., Lakes: Chemistry, geology, physics: New York, Springer-Verlag, p. 363.

Kirkland, J.I., 2006, Fruita paleontological area (Upper Jurassic, Morrison Formation), western Colorado; an example of terrestrial taphofacies analysis: Bulletin - New Mexico Museum of Natural History and Science, v. 36, p. 67-95.

Kraus, M.J., 1997, Lower Eocene alluvial paleosols: pedogenic development, stratigraphic relationships, and paleosol/landscape associations: Palaeogeography, Palaeoclimatology, Palaeoecology, v. 129, p. 387-406.

Kraus, M.J., 1999a, Paleosols in clastic sedimentary rocks: their geologica applications: Earth-Science Reviews, v. 47, p. 41-70.

Kraus, M.J., 1999b, Paleosols in clastic sedimentary rocks: their geological applications: Earth-Science Reviews, v. 47, p. 41-70.

Kraus, M.J., and Gwinn, B., 1997, Facies and facies architecture of Paleogene floodplain deposits, Willwood Formation, Bighorn Basin, Wyoming, USA: Sedimentary Geology, no. 114, p. 33-54.

Kuenzi, W.D., Horst, O.H., and McGehee, R.V., 1979, Effect of volcanic activity on fluvial-deltaic sedimentation in a modern arc-trench gap, southwestern Guatemala: Geological Society of America Bulletin, v. 90, no. Part 1, p. 827-838.

Lawton, T.F., 1994, Tectonic setting of Mesozoic sedimentary basins, Rocky Mountain region, United States, *in* Caputo, M.V., Peterson, J.A., and Franczyk, K.J., eds., Mesozoic Systems of the Rocky Mountain Region, USA: Rocky Mountain Section, Society of Economic Paleontolgists and Mineralogists, Special Publication, p. 1-25.

Liuqi, W., Zaixing, J., Yingchang, C., Wentao, H., and Jing, W., 1997, Lake sequence stratigraphy of the Shahejie Formation in the Zhanhua Hollow, Shandong Province: Acta Geologica Sinica, v. 71, no. 1, p. 104-114.

Liutkus, C.M., Wright, J.D., Ashley, G.M., and Sikes, N.E., 2005, Paleoenvironmental interpretation of lake-margin deposits using d13C and d18O results from early Pleistocene carbonate rhizoliths, Olduvai Gorge, Tanzania: Geology, v. 33, no. 5, p. 377-380.

Lockley, M., 1986, The paleobiological and paleoenvironmental importance of dinosaur footprints: Palaios, v. 1, p. 37-47.

Lockley, M.G., Houck, K.J., and Prince, N.K., 1986, North America's largest dinosaur trackway site: implications for Morrison Formation paleoecology: Geological Society of America Bulletin, v. 97, no. 10, p. 1163-1176.

Lovelace, D., 2006, An Upper Jurassic Morrison Formation fire-induced debris flow: taphonomy and paleoenvironment of a sauropod (Sauropoda: *Supersaurus vivianae*) locality, East-Central Wyoming: New Mexico Museum of Natural History Bulletin, v. 36, p. 47-56.

Lucas, S.G., and Kirkland, J.I., 1998, Preliminary report on conchostraca from the Upper Jurassic Morrison Formation, western United States: Modern Geology, v. 22, p. 415-422.

Luo, Z., and Wible, J.R., 2005, A Late Jurassic digging mammal and early mammalian diversification: Science, v. 308, p. 103-107.

Major, J.J., Pierson, T.C., and Costa, J.E., 2000, Sediment yield following severe volcanic disturbance--a two-decade perspective from Mount St. Helens: Geology, v. 28, no. 9, p. 819-822.

Mausbach, M.J., and Parker, W.B., 2001, Background and history of the concept of hydric soils, *in* Richardson, J.L., and Vepraskas, M.J., eds., Wetland Soils: genesis, hydrology, landscapes, and classification: New York, Lewis Publishers, p. 19-33.

Meunier, A., and Velde, B., 2004, Illite: origins, evolution, and metamorphism: New York, Springer-Verlag, 286 p.

Meyers, P.A., and Ishiwatari, R., 1993, Lacustrine organic geochemistry -- an overview of indicators of organic matter sources and diagenesis in lake sediments: Organic Geochemistry, v. 20, no. 7, p. 867-900.

Milroy, P.G., and Wright, V.P., 2000, A highstand oolitic sequence and associated facies from a Late Triassic lake basin, south-west England: Sedimentology, v. 47, p. 187-209.

Ming, D.W., and Dixon, J.B., 1988, Occurrence and weathering of zeolites in soil environments., *in* Kiado, A., ed., Occurrences, Properties, and Utilization of Natural Zeolites: Budapest, Hungary, p. 699-715.

Moore, D.M., and Reynolds, R.C., 1997, X-ray Diffraction and the Identification and Analysis of Clay Minerals: New York, Oxford University Press, 378 p.

NRCS, 2010, NRCS Soils Website, http://soils.usda.gov/.

Owen, D.E., Turner-Peterson, C.E., and Fishman, N.S., 1989, X-ray Diffraction Studies of the <0.5-um Fraction from the Brushy Basin Member of the Upper Jurassic Morrison Formation, Colorado Plateau, *in* Interior, D.o.t., U.S. Geological Survey, v. 1808-G, p. G1-G25.

Parrish, J.T., Peterson, F., and Turner, C.E., 2004, Jurassic "savannah"--plant taphonomy and climate of the Morrison Formation (Upper Jurassic, Western USA): Sedimentary Geology, v. 167, p. 137-162.

Paz, J.D.S., and Rossetti, D.F., 2005, Linking lacustrine cycles with syn-sedimentary tectonic episodes: an example from the Codo Formation (late Aptian), northeastern Brazil: Geology Magazine, v. 142, no. 3, p. 269-285.

Pedons, V.A., 2002, Oxygen-isotope composition of Great Salt Lake, 1979 to 1996, *in* Richmond, M.W., Great Salt Lake: an overview of change: Salt Lake City, Special Publication - Utah Department of Natural Resources, p. 121-126.

Peterson, F., 1988, Pennsylvanian to Jurassic eolian transportation systems in the western United States: Sedimentary Geology, v. 56, p. 207-260.

Peterson, F., 1994, Sand dunes, sabkhas, streams, and shallow seas: Jurassic paleogeography in the southern part of the Western Interior basin, *in* Caputo, M.V., Peterson, J.A., and Franczyk, K.J., eds., Mesozoic systems of the Rocky Mountain region, USA, p. 233-272.

Pipujol, M.D., and Buurman, P., 1994, The distinction between ground-water gley and surface-water gley phenomena in Tertiary paleosols of Ebro basin, NE Spain: Palaeogeography, Palaeoclimatology, Palaeoecology, v. 110, p. 103-113.

Platt, S.G., Rainwater, T.R., and Brewer, S.W., 2004, Aspects of the burrowing ecology of nine-banded armadillos in northern Belize: Mammalian Biology, v. 69, no. 4, p. 217-224.

Renaut, R.W., 1993, Zeolitic diagenesis of late Quaternary fluvio-lacustrine sediments and associated calcrete formation in the Lake Borgoria Basin, Kenya Rift Valley: Sedimentology, v. 40, p. 271-301.

Richardson, J.L., Arndt, J.L., and Montgomery, J.A., 2001, Hydrology of wetland and related soils, *in* Richardson, J.L., and Vepraskas, M.J., eds., Wetland Soils: genesis, hydrology, landscapes and classification: New York, Lewis Publishers, p. 35-84.

Richardson, J.L., and Brinson, M.M., 2001, Wetland soils and hydrogeomorphic classification of wetlands, *in* Richardson, J.L., and Vepraskas, M.J., eds., Wetland Soils: genesis, hydrology, landscapes, and classification: New York, Lewis Publishers, p. 209-227.

Santos, E.S., and Peterson, C.E., 1986, Tectonic setting of the San Juan Basin in the Jurassic, *in* Turner-Peterson, C.E., Santos, E.S., and Fishman, N.S., eds., A Basin Analysis Case Study: the Morrison Formation, Grants Uranium Region, New Mexico: American Association of Petroleum Geologists p. 27-33.

Scheiber, J., 2003, Simple gifts and buried treasures -- implications of finding bioturbation and erosion surfaces in black shales: The Sedimentary Record, v. 1, no. 2, p. 4-8.

Schnurrenberger, D., Russell, J., and Kelts, K., 2003, Classification of lacustrine sediments based on sedimentary components: Journal of Paleolimnology, v. 29, p. 141-154.

Schudack, M.E., Turner, C.E., and Peterson, F., 1998, Biostratigraphy, paleoecology, and biogeography of charophytes and ostracodes from the Upper Jurassic Morrison Formation, Western Interior, USA: Modern Geology, v. 22, p. 379-414.

Scott, A.C., 2000, The Pre-Quaternary history of fire: Palaeogeography, Palaeoclimatology, Palaeoecology, v. 164, p. 281-329.

Seal, I., Robert R., Alpers, C.N., and Rye, R.O., 2000, Stable isotope systematics of sulfate minerals, *in* Alpers, C.N., Jambor, J.L., and Nordstrom, D.K., eds., Sulfate minerals: crystallography, geochemistry, and environmental significance: Washington D.C., Mineralogical Society of America, p. 541-602.

Shanley, K.W., and McCabe, P.J., 1994, Perspectives on the sequence stratigraphy of continental strata: AAPG Bulletin, v. 78, no. 4, p. 544-568.

Smith, E., Hamilton-Taylor, J., Davison, W., Fullwood, N.J., and McGrath, M., 2004, The effect of humic substances on barite precipitation -- dissolution behaviour in natural and synthetic lake waters: Chemical Geology, v. 207, p. 81-89.

Smith, G.A., 1988, Sedimentology of proximal to distal volcaniclastics dispersed across an active foldbelt: Ellensburg Formation (late Miocene), central Washington: Sedimentology, v. 35, p. 953-977.

Soils, N.T.C.H., 1987, Hydric Soils of the United States: Washington, DC, USDA Soil Conservation Service.

Stoops, G., and Poch, R.M., 1994, Micromorphological classification of gypsiferous soil materials, in IX International Working Meeting on Soil Micromorphology, Townsville, Australia, Developments in Soil Science, Elsevier, p. 327-332.

Stoops, G., and Zavaleta, A., 1978, Micromorphological evidence of barite neoformation in soils: Geoderma, v. 20, no. 1, p. 63-70.

Sullivan, L.A., and Koppi, A.J., 1995, Micromorphology of authigenic celestobarite in a duripan from central Australia: Geoderma, v. 64, no. 3-4, p. 357-361.

Surdam, R.C., and Eugster, H.P., 1976, Mineral reactions in the sedimentary deposits of the Lake Magadi region, Kenya: Geological Society of America Bulletin, v. 87, p. 1739-1752.

Suttner, L.J., 1969, Stratigraphic and petrographic analysis of Upper Jurassic-Lower Cretaceous Morrison and Kootenai formations, southwest Montana: American Association of Petroleum Geologists Bulletin, v. 53, no. 7, p. 1391-1410.

Swirydczuk, K., and Wilkinson, B.H., 1979, The Pliocene Glenns Ferry oolite: lake-margin carbonate deposition in the southwestern Snake River Plain: Journal of Sedimentary Petrology, v. 49, no. 3, p. 995-1004.

Takehito, I., Watkins, P., and Gray, D., 2006, Stratigraphy, sedimentology, and taphonomy of a sauropod quarry from the Upper Morrison Formation of Thermopolis, Central Wyoming: New Mexico Museum of Natural History and Science Bulletin, v. 36, p. 39-46.

Tanner, W.F., 1968, Shallow lake deposits, lower part of Morrison Formation (late Jurassic), northern New Mexico: The Mountain Geologist, v. 5, no. 4, p. 187-195.

Taylor, M.W., and Surdam, R.C., 1981, Zeolite reactions in the tuffaceous sediments at Teels Marsh, Nevada: Clays and Clay Minerals, v. 25, no. 5, p. 341-352.

Tidwell, W.D., 1990, Preliminary report on the megafossil flora of the Upper Jurassic Morrison Formation: Hunteria, v. 2, no. 8, p. 12.

Tiercelin, J., Vincens, A., Barton, C.E., Carbonel, P., Casanova, J., Delibrias, G., Gasse, F., Grosdidier, E., Herbin, J., Huc, A.Y., Jardine, S., Le Fournier, J., Palacios, C., Paquet, H., Peniguel, G., Peypouquet, J., Raynaud, J., Renaut, R.W., de Reneville, P., Richert, J., Riff, R., Robert, P., Seyve, C., Vandenbroucke, M., and Vidal, G., 1987, Le demi-graben de Baringo-Bogoria Rift Gregory, Kenya. 30 000 ans d'histoire hydrologique et seddimentaire (The Baringo-Borgoria Half-graben, Gregory Rift, Kenya, 30,000 years of Hydrological and Sedimentaty History), Societe National Elf Aquitaine (Production), 540 p.

Tiner, R.W., 1999, Wetland Indicators: A Guide to Wetland Identification, Delineation, Classification, and Mapping: New York, Lewis Publishers.

Tiner, R.W., 2003, Geographically isolated wetlands of the United States: Wetlands, v. 23, no. 3, p. 494-516.

Trujillo, K.C., 2003, Stratigraphy and Correlation of the Morrison Formation (Late Jurassic-?Early Cretaceous) Across the Western Interior, U.S.A., with special emphasis on southeastern Wyoming: Laramie, University of Wyoming, Dissertation, 192 p.

Turner, C.E., and Fishman, N.S., 1991, Jurassic Lake T'oo'dichi': a large alkaline, saline lake, Morrison Formation, eastern Colorado Plateau: Geological Society of America Bulletin, v. 103, p. 538-558.

Turner, C.E., and Fishman, N.S., 1998, Late Jurassic Lacustrine Deposits and Implications for Paleohydrology: Deposition to Early Compaction, *in* Pitman, J.K., and Carroll, A.R., eds., Modern and Ancient Lake Systems: Utah Geological Association, p. 31-49.

Turner, C.E., and Peterson, F., 2004, Reconstruction of the Upper Jurassic Morrison Formation extinct ecosystem -- a synthesis: Sedimentary Geology, v. 167, p. 309-355.

Vepraskas, M.J., 2001, Morphological features of seasonally reduced soils, *in* Richardson, J.L., and Vepraskas, M.J., eds., Wetland Soils: genesis, hydrology, landscapes, and classification: New York, Lewis Publishers, p. 163-182.

Vepraskas, M.J., and Faulkner, S.P., 2001, Redox chemistry of hydric soils, *in* Richardson, J.L., and Vepraskas, M.J., eds., Wetland Soils: genesis, hydrology, landscapes, and classification: New York, Lewis Publishers, p. 85-105.

Vepraskas, M.J., Wilding, L.P., and Drees, L.R., 1992, Aquic conditions for Soil Taxonomy: concepts, soil morphology and micromorphology, in IX International Working Meeting on Soil Micromorphology, Townsville, Australia, Elsevier, p. 117-131.

Walker, R.G., and Cant, D.J., 19984, Sandy fluvial systems, *in* Walker, R.G., ed., Facies Models: (2nd ed.) Newfoundland, Canada, Geological Association of Canada, p. 71-89.

Warner, B.G., and Rubec, C.D.A., eds., 1997, The Canadian Wetland Classification System (2nd ed.): Waterloo, Ontario, National Wetlands Working Group, 7 p.

Wood, J.R., Worthy, T.H., Rawlence, N.J., Holdaway, R.N., and Reed, S.E., 2008, A deposition mechanism for Holocene miring bone deposits, South Island, New Zealand: Journal of Taphonomy, v. 6, no. 1, p. 1-20.

Wright, V.P., Marriott, S.B., and Vanstone, S.D., 1991, A 'reg' palaeosol from the Lower Triassic of south Devon: stratigraphic and palaeoclimatic implications: Geological Magazine, v. 128, no. 3, p. 517-523.

CHAPTER THREE

Understanding Barite and Gypsum Precipitation in Upland Acid-sulfate Soils: An example from a Lufkin Series toposequence, south-central Texas, USA

This chapter published as: Jennings, D.S., and Driese, S.G., 2014, Understanding barite and gypsum precipitation in upland acid-sulfate soils: An example from a Lufkin Series toposequence, south-central Texas, USA: Sedimentary Geology, v. 299, p. 106-118.

Abstract

Although low-temperature barite precipitation has been previously documented in soils and paleosols, pedogenic barite precipitation remains poorly understood. This study characterizes the micromorphology, elemental trends, and stable isotope geochemistry of sulfates in a barite-bearing soil (Lufkin Series) toposequence using optical microscopy, XRD, ICP-MS, and stable S and O isotope data. Synthesized data indicate that fluctuating redox processes and microbial activity resulting from epiaquatic and evaporative conditions lead to the precipitation of sulfates in the Lufkin soils. Stable sulfur and oxygen isotopes indicate that the primary source of sulfur is the partial dissolution of jarosite during microbial sulfate reduction. Barium-rich parent material provides adequate barium for barite precipitation. Barium is mobilized and concentrated in Btg horizons ~100-160 cm below the surface. The presence of humic acids in profiles lower on the landscape prevents barite precipitation and drives the precipitation of gypsum between saturated, anoxic conditions (November to May) and drier, more oxic conditions (May to November). Barite precipitation is a slow, punctuated process. Micromorphological data reveal that barite precipitates first along evacuated macropores and then in the adjacent

matrix. In general, optimal conditions for pedogenic barite precipitation in upland wetland acid-sulfate soils are: 1) warm soil temperature that supports active sulfur-reducing and sulfur oxidizing microbes; 2) distinct wet/dry seasons that allow alternating redox conditions; 3) low-gradient landscape; 4) parent material that contains barium- and sulfur-rich constituents; and 5) a long-lived, stable landscape.

Introduction

Modern pedogenic barite has been reported from soils in Australia (Beattie and Haldane, 1984), Peru (Stoops and Zavaleta, 1978), New Caledonia (Podwojewski, 1995), and several soils in the US (Lynn and others, 1971; Carson and others, 1982; Darmoody and others, 1989; NRCS, 2010). Early authigenic barite has also been documented in several paleosols (i.e., Sullivan and Koppi, 1993; Triplehorn and others, 2001; McCarthy and Plint, 2003; Kirkland, 2006; Retallack and Kirby, 2007; White and Schiebout, 2008; Buck and others, 2010; Jennings and others, 2011). Although barite precipitation is well-studied in modern marine sediments (Hanor, 2000; Seal and others, 2000) and lacustrine settings (Felmlee and Cadigan, 1978; Hocking and Pirajno, 2000; Hocking, 2001; Smith and others, 2004a; Jennings and others, 2011), the pedogenic processes leading to barite precipitation in soils are poorly understood (Stoops and Zavaleta, 1978; Carson and others, 1982; Darmoody and others, 1989; Hanor, 2000). Several hypotheses have been proposed to explain pedogenic barite precipitation (i.e., Childs and others, 1975; Stoops and Zavaleta, 1978; Carson and others, 1982; Beattie and Haldane, 1984; Sullivan and Koppi, 1995; Triplehorn and others, 2001; Buck and Van Hoesen, 2002; Brock and Buck, 2009), which include precipitation during active sulfurization of exposed wetland soils and biomineralization by bacteria and in the rhizosphere. Although few subsequent

detailed studies have been conducted on modern, barite-bearing soils to test these hypotheses, barite-bearing paleosols have been applied to answer complex geologic questions such as the development of sequence stratigraphic models (McCarthy and Plint, 2003), paleoenvironmental reconstructions (Kirkland, 2006; Jennings and others, 2011), and paleoclimate studies (Retallack and Kirby, 2007). The key to accurately interpreting pedogenic processes and landscape relationships of ancient, barite-bearing paleosols is an understanding of the genesis of modern barite-bearing soils, the resulting distribution of sulfate minerals in associated soil profiles, and their link to the surrounding landscape. The purpose of this study is to: 1) determine how acid-sulfate soil physical and chemical characteristics vary along a modern toposequence, and (2) integrate data from this study with previously published data to interpret the important pedogenic processes that control barite precipitation, based on a previously reported example from the Lufkin Series in south-central Texas, USA.

Previous Work

Barite-bearing soils commonly are mature soils (typically U.S. Department of Agriculture Natural Resources Conservation Service (USDA-NRCS) Alfisols or Ultisols) with high background levels of barium that exhibit slow permeability and imperfect drainage, hydromorphic characteristics such as mottling and iron oxyhydroxide nodules, relatively low pH, and high base saturation (Lynn and others, 1971; Stoops and Zavaleta, 1978; Carson and others, 1982; Darmoody and others, 1989). Barite in upland acid-sulfate soils contains little strontium (Stoops and Zavaleta, 1978) and occurs in subsurface horizons (usually Bt horizons) ≥100cm below the surface. Soil barite is typically present as loose clusters of fine, microscopic, prismatic crystals (microlites) in

root channels and macropores, and as soft, white powdery masses in the matrix (Stoops and Zavaleta, 1978; Carson and others, 1982; Darmoody and others, 1989). Masses commonly display associated clay skins or clay coatings, indicating that they formed during pedogenesis and were not inherited from the parent material (Lynn and others, 1971; Darmoody and others, 1989; Brock-Hon and others, 2012). Barite, gypsum, and jarosite are commonly documented in close proximity to each other, but are not always present in individual profiles across the landscape (Carson and others, 1982). The micromorphology of barite-bearing soils suggests that alternating reducing and oxidizing conditions occur at depth within the soil profile, and some authors have suggested that these fluctuations in redox conditions, combined with the introduction of saline groundwater resulting from fluctuating groundwater levels, may together contribute to barite precipitation (Stoops and Zavaleta, 1978; Carson and others, 1982) Translocated clay covering barite crystals supports polygenetic pedogenic processes (Darmoody and others, 1989).

Darmoody et al., (1989) suggested that barium is the limiting species in pedogenic barite precipitation. The problem with this hypothesis is that barium is generally considered an immobile, large lithophile element because it is easily precipitated as sulfates and carbonates, is strongly adsorbed by clays, is concentrated in Mn and P concretions, and is sorbed onto oxides and hydroxides, particularly in temperate humid climate zones (Kabata-Pendias, 2001). However, barium may be released from clays and feldspars under reducing conditions (Zang and others, 2001; Atun and Bascetin, 2003). Because the process by which free barium (Ba^{2+}) becomes available in the lower parts of a soil profile for barite precipitation is not completely understood (Darmoody and others,

1989), the distribution of elements (particularly reducible elements) and minerals in the Lufkin soil may provide evidence of the source of barium and redox processes that occur in the soil profile. Variations in elemental trends and authigenic minerals along a toposequence may also supply critical information related to pedogenic thresholds in soil profiles across the landscape (Chadwick and Chorover, 2001).

As a result of previous studies, Carson et al., (1982) hypothesized that stable sulfates in the Lufkin soil precipitated during the post sulfurization stage of a coastal wetland soil and that the source of sulfate is the oxidation of marine pyrite. However, no data were offered that definitively supports this hypothesis. Due to its high ionic potential Ba^{2+} is easily accommodated in aqueous solutions as a hydrated divalent cation. Sulfate is also incorporated into solution readily as a hydrated anion. When barium-rich and sulfate-rich solutions come into contact, reactions between Ba^{2+} and SO_4^{2-} precipitate highly stable solids resistant to diagenesis and dissolution (Hanor, 2000). Barite melts at 1580ºC and its solubility is very low up to 300°C, increasing slightly with burial depth in saline solutions (Blount, 1977). Consequently, it is stable over the entire pressure/temperature range of the earth's crust. In general, equilibrium prevails at low pH and high temperatures whereas kinetic factors dominate at low temperatures, even at low pH. Because the kinetics of oxygen and sulfur are so slow (exchange rates with water are billions of years, below 100ºC), stable isotopic compositions of barite record the sources and processes that initially produced sulfate because ratios tend not to re-equilibrate during fluid transport and mineral precipitation (Seal and others, 2000). Subsequently, $\delta^{18}O$ and $\delta^{34}S$ values fingerprint the sources of oxygen and sulfur and help identify physical and chemical processes of sulfate formation, which in turn are useful in

discerning pedogenic factors such as climate, sedimentary processes, geomicrobiology, and hydrologic conditions. In ancient deposits, $\delta^{18}O$ and $\delta^{34}S$ values of early diagenetic barite nodules have been used to discern authigenic from epigenic barite nodules and understand the original processes and environmental conditions of formation (see Hanor, 2000 ; Seal and others, 2000). It follows that stable isotopic signatures of soil sulfates are invaluable data necessary for understanding the source of sulfate in barite-bearing soils and their ancient analogues.

Materials and Methods

Site Description

Two long cores (5.1 cm diameter and ~3 m long) were collected using a truck-mounted Giddings probe along a toposequence in south-central Texas, immediately adjacent to previously documented profiles (Carson and others, 1982), just southeast of Easterwood Airport near the Texas A&M campus in College Station (Fig. 3.1, A). The study area is predominantly pristine and undisturbed (Joe Dixon, personal communication). The Lufkin Series in south-central Texas is classified as a fine, smectitic, thermic, vertic, Albaqualf according to USDA Soil Taxonomy (Chervenka, 2002; NRCS, 2010), and interpreted as an upland acid sulfate soil that developed in terrestrial, coastal plain deposits of the Eocene Yegua Formation (Routh and others, 1999). An ash bed that was deposited in a coastal wetland and predominantly composed of kaolinite and smectite occurs ~ 2-3 m below the modern soil profile (Senkayi and others, 1984). The two Lufkin soil pedons occupy erosional uplands that have a 1-4% slope. Vegetation in wooded portions of the study area is dominated by scrub post oak and live oak. The climate in this area is moist subhumid with a mean annual precipitation

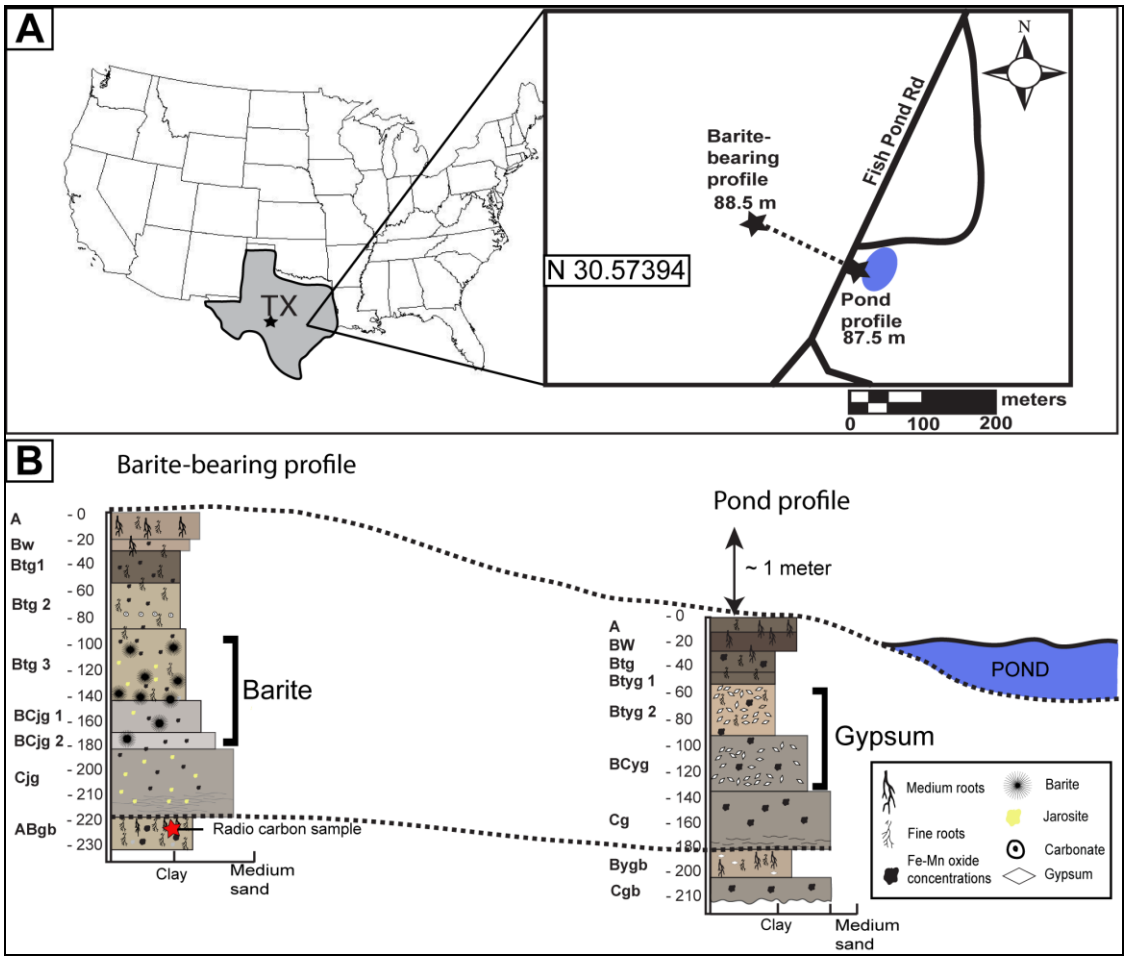

Figure 3.1 Study Area and representative soil profiles. A) Study area map and relative topographic position of the barite-bearing profile and the barite-poor profile (PP). B) Cross-section of the toposequence and soil profiles. Dashed lines delineate the top and base of the profiles.

(MAP) of 1008 mm and a mean annual temperature (MAT) of 20° C (NCDC, 2012). A temporary perched water table occurs above clay-rich Btg horizons during rainy periods (NRCS, 2010). Surface horizons may remain saturated for weeks at a time from November to May (NRCS, 2010). Dry conditions dominate from May to November. Surface runoff is slow to very slow. Although soil profiles in nearby areas display gilgai relief with microhighs and microlows 1.8 to 4.5 meters in diameter, indicating high shrink-swell (i.e., vertic) properties, no slickensides are observed (Routh and others,

1999; NRCS, 2010). The A and uppermost Btg horizons are typically slightly to strongly acid (pH = 5.3-6.7). Lower Btg horizons range from slightly acid to slightly alkaline (pH = 6.9-7.7). BC and C-horizons are slightly to moderately alkaline (pH = 7.5-7.9) (NRCS, 2010). Faint, remnant laminations are present and roots are absent near the base of the Cjg horizon in both profiles. The underlying ABgb horizon contains remnant root traces, FeMn nodules, and no remnant bedding.

The first core (Pond Profile) was collected adjacent to the edge of a pond at an elevation of 87.5 m. The second core (Barite Profile) was collected from a wooded area up- gradient and ~ 150 m west of the pond at an elevation of 88.5 m. Profile descriptions are summarized in Table 3.1. Sample material was isolated from the middle of each core every 10 cm. Samples were then split for preparation of thin-section billets and geochemical analyses to minimize lateral distances between samples. High-magnification images were taken of fresh, broken whole core samples to document the distribution of pedogenic minerals throughout the matrix.

Microscopy and Clay Mineralogy

Thin sections from representative genetic horizons were analyzed using methods described by Bullock et al. (1985) and Fitzpatrick (1993). Adjacent soil samples were analyzed with powder X-ray diffraction (XRD) to identify mineral compositions. Clays were separated by standard centrifugation methods as described in Moore and Reynolds (1997). Individual samples were then saturated with 10% KCl or 10% MgCl (Moore and Reynolds, 1997), mounted on glass slides using the Millipore method (Drever, 1973), and glycolated for two days. Samples that displayed peaks ≥ 14Å were heated at 300ºC for 1 hour to differentiate individual 2:1 clay phases and mixed-layer clays. Mounted clay

samples and randomly oriented powdered samples of individual minerals were analyzed on a Siemens D5000 X-ray diffractometer with CuK α radiation at Baylor University, Waco, TX. Dominant clay compositions were documented from at least three XRD peaks whenever possible to avoid misidentification resulting from peak interferences from multiple clay phases (Moore and Reynolds, 1997). Randomly oriented powder mounts were used to verify the composition of sulfates.

Elemental Analyses

Whole soil samples were dried at low temperature, crushed, and split into representative samples. Elemental analyses were conducted by ICP-MS at ALS Chemex using a four-acid "total" digestion method. Reducible Fe, Mn, and Al analyses were performed at the USDA-NRCS National Soil Survey Laboratory in Lincoln, Nebraska using methods described in Jackson et al. (1986a). Citrate-dithionite-bicarbonate extractable (CDB) elemental data are reported in ppm.

Stable Isotope Analysis

Two samples of free sulfate were collected from whole-soil samples (*sensu*, Van Stempvoort and others, 1990). Soil material was rinsed with distilled water and the supernatant liquid was poured through an 80µm mesh sieve and centrifuged to remove clay-sized particles.

Sulfate was desorbed with 0.5 M NaCl and then precipitated as barite by adding 0.5 M $BaCl_2$ solution. Barite was filtered through a 0.45µm membrane, dried, and removed from the membrane. This procedure was repeated until no barite precipitated from solution.

Table 3.1. Barite-Bearing profile (BB, pedon 1) and non-barite-bearing Pond-Profile (PP, pedon 2) characteristics.

Barite-bearing profile (BB)

Horizon	Depth (cm)	Color	Texture	Pedogenic features	Micromorphology
A	0-8	10YR 5/3	very fine sandy loam	abundant roots; Fe concentrations and hypocoatings along macropores (10YR 6/3);	
Bw	8-20	10YR 3/2	fine sandy loam	decreased root activity; mm-scale Fe_2O_3 nodules; few leached zones; Fe hydroxides-oxyhydroxides lining small macropores	depletion zones; FeMn concentrations and mm-scale typic, Fe_2O_3 nodules; clay between framework grains (microcline, quartz)
Btg1	20-58	10YR 3/2 to 10YR 4/2	fine sandy clay loam	small roots; clay-rich; clusters of sub-mm-scale calcite masses; pH - 5.3-6.7	clay-lined grains; clay in macropores; sub-mm-scale, typic calcite nodules
Btg2	58-91	10YR 3/3 to 5YR 4/6, some 10 GY 7 and 10YR 3/2 mottles	clay loam	fine roots; clay-rich; Fe hydroxides-oxyhydroxides lining small macropores; mm-scale MnO nodules	few mm-scale, typic calcite nodules; mm-scale FeMn nodules with irregular boundaries
Btg3	91-142	10YR 6/2 to 10YR5/2, some 10YR4/2 mottles	clay loam	few fine roots; depletion zones; FeMn concentrations; barite in macropores; FeOOH hypocoatings; MnO nodules; depletion zones (10GY 7); mm-scale barite masses; clay coatings; pH -- 6.9-7.7	barite crystals in macropores; common clay pseudomorphs after feldspar; clay in macropores
BCjg1	142-169	10YR 6/1 , some 10YR 7/1 to 10YR 6/1 mottles	fine sandy clay loam	no roots observed; depletion zones; jarosite mottles; mm-scale MnO nodules	barite crystals in macropores; clusters of mm-scale radial barite nodules with radial fibrous habit; clay pseudomorphs after feldspar; clay in macropores

Table continued

Barite-bearing profile (BB)

Horizon	Depth (cm)	Color	Texture	Pedogenic features	Micromorphology
BCjg2	169-180	10YR 7/1 to 10YR 6/1	fine sandy loam	Fe_2O_3, FeOOH, jarosite mottles, FeMn nodules	FeMn concentrations; jarosite in matrix
Cjg	180-218	10YR 5/2 with 10YR 6/1 to 10YR 6/2 mottles	fine-grained sand	jarosite mottles; FeOOH hypocoatings; faint laminations; pH -- 7.5-7.9	FeMn concentrations with associated jarosite; pseudomorphs after feldspar

Pond profile (PP)

Horizon	Depth (cm)	Color	Texture	Pedogenic features	Micromorphology
A	0-8	10YR 5/3	very fine sandy loam	abundant roots; Fe concentrations and hypocoatings along macropores (10YR 6/3); abundant roots	
Bw	8-25	10YR 3/2	fine sandy loam	decreased root activity; mm-scale FeMn nodules; few leached zones; Fe hydroxides-oxyhydroxides lining small macropores	depletion zones adjacent to roots; FeMn concentrations; clay between framework grains (microcline, quartz)
Btg	25-43	10YR 3/2 to 10YR 4/2	sandy clay loam	small roots; increased clay	clay-lined grains; clay in macropores
Bytg1	43-50	10YR 3/3 to 5YR 4/6, some 10 GY 7 and 10YR 3/2 mottles	clay loam	fine roots; clay-rich; Fe hydroxides-oxyhydroxides lining small macropores; mm-scale MnO nodules; sparse gypsum crystals	scattered gypsum crystals in macropores; common Fe hydroxides in matrix and along root pores
Btyg2	50-72	10YR 6/2 to 10YR5/2, some 10YR4/2 mottles	clay loam	few fine roots; depletion zones; FeMn concentrations; gypsum in macropores; FeOOH hypocoatings; MnO nodules; depletion zones (10YR 5/2)	gypsum crystals in macropores; clay pseudomorphs after feldspar; clay in macropores
BCyg	72-80	10YR 5/2	sandy clay loam	fine roots and macerated organic matter; FeMn concentrations; Fe hypocoatings along root pores	scattered gypsum crystals in matrix and larger gypsum crystal in macropores; FeMn concentrations;

Table continued

Pond profile (PP) Horizon	Depth (cm)	Color	Texture	Pedogenic features	Micromorphology
Cg	80-180	10YR 5/2 to 10YR 5/3	sandy clay loam	no roots observed; 10YR 6/2 to 10YR 6/1 depletion zones depletion zones; jarosite mottles; scattered, fine laminations; mm-scale MnO nodules	FeMn concentrations; depletion zones; pseudomorphs after feldspar; quartz and feldspar dominant framework grains;

Barite and gypsum were handpicked from whole-soil samples (2 each), rinsed with distilled water, and the composition was verified with XRD before analysis. Jarosite-bearing soil material with water-soluble sulfate removed was immersed in 1 M NaOH solution, heated to 50-60°C, and then allowed to cool and settle. Decanted liquid was filtered to remove any remaining sediment. Dissolved sulfate was precipitated from solution as barite by adding $BaCl_2$. Barite was then filtered through 0.45µm membrane, dried, and collected from the membrane (4 samples).

Stable sulfur and oxygen isotope analyses were conducted at the University of Arizona Environmental Isotope Laboratory. Values of $\delta^{34}S$ were measured for SO_2 gas in a continuous-flow gas-ratio mass spectrometer (ThermoQuest Finnigan Delta PlusXL). Precision is estimated as ±0.15‰ or better, based on repeated internal standards. Values of $\delta^{18}O$ were measured on a continuous-flow gas-ratio mass spectrometer (ThermoQuest Finnigan Delta PlusXL). Standardization is based on international standard OGS-1. Precision is estimated as ±0.3‰ or better, based on repeated standards. Values for $\delta^{18}O$ are reported relative to VSMOW (Vienna Standard Mean Ocean Water) and $d^{34}S$ values are reported relative to VCDT (Vienna Canyon Diablo Troilite).

Radiocarbon Dating

Radiocarbon dating was conducted on the bulk organic fraction of a sample from the uppermost horizon of the underlying buried soil (ABgb) of the barite-bearing profile by accelerator mass spectrometry at Beta Analytical Inc. The sample was sieved to < 180 microns to remove any roots or microfossils and then acid washed to remove carbonates. The Measured Radiocarbon Age was corrected for isotopic fractionation, and calculated using the $\delta^{13}C_{PDB}$. Results are reported as radiocarbon years before present (RCYBP -- "present" = AD 1950).

Results

Barite-bearing Profile

Photomicrographs of the A horizon reveal that mm-scale, typic Fe_2O_3 nodules and FeMn concentrations are present (Fig. 3.2 A). Depletion zones are also common. Quartz and feldspar are the primary mineral grains. The predominant clay phases present throughout the profile (see representative XRD pattern in Fig. 3.3) are kaolinite-montmorillonite or mixed-layer, kaolinite-expandable clay (K/E, e.g., Hughes and others, 1993). Mixed-layer, K/E clays documented in Texas soils contain relatively large amounts of Fe in the octahedral layer (15-25%). The Btg1 and Btg2 horizons display increased clay content and FeMn concentrations with irregular boundaries. Sub-mm-scale, typic, micritic, calcite nodules are locally present in the Btg2 horizon (Fig. 3.2 B). A photomicrograph of the Btg3 horizon taken under cross-polarized light reveals that the

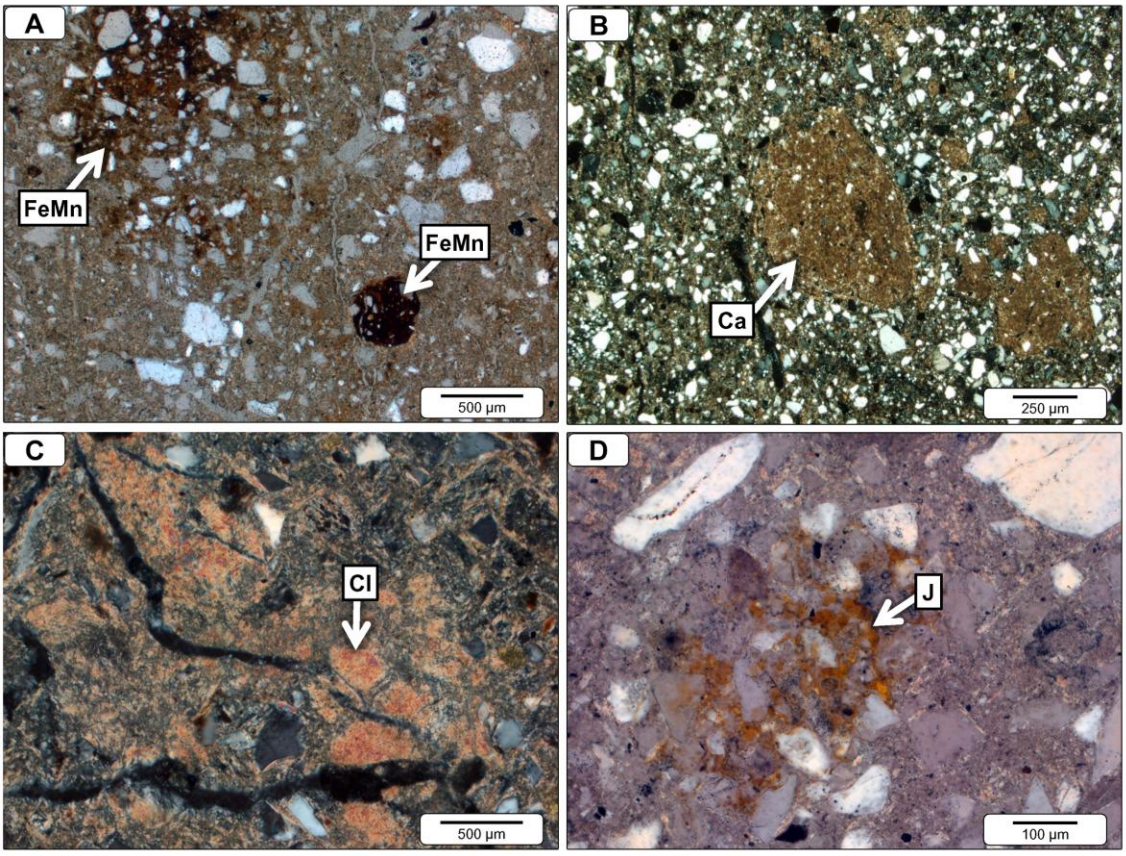

Figure 3.2. Photomicrographs of the barite-bearing profile. A) FeMn nodules and diffuse concentrations (FeMn) present in the A horizon (PPL). Mineral grains include quartz and feldspar. B) Sub-mm-scale, typic, micritic, calcite nodules locally present in the Btg2 horizon, immediately above the barite-bearing zone (PPL). C) Clay pseudomorphs after feldspar (Cl) are common in all Btg horizons and increase in abundance with depth (XPL). D) Jarosite (J) is most abundant as a matrix mineral in the Cjg horizon (PPL).

clay matrix contains abundant clay pseudomorphs after feldspar (Fig. 3.2 C). Clay-coated framework grains are common, particularly near the bottom of the horizon. Jarosite is present as a matrix mineral in the Cjg horizon (Fig. 3.2 D). The Cjg horizon also contains abundant feldspars (40%) and microcrystalline quartz. XRD reveals that feldspars are microcline and albite, with minor amounts of anorthite. Mineral grains are poorly sorted and angular to subangular. This mineralogical composition is similar to tonstein beds below the underlying the parent material (Senkayi and others, 1984). No pyrite is documented in the parent material or in the soil profile. Recent work suggests that no

pyrite is present for ~ 20 meters below the surface (Senkayi and others, 1984; Ulrich and others, 1998).

In barite-bearing horizons, jarosite occurs immediately adjacent to barite and in the soil matrix (Fig. 3.4 A, C). Coarse, tabular grains of barite that occur adjacent to macropores typically display a sharp contact with jarosite that lines the pores (Fig. 3.4 B). FeMn concentrations with diffuse boundaries are also common in the matrix and along root pores near barite (Fig. 3.4 A, C). Clusters of sub-mm-scale barite nodules with radial fibrous crystals and a coarser-grained center also occur in the adjacent matrix (Fig. 3.4 D). The uppermost ABgb horizon in the buried soil exhibits FeMn hypocoatings around root pores, diffuse FeMn concentrations in the matrix, and depletion zones. Clusters of sub-mm-scale barite nodules with radial fibrous crystals and a coarser-grained center also occur in the adjacent matrix (Fig. 4 D). The uppermost ABgb horizon in the buried soil exhibits FeMn hypocoatings around root pores, diffuse FeMn concentrations in the matrix, and depletion zones.

Several significant geochemical trends are apparent in the barite-bearing profile (see Fig. 3.5). First, a major increase in barium, strontium, MnO, and sulfur occurs at the depth of highest barite abundance (130 cm) in the barite-bearing horizons (Fig. 3.5 A, B, D, G). A peak in Mn occurs at 110 cm. An increase in Ca occurs just above the barite-bearing horizons, coincident with the occurrence of calcite nodules (Fig. 3.5 C). Potassium concentration increases dramatically in the lowermost horizons, from the top of the barite-bearing horizons to the base of the BCjg1 horizon, where jarosite occurs in conjunction with abundant feldspar grains and clay pseudomorphs (Fig. 3.5 E).

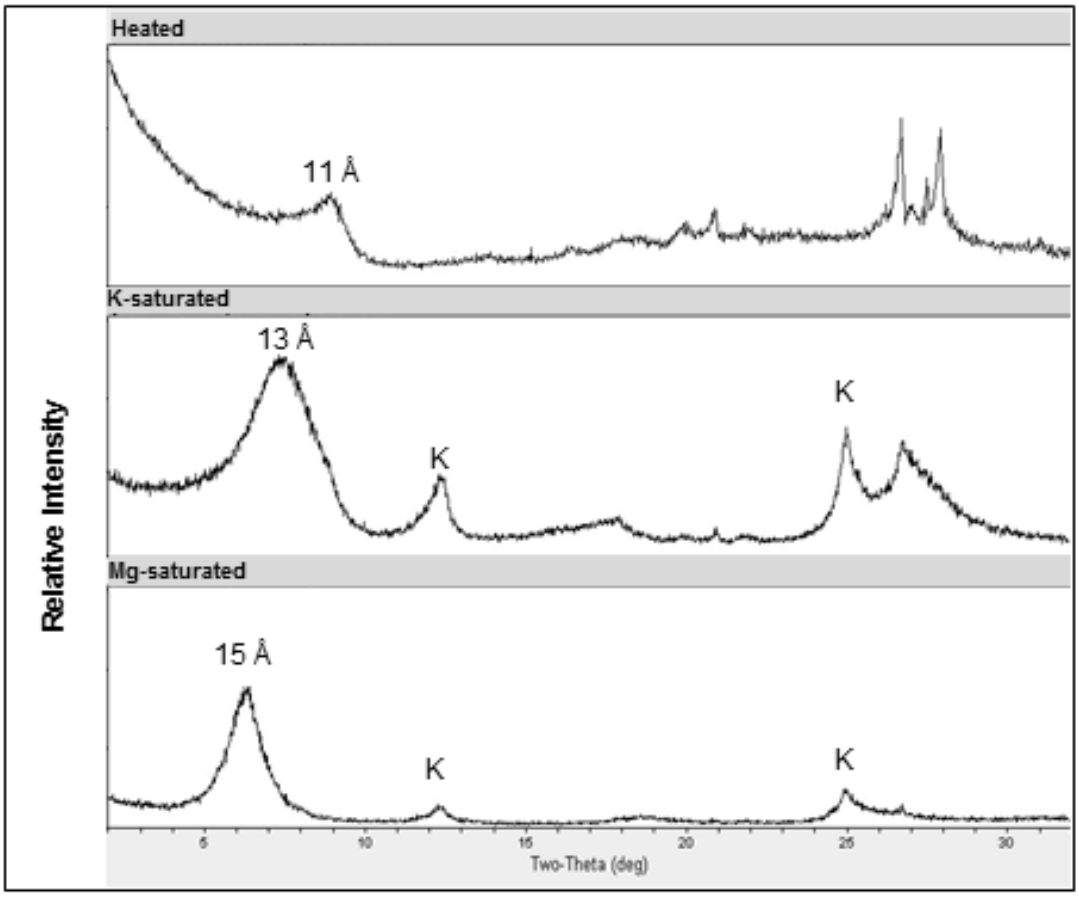

Figure 3.3. Representative X-ray diffraction patterns for kaolinite-expandable (K/E) clays. Expandable clays collapse upon K-saturation and heating. Kaolinite peaks (K) become more defined with K-saturation and partially collapse with heating.

Three peaks in Fe_2O_3 occur in the Btg horizons and in the BCjg2 horizon (Fig. 3.5 F). However, the highest value of extractable Fe (Fe_{CDB}) occurs near the base of the barite-bearing zone (Fig. 3.5 J). Overall total aluminum concentration increases with depth below 70 cm (Fig. 3.5 H). A peak in P occurs at 160 cm and then gradually decreases to the Cjghorizon (Fig. 3.5 I). An increase in extractable Al (Al_{CDB}) is coincident with low values of extractable Fe (Fig. 3.5 B, J, and K). The Ba/Sr ratio displays a sharp increase at 130 cm, but otherwise remains relatively constant throughout the rest of the profile (Fig. 3.5 L).

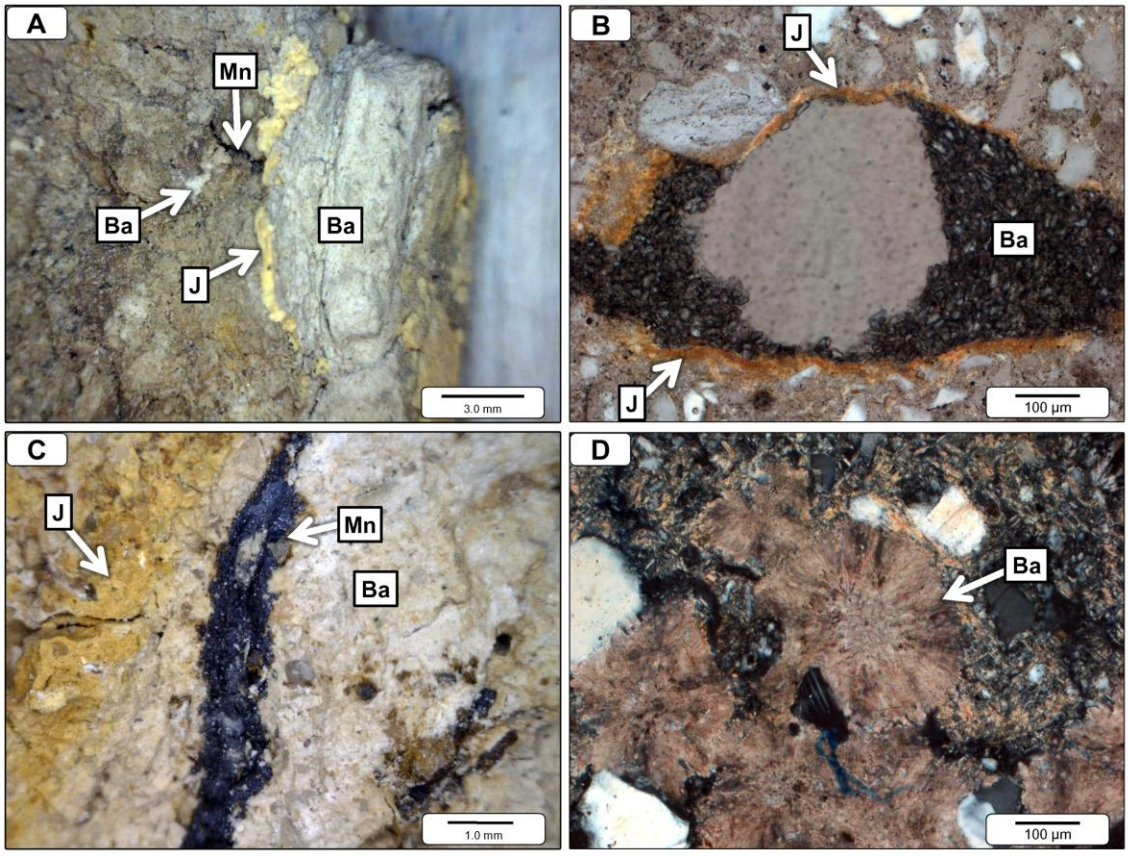

Figure 3.4. Photomicrographs of barite and associated mineral relationships. Images A and C were taken under reflected light (RL). A) Silt-sized, tabular, barite crystals within macropores (Ba, right) and in the adjacent matrix (Ba, left). Jarosite (J) and Mn oxide immediately adjacent to the barite. Vacant root pore in center. B) Close relationship between barite (Ba) and jarosite in evacuated root pores (XPL). C) Spatial relationship between fine-grained barite crystals (Ba), jarosite (J), and Mn oxides. D) Clusters of sub-mm-scale barite nodules (Ba) (as illustrated in C) with radial fibrous crystals and a coarser-grained center (XPL).

The $\delta^{34}S$ and $\delta^{18}O$ values of exchangeable sulfate in the barite-bearing profile are -4.14‰ and +10.4‰, respectively (Fig. 3.6). Barite $\delta^{34}S$ values range from +5.4 to +5.5‰, averaging +5.45‰. Barite $\delta^{18}O$ ranges from +13.0 to +13.4‰, averaging +13.2‰. Jarosite samples have $\delta^{34}S$ values that range from -12.5 to -12.7‰ and average -12.6‰. Jarosite $\delta^{18}O$ values average +12.2‰. The conventional radiocarbon age

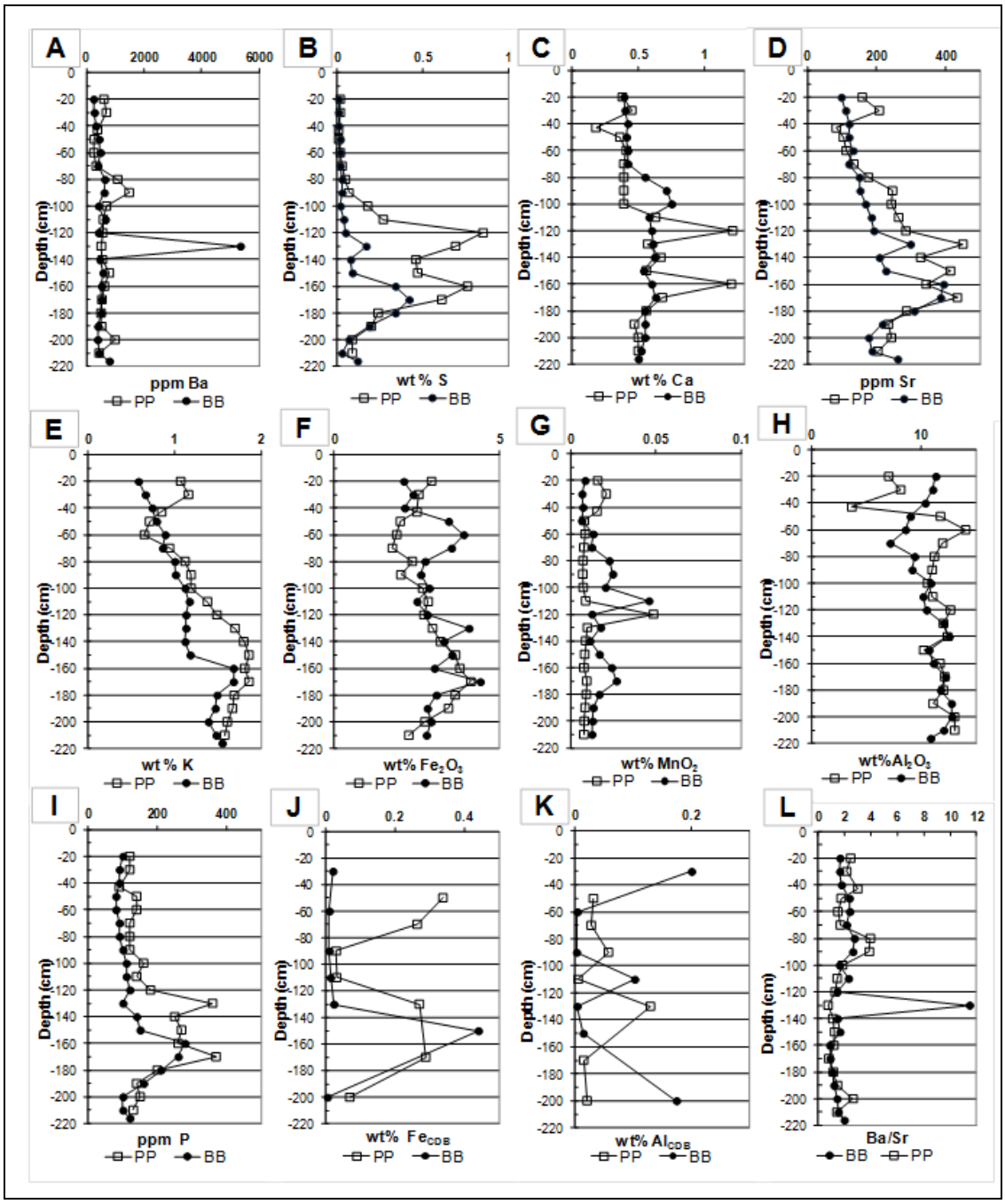

Figure 3.5. Elemental chemistry for the barite-bearing (BB) and the barite-poor pond (PP) profiles. A-I) wt% Ba, Sr, and P and ppm S, Ca, K, Fe_2O_3, MnO_2, and Al_2O_3 vs. depth showing different trends. J-K) Citrate dithionate bicarbonate extractable elements (Fe_{CDB} and Al_{CDB}) are reported in weight % and plotted vs. depth. L) Ba/Sr molecular ratio distribution with depth.

(corrected for isotopic fractionation) for a sample from the ABgb horizon is 13,010 ± 50 BP (Beta 344657).

Pond Profile

Overall, the pond profile is slightly less thick, coarser-grained, and appears less weathered than the barite-bearing profile (Fig. 3.1 B). Roots are abundant in the brown (10YR 5/3) A horizon. Below the A horizon, root abundance decreases. The very dark grayish-brown (10YR 3/2) Bw horizon displays scattered leached zones, and common, mm-diameter, FeMn nodules. Iron hydroxides and oxyhydroxides line small macropores. During the rainy season, iron oxides in the upper A and Bw horizons are reduced and the soil matrix color normally ranges between 10YR 5/3 - 10YR 4/2 and changes to 10BG 4/2, due to the presence of abundant reducible iron in the upper part of the profile.

The Btg horizons are significantly thinner as compared to those in the barite-bearing profile. No hematite nodules occur in this profile, but small FeMn nodules are common. Iron oxide hypocoatings around root pores and light greenish-gray (10GY 7), leached zones are common in the Btyg and BCyg horizons. Roots decrease with depth to the C-horizon, where there is remnant bedding and no roots are visible. An abrupt increase in abundance of medium-fine roots below the C-horizon marks the top of a buried soil. Jarosite was documented only in the Cg horizon, whereas pyrite was not identified in any part of this profile.The dominant clay phase present in this profile is mixed-layer K/E. No barite was identified in this profile. Depletion zones occur adjacent to roots and are scattered throughout the matrix (Fig. 3.7A). FeMn concentrations with diffuse boundaries and clay-coated framework grains are common in the sandy matrix.

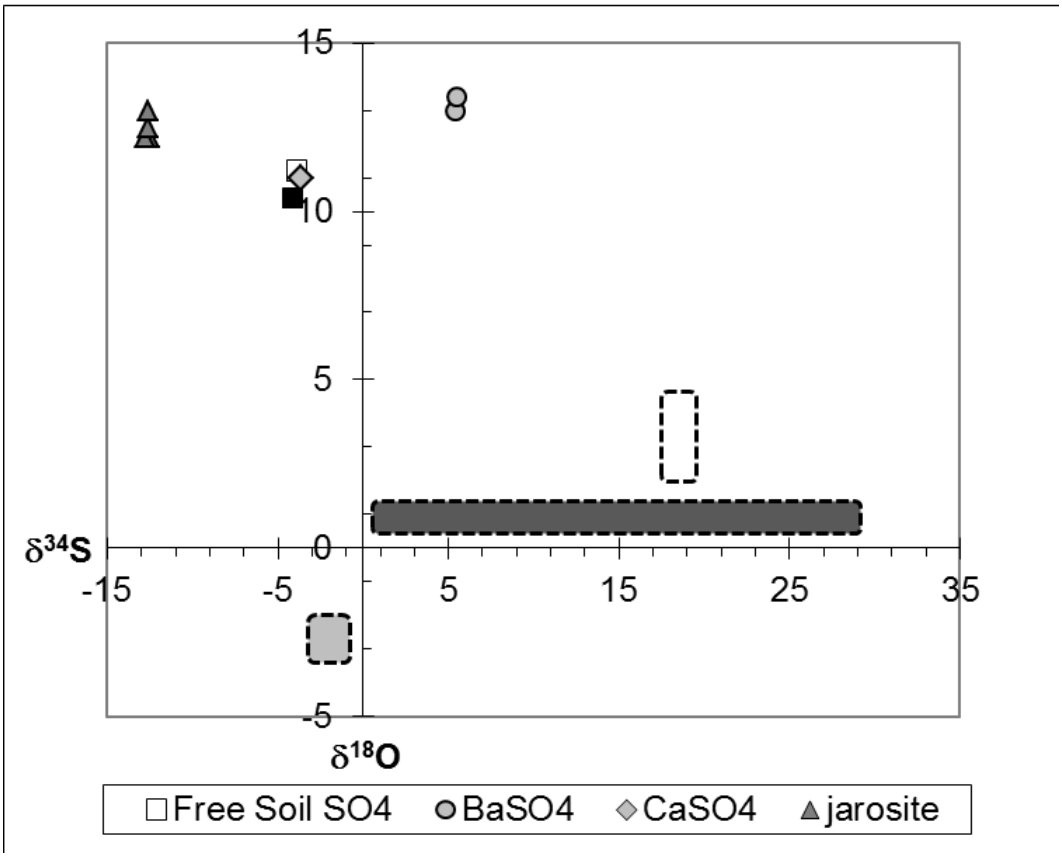

Figure 3.6. Stable sulfur and oxygen isotopic composition of sulfate minerals and free sulfate. White box represents the range of middle Eocene marine barite. The light gray box is local meteoric water values. The dark gray box is the range of groundwater values documented in the study area.

Photomicrographs of the Btg2 horizon reveal that FeOOH concentrations are dispersed throughout matrix (Fig. 3.7 B). Abundant, lenticular, gypsum crystals infill macropores and are commonly associated with FeMn concentrations (Fig. 3.7 C). Mineral grains in the BCyg and Cjg horizons are mainly composed of quartz, albite, and microcline (Fig. 3.7 D). Clay pseudomorphs after feldspar are common.

Barium peaks occur at 80-90 cm and at 200 cm (Fig. 3.5A). Otherwise, the concentration of barium remains relatively uniform throughout the profile. Strontium, calcium, phosphorus, and sulfur peaks were identified in the gypsum bearing horizons (Fig. 3.5 A, B, I). Potassium gradually increases with depth, with the highest

concentration occurring from 140-170 cm (Fig. 3.5 E). Fe_2O_3 concentrations also increase with depth from 70-170 cm (Fig. 3.5 F). A significant peak in MnO_2 occurs at 120 cm (Fig. 3.5 G). Aluminum is highest in abundance below 50 cm (Fig. 3.5 H). A peak in reducible Al occurs at 130 cm (Fig. 3.5 K). Al_{CDB} is significantly higher above 130 cm compared to the barite-bearing profile. From 130-170 cm, there is an increase in Fe_{CDB} similar to that documented in the barite-bearing profile. However, unlike the barite-bearing profile there is a coincident decrease in Al_{CDB} (Fig.3.5 J, K). Although slight increases in Ba/Sr ratio (up to 3.94) occur at 80-90 cm and at 200 cm in the parent material, Ba/Sr values remain near 2 throughout the profile (Fig. 3.5 L). This profile contains significantly more Fe_{CDB} in the upper horizons compared to the barite-bearing profile (See Fig. 3.5 J). The underlying soil displays a decrease in Fe_{CDB} similar to that of the barite-bearing profile.

The $\delta^{34}S$ and $\delta^{18}O$ values of exchangeable sulfate in the pond profile are -3.9‰ and +11.2‰, respectively (See Fig. 3.6). Gypsum $\delta^{34}S$ values average -3.7‰. The $\delta^{18}O$ values of gypsum average +11.0‰. Jarosite samples have $\delta^{34}S$ values of -12.6‰ and $\delta^{18}O$ values ranging between +12.5‰ and +13.0‰, with an average of 12.75‰.

Discussion

Acid-sulfate Soil Genesis

In soils that form in exposed wetland sediments, such as the buried soil in the study area (Senkayi and others, 1984), the active sulfurization state of acid- sulfate soil genesis occurs once the moisture content reaches field capacity, usually within a few weeks of exposure (Pons, 1973). The oxidation of reduced iron sulfides releases FeOOH,

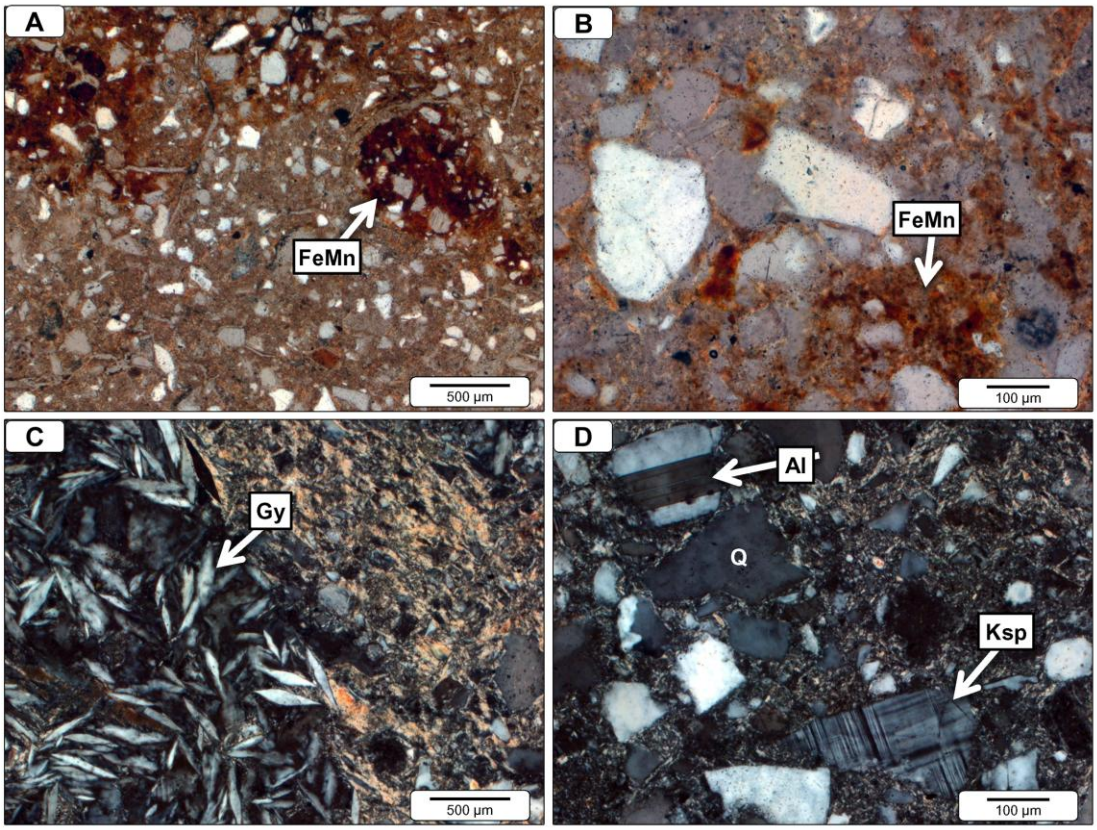

Figure 3.7. Photomicrographs of the pond profile. A) Depletion zones and diffuse FeMn masses (FeMn) common in the silty matrix of the Btg1 horizon (PPL). B) Dispersed FeOOH in the Btg2 horizon (PPL). C) Abundant lenticular gypsum (Gy) in macropores (XPL). D) Primary mineral grains in the BCyg and Cjg horizons include albite (Al), quartz (Q), and potassium feldspar (Ksp) XPL.
(Fig. 3.5 A, B, I).

sulfate and H^+ into the soil solution (Pons, 1973; Smolders and others, 2006). During the initial stages of acid-sulfate soil genesis, extreme acidification results in the mobilization of Al. Dissolution of oxidized iron at low pH also results in phosphate release (Smolders and others, 2006). With continued exposure, acids attack feldspars and clay minerals (active sulfurization), liberating more Al.

Jarosite typically forms in association with acidic, oxidizing conditions resulting from the weathering of pyrite (Stoffregen and others, 2000). Pyrite oxidation in exposed, pyritic, wetland soils of the Yegua Formation coastal plains and nearshore mudstones

(Routh and others, 1999) led to the formation of jarosite-rich sediments. Although Lufkin jarosite likely precipitated during the active sulfurization stages in exposed coastal marine deposits, the absence of pyrite in surficial soils and the presence of a buried wetland soil (Routh et al., 1999) suggest that the Lufkin soil developed in reworked wetland and underlying altered ash sediments during the extended post-sulfurization stage, contrary to previous hypotheses (Carson and others, 1982).

Experimental studies reveal that reduction of redox potential (Eh) of the soil destabilizes jarosite during saturated, reducing conditions and the presence of organic acids increases jarosite dissolution (Chu and others, 2006). The relatively high Fe_{CDB} in the upper portion of the pond profile suggests that this profile likely seldom reaches field capacity, except in the topmost horizons (<20 cm). Increased phosphorus sorption in the pond profile is coincident with sulfate adsorption in lower horizons that contain abundant Fe_{CDB} and Al_{CDB}, and likely results in gypsum precipitation (Serrano and others, 1999). In general, the presence of higher amounts of organic matter in the pond profile results in more rapid development of reduced conditions during epiaquatic events. Under these conditions, the dissolution rate of jarosite would be significantly higher (Chu and others, 2006) and would explain the paucity of jarosite in the pond profile. Alternatively, but less likely, it is possible that the presence of jarosite in the reworked sediments may have been localized and jarosite may not have been distributed evenly across the landscape.

In well-developed, acid sulfate soils, SO_4^{2-} translocation and adsorption is controlled by saturation time (longer and more common in the pond profile), presence of clay, free iron oxyhydroxides, and Al_{CDB} (Ajwa and Tabatabai, 1995). Humic acids

significantly decrease the rate of SO_4^{2-} retention because SO_4^{2-} and organic anions compete for sorption sites (Courchesne and others, 1995). Consequently, in the upper part of the pond profile, where organic matter is not completely oxidized, sulfate is released and then translocated deeper in the soil profile, where Al_{CDB} and clay content increases. During times of high evaporative stress, SO_4^{2-} adsorption would be high at the redox boundary during dry times and the lower part of the pond profile becomes oversaturated with respect to gypsum (Van Den Ende, 1991; Courchesne and others, 1995).

Factors Controlling Barite Precipitation

Low-temperature barite precipitation in surface sediments such as soils, lakes, and marine deposits requires the presence of adequate concentrations of SO_4^{2-} and Ba^{2+} in separate aqueous solutions that converge in the barite-bearing horizons (Hanor, 2000). In marine sediments, the convergence of barium-rich solutions with sulfate-rich marine waters is attributable to the abundance of sulfate in ocean water and more possible sources of barium. In soils, the source(s) of sulfur- and barium-rich fluids are more challenging to explain.

Source of barium. The presence of abundant clay pseudomorphs after feldspar and the absence of other barium-rich minerals (Senkayai et al., 1984), suggests that preferential weathering of Ba-rich feldspars and Ba-rich clays present in the parent material are the most likely source of Ba^{2+} in the Lufkin soil profiles (Kunze and Oakes, 1957; Senkayi and others, 1984; Singer, 1984; Kabata-Pendias, 2001). Barium is common in microcline in volcanic rocks. Feldspars in volcanic rocks are the source of barium in most soils (Dunham and Hanor, 1967). The release of free Ba^{2+} into the soil solution occurs largely because the solubility of Ba-rich compounds increases with

decreasing pH during reducing conditions (Fiedler and Sommer, 2004; Scarciglia and others, 2009). The increased concentration of Ba^{2+} in the BCjg1 horizon and associated clay pseudomorphs suggest that at least some Ba^{2+} may be translocated with Ba-rich clays or as a mobile element during saturated, low pH conditions (Zang and others, 2001) The increase in Al_{CDB} combined with the presence of K/E in the Btg3 horizon in the barite-bearing profile also promotes SO_4^{2-} adsorption during dry conditions (Gambrell, 1994). The presence of manganese oxides would contribute to the retention of barium and to the oxidation of iron (Dixon, 1991) observed in barite-bearing horizons.

Although there is a peak in Ba^{2+} concentration in the pond profile, low sulfate concentration, the presence of humic acids, and common reducing conditions likely prohibit barite precipitation (Smith and others, 2004a). Instead, we suggest that Ba^{2+} mobility is more limited and there is a downward movement of sulfur in the form of organic sulfides because of reducing conditions that occur during the wet season to lower horizons, below the highest Ba^{2+} accumulation, where sulfides are reoxidized, either by microbial activity or by communication with meteoric water.

Sources of sulfate. The principal source of sulfur in soils is pyrite in the parent material (acid sulfate soils) and organically derived phases (Stevenson and Cole, 1999; Hutchinson and others, 2001). The influx of sulfur into soil also results from atmospheric SO_2^{2-} (via gas or acid rain), groundwater leaching of subsurface minerals (i.e., dissolution of gypsum in the parent material), the application of fertilizer, and biologically produced HS released during the decay of organic matter, particularly the decay of roots within macropores (Andreae and Jaeschke, 1988; Krouse and others, 1991; Stevenson and Cole, 1999). No introduction of fertilizer occurs in the study area (Joe Dixon, personal

communication) nor has gypsum been observed in the parent material, eliminating these factors for further consideration. All likely sources of sulfur species in Lufkin soils, including the weathering and reduction of sulfide minerals in the parent material, residual sea salts from marine regressions, decaying organic material, atmospheric SO_2, groundwater¸ meteoric surface water, and existing sulfates have relatively distinct $\delta^{34}S$ values (i.e., Lyons and others, 1994; Delmelle and Bernard, 2000; Hanor, 2000).

Sulfur Isotopic Composition. Most barite studies focus on $\delta^{34}S$ because significant sulfur fractionation occurs when sulfate is reduced, but there is little fractionation during the oxidation of sulfide (Seal and others, 2000). Lighter isotopes are preferentially partitioned into sulfide during microbial reduction resulting in a product (usually pyrite) that is much more depleted in ^{34}S than the original sulfate (Seal and others, 2000). The residual sulfate in the aqueous solution is enriched in ^{34}S as the pore water evolves, if the system is closed. In oceans, the sulfur isotopic composition of water equals the proportion of sulfide and sulfate removed divided by $\delta^{34}S$ of river input. However, in terrestrial systems such as lakes and soils, sulfate in meteoric water, overland flow, groundwater, and decaying plant material have a more significant impact on the sulfur isotopic composition of available sulfate.

All soluble and insoluble sulfur compounds/species in both profiles have $\delta^{34}S$ values that are much lower than those of present-day seawater (Seal and others, 2000) and those of evaporative Eocene marine sulfates (Turchyn and Schrag, 2006). This suggests that evaporites are not a source of sulfur in Lufkin soils. Instead, the results of this study indicate that the $\delta^{34}S$ of jarosite in the Lufkin soil is consistent with pyrite that formed in coastal plain deposits (Trust and Fry, 1992). If the source of sulfate for both

jarosite and barite were the oxidation of sulfide minerals during the active sulfurization stage as hypothesized by Darmoody et al., (1989), the $\delta^{34}S$ and $\delta^{18}O$ values of these minerals would be nearly identical (Seal and others, 2000). If groundwater is a contributor, a much more positive $\delta^{34}S$ (~+20.0-30.0‰) would be predicted (Ulrich and others, 1998). Isotopic values for Lufkin sulfates exhibit disparities that indicate that the source of sulfate is different for free sulfate, gypsum, barite, and jarosite.

The narrow range of $\delta^{34}S$ values of both free soil sulfate and gypsum lends additional evidence that $SO_{4gypsum}$ and free soil sulfate have a common origin. The sulfur isotopic signatures of these species are consistent with modern meteoric water in the study area (Chowdhury, 2004; Dutton and others, 2005). The slight depletion with respect to ^{34}S in gypsum is likely due to a slight fractionation effect attributable to the presence of organic sulfur in the pond profile (Trust and Fry, 1992). Assuming that jarosite is the primary source of free sulfate in the soil, then the difference in the isotopic composition between free sulfate and jarosite may reflect the kinetic isotope fractionation during partial reduction of jarosite and subsequent oxidation of sulfides to sulfate (Habicht and Canfield, 2001). The introduction of a small amount of atmospheric sulfur into the soil via plant metabolic processes may also contribute to a difference in the sulfur isotopic composition. However, it is most likely that a combination of these two factors best explains the overall total sulfur isotopic signatures of the free sulfate (Dowuona and others, 1992).

In sandy materials such as the Lufkin soil parent material, sulfide oxidation occurs rapidly and soil-buffering reactions are usually sufficient to prevent significant acidification. Typically, jarosite precipitates and remains stable under oxidized, post-

sulfurization conditions (Chu and others, 2006). However, if the soil is inundated long enough to become anoxic, particularly if organic matter is present, jarosite may destabilize and dissolve, and K^+, SO_4^{2-}, Fe^{2+}, and H^+ may be released into the soil solution (Jones and others, 2006). In this way jarosite becomes a secondary source of soluble acid and sulfate in the soil solution. Under reducing, inundated conditions, transformations of Fe^{3+} into soluble Fe^{2+} and SO_4^{2-} into H_2S may take place, consuming H^+ and increasing pH, conditions that are favorable for sulfate reducing bacteria (SRB) to flourish. Recent work in the study area documents the presence of SRB and sulfur-oxidizing bacteria (SOB) in surficial soils within a kilometer of the study area (Martino and others, 1998). SRB are most active in lower part of the $BaSO_4$ profile (below the redox boundary) where jarosite is most abundant and electron donors are most available to stimulate microbial respiration (Ulrich and others, 1998). SOB, on the other hand, are most active in the upper, more oxic portion of the surficial soil (above the redox boundary).

Sulfate reduction results in $\delta^{34}S$ values ranging from +19.0 to +71.0‰ (or more), depending on the availability of SO_4^{2-} and rate of sulfate reduction (Seal and others, 2000). Unlike marine deposits, SO_4^{2-} availability in soils is limited and reducing conditions are time-limited. Consequently, sulfate reduction in soils may be faster, but more punctuated compared to marine environments (D'Angelo and Reddy, 1999) due to the metabolization of organic carbon by aerobic bacteria in the oxic zone (Lyons and others, 1994). Lufkin soil barite $\delta^{34}S$ values have an average of +18.05‰ enrichment in the heavy isotope (^{34}S) compared to the $\delta^{34}S_{\text{jarosite}}$, suggesting that the sulfate in the barite resulted from dissolution of jarosite due to bacterial sulfate reduction during reducing

conditions (Seal and others, 2000). Subsequent more direct sulfide oxidation through metabolic processes of SOB with the onset of the dry season would lead to comparatively less enriched free sulfate and the incorporation of residual heavy sulfate into the barite (Habicht and Canfield, 2001). Although $\delta^{34}S_{barite}$ reported in this study is inconsistent with sulfate derived from the oxidation of decaying plant material (Trust and Fry, 1992), the overall fractionation effect may be slightly reduced by mixing of exchangeable sulfur phases that are also reduced during saturated conditions (Jorgensen, 1983). Because conditions in the barite-bearing profile would have been too oxidized and reducing conditions limited enough so as to prevent sulfate reduction to occur above the redox boundary, we suggest that mixing would be considerably limited due to greater O_2 availability.

Oxygen Isotopic Composition: According to Seal et al. (2000), the $\delta^{18}O$ value of sulfates records the sources of oxygen, except under the most acidic conditions because the slow kinetics of sulfate-water isotope exchange are limiting. The $\delta^{18}O$ values, as with the $\delta^{34}S$ values, for free sulfate in both profiles, are nearly uniform and similar to the isotopic composition of gypsum in the pond profile. This uniformity agrees with the interpretation that the soil sulfate is derived from the same source(s). The oxygen isotopic signatures of free sulfate and gypsum in the Lufkin soils are slightly less enriched with respect to ^{18}O. Because there is little or no fractionation associated with sulfate adsorption or dissolution, it is likely that the slight difference in the oxygen isotopic composition is related to sulfate reduction processes (Habicht and Canfield, 2001). It also supports the hypothesis that sulfate is advectively transported down-gradient from the upper profile to areas lower on the landscape (Ulrich and others, 1998). Because free

sulfate and gypsum are both depleted in ^{18}O compared to jarosite, it is reasonable to hypothesize that the oxidation of sulfides that are released after the bacterial degradation of jarosite contributes to the isotopic composition of free sulfates and gypsum. Given the differences in sulfur and oxygen isotopic compositions of gypsum, free sulfate, and barite documented in this study, it is reasonable to conclude that sulfate that is enriched in $\delta^{34}S$ is preferentially incorporated into barite, while less-enriched sulfate is adsorbed to kaolinite as the soil dries (Rao and Sridharan, 1984; Seal and others, 2000). Our results reveal a 2.4‰ enrichment in $\delta^{18}O_{BaSO4}$, which would also be a reasonable result of bacterial sulfate reduction of jarosite (Turchyn and others, 2010). Meteoric water (mixing) may have also contributed to a lower overall fractionation, particularly if phototrophic sulfide-oxidizing bacteria are present (Senko and others, 2004).

Barite Precipitation

During reducing conditions, H_2S (sourced from decaying organic compounds and weathering of existing sulfate minerals) and Ba^{2+} are in solution together at the redox boundary or redoxicline (sensu, Fiedler and Sommer, 2004), particularly if sulfate-reducing bacteria (SRB) are present. As the soil begins to dry, organic matter is completely oxidized, soil pH increases, H_2S is oxidized to SO_4, first in open channels (vacated root pores and along ped faces) and then in the soil matrix (Sharpley, 1990; Agbenin, 1997; Biswas and others, 2003). As drying continues, SO_4^{2-} adsorbed to kaolinite is also desorbed (Biswas and others, 2003). It is most likely that barite precipitation occurs as the soil solution changes from saturated to dry conditions when Ba^{2+} and SO_4^{2-} would be in solution together,.

Crystal size, morphology, and texture partially indicate the conditions of crystallization (Hanor, 2000). Experimental studies by Sanchez-Pastor et al. (2006) indicate that rapid precipitation results in anhedral, microgranular and scalloped barite crystals (i.e., radial, fibrous texture in the Lufkin soil) and that tabular barite crystals (i.e., in larger macropores above zone of most abundant jarosite concentrations) form under conditions of lower supersaturation (Sanchez-Pastor and others, 2006). The occurrence of both types of crystal habits in the Lufkin soil adjacent to jarosite along macropores suggests localized heterogeneity of precipitation rates and concentrations of Ba^{2+} and soil SO_4^{2-}.

The release of dissolved organic matter along pores as roots senesce/decay may also fuel bacterial sulfate reduction when sulfates are present (Andreae and Jaeschke, 1988). Additional sulfur introduced during root decay and localized reducing conditions that release barium into solution may provide nucleation sites for barite precipitation first in vacated macropores, (Blount, 1977), and then in the matrix adjacent to FeMn concentrations.

Under reducing conditions, Ba^{2+} is released into soil solution and sulfate reduction releases H_2S into solution. As sulfides are reoxidized and the sulfate content increases during drier conditions, sulfate ions are captured by the Ba^{2+} ions, giving rise to a barite growth nucleus (Gonzalez-Munoz and others, 2003). This would explain the presence of radial fibrous and bladed barite within, and near, evacuated root pores, and supports interpretations of the timing of barite precipitation. At the redox boundary in the barite-bearing profile, the absence of humic acids would allow the precipitation of well-formed crystals as euhedral crystals and spherulites (Smith and others, 2004a). In the

pond profile, barite crystal growth is likely inhibited by the adsorption of humic acids to spherulite surfaces, blocking active growth sites (Smith and others, 2004a). The sorption of Ca^{2+} by organic matter likely drives the precipitation of gypsum lower in the profile during times of high evaporative stress (Van Den Ende, 1991).

Synthesized data indicate that the Lufkin series is an acid sulfate soil that developed in reworked wetland soil and altered ash sediments over the last ~ 13,000 years (Senkayi and others, 1984) Redox features suggest that that the soil may be saturated as much as 18% (low-chroma Fe-depletion features) to 50% (gray matrix - chroma ≤2) of the time during the growing season (Jacobs and others, 2002). Based on the $\delta^{34}S$ values, we suggest that during saturated conditions, partial jarosite dissolution, and subsequent bacterial sulfate reduction occurs in the barite-bearing profile (Fig. 8A).Alternating saturated, anoxic and dry, oxic conditions in the Lufkin soil profiles provide the optimal conditions for mineralization of free sulfate and mobilized Ca^{2+}, Ba^{2+}, and Fe^{2+} at a redoxicline in the Btg horizons (Fiedler and Sommer, 2004). Consequently, it is likely that most barite in the Lufkin soils precipitates at the transition between the wet season (November to May) and the dry season (May to November) when the soil experiences drying conditions, an increase in pH, and SO_4^{2-}, Ca^{2+} and Ba^{2+} are in solution together. At lower positions on the landscape where ponding is more prolonged and organic matter is not completely oxidized, the presence of humic acids prevents barite precipitation and gypsum is the predominant sulfate (Fig. 3.8 B).

Conclusions

Results presented here illustrate that the most important pedogenic redox processes that control barite precipitation in the Lufkin soil are as follows: 1) warm soil

temperature that supports sulfur-reducing and sulfur oxidizing microbial activity, 2) distinct wet/dry seasons that allow for alternating redox conditions, 3) a low-gradient landscape, 4) parent material that contains barium- and sulfur-rich constituents, and 5) a long-lived, stable landscape.

Conditions that lead to pedogenic barite precipitation may be slightly different in soils that develop in gypsum-rich parent materials (Buck and others, 2010) or have better communication with sulfate-rich groundwater (Stoops and Poch, 1985). Consequently, additional studies of modern barite-bearing soils is needed to document a full spectrum conditions and landscape relationships that allow improved interpretation and application of barite-bearing paleosols.

Redoximorphic features, micromorphology, mineralogy, elemental trends, and stable isotopes data presented in this study are typically well preserved in paleosols and microbial processes, and the paleotopography of ancient acid sulfate soils. Actuo-taphonomic studies of barite-bearing paleosols/modern soils, using these lines of data, may help refine current interpretations of ancient landscapes and climate. Because significant Fe fractionation occurs during redox soil processes (due to bacterial dissimilatory Fe reduction), Fe isotopes may provide an additional way to trace biogeochemical processes in barite-bearing paleosols, especially if they are compared with modern soils (Stiles and others, 2001; Beard and others, 2003).

One of the original motivations for undertaking this study was to try to identify the processes involved in barite precipitation in soils so that we could understand barite occurrences in paleosols (e.g., Morrison Fm., Jennings and others, 2011). Although the soil site at College Station is not strictly a floodplain-lacustrine system like that

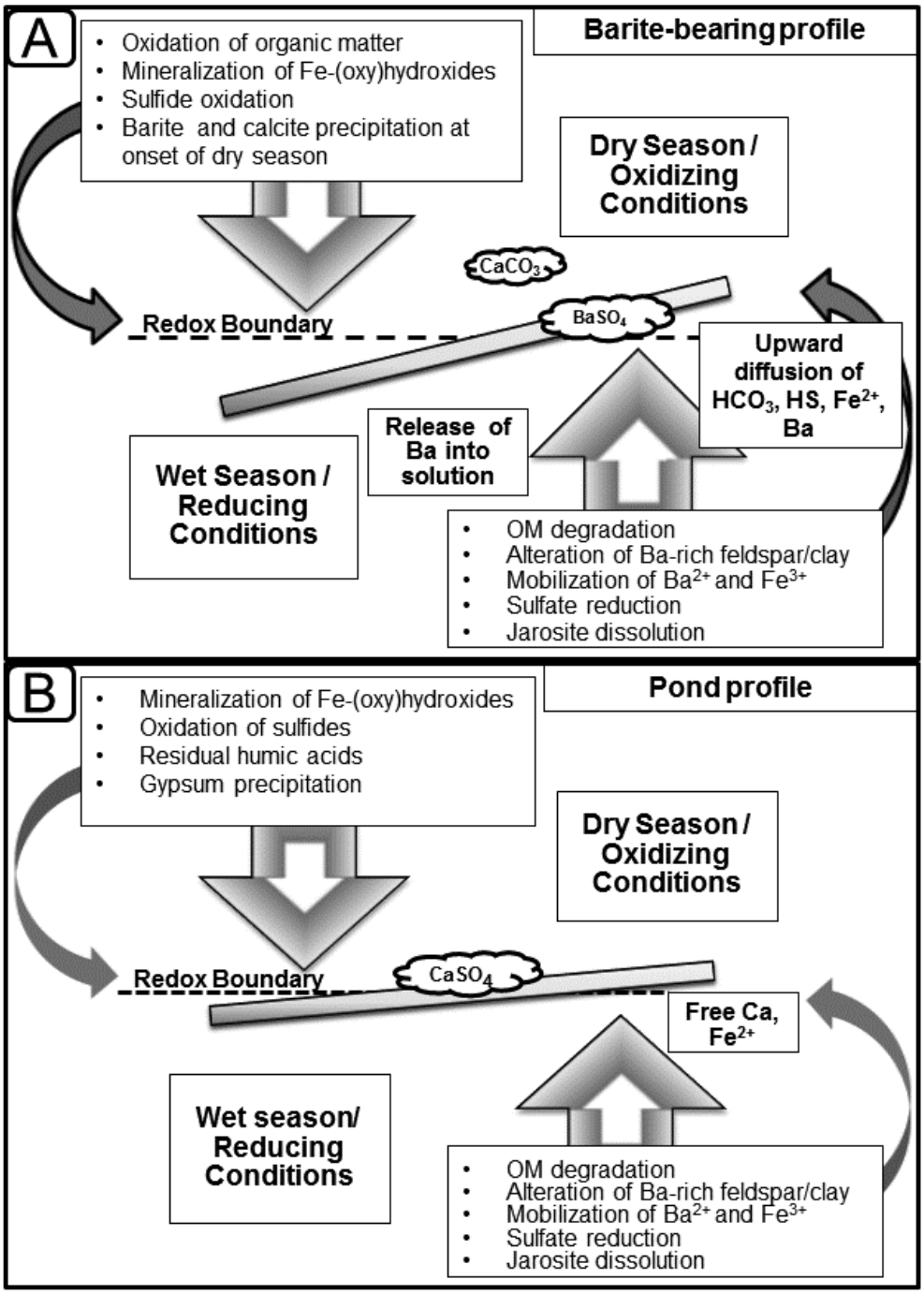

Figure 3.8. Generalized, schematic model. Model illustrates the topographic- and redox-dependent pedogenic processes and redox reactions that occur in the A) the barite-bearing profile and B) the pond profile as a result of fluctuating redox conditions.

envisioned for Morrison Fm. paleosols, it still provides valuable insights in understanding barite precipitation processes and should serve as a springboard for future studies of paleosols containing pedogenic barite and for studies using barium to track weathering intensity and leaching. For example, an unexpected result of this study is the discovery of elemental evidence of Ba^{2+} mobility and concentration in a Btg3 horizon. Because an enrichment of Ba/Sr ratio is commonly used as evidence for ancient paleosol surface horizons, the results of this study indicate that an enrichment may instead occur 70-100 cm below the surface in ancient acid sulfate soils and lower horizons of paleosols.

Additionally, although it is commonly assumed that a Ba/Sr molecular ratio of 10 or more indicates strongly leached soils, the significant peak in the barite-bearing soil, and to a lesser extent in the pond profile, would give a false impression of enhanced leaching. Instead, the Ba peak more likely is fixed by Fe-oxides at depth near the base of the barite-bearing zone. Contrary to previous interpretations (e.g., Retallack and Kirby, 2007; Retallack and Huang, 2010) of paleohorizons in gypsic and baritic paleosols, related calcite nodules in barite-bearing soils occurs at a shallower depth than barite-bearing horizons. Barite-bearing horizons also occur relatively deeper than gypsum-bearing horizons associated with profiles lower on the landscape. Using the proposed relationship between mean annual precipitation (P, in millimeters) and depth to the By horizons for the pond profile (D, in centimeters) proposed by Retallack and Huang (2010) ($P=87.593e^{0.0209D}$), distinctly different values for mean annual precipitation are calculated for the two gypsum-bearing horizons (873 and 1075 mm). Compared to the actual mean annual precipitation (1008 mm) these values fall well outside the suggested standard deviation, indicating that data from gypsum-bearing paleosols associated with barite-

bearing paleosols may not be useful proxies for mean annual precipitation. These data should be used with caution, particularly in paleosols that developed in volcanically influenced systems (i.e., Retallack and others, 1999; Retallack and Kirby, 2007), and paleosols that contain jarosite and other sulfate minerals (e.g., Kraus, 1997; Kraus and Hasiotis, 2006).

REFERENCES

Agbenin, J.O., 1997, Sulfate retention by kaolinitic Alfisols from Nigerian savannah: Soil Science Society of America Journal, v. 61, p. 53-57.

Ajwa, H.A., and Tabatabai, M.A., 1995, Metal-induced sulfate adsorption by soils: I. effect of pH and ionic strength: Soil Science, v. 159, no. 1, p. 32-42.

Andreae, M.O., and Jaeschke, W.A., 1988, Exchange of sulphur between biosphere and atmosphere over temperate and tropical regions, *in* Howarth, R.W., Stewart, J.W.B., and Ivanov, M.V., eds., Sulphur Cycling on the Continents: Wetlands, Terrestrial Ecosystems and Associated Water Bodies: New York, John Wiley & Sons, p. 27-61.

Atun, G., and Bascetin, E., 2003, Adsorption of barium on kaolinite, illite, and montmorillonite at various ionic strengths: Radichimica Acta, v. 91, p. 223-228.

Beard, B.L., Johnson, C.M., Skulan, J.L., Nealson, K.H., Cox, L., and Sun, H., 2003, Application of Fe isotopes to tracing the geochemical and biological cycling of Fe: Chemical Geology, v. 195, no. 1-4, p. 87-117.

Beattie, J.A., and Haldane, A.D., 1984, The occurrence of palygorskite and barytes in certain parna soils of the Murrumbidgee region, New South Wales: Australian Journal of Science, v. 20, p. 274-275.

Biswas, H., Datta, S.P., and Singh, A.K., 2003, Adsorption and translocation of sulfur in some tropical acid soils: Journal of Plant Nutrition and Soil Science, v. 166, p. 519-524.

Blount, C.W., 1977, Barite solubilities and thermodynamic quantities up to 300 C and 1400 bars: American Mineralogist, v. 62, p. 942-957.

Brock-Hon, A.L., Robins, C.R., and Buck, B.J., 2012, Micromorphological investigation of pedogenic barite in Mormon Mesa petrocalcic horizons, Nevada, USA: Implications for genesis: Geoderma, v. 179-180, p. 1-8.

Brock, A.L., and Buck, B.J., 2009, Polygenetic develpment of the Mormon Mesa, NV petrocalcic horizons: geomorphic and paleoenvironmental interpretations: Catena, v. 77, p. 65-75.

Buck, B.J., Lawton, T.F., and Brock, A.L., 2010, Evaporitic paleosols in continental strata of the Carroza Formation, La Popa Basin, Mexico: record of Paleogene climate and salt tectonics: Geological Society of America Bulletin, v. 122, no. 7/8, p. 1011-1026.

Buck, B.J., and Van Hoesen, J.G., 2002, Snowball morphology and SEM analysis of pedogenic gypsum, southern New Mexico, U.S.A.: Journal of Arid Environments, v. 51, p. 469-487.

Bullock, P., Fedoroff, N., Jongerius, A., Stoops, G., Tursina, T., and Babel, U., 1985, Handbook for Soil Thin Section Description: Woverhampton, UK, Waine Research Publications, 152 p.

Carson, C.D., Fanning, D.S., and Dixon, C.J., 1982, Alfisols and Ultisols with acid sulfate weathering features in Texas, *in* Kittrick, J.A., ed., Acid Sulfate Weathering: Madison, WI, Soil Science Society of America, p. 127-146.

Chadwick, O.A., and Chorover, J., 2001, The chemistry of pedogenic thresholds: Geoderma, v. 100, p. 321-353.

Chervenka, G., 2002, Soil Survey of Brazos County, Texa, *in* United States Department of Agriculture, N.R.C.S.: College Station, United States Department of Agriculture, p. 268.

Childs, C.W., Searle, P.L., and Weatherhead, A.V., 1975, Note on occurrence of barite in B horizons of paleosols in loess, South Canterbury, New Zealand: New Zealand Journal of Science, v. 18, no. 2, p. 227-230.

Chowdhury, A.H., 2004, Hydraulic interaction between groundwater, Brazos River, and oxbow lakes: evidences from chemical and isotopic compositions, Brazos River Basin, Texas, *in* Groundwater Resources Division, T.W.D.B.: Austin, TX, p. 22.

Chu, C., Lin, C., Wu, Y., Lu, W., and Long, J., 2006, Organic matter increases jarosite dissolution in acid sulfate soils under inundation conditions: Australian Journal of Soil Research, v. 44, no. 1, p. 11-16.

Courchesne, F., Gobran, G.R., and Dufresne, A., 1995, The role of humic acid on sulfate retention and release in a podzol: Water, Air and Soil Pollution, v. 85, p. 1813-1818.

D'Angelo, E.M., and Reddy, K.R., 1999, Regulators of heterotrophic microbial potentials in wetland soils: Soil Biology and Biochemistry, v. 31, p. 815-830.

Darmoody, R.G., Harding, S.D., and Hassett, J.J., 1989, Barite authigenesis in surficial soils of mid-continental United States, *in* Miles, ed., Rock-Water Interaction: Rotterdam, p. 183-186.

Delmelle, P., and Bernard, A., 2000, Downstream composition changes of acidic volcanic waters discharged into the Banyupahit Stream, Ijen caldera, Indonesia: Journal of Volcanology and Geothermal Research, v. 97, no. 1-4, p. 55-75.

Dixon, J.B., 1991, Roles of clays in soils: Applied Clay Science, v. 5, p. 489-503.

Dowuona, G.N., Mermut, A.R., and Krouse, H.R., 1992, Stable isotopes of salts in some acid sulfate soils of North America: Soil Science Society of America Journal, v. 56, p. 1646-1653.

Drever, J.I., 1973, The preparation of oriented clay mineral specimens for X-ray diffraction analysis by a filter-membrane peel technique: American Mineralogist, v. 58, p. 553-554.

Dunham, A.C., and Hanor, J.S., 1967, Controls on barite mineralization in the western United States: Economic Geology, v. 62, p. 82-94.

Dutton, A., Wilkinson, B.H., Welker, J.M., Bowen, G.J., and Lohmann, K.C., 2005, Spatial distribution and seasonal variation in 18O/16O of modern precipitation and river water across the conterminous USA: Hydrological Processes, v. 19, p. 4121-4146.

Felmlee, J.K., and Cadigan, R.A., 1978, Spring-deposited radioactive barite in the Great Salt Lake area of Utah: U. S. Geological Survey Professional Paper, v. 38.

Fiedler, S., and Sommer, M., 2004, Water and redox conditions in wetland soils -- their influence on pedogenic oxides and morphology: Soil Science Society of America Journal, v. 68, p. 326-335.

Fitzpatrick, E.A., 1993, Soil Microscopy and Micromorphology: New York, John Wiley, 304 p.

Gambrell, R.P., 1994, Trace and toxic metals in wetlands -- a review: Journal of Environmental Quality, v. 23, p. 883-891.

Gonzalez-Munoz, M.T., Fernandez-Luque, B., Martinez-Ruiz, F., Chekroun, K.B., Arias, J.M., Rodriguez-Gallego, M., Martinez-Canamero, M., de Linares, C., and Paytan, A., 2003, Precipitation of barite by *Mycoccus xanthus*: possible implications for the biogeochemical cycle of barium: Applied and Environmental Microbiology, v. September, p. 5722-5725.

Habicht, K.S., and Canfield, D.E., 2001, Isotope fractionation by sulfate-reducing natural populations and the isotopic composition of sulfide in marine sediments: Geology, v. 29, no. 6, p. 555-558.

Hanor, J.S., 2000, Barite-celestine geochemistry and environments of formation, *in* Alpers, C.N., Jambor, J.L., and Nordstrom, D.K., eds., Sulfate Minerals: crystallography, geochemistry, and environmental significance: Washington D.C., Mineralogical Society of America, p. 193-275.

Hocking, R., 2001, Remote Quadrio Lake; a new base metal frontier?: Prospect (Perth. 1992), v. 2001, no. March, p. 24-25.

Hocking, R.M., and Pirajno, F., 2000, Quadrio Lake; we've found the barite, where are the sulfides?: Record - Geological Survey of Western Australia, p. 25-27.

Hughes, R.E., Moore, D.M., and Reynolds, J., R.C., 1993, The nature, detection, occurrence, and origin of kaolinite/smectite, *in* Kaolin genesis and utilization: a collection of papers presented at the Keller '90 Kaolin Symposium, p. 291-323.

Hutchinson, K.J., Hesterberg, D., and Chou, J.W., 2001, Stability of reduced organic sulfur in humic acid as affected by aeration and pH: Soil Science Society of America Journal, v. 65, p. 704-709.

Jackson, M.L., Lim, C.H., and Zelazny, W., 1986, Oxides, hydroxides, and aluminosilicates, *in* Klute, A., ed., Methods of Soil Analysis, Part I -- Agronomy Monograph 9: (2nd ed.) Madison, Wisconsin, American Society of Agronomy, Inc., p. 101-142.

Jacobs, P.M., West, L.T., and Shaw, J.N., 2002, Redoximorphic features as indicators of seasonal saturation, Lowndes County, Georgia: Soil Science Society of America Journal, v. 66, p. 315-323.

Jennings, D., Lovelace, D., and Driese, S.G., 2011, Differentiating paleowetland subenvironments using a multi-disciplinary approach: An example from the Morrison formation, South Central Wyoming, USA: Sedimentary Geology, v. 238, p. 23-47.

Jones, E., J.P., Nadeau, T.-L., Voytek, M.A., and Landa, E., R., 2006, Role of microbial iron reduction in the dissolution of iron hydroxysulfate minerals: Journal of Geophysical Research, v. 111, no. G01012, p. 1-8.

Jorgensen, R.R., 1983, The microbial sulphur cycle, *in* Krumbein, W.E., ed., Microbial Geochemistry: Oxford, Blackwell Science Ltd, p. 91-124.

Kabata-Pendias, A., 2001, Trace Elements in Soils and Plants (3rd ed.): New York, CRC Press, 432 p.

Kirkland, J.I., 2006, Fruita paleontological area (Upper Jurassic, Morrison Formation), western Colorado; an example of terrestrial taphofacies analysis: Bulletin - New Mexico Museum of Natural History and Science, v. 36, p. 67-95.

Kraus, M.J., 1997, Lower Eocene alluvial paleosols: pedogenic development, stratigraphic relationships, and paleosol/landscape associations: Palaeogeography, Palaeoclimatology, Palaeoecology, v. 129, p. 387-406.

Kraus, M.J., and Hasiotis, S.T., 2006, Significance of different modes of rhizolith preservation to interpreting paleoenvironemtns and paleohydrological setting: examples from Paleogene paleosols, Bighorn Basin, Wyoming, U.S.A: Journal of Sedimentary Research, v. 76, p. 633-646.

Krouse, H.R., Stewart, J.W.B., and Grinenko, V.A., 1991, Pedosphere and Biosphere, *in* Krouse, H.R., and Grinenko, V.A., eds., Stable Isotopes in the Assessment of Natural and Anthropogenic Sulphur in the Environment: John Wiley & Sons, Ltd, p. 267-306.

Kunze, G.W., and Oakes, H., 1957, Field laboratory studies of the Lufkin soil, a planosol: Soil Science Society of America Proceedings, v. 21, p. 330-335.

Lynn, W.C., Tu, H.Y., and Franzmeier, D.P., 1971, Authigenic barite in soils: Soil Science Society of America Journal Proceedings, v. 35, p. 160-161.

Lyons, W.B., Hines, M.E., Last, W.M., and Lent, R.M., 1994, Sulfate reduction rates in microbial mat sediments of differing chemistries: implications for organic carbon preservation in saline lakes, Sedimentology and Geochemistry of Modern and Ancient Saline Lakes, SEPM Publication: SEPM (Society for Sedimentary Geology), p. 13-20.

Martino, D.P., Grossman, E.L., Ulrich, G.A., Schlichenmeyer, J.L., Suflita, J.M., and Ammerman, J.W., 1998, Microbial abundance and activity in a low-conductivity aquifer system in east-central Texas: Microbial Ecology, v. 35, p. 224-234.

McCarthy, P.J., and Plint, A.G., 2003, Spatial variability of palaeosols across Cretaceous interfluves in the Dunvegan Formation, NE British Columbia, Canada: palaeohydrological, palaeogeomorphological and stratigraphic implications: Sedimentology, v. 50, p. 1187-1220.

Moore, D.M., and Reynolds, R.C., 1997, X-ray Diffraction and the Identification and Analysis of Clay Minerals: New York, Oxford University Press, 378 p.

NCDC, 2012, Climatography of the United States, No. 20, National Oceanic & Atmospheric Administration, v. 2011.

NRCS, 2010, NRCS Soils Website, http://soils.usda.gov/.

Podwojewski, P., 1995, The occurrence and interpretation of carbonate and sulfate minerals in a sequence of Vertisols in New Caledonia: Geoderma, v. 65, no. 3-4, p. 223-248.

Pons, L.J., 1973, Outline of the genesis, characteristics, classification and improvement of acid sulphate soils, *in* Acid Sulphate Soils, Proceedings of the International Symposium, Wageningen, The Netherlands, International Land Reclamation Insititute, p. 3-27.

Rao, S.M., and Sridharan, A., 1984, Mechanism of sulfate adsorption by kaolinite: Clays and Clay Minerals, v. 32, no. 5, p. 414-418.

Retallack, G.J., Bestland, E.A., and Fremd, T.J., 1999, Eocene and Oligocene Paleosols of Central Oregon, Geological Society of America, Inc., v. Special Paper no. 344, 192 p.

Retallack, G.J., and Huang, C., 2010, Depth to gypsic horizon as a proxy for paleoprecipitation in paleosols of sedimentary environments: Geological Society of America Bulletin, v. 38, no. 5, p. 403-406.

Retallack, G.J., and Kirby, M.X., 2007, Middle Miocene global change and paleogeography of Panama: Palaios, v. 22, p. 667-679.

Routh, J., McDonald, T.J., and Grossman, E.L., 1999, Sedimentary organic matter sources and depositional environment in the Yegua formation (Brazos County, Texas): Organic Geochemistry, v. 30, p. 1237-1453.

Sanchez-Pastor, N., Pina, C.M., and Fernandez-Diaz, L., 2006, Relationship between crystal morphology and composition in the (Ba, Sr)SO_4--H_2O solid solution -- aqueous solution system: Chemical Geology, v. 225, p. 266-277.

Scarciglia, F., Barca, D., De Rosa, R., and Pulice, I., 2009, Application of laser ablation ICP-MS and traditional micromorphological techniques to the study of an Alfisol (Sardinia, Italy) in thin sections: Insights into trace element distribution: Geoderma, v. 152, p. 113-126.

Seal, I., Robert R., Alpers, C.N., and Rye, R.O., 2000, Stable isotope systematics of sulfate minerals, *in* Alpers, C.N., Jambor, J.L., and Nordstrom, D.K., eds., Sulfate minerals: crystallography, geochemistry, and environmental significance: Washington D.C., Mineralogical Society of America, p. 541-602.

Senkayi, A.L., Dixon, J.B., Hossner, L.R., Abder-Ruhman, M., and Fanning, D.S., 1984, Mineralogy and genetic relationships of tonstein, bentonite, and lignitic strata in the Eocene Yegua Formation of East-central Texas: Clays and Clay Minerals, v. 32, no. 4, p. 259-271.

Senko, J.M., Campbell, B.S., Henriksen, J.R., Elshahed, M.S., Dewers, T.A., and Krumholz, L.R., 2004, Barite deposition resulting from phototrophic sulfide-oxidizing bacterial activity: Geochemica et Cosmochimica Acta, v. 68, no. 4, p. 773-780.

Serrano, R.E., Arias, J.S., and Fernandez, P.G., 1999, Soil properties that affect sulphate adsorption by Palexerults in western and central Spain: Communications in Soil Science and Plant Analysis, v. 30, no. 9&10, p. 1521-1530.

Sharpley, A.N., 1990, Kinetics of sulfate desorption from soil: Soil Science Society of America Journal, v. 54, p. 1571-1575.

Singer, A., 1984, The paleoclimatic interpretation of clay minerals in sediments -- a review: Earth-Science Reviews, v. 21, p. 251-293.

Smith, E., Hamilton-Taylor, J., Davison, W., Fullwood, N.J., and McGrath, M., 2004, The effect of humic substances on barite precipitation-dissolution behaviour in natural and synthetic lake waters: Chemical Geology, v. 207, no. 1-2, p. 81-89.

Smolders, A.J.P., Moonen, M., Zwaga, K., Lucassen, E.C.H.E.T., Lamers, L.P.M., and Roelofs, J.G.M., 2006, Changes in pore water chemistry of desiccating freshwater sediments with different sulphur contents: Geoderma, v. 132, p. 372-383.

Stevenson, F.J., and Cole, M.A., 1999, Cycles of Soil: carbon, nitrogen, phosphorus, sulfur, micronutrients: New York, John Wiley & Sons, Inc., 427 p.

Stiles, C.A., Mora, C.I., and Driese, S.G., 2001, Pedogenic iron-manganese nodules in Vertisols: a new proxy for paleoprecipitation?: Geology, v. 29, no. 10, p. 943-946.

Stoffregen, R.E., Alpers, C.N., and Jambor, J.L., 2000, Alunite-jarosite crystallography, thermodynamics, and geochronology, *in* Alpers, C.N., Jambor, J.L., and Nordstrom, D.K., eds., Sulfate Minerals: Crysallography, Geochemistry, and Environmental Significance: Washington, DC, The Mineralogical Society of America, p. 453-479.

Stoops, G., and Poch, R.M., 1985, Micromorphological classification of gypsiferous soil materials, *in* IX International Working Meeting on Soil Micromorphology, Townsville, Australia, Developments in Soil Science, Elsevier, p. 327-332.

Stoops, G., and Zavaleta, A., 1978, Micromorphological evidence of barite neoformation in soils: Geoderma, v. 20, no. 1, p. 63-70.

Sullivan, L.A., and Koppi, A.J., 1993, Barite pseudomorphs after lenticular gypsum in a buried soil from Central Australia: Australian Journal of Soil Research, v. 31, p. 393-396.

---, 1995, Micromorphology of authigenic celestobarite in a duripan from central Australia: Geoderma, v. 64, no. 3-4, p. 357-361.

Triplehorn, D.M., Blake, B.M., and Anonymous, 2001, Authigenic barite precipitated in Paleosols below marine transgressions: Abstracts with Programs - Geological Society of America, v. 33, no. 6, p. 445.

Trust, B.A., and Fry, B., 1992, Stable sulphur isotopes in plants: a review: Plant, Cell, and Environment, v. 15, p. 1105-1110.

Turchyn, A.V., Bruchert, V., Lyons, T.W., Engel, G.S., Balci, N., Schrag, D.P., and Brunner, B., 2010, Kinetic oxygen isotope effects during dissimilatory sulfate reduction: a combined theoretical and experimental approach: Geochimica et Cosmochimica Acta, v. 74, p. 2011-2024.

Turchyn, A.V., and Schrag, D.P., 2006, Cenozoic evolution of the sulfur cycle: insight from oxygen isotopes in marine sulfate: Earth and Planetary Science Letters, v. 241, p. 763-779.

Ulrich, G.A., Burger, K., Routh, J., Grossman, E.L., Ammerman, J.W., and Suflita, J.M., 1998, Sulfur cycling in terrestrial subsurface: commensal interactions, spatial scales, and microbial heterogeneity: Microbial Ecology, v. 36, p. 141-151.

Van Den Ende, J., 1991, Supersaturation of soil solutions with respect to gypsum: Plant and Soil, v. 133, p. 65-74.

Van Stempvoort, D.R., Reardon, E.J., and Fritz, P., 1990, Fractionation and sulfur and oxygen isotopes in sulfate soil by sulfate sorption: Geochimica et Cosmochimica Acta, v. 54, p. 2817-2826.

White, P.D., and Schiebout, J., 2008, Paleogene paleosols and changes in pedogenesis during the initial Eocene thermal maximum: Big Bend National Park, Texas, USA: Geological Society of America Bulletin, v. 120, p. 1347-1361.

Zang, P.-C., Brady, P.V., Arthur, S.E., Zhou, W.-Q., Sawyer, D., and Hesterberg, D., 2001, Adsorption of barium (II) on montmorillonite: an EXAFS study: Colloids and Surfaces A: Physicochemical and Engineering Aspects, v. 190, p. 239-249.

CHAPTER FOUR

Comparison of Modern and Ancient Barite-bearing Acid-sulfate Soils Using Micromorphology, Geochemistry, and Field Relationships

This is the pre-peer-reviewed version of the article which has been accepted for publication *Sedimentology*

Abstract

Although pedogenic barite has been documented in many modern soils and paleosols, no actualistic studies on its formation have been reported. Because barite is stable over the entire range of pressure and temperature of the earth's crust, it preserves reliable data about the original environment in which it formed. Pedogenic barite and barite-bearing soils have been used as indicators of landscape stability, environmental conditions, climate, and microbial activity. This study compares field data, micromorphology, and stable isotope geochemistry of a barite-bearing paleosol from the Morrison Formation (Jurassic) and a modern analog soil in south-central Texas, USA. Morrison barite-bearing paleosols are over-thickened cumulic paleosols that developed in subaerially exposed lacustrine sediments during an extended lake contraction event. Lateral facies relationships document changes in hydrology and duration of episaturated conditions that correspond to differences in barite nodule morphology and abundance. Barite precipitation occurred at a redox boundary higher on the landscape after organic matter was completely oxidized. Sulfur isotope data indicate that the initial source of sulfur was soil organic matter. Meteoric water is the likely source of oxygen for the

sulfate. Barium sourced from weathering feldspars and clays. The modern analog displays similar catenary relationships, redox features, and micromorphological characteristics compared to the Morrison paleosols, suggesting that similar pedogenic processes led to barite precipitation. Synthesized data suggest that conditions favorable to barite-bearing soil formation are low-gradient basins that have received feldspar-rich sediments (i.e. volcanically influenced basins), soils that developed near salt domes, soils that developed in exposed wetland or lacustrine sediments, and coastal plain deposits. When studied in a well-documented paleogeographic context, barite-bearing soils are valuable to paleoclimate, paleoenvironmental, and paleohydrological studies. Combined with regional interfluve paleosols, barite-bearing paleosols may document temporal changes in drainage, surface stability, and accommodation consistent with sequence boundaries/maximum flooding surfaces, and climate changes.

Introduction

Once thought to be a rare phenomenon, barite-bearing soils and paleosols have been receiving increasing attention in the literature (see summary Table 4.1). Whereas large volumes of barite precipitated in early Archean oceans and their understanding has provided important constraints on early ocean and atmospheric chemistry (Strauss, 1997; Huston and Logan, 2004), the use of pedogenic barite formed in terrestrial systems for paleoenvironmental reconstructions has been less common. Pedogenic barite documented previously in many modern soils and paleosols has been used as indicators of landscape stability, environmental conditions, climate, and microbial activity. Barite may also precipitate in lakes (Felmlee and Cadigan, 1978; Finlay and others, 1983; Garces and

Table 4. 1. Examples of barite-bearing paleosols and soils.

Age	Formation	Location	Reference
Modern soils		Texas, Illinois, Indiana Louisiana, USA	(Carson et al., 1982; Crum and Franzmeier, 1980; Darmoody et al., 1989; Jones, 1986; Lynn et al., 1971)
		Peru	(Stoops and Zavaleta, 1978)
		Australia	(Beattie and Haldane, 1984; Sullivan and Koppi, 1995)
Quaternary	Pampean loess	Argentina	(Cumba and Imbellone, 2004)
	Loess	New Zealand	(Childs et al., 1975)
	Muddy Creek Fm.	Nevada, USA	
Eocene	Carroza	La Popa, Mexico	(Buck et al., 2010)
	Canoe	Big Bend, Texas, USA	(White and Schiebout, 2008)
Cretaceous/Paleocene	Dasdap beds	South Africa	(Brandt et al., 2005)
K/T boundary	Javelina	Texas, USA	(Schmidt, 2009)
Cretaceous	Dunvegan	Canada	(McCarthy and Plint, 2003)
Jurassic/Cretaceous	Morrison	Wyoming, USA	(Baar et al., 2005; Jennings et al., 2011; Jennings and Hasiotis, 2006)
		Colorado, USA	(Kirkland, 2006)

Aguilar, 1994; Hocking and Pirajno, 2000; Aspler and others, 2004; Jennings and others, 2011) and associated wetland soils (Jennings and others, 2011). Low-temperature barite typically precipitates as sulfate-rich and barium-rich fluids mix (Hanor, 2000), as a result of persistent fluctuating redoximorphic conditions, and as a result of microbially induced early diagenetic processes (Gonzalez-Munoz and others, 2003; Senko and others, 2004; Bonny and Jones, 2008; Jennings and others, 2011) on stable landscapes. Although many barite-bearing soils and paleosols have been documented and employed in a variety of studies such as sequence stratigraphy (Plint and others, 2001), paleoclimate studies (Retallack and Kirby, 2007), and paleoenvironmental reconstruction (Brock and Buck, 2009; Buck and others, 2010; Jennings and others, 2011), we are aware of no direct (i.e.,

actualistic) comparisons between modern and ancient barite-bearing soils. Indeed, for many paleosol researchers the genesis of pedogenic barite is an enigma and thus our study will contribute significant insights towards a long-standing problem.

Taxonomic uniformitarianism (sensu, Lovely and others, 1998) is fundamental to understanding and accurately interpreting paleopedogenic process and ancient landscape development. One particular limitation to taxonomic uniformitarianism is that it may be difficult to establish that pedogenic processes that occurred in paleosols and soils are truly analogous. However, barite-bearing soils are unique in that the conditions that lead to pedogenic barite precipitation may be documented by micromorphological features and geochemical data, specifically stable isotope geochemistry, which is little-affected by diagenetic overprinting (Lovely and others, 1998; Seal and others, 2000). The physicochemical stability of barite under nearly the entire range of pressure and temperature of the earth's crust makes pedogenic barite particularly useful for identifying the source of soil sulfur (Hanor, 2000). In addition to a source of free sulfate, barite precipitation also requires an adequate amount of barium in the parent material. The modern and ancient soil examples investigated in this paper developed in terrigenous sediments up-gradient from a standing body of water (Darmoody and others, 1989; Jennings and others, 2011; Jennings and Driese, 2014) and outside the influence of marine sulfate sources, making delineation of sulfur and barium sources less tenuous. Micromorphological data and lateral facies relationships document the composition of the parent material, possible biogenic activity, and hydrological conditions that prevailed during pedogenesis (Richardson and Brinson, 2001; Vepraskas, 2001; Vepraskas and Faulkner, 2001). The purpose of this study is to compare the field data,

micromorphology, and stable isotope geochemistry of a barite-bearing paleosol and a modern analog soil. Specifically, we will test the hypothesis that barite-bearing paleosols from the Upper Jurassic Morrison Formation in north-central Wyoming, USA and the Lufkin soil series in south-central Texas developed under similar pedogenic conditions by comparing data that are the least susceptible to the influences of diagenesis (Lovely and others, 1998; Seal and others, 2000).

Background Information

During the Late Jurassic-Early Cretaceous, the Morrison depositional basin lay midway between a subduction zone to the west and the retreating marine coastline to the northeast (Lawton, 1994a) and spanned more than 1.5×10^6 km^2 (Fig. 4.1). The Morrison study area is located near the center of the Morrison basin in north-central Wyoming. Increased sedimentation from plinian eruptions and uplift along the developing Andean-type magmatic arc increased siliciclastic input exponentially. Reworked, fine-grained, volcaniclastic material was delivered to the area by punctuated volcanic events in the volcano-plutonic arc source area to the west (Blue Mountains and the Salmon River belt) as the back bulge migrated to the east (DeCelles, 2004; Gray and Oldow, 2005; Swartz and others, 2011). Subsequent thrust faulting and folding contributed to continued lacustrine development in semi-isolated to isolated basins throughout the Western Interior (Dunagan, 2000).

A detailed paleoenvironmental reconstruction of the study area during the latest Jurassic indicates that barite-bearing paleosols developed in exposed alkaline-saline lake deposits during an extended time of landscape stability and lake contraction (Jennings et

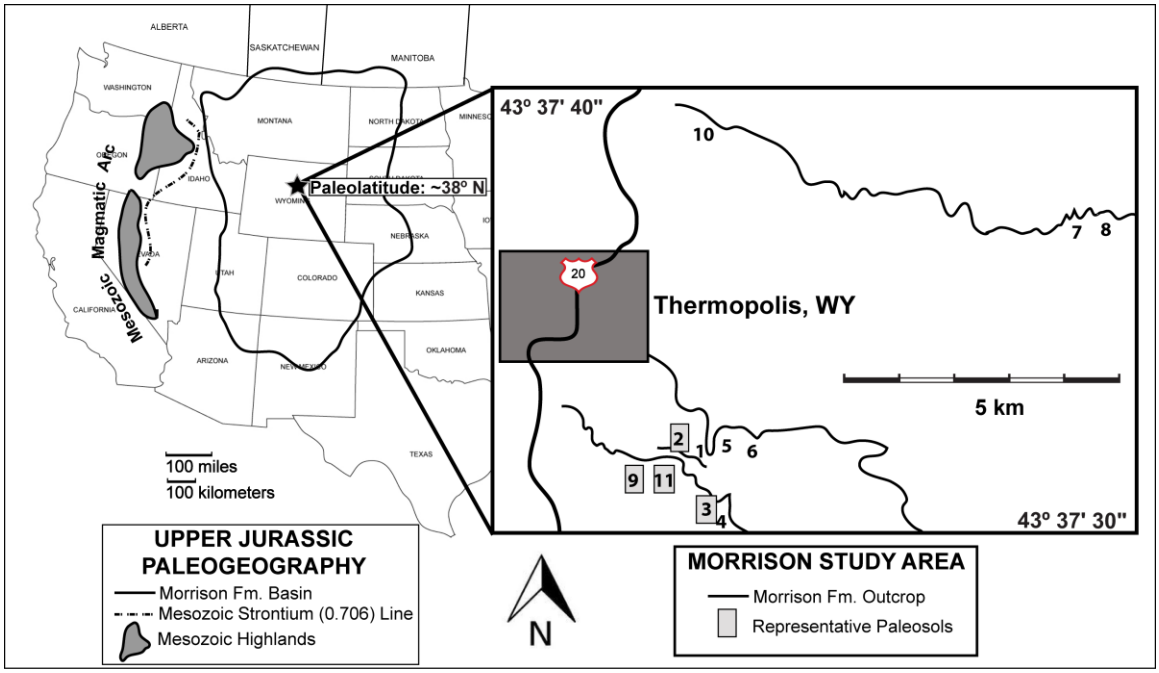

Figure 4.1. Location map for Morrison Formation paleosols (black star). Paleogeographic map modified from Elison et al., (1990) and Swartz et al., (2011). Measured stratigraphic sections are numbered. Representative paleosol profiles described from sections 2, 3, 9, and 11. Latest Jurassic marine deposits were located west of the magmatic arc and in what is now northern Canada.

al., 2011). Jennings et al. (2011) also documented that high evapotranspirative stress in a semi-arid climate regime resulted in gypsum precipitation in low-lying marshy areas adjacent to the lake body. Millimeter- to cm-scale pedogenic barite nodules precipitated in paleosols that developed in topographically higher areas during an extended lake contraction event. The overall topography was low-gradient, resulting in sluggish drainage conditions. Fluctuating groundwater levels resulted in saturated, reducing conditions alternating with dry, oxidizing conditions, which had a major impact on soil chemistry, particularly pH conditions. Mobile Fe^{2+} (potentially competing for S species) was translocated down-gradient and accumulated in less well-drained soils as Fe mottles and concentrations.

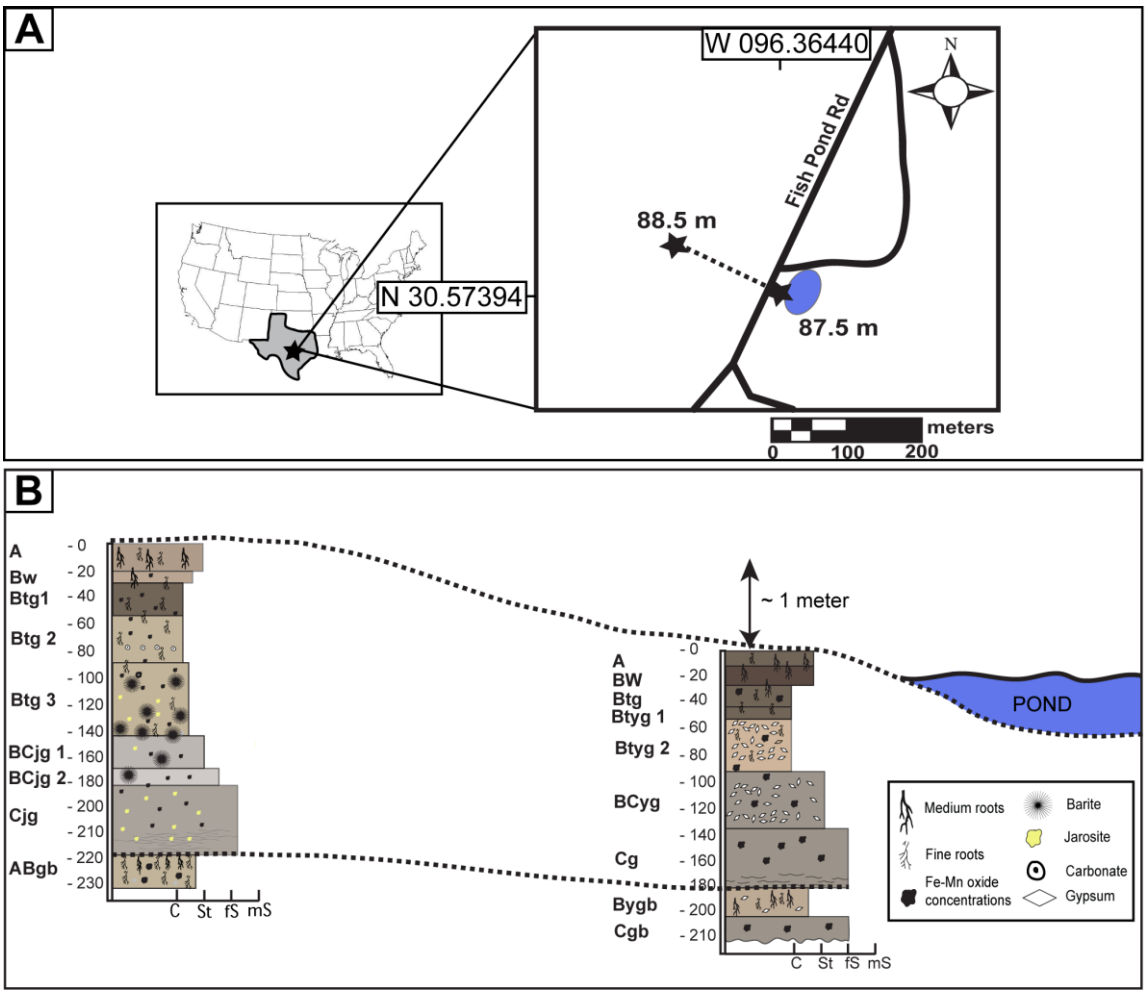

Figure 4.2. Lufkin location map and profiles. A) Lufkin soil location map. The barite-bearing profile is 88.5m above sea level. The profile collected adjacent to the existing pond is 87.5m above sea level. B) Soil profiles along a toposequence. Approximately 1 meter of elevation change occurs between the upper profile (left) and the profile adjacent to the pond.

The analog surface soil is the Lufkin series located in south-central Texas (Fig. 4.2 A). The Lufkin series is classified as a fine, smectitic, thermic, vertic, Albaqualf according to USDA Soil Taxonomy (NRCS, 2010). The Lufkin series developed in reworked slightly acid to alkaline, fine- to medium-grained sand, silt, and carbonaceous clay, and lignitic nearshore to terrestrial, coastal plain sediments of the Eocene Yegua Formation (Jennings and Driese, 2014). The Yegua aquifer is anaerobic at shallow depths (< 30 m) because of slow recharge and low hydraulic conductivity (Martino and others,

1998). Yegua groundwater is fresh to somewhat saline. The Lufkin soil profiles in this study occur in erosional uplands that have a 1-4% slope. Vegetation in wooded portions of the study area is dominated by scrub post oak and live oak. The climate in this area is moist subhumid with a mean annual precipitation (MAP) of 1008 mm and a mean annual temperature (MAT) of 20° C classified as thermic (NRCS, 2010). A temporary perched water table occurs above Btg horizons during rainy periods. Surface horizons may remain saturated for weeks at a time from November to May during times of reduced water utilization by plants and lower evaporative rates. Dry conditions dominate from May to November. Surface runoff is slow to very slow. Although soil profiles in nearby areas display gilgai relief, indicating high shrink-swell activity, no pedogenic slickensides are observed (Routh and others, 1999; NRCS, 2010). The A and uppermost Btg horizons are typically slightly to strongly acidic (pH = 5.3-6.7). Lower Btg horizons range from slightly acidic to slightly alkaline (pH = 6.9-7.7). BC and C-horizons are slightly to moderately alkaline (pH = 7.5-7.9) (NRCS, 2010). Geochemical and microbiological studies reveal that both sulfate-reducing (SRB) and sulfur-oxidizing (SOB) bacteria commonly occupy the soil zone (Martino and others, 1998).

Site locations and Methodology

Morrison Formation Paleosols

The Morrison study area is located on the Warm Springs Ranch and adjacent Bureau of Land Management (BLM) lands near Thermopolis, Wyoming, at the southeastern most corner of the Bighorn Basin (Fig. 4.1). Descriptions of representative barite-bearing profiles were measured and described from freshly excavated trenches of outcrops. Profile descriptions include unit thickness, sedimentary structures, pedogenic

features, grain size, body and trace fossils, and color. Colors were described using a Munsell rock-color chart. Rock samples of the matrix and pedogenic minerals were collected from each unit for geochemical analyses and thin section preparation. Thin sections from each horizon, representative barite nodules, and associated carbonates were analyzed using methods describe by Bullock et al., (1985) and Fitzpatrick (1993). Gold-coated chips from representative barite nodules were imaged with a Leo 1550 field-emission scanning electron microscope at Baylor University.

Stable sulfur and oxygen isotope analyses were conducted on 100 samples from 29 barite nodules at the University of Arizona Environmental Isotope Laboratory. Preliminary samples were collected from the center of each nodule. Additional samples were collected systematically across the nodule. Samples were harvested with a dremel tool with a diamond tip that was cleaned between each sample to limit contamination. Values of $\delta^{34}S$ were measured for SO_2 gas in a continuous-flow gas-ratio mass spectrometer (ThermoQuest Finnigan Delta PlusXL). Precision is estimated as ± 0.15‰ or better, based on repeated internal standards. Values of $\delta^{18}O$ were measured on a continuous-flow gas-ratio mass spectrometer (ThermoQuest Finnigan Delta PlusXL). Standardization is based on international standards. Values for $\delta^{18}O$ are reported relative to VSMOW (Vienna Standard Mean Ocean Water) and $\delta^{34}S$ values are reported relative to VCDT (Vienna Canyon Diablo Troilite).

Select barite powders were treated with 2N HCl to destroy any carbonate minerals. Exchangeable Sr was then removed using 1N ammonium acetate. Barite was dissolved by chelation in cation exchange resin at 90°C (*sensu*, Church, 1970). The cations were stripped from the resin and strontium was separated using conventional ion

chromatography. Once Sr was isolated is was placed onto tantalum filaments and measured for isotope abundances on a Finnigan MAT 261 mass spectrometer at the Department of Geological Sciences at the University of Texas at Austin. Fractionation was corrected by assuming $^{86}Sr/^{88}Sr = 0.1194$ and employing an exponential fractionation law. Precision on all analyses is less than 0.000020. The average measured value for NIST-SRM 987 during the course of this analysis was 0.710257 (n=7).

Lufkin Soil

Two long cores (~5 cm diameter) were collected using a truck-mounted Giddings probe along a toposequence in south-central Texas, approximately 1km southeast of Easterwood Airport near the Texas A&M University campus in College Station (Fig. 4.2 A). The first core was collected adjacent to a pond at an elevation of 87.5 m. The second core was collected from a wooded area approximately 250 meters west of the pond at an elevation of 88.5 m. After the cores were air-dried and stabilized with epoxy, they were slabbed with a dry tile saw. Profile descriptions were compiled from a dry core. A Munsell soil color chart was used to document matrix and mottle colors. Samples of each horizon were collected from the middle of each core for thin section analyses. Thin sections from each horizon, representative barite nodules, and associated carbonates were analyzed using methods describe by Bullock et al., (1985) and Fitzpatrick (1993).

Samples of free sulfate were collected from whole-soil samples (sensu, Van Stempvoort and others, 1990). Soil material was rinsed with distilled water and the supernatant liquid was poured through an 80µm mesh sieve and centrifuged to remove clay-sized particles. Sulfate was desorbed with 0.5 M NaCl and then precipitated as barite by adding 0.5 M $BaCl_2$ solution. Barite was filtered through a 0.45µm membrane, dried,

and removed from the membrane. This procedure was repeated until no additional barite precipitated from solution.

Barite and gypsum were handpicked from whole-soil samples, rinsed with distilled water, and mineralogy was verified with X-ray Diffraction (XRD) before analysis. Jarosite-bearing soil material with water-soluble sulfate removed was immersed in 1 M NaOH solution, heated to 50-60°C, and then allowed to cool and settle. Decanted liquid was filtered to remove any remaining sediment. Dissolved sulfate was precipitated from solution as barite by adding $BaCl_2$. Barite was then filtered through 0.45µm membrane, dried, and collected from the membrane.

All stable sulfur and oxygen isotope analyses were conducted at the University of Arizona Environmental Isotope Laboratory. Values of $\delta^{34}S$ were measured for SO_2 gas in a continuous-flow gas-ratio mass spectrometer (ThermoQuest Finnigan Delta PlusXL). Precision is estimated as ±0.15‰ or better, based on repeated internal standards. Values of $\delta^{18}O$ were measured on a continuous-flow gas-ratio mass spectrometer (ThermoQuest Finnigan Delta PlusXL). Standardization is based on international standard OGS-1. Precision is estimated as ±0.3‰ or better, based on repeated standards. Values for $\delta^{18}O$ are reported relative to VSMOW (Vienna Standard Mean Ocean Water) and $\delta^{34}S$ values are reported relative to VCDT (Vienna Canyon Diablo Troilite).

Radiocarbon dating was conducted on a sample from the uppermost horizon of the underlying buried soil (ABgb) of the barite-bearing profile by accelerator mass spectrometry at Beta Analytical Inc. The sample was sieved to < 180 microns to remove any roots or microfossils and then acid washed to remove carbonates. The Measured Radiocarbon Age was corrected for isotopic fractionation, and calculated using the

$\delta^{13}C_{PDB}$. Results are reported as radiocarbon years before present (RCYBP -- "present" = AD 1950).

Soil and Paleosol Description

Macromorphology of Morrison Formation Paleosols

Jennings et al., (2011) documented 4 barite-bearing paleosols (pedotype C, D, E, and F) and one gypsic paleosol (pedotype G) that can be traced along a roughly west to east transect (Figs. 4.1and 4.3A). Pedotype C is a palustrine paleosol that occurs slightly lower in the section than pedotypes D, E, F, and G. Relative stratigraphic positions and lateral relationships are illustrated on the stratigraphic sections in Fig. 4.3A. Representative paleosol profiles are shown in Fig. 4.3 B. The most abundant, best developed, typic nodules occur in the west and smaller, less abundant and less well-developed, barite nodules towards the east. Parent material for all but pedotype C was sandy to silty, lacustrine and wetland sediments that were subaerially exposed during an extended period of lake-level lowering and contraction (Fig. 4.4A). Embayed quartz grains, potassium feldspar, and plagioclase are the most common framework grains (Fig. 4.4A inset). Clay and patchy calcite clay are also present.

Fine-grained barite nodules in pedotype C are commonly packed around dinosaur bones and sometimes contain bone inclusions (Fig. 4.4C). These nodules are the largest, ranging from ~3.5 to 13.0 cm long and 3.0 to 6.7 cm wide. Nodules are compacted parallel to bedding and sediments are differentially compacted around them. Larger barite nodules display vertical to subvertical desiccation cracks filled with calcite and coarser-grained barite. Above the B/Cg horizon a distinct Bkg horizon with bone fragments and a Btg horizon with slickensides, burrows, and root traces complete the profile (Fig. 4.3 B).

Pedotypes D, E, F, and G vary in thickness from 1-6 m and are composed of stacked B-horizons with mottles and matrices that vary in color. Pedotype D is characterized by stacked, black horizons, with common disarticulated dinosaur bones, well preserved tree trunks, and scattered, circular barite nodules (1.0-3.0 cm diam.). Slickensides are observed in uppermost, silty Bw horizons in paleosols that developed higher on the paleolandscape (pedotype E). Greenish-gray (10Y 5/1), weak red (10R 4/2), and light greenish-gray (10Y 7/1) mottles are abundant (Fig. 4.4 B inset). Matrix color in Bt horizons varies from grayish-purple to grayish red-purple (5P4/2; 5P6/2; 5RP4/2). Mottles are less abundant in the Bt horizons and generally are greenish-gray (10Y 5/1). Btk horizons contain decimeter-scale, cone-shaped or ovoid carbonate steinkerns with barite cores and large clusters of cm-scale, micritic carbonate nodules (Jennings et al., 2011). Illuviated illite-rich clay fills cracks between clusters of carbonate nodules. Depleted mottles are common. Bg horizons that underlie barite-bearing horizons are characterized by a silty, greenish-gray (10Y 5/1) matrix with dark purple-gray (5P 5/1) mottles. Fragmented clay skins are common in these Bg horizons. Lowermost 2Bg horizons contain grayish-green (10Y 4/2) mottles.

Barite-bearing paleosols that developed in argillaceous, fine-grained sandstone lower on the paleolandscape (pedotype F) are characterized by 4.0-4.5 m thick intervals of stacked B-horizons with mottles that developed in greenish-black (5GY 5/1) to greenish-gray (10GY 5/1) matrices. Barite nodules that precipitated in this paleosol range from 2.0-5.0 cm in diameter, display a rough exterior, and are finer-grained than other pedogenic barite nodules in the area.

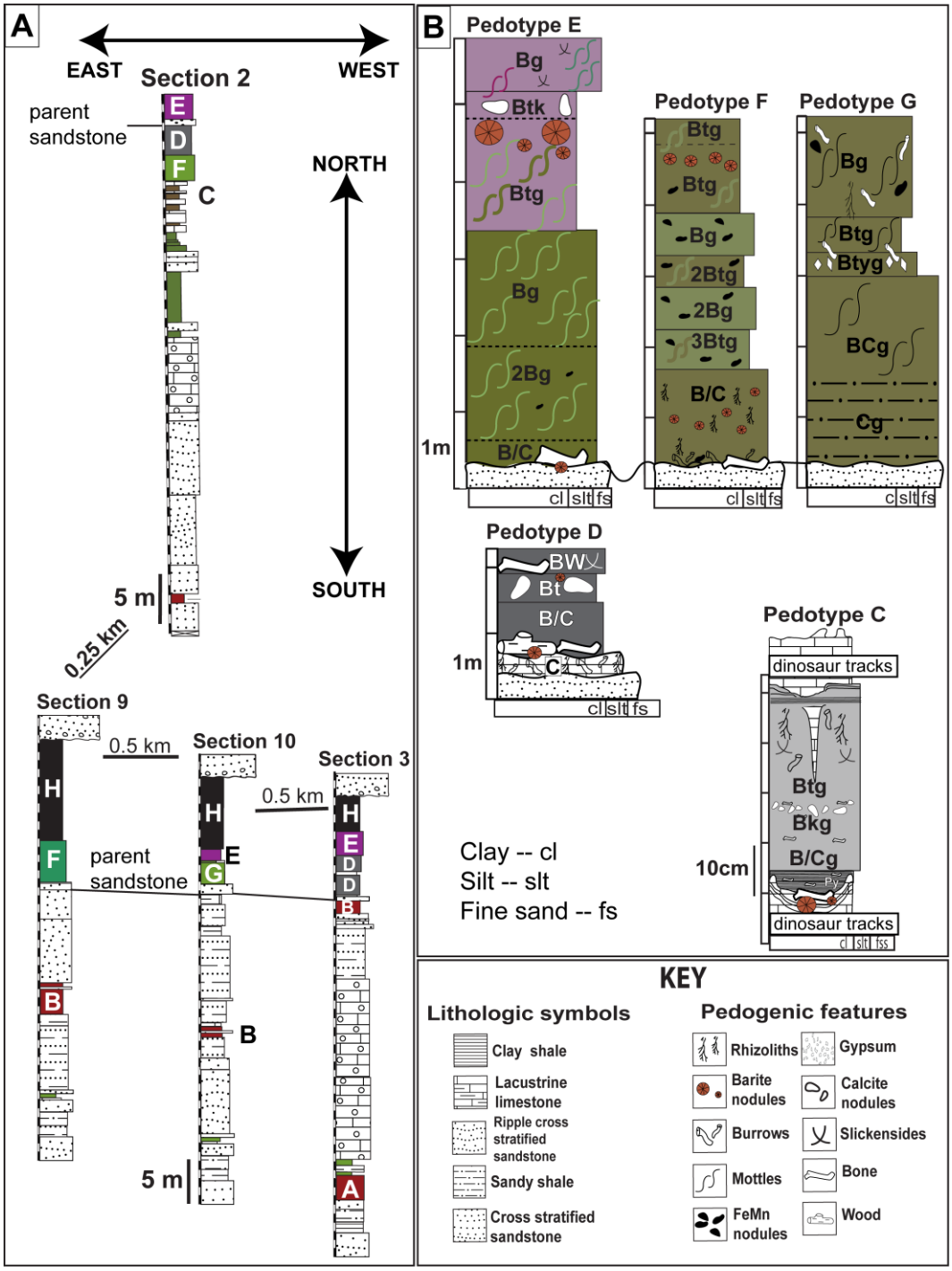

Figure 4.3. Relative stratigraphic position of barite- and gypsum-bearing paleosols. Correlative parent sandstone is correlated along strike. Pedotype C occurs slightly lower than pedotypes D, E, F, and G. A) Morrison barite-bearing and gypsiferous paleosols occur laterally adjacent to lacustrine deposits. B) Paleosol profiles.

Pedotype G occurs laterally adjacent to pedotype F and is characterized by Cg/BCg/Btyg/ Btg/Bg profile. Burrows, root traces, light greenish gray mottles and FeMn nodules are common. No barite nodules are not documented in this pedotype; however, calcite-replaced gypsum crystals are common.

Micromorphology of Morrison Formation paleosols

Morrison Fm. barite nodules are composed of micron-scale, interlocking barite crystals with the coarsest crystals near the center of the nodule (Fig. 4.5A). Nodules commonly contain matrix and quartz silt inclusions (Fig. 4.5A) and micrometer-scale Fe-Mn masses or oxidized pyrite grains (Jennings and others, 2011). SEM images reveal mineralized filaments in barite nodules similar to those documented in experimental studies (Bonny and Jones, 2008) of bacterially mediated barite precipitation (Fig 4.5B). Euhedral pyrite grains with diffuse hypocoatings arelocally present in the siliceous parent material (Jennings and others, 2011). Potassium feldspar grains are scattered throughout all profiles.

Depleted zones and Fe-Mn nodules with irregular (diffuse) boundaries are common in most Bg horizons (Fig. 4.5C). Reworked clay skins are common in siltier Bg horizons (Fig. 4.5D). Btg-horizons contain mm-scale, barite rhizoliths. Many rhizoliths have an Fe-Mn center (Fig. 4.5E) from which fine-grained barite radiates. Dogtooth calcite spar cement fills pores between granular peds in upper horizons. Photomicrographs of adjacent, poorly developed paleosols with no barite nodules (pedotype G) contain abundant calcite pseudomorphs after gypsum in macropores (Fig 4.5F).

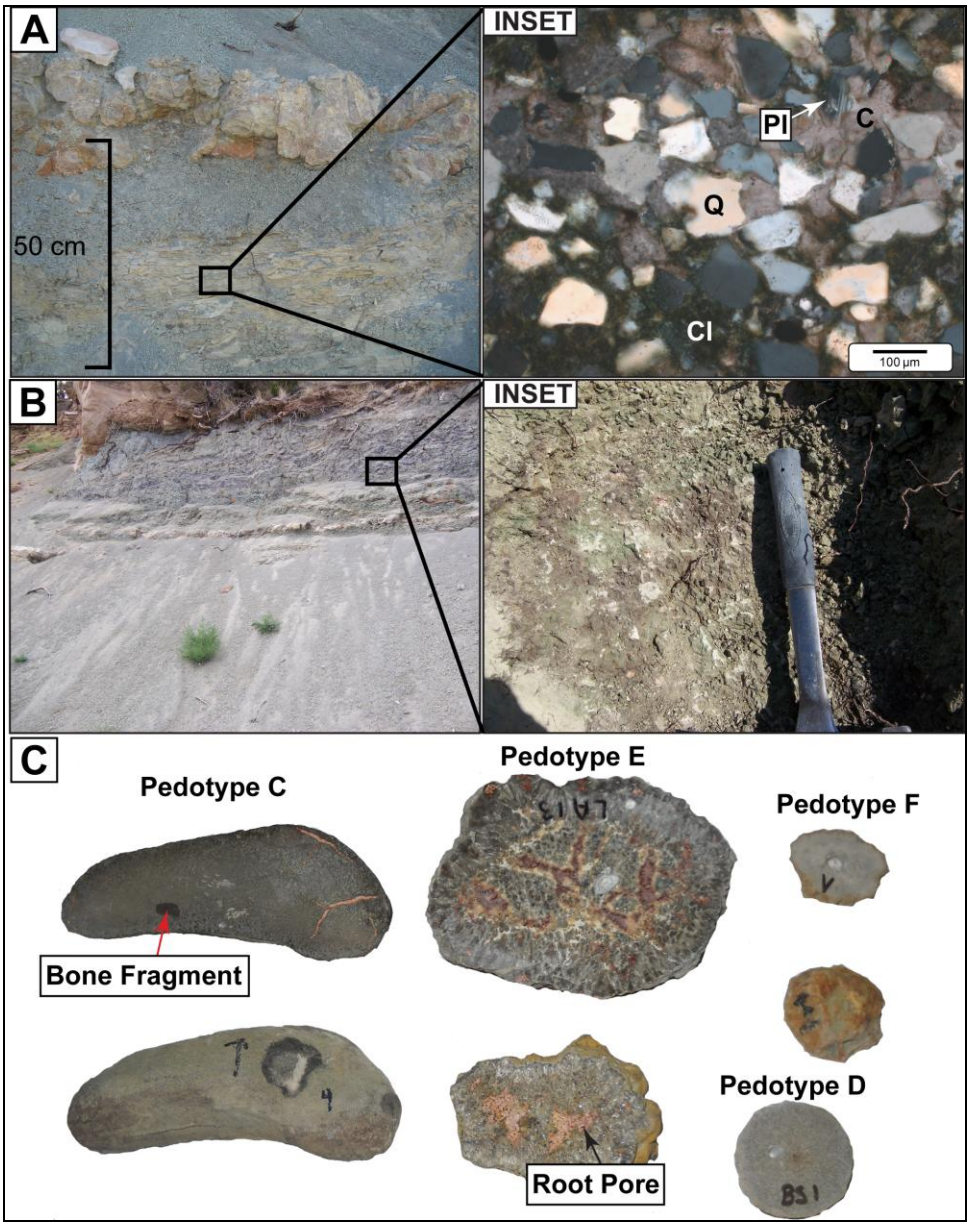

Figure 4.4. Morrison barite-bearing paleosols. A) Outcrop image of pedogenically modified fine-grained sandstone to siltstone. Inset: Sandstone is composed of embayed quartz grains (Q), plagioclase (Pl), clay (Cl), and calcite cement (C). B) Pedotype E displays complex mottling (Inset). C) Barite nodules collected from pedotype C are commonly compacted parallel to bedding. Internal structure reveals bone fragments, matrix inclusions, and desiccation cracks filled with barite. Nodules from pedotype E are coalesced millimeter- to centimeter-scale nodules with vacant root pores and iron hypocoatings. Discrete nodules from pedotype F exhibit a rough exterior with iron coatings. Pedotype D nodules are circular and much smaller and less abundant than nodules in other pedotypes.

Macromorphology of Lufkin Soil Profiles

The Lufkin series near College Station, Texas is interpreted as a very deep, moderately well-drained, lower permeability soil that formed in upland settings from slightly acid to alkaline clayey Neogene sediments (Fig. 4.2B). The conventional radiocarbon age (corrected for isotopic fractionation) for a sample from the underlying buried soil is 13,010 ± 50 BP (Beta – 344657). Slightly wavy laminated, sand and clay delineates the modern soil from an underlying buried soil at ~160-170 cm in the upper, barite-bearing soil profile. The contact between the laminated sediments and the soil is gradational to sharp. The sandy BCjg horizon is grayish-brown with redox concentrations of yellow or brown. Remnant laminations are locally present and roots are absent near the base of both profiles. Jarosite concentrations are locally present. A significant increase in clay content marks the transition between the BCjg horizon and the Btg3 horizon in the barite-bearing profile. Barite, FeMn nodules, and FeOOH and jarosite hypocoatings are most abundant between 130-140 cm. Mottles range in color from dark grayish-brown (10YR 4/2) to light greenish-gray (10GY 7). Few fine roots are present. Scattered, small clusters of sub-mm-scale, calcite nodules occur in the lower portion of the dark brown (10YR 3/2 - 10YR 4/2) Btg1 horizon. Submillimeter-scale, calcite nodules are sparse. FeMn coatings along macropores, mm-scale FeMn masses, and light greenish-gray, sandy depletion zones (10 GY 7) are disseminated in a yellowish-red to light brownish-gray (10YR 3/2 to 10YR 6/2) clayey matrix in the Btg2 and Btg3 horizons. Sand-sized, white (N8) barite crystals occur in macropores at ~100 cm in the highly mottled Btg3 horizon. A significant increase in clay content marks the boundary between the Btg1

horizon and the Bw horizon. Millimeter-scale, typic, hematite nodules and clay-coated skeletal grains are common in the brown (10YR 5/3) A horizon.

The soil profile sampled adjacent to the pond is slightly less thick, coarser-grained, and appears less weathered than the barite-bearing profile (Fig. 4.2B). Similar to the barite-bearing profile, the absence of roots and presence of remnant laminations mark the gradational contact between the sand-rich Cjg horizon and the BCyg horizon. Jarosite was documented only in the Cg horizon. Pyrite was not identified in any part of this profile. Iron oxide hypocoatings around root pores and light greenish-gray (10GY 7), leached zones are common in the Btyg and BCyg horizons. The Btg horizons are significantly thinner as compared to the Btg horizons in the barite-bearing profile. No hematite nodules occur in this profile, but small FeMn nodules are common. The very dark grayish-brown (10YR 3/2) Bw horizon displays scattered leached zones, and common, mm-diameter, FeMn nodules. Iron hydroxides and oxyhydroxides line small macropores. During the rainy season, iron oxides in the upper A and Bw horizons are reduced and the soil matrix color normally ranges between 10YR 5/3 - 10YR 4/2 changes to 10BG 4/2, due to the presence of abundant reducible iron in the upper part of the profile.

Micromorphology of Lufkin Soil Profiles

The Cjg horizons in both profiles contain abundant microcline and albite (40%) and microcrystalline quartz. This mineralogical composition is consistent with tonstein beds below the underlying the parent material (Senkayi and others, 1984). No pyrite is present in the parent material or in the soil profiles.

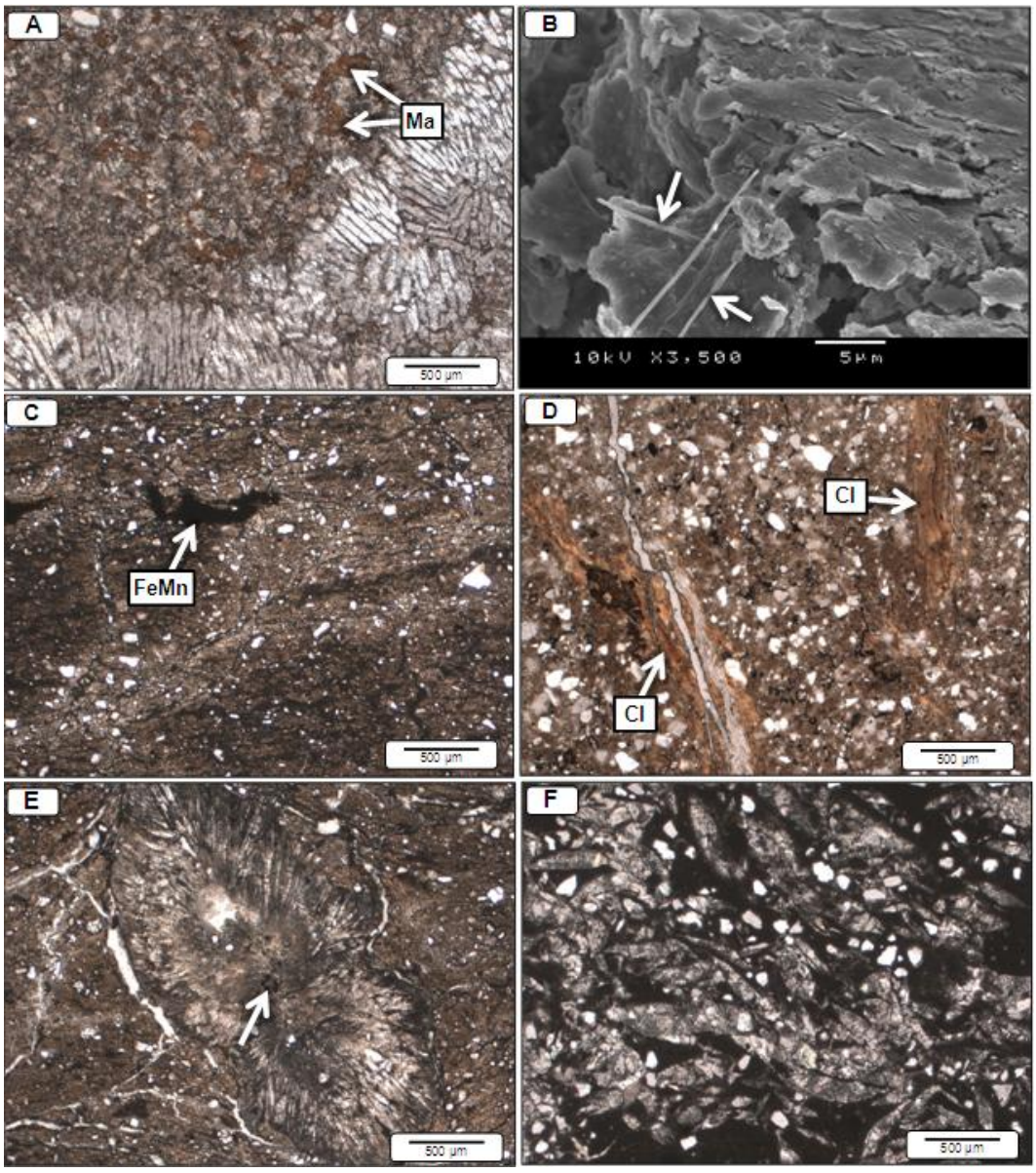

Figure 4.5. Photomicrographs of Morrison paleosols. A) Matrix (Ma) and silt (white grains) inclusions in the center of a barite nodule. Coarser, interlocked crystals occur near the center of the nodule. B) Filaments documented in barite nodule (white arrows). C) Depletion zones and irregular FeMn masses with irregular diffuse boundaries. D) Reworked clay skins (Cl) in a Bg horizon. E) Radial fibrous barite crystals surrounding a FeMn-coated root pore (white arrow). F) Calcite pseudomorphs after gypsum in the barite-poor paleosol. White grains are quartz and feldspar silt.

In barite-bearing horizons, jarosite occurs immediately adjacent to barite and in the soil matrix (Fig. 4.6A). Jarosite is also present as a matrix mineral in the Cjg horizon. Barite crystals typically display a sharp contact with jarosite that lines the pores.

Photomicrographs reveal coarse, tabular grains of barite that occur within vacant macropores (Fig. 4.6B). Clusters of sub-mm-scale barite nodules with radial fibrous crystals and a coarser-grained center also occur in the adjacent matrix (Fig. 4.6C). The clay-rich matrix of the Btg3 horizon is mostly composed of clay pseudomorphs after feldspar (Fig. 4.6D). Clay-coated framework grains are common, particularly near the bottom of the horizon. FeMn concentrations with diffuse boundaries in the matrix and along root pores are also common near barite (Fig. 4.6E). The Btg1 and Btg2 horizons display increased clay content and FeMn concentrations with irregular boundaries. Sub-mm-scale, typic, calcite nodules are locally present in the Btg2 horizon. Millimeter-scale, typic, Fe_2O_3 nodules and FeMn concentrations are present in the A horizon. Depletion zones are common. Quartz and feldspar are the primary framework grains. No barite was identified in the core taken from adjacent to the pond (Fig. 4.2 A).

Redox depletion zones occur adjacent to roots, and are scattered throughout the matrixand sharply decrease to the Cjg horizon. Framework grains in the BCyg and Cjg horizons are mainly composed of quartz, albite, and potassium feldspar. Clay pseudomorphs after feldspar are common. FeMn concentrations with diffuse boundaries and clay-coated framework grains are common in the sandy matrix. Photomicrographs of the Btg2 horizon reveal that FeOOH concentrations are dispersed throughout matrix (Fig. 4.6F). Abundant, lenticular, gypsum crystals infill macropores and are commonly associated with FeMn concentrations (Fig. 4.6F).

Isotope Geochemistry of Soil and Paleosol Sulfates

Isotopic data are summarized in Table 4.2. The $\delta^{34}S$ and $\delta^{18}O$ values of exchangeable sulfate in the barite-bearing Lufkin soil profile are -4.14‰ and +10.4‰,

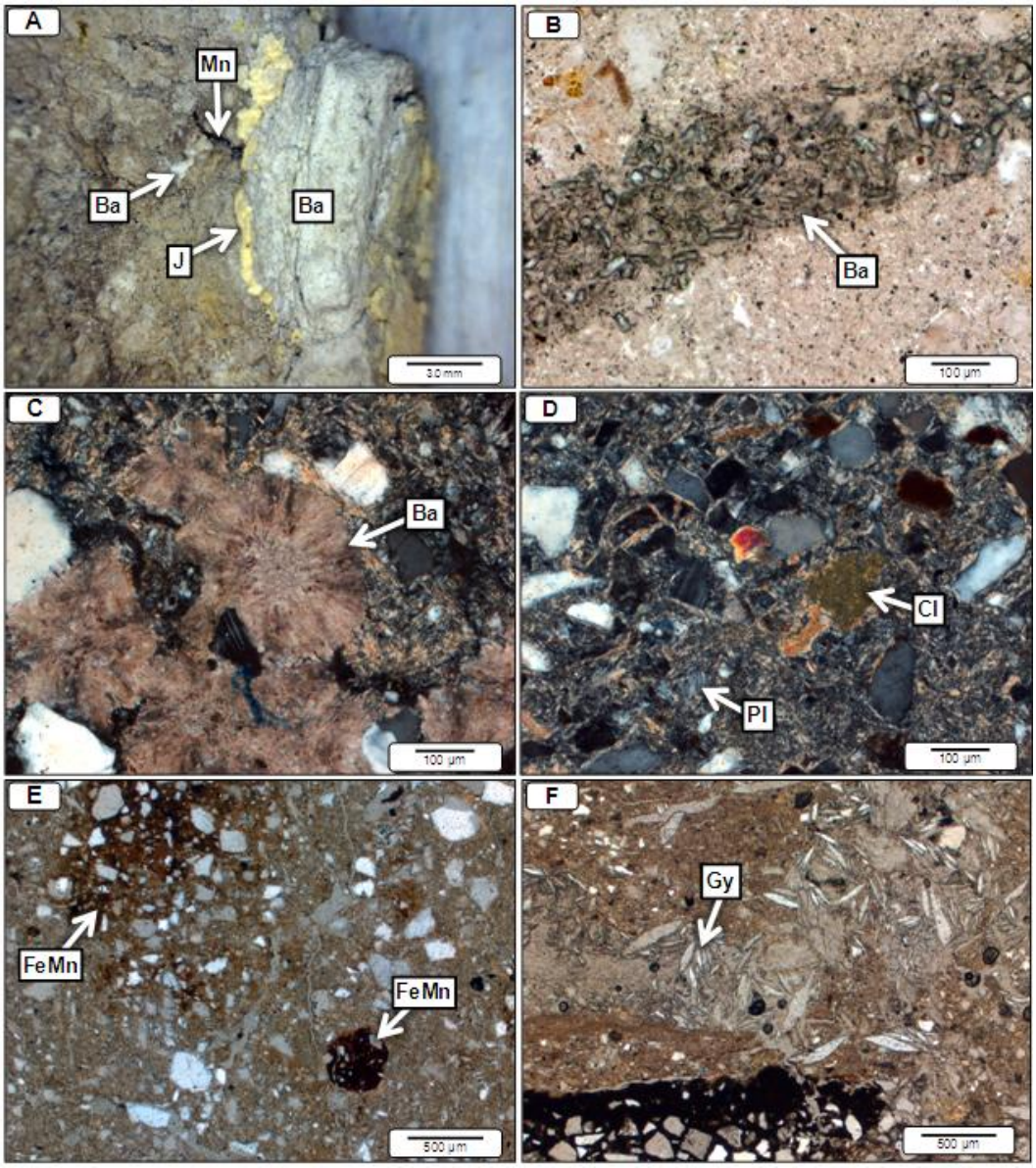

Figure 4.6. Lufkin Series photomicrographs. A) Reflected light image of the spatial relationships of barite (Ba), jarosite (J) and manganese oxide concentrations (Mn) in the Lufkin barite-bearing soil. B) Plane light photomicrograph of tabular barite crystals in a vacant root pore. C) Clusters of sub-mm-scale barite nodules with radial fibrous crystals and a coarser-grained center (Ba) in a Btg3 horizon (taken under cross-polarized light (XPL). D) Clay pseudomorphs after feldspar (Cl) in the Btg3 horizon; albite (Pl) and clay-coated, quartz (gray grains) framework grains are common in the Cjg horizons (taken under cross-polarized light (XPL). E) Diffuse (left) and concentrated (right) FeMn masses (taken under cross-polarized light (XPL). F) Lenticular gypsum crystals (Gy) in the barite-poor Lufkin profile are common in vacated root pores. FeMn masses are common (bottom).

respectively. Barite $\delta^{34}S$ values range from +5.4 to +5.5‰, averaging +5.45‰. Barite $\delta^{18}O$ ranges from +13.0 to +13.4‰, averaging +13.2‰. Jarosite ($KFeSO_4$) samples have

$\delta^{34}S$ values that range from -12.5 to -12.7‰ and average -12.6‰. Jarosite $\delta^{18}O$ values have an average of +12.2‰. The $\delta^{34}S$ and $\delta^{18}O$ values of exchangeable sulfate in the pond profile are -3.9‰ and +11.2‰, respectively. Gypsum $\delta^{34}S$ values average -3.7‰. The $\delta^{18}O$ values of gypsum average +11.0‰. Jarosite samples have $\delta^{34}S$ values of -12.6‰ and $\delta^{18}O$ values ranging between +12.5‰ and +13.0‰, with an average of 12.75‰.

Barite $\delta^{34}S$ values from the most well developed paleosols range from +5.5 to +20.7‰ and have $\delta^{18}O$ values that range from +41.2 to +19.5‰ (Fig. 5). Barite in paleosols that developed lower on the landscape have $\delta^{34}S$ values that range from +9.7 to +19.4‰ and $\delta^{18}O$ values range from +10.4 to +17.0‰. Sulfur and oxygen isotope values are most consistent in nodules from pedotypes D, and E (Fig. 4.7A and B). Sulfur and oxygen isotope values are progressively more positive towards the outer rim of the nodules in the best developed nodules from pedotypes C, E and F (Fig. 4.7A-C). $^{87}Sr/^{86}Sr$ ratios range from 0.70775 to 0.70784 with one outlier at 0.70798 (Fig. 4.7D).

Discussion

Critical to the precipitation of barite is the presence of ample concentrations of free barium and sulfate and conditions that allow these two components to be available in separate solutions(Hanor, 2000). Clay pseudomorphs after feldspar and the presence of microcline in both the Morrison barite-bearing paleosols and the Lufkin soil suggest that weathering of Ba-rich feldspars and clays is a consistent factor in the development of barite-bearing soils. Preferential weathering of Ba-rich feldspars and Ba-rich clays releases free Ba^{2+} into solution during reducing conditions (Fiedler and Sommer, 2004).

Ba-rich clays that accumulate in a Bt horizon would provide an increasingly concentrated source of Ba^{2+} during episaturated conditions. In more organic-rich sediments such as pedotype G, the presence of humic acids and more extended reducing conditions would limit barite precipitation by blocking active growth sites (Smith and others, 2004b). Instead, the sorption of Ca^{2+} by organic matter would drive the precipitation of gypsum preferentially along vacated root pores during times of higher evaporative stress (Van Den Ende, 1991).

$^{87}Sr/^{86}Sr$ values of plutons east of the 0.706 line, (sensu, Armstrong and others, 1977) from the Morrison source area are consistent with those documented in barite nodules, indicating that Sr sourced from the weathering of silicates. Although $^{87}Sr/^{86}Sr$ values are also similar to Late Triassic marine values (Korte and others, 2003), there is little evidence that significant volumes of Triassic sediments were delivered into the study area during Morrison time (May and others, 2013). Instead, extreme magmatism at the end of the Jurassic as evidenced by geochronometric data from all plutons of the Klamath mountains, eastern Oregon, and western and northern Idaho coupled with the subsequent increased subsidence precluded distribution of Late Triassic sediments in the Big Horn Basin (Armstrong and others, 1977; LaMaskin and others, 2011).

Lateral pedofacies relationships in both Morrison paleosols and the Lufkin series suggest that similar variations in hydrological conditions, concentrations of organic matter, and duration of reducing conditions correlate with topographic position. Soils that developed higher on both the ancient and modern landscapes (Jennings and others, 2011; Jennings and Driese, 2014) display evidence of seasonal episaturated conditions of sufficient duration for reducing conditions to develop (i.e., Fe/Mn nodules, illuviated

clay, and evidence of reduction along root pores). The presence of fragmented clay skins in the paleosols indicates that the uppermost portion of the soil experienced episodic dry conditions. However, the abundance of gleyed mottles and paucity of slickensides suggest that epiaquatic conditions limited the shrink-swell capacity of the soil, and prevented clay flocculation long enough to allow clay to accumulate in a Btg horizon, similar to the conditions observed in the Lufkin soil.

The presence of matrix inclusions in Morrison barite nodules and barite-filled rhizoliths support the hypothesis that barite precipitation occurred because of alternating redox conditions in the Bt horizons. Reducing conditions resulted in oxidation of organic matter, the liberation of Ba^{2+} from clays and feldspars, and mobilization of reducible iron. Coincident bacterial sulfate reduction, as evidenced by the presence of microbial filaments (Fig. 4.5B), similar to that documented in modern laboratory studies (Gonzalez-Munoz and others, 2003) released HS and HCO_3into soil solution, which in turn diffused upward to a redox boundary within the soil profile.

Paleosols that developed lower on the topography (i.e., pedotypes F and G) display evidence of more groundwater gleying (Pipujol and Buurman, 1994), suggesting that more sluggish drainage conditions and extended reducing conditions similar to those documented in the Lufkin series (Jennings and Driese, 2014) occurred in the Morrison system. Barite precipitation may have been more limited due to the presence of humic acids and organic matter in low-lying areas, which resulted in the precipitation of gypsum instead.

Table 4. 2. Isotopic composition of modern and ancient barite.

Sample ID	Sample Location	Nodule Size (cm)	$\delta^{34}S$	$\delta^{18}O$	$^{87/86}Sr$	Pedotype	Relative Position on Nodule
SI-1	A	6.5x3.7	7.07	11.30			center
SI-1	B		7.00	12.50			middle
SI-1	C		19.08	17.10			outside, top
SI-1	B		7.40	11.80			center
SI-1	B		7.00	12.50			center
SI-2	A	5.4x3.0	6.50	12.93			center
SI-2	B		6.90	10.80			center
SI-2	C		16.48	16.30			outside, bottom
SI-2	B		6.90	12.70			center
SI-2	B		6.90	10.80			center
SI-3	A	3.5x3.1	9.57	12.30			center
SI-3	B		9.80	10.20			middle
SI-3	C		8.47	10.30			outside
SI-5	A		8.49	12.20			outside, bottom
SI-5	B		6.60	12.20			center
SI-5	C		8.60	12.40			center
SI-6a	A	6.2X4.1	17.65	17.24			outside, bottom
SI-6b	B		19.54	19.46			middle, bottom
SI-6c	C		9.25	13.95			center
SI-6d	D		8.42	12.71			center
SI-6e	E		10.28	15.01			middle, top
SI-6f	F		16.14	14.88		Pedyotpe C	outside, top
SI-7	A	7.8x2.5	17.73	15.85			outside, top
SI-7	B		8.47	13.58			middle, top
SI-7	C		8.41	14.39			center
SI-7	D		8.37	13.78			middle, bottom
SI-7	E		7.77	13.04			outside, bottom
SI-8	A	6.0x4.7	11.82	13.80			center
SI-8	B		10.60	13.90			middle
SI-8	C		9.17	12.40			outside
SI-8	B		7.13	12.46			center
SI-9	A	10.2X5.0	9.30	13.30			outside, bottom
SI-9	B		7.10	12.60			middle outside, bottom
SI-9	C		11.96	13.20			center
SI-9	B		7.50	13.10			center
SI-9	B		7.10	12.60			center
SI-9	A		7.52	13.12			center
SI-10	A	13.0x6.7	9.34	12.50			center
SI-10	B		9.40	12.00			middle
SI-10	C		10.35	13.90			outside
SI-11	A	4.1x3.0	14.57	11.50			outside, bottom
SI-11	B		5.50	11.20			center

Table continued

Sample ID	Sample Location	Nodule Size (cm)	$\delta^{34}S$	$\delta^{18}O$	$^{87/86}Sr$	Pedotype	Relative Position on Nodule
SI-11	C		7.23	11.40	0.7078370		outside, top
SI-12	A	12.7x6.5	19.37	17.50			center
SI-12	C		20.71	17.30			outside
SI-13	A		10.16	13.40			center
SI-13	B		8.80	11.30			middle
SI-13	C		19.96	17.70			outside
SI19	A	7.0x4.0	15.20	14.30			outside, bottom
SI19	B		15.60	14.50			middle, bottom
SI19	C		16.20	14.90	0.7077540		center
SI19	D		14.90	14.50			middle, top
SI19	E		13.50	14.00			outside, top
BBS1	A		17.50		0.7078250		center
BBS2	A		18.60	15.10			outside
BBS2	B		17.50	15.90			middle
BBS2	C		17.20	15.90			center
BBS3	A		17.20		0.707794		center
BS1	A	3.5X3.4	18.67	15.45			outside, top
BS1	B		19.08	15.13		Pedotype D	middle, top
BS1	C		19.42	15.69			center
BS1	D		19.44	15.74	0.707987		middle, bottom
BS1	E		19.15	15.59			outside, bottom
LA-2	A	8.0x6.5	18.40	15.90			outside, left
LA-2	B		19.80	15.50			middle, left
LA-2	C		19.30	14.50			middle-center left
LA-2	D		20.00	15.50			center
LA-2	E		18.30	15.80			middle-center right
LA-2	F		18.90	15.90			middle-outside, right
LA-2	G		18.70	15.50			outside right
LA-2	H		13.10	15.40			outside right
LA-2	I		19.30	15.70			outside right
LA-9	A	7.6x6.4	19.20	16.28			outside, bottom
LA-9	B		19.81	15.59			outside, left
LA-9	C		20.02	15.36		Pedotype E	outside
LA-9	D		20.05	16.70			middle
LA-9	E		18.66	17.29			outside, top
LA-10	A	5.7x7.0	18.90	15.90			outside, bottom
LA-10	B		18.70	15.50			middle
LA-10	C		13.10	15.40			center
LA-10	D		19.30	15.70			middle, top

Table continued

LA-10	E		19.10	15.50			outside, top
LA-12	A		19.37	17.50			within calcite steinkern
LA-12	C		19.00	15.40			outside edge
LA-13	B		8.80	11.30			fine-grained center

Sample ID	Sample Location	Nodule Size (cm)	$\delta^{34}S$	$\delta^{18}O$	$^{87/86}Sr$	Pedotype	Relative Position on Nodule
LA-13	B		10.80	12.60			coarse-grained center
LA-16	A	7.5X4.3	19.27	16.67			outside, bottom
LA-16	B		18.81	15.45			middle, bottom
LA-16	C		11.07	13.17	0.707837		center
LA-16	D		19.30	14.93			middle, top
LA-16	E		18.47	18.41			outside top
V-1		4.3X4.5	12.80		0.707784		center
V2-2	A	4.0X3.9	16.18	17.04			outside
V2-2	B		9.89	10.37			center
V2-2	C		12.80	11.51			middle
V2-2	D		17.96	15.92			outside
V2-2	B		9.70	14.40			center
V2		3.0X3.0	9.70		0.707856	Pedotype F	center
V2-6		2.5X2.0	18.00		0.707802		center
V2-7			9.90		0.707888		center

Lufkin Series Sample ID			δ34S ‰	δ18O ‰			
BB-120			5.40	13.00			
BB-120				5.50	13.40		
LBB110 Exch			-4.136769	10.4			
LPP120 Exch			-3.901955	11.2			
LPP120 CaSO4			-3.664505	11.0			
LBB160 KFeSO4			-12.52677	12.2			
LBB160 KFeSO4			-12.74132	12.2			
LBB160 KFeSO4			-12.60618	12.5			
LBB160 KFeSO4			-12.62494	13.0			

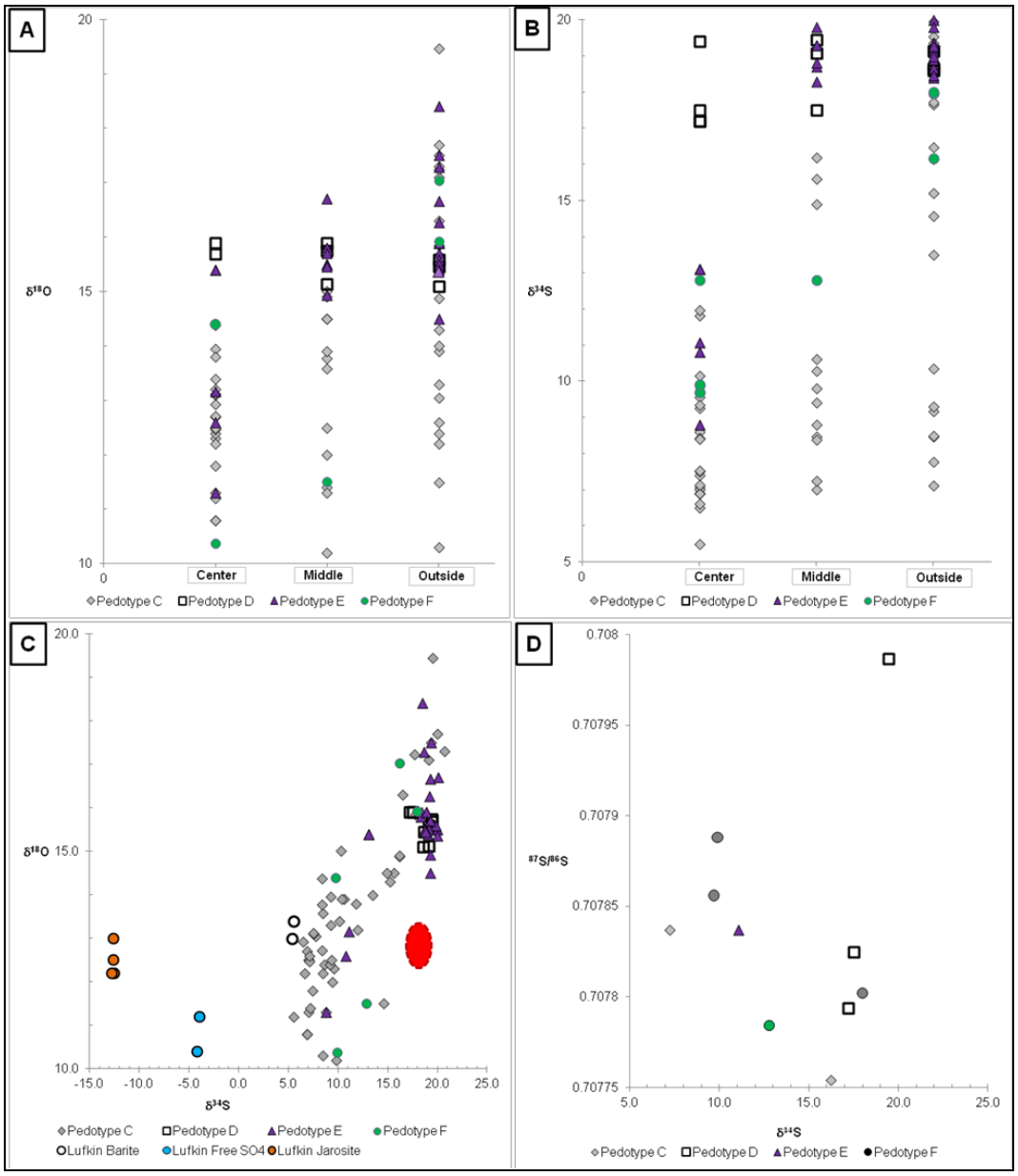

Figure 4.7. Morrison and Lufkin sulfate isotopes. A) Oxygen isotope values from the center to the outside edge of the nodule. B) Sulfur isotope values from the center to the outside edge of the nodules. C) Sulfur and oxygen isotope values for Lufkin and Morrison barite. Note that $\delta^{18}O$ values of Lufkin barite is very similar to Morrison paleosols values, whereas $\delta^{18}O$ values of other Lufkin soil sulfate minerals are much more negative than $\delta^{18}O$ values of Morrison paleosols barite. Sulfur isotope values are similar and their resulting fields overlap for all minerals analyzed. Red dashed circle: Late Jurassic marine evaporite values (from (Claypool and others, 1980; Burke and others, 1982; Lo Forte and others, 2005). See text for discussion. D) Cross plot of $^{87}Sr/^{86}Sr$ vs. $\delta^{34}S$.

Also essential to pedogenic barite precipitation is the presence of free sulfate. The primary sources of sulfur in soils are typically organic phases (derived from the decay of

soil organic matter) and pyrite in the parent material (Stevenson and Cole, 1999; Hutchinson and others, 2001). Other sources include influx of atmospheric SO_2, groundwater leaching of sulfate minerals (usually gypsum in the parent material), and application of fertilizer (Andreae and Jaeschke, 1988; Krouse and others, 1991; Stevenson and Cole, 1999). In well-developed, acid-sulfate soils such as the Morrison and Lufkin soils, SO_4^{2-} is translocated down through the profile and concentrated at a depth where it is adsorbed by Al and Fe compounds, typically in a Bt horizon (Sharpley, 1990; Ajwa and Tabatabai, 1995; Agbenin, 1997). Free soil sulfate retains the isotopic signature of the sulfur and oxygen because no significant fractionation occurs during sulfate adsorption (Van Stempvoort and others, 1990). All likely sources of soil sulfate have relatively distinct $\delta^{34}S$ and $\delta^{18}O$ values that are preserved in sulfate minerals.

Although gypsum is documented in Btyg horizon of pedotype G (Fig. 4.5F), it is not present in the parent material (Fig. A inset). Fertilizer may also be excluded as a possible sulfur source because fertilizer is not introduced to the Lufkin series field area (T. Hallmark, pers. comm., 2006) and would not have been a consideration during Morrison time. Because the Morrison study area was hundreds of km from the marine realm (Fig. 4.1), it is also unlikely that coeval marine derived sulfate was a source of Morrison soil sulfate.

The $\delta^{34}S$ values from the Lufkin jarosite are consistent with pyrite that formed in coastal plain deposits (Trust and Fry, 1992). The Lufkin barite is significantly less enriched in ^{34}S compared to area groundwater (Ulrich and others, 1998). Instead, its isotope value is more consistent with fractionation that occurs during the bacterial sulfate reduction of existing jarosite during cyclic, reducing conditions and subsequent sulfide

oxidation through the metabolic processes of sulfur-oxidizing bacteria at the onset of drier conditions (Seal and others, 2000; Habicht and Canfield, 2001). The presence of both SOB and SRB in area soils also supports this interpretation (Marfil et al., 1998). Conversely, gypsum in the lower profile and free sulfate display a narrow range of $\delta^{34}S$ values, suggesting that they share a common origin, which is more consistent with modern meteoric water (Chowdhury, 2004). A slight fractionation effect attributable to the presence of abundant organic sulfur in the lower profile likely explains the slight depletion with respect to ^{34}S in the gypsum compared to the free sulfate (Trust and Fry, 1992).

Comparatively, samples from the center of most Morrison barite nodules (pedotypes C, E, and F) and Lufkin barite display similar $\delta^{18}O$ and $\delta^{34}S$ values, suggesting that the soil sulfate had a similar signature. However, unlike the Lufkin soil, Morrison paleosols developed on exposed lacustrine sediments rather than marine deposits. Additionally, all barite nodules from pedotype C are closely associated with dinosaur skeletal elements. Oxygen and sulfur isotopic signatures are significantly more negative than upper Jurassic marine evaporites (Fig. 4.7C), indicating that groundwater interaction with earlier marine evaporites is also an unlikely source of sulfate for Morrison barite nodules.

If a system is relatively closed to free access of sulfate, the removal of sulfate gives rise to lower overall fractionation effects and non-steady-state reduction (Coleman and Raiswell, 1981). As a result, soil sulfate would have a slightly more positive $\delta^{34}S$ signature compared to parent S material (Coleman and Raiswell, 1981). Typically, the primary sources of sulfur available to plants (and animals that consume them) are

atmospheric SO_2, sulfide minerals, and free SO_4 in soil (Trust and Fry, 1992; Peterson and others, 2003). Organically bound sulfur experiences a 1.2‰ fractionation that occurs during assimilatory sulfate reduction (Trust and Fry, 1992). If the average land plant $\delta^{34}S$ ranges from -2.0 to 0.5‰ (Trust and Fry, 1992), and the $\delta^{34}S$ of soil organic matter is intermediate between that of plants and free soil sulfate (Kusakabe and others, 1976), the $\delta^{34}S$ of barite from the interior of Morrison barite nodules suggests that free soil sulfate may have been slightly less enriched with respect to ^{34}S compared to the Lufkin soil profile. Because there is no evidence of jarosite or marine pyrite in the Morrison parent materials, it is likely that the predominant initial source of sulfur for the Morrison pedotypes C, E, and F was sulfides and ester sulfates released during the decay of organic matter. The close association of barite nodules with dinosaur bone also supports this interpretation. Covariance of $\delta^{34}S$ and $\delta^{18}O$ values toward the outside of the barite nodules indicate that subsequent sulfate reduction resulted in continued fractionation of pore water sulfate with depth (Seal and others, 2000).

Higher $\delta^{34}S$ and $\delta^{18}O$ values and less covariance across the nodules documented in pedotype D indicate that alternating redox processes and oxidation of organic matter were less dominant in marshy areas (Jennings and others, 2011), and the rate of sulfate reduction higher. Paucity of barite nodules in this pedotype also supports this hypothesis.

One problem with comparing barite-bearing paleosols and modern soils is the disparity in the size of the barite masses (Retallack and Kirby, 2007). Texture, apparent matrix permeability, and abundance of quartz, plagioclase, and potassium feldspar are very similar to that documented in both the Morrison paleosols and the Lufkin soil. The changes in barite nodule size and morphology across the Morrison landscape documented

in this study suggests a possible relationship between the shrink/swell potential, topographic position, and abundance of humic acids in the soil profile. Larger, typic nodules formed higher on the landscape where there is evidence of higher shrink/swell potential, whereas less well-formed and smaller nodules or rhizoliths formed lower on the landscape where saturated conditions and the abundance of humic acids would have been significantly higher.

Time is also a factor that would contribute to the overall nodule size. Based on the presence of stacked, over-thickened paleosol profiles, we suggest that it is likely that pedogenesis of modern soils has not occurred over as extended a time as with the paleosols. Based on the conventional radiocarbon age of 13,010 ± 50 BP for the buried soil, landscape stability and continued barite precipitation may have occurred over a period of tens of thousands of years or more. Additionally, compaction during burial may have caused smaller nodules and masses in the matrix to coalesce as in the Morrison paleosols. Another explanation would be variability in the abundance of SRB and the rate of sulfate reduction, which may result in larger masses. However, because the sulfur isotopic signatures are so similar, we suggest that microbial activity is not a factor in nodule size in this study.

Conclusions

Although Morrison paleosols and the Lufkin soil at College Station are not identical with respect to landscape location, we argue that they are analogous with respect to pedogenic processes and relative landscape relationships. Overall, the Lufkin soil and the Morrison paleosols display many similar characteristics including:

1. Lateral topofacies relationships, with barite-bearing profiles occurring higher on the landscape and gypsum-bearing profiles in lower, more persistently saturated and organic-rich areas.
2. Feldspar-rich parent materials that provide a source of Ba^{2+}.
3. Abundant redoximorphic features (i.e., Fe/Mn nodules, gleyed mottles, and reworked clay skins) indicative of fluctuating redox conditions.
4. Evidence of bacterial sulfate reduction during reducing, episaturated conditions, and subsequent sulfide oxidation and barite precipitation at the onset of drier conditions.

Results presented here illustrate that the most important pedogenic processes that control barite precipitation in upland soils are: 1) barium-rich parent materials; 2) alternating redox conditions, with reducing conditions that last long enough to release sulfides and barium into solution; 3) extended landscape stability; 4) the presence of a diverse microbial community that allows both dissimilatory sulfate reduction and sulfide oxidation, and 5) a low-gradient landscape that has sluggish drainage conditions. These conditions are common in many modern and ancient systems, particularly those in low-gradient basins that have received feldspar-rich sediments (i.e., volcanically influenced basins), soils that developed near salt domes, soils that developed in exposed wetland or lacustrine sediments, and coastal-plain deposits.

One of the most important implications of barite-bearing paleosols and soils is the extended landscape stability that is necessary for their development. Contrary to past interpretations, the modern analogue in this study documents that barite-bearing soils and gypsum-bearing soils occur in close proximity and develop coevally. The key to

understanding and accurate interpretation of barite-bearing paleosols and modern soils is lateral, topofacies relationships, stable isotope geochemistry, and micromorphology. When studied in a well-documented paleogeographic context, barite-bearing soils are valuable to paleoclimate, paleoenvironmental, and paleohydrological studies. Combined with regional interfluvial paleosols, barite-bearing soils may document temporal changes in drainage, surface stability, and accommodation consistent with sequence boundaries and climate changes.

CHAPTER FIVE

Conclusions

Only in the last 3 decades have scientists realized the value of wetland studies in Critical Zone research and their impact on our understanding of long-term global climate change and large-scale environmental perturbations. As archives of paleoenvironmental and paleoecological data, wetland paleosols offer an excellent source of information about the impact of climate change on wetlands, how they recover from major environmental disruptions, and how wetland biotas interact with those of surrounding environments. When combined with detailed paleopedological studies of laterally equivalent paleosols they offer the unique potential to document high-resolution paleoclimatic and paleoecological data across a wide area. Differentiating hydrogeomorphological subenvironments within paleowetland-lacustrine systems is vital to the study of ancient terrestrial landscapes and climate, which in turn increase our understanding of the repercussions of anthropogenic and climatic influences on modern wetlands. This study establishes a genetic wetland classification scheme that uses data preserved or easily inferred in the rock record, thereby facilitating future paleowetland studies.

Results presented here illustrate that the most important pedogenic processes that control barite precipitation in upland soils are: 1) barium-rich parent materials; 2) alternating redox conditions, with reducing conditions that last long enough to release sulfides and barium into solution; 3) extended landscape stability; 4) the presence of a diverse microbial community that allows both dissimilatory sulfate reduction and sulfide

oxidation, and 5) a low-gradient landscape that has sluggish drainage conditions. These conditions are common in many modern and ancient systems, particularly those in low-gradient basins that have received feldspar-rich sediments (i.e., volcanically influenced basins), soils that developed near salt domes, soils that developed in exposed wetland or lacustrine sediments, and coastal-plain deposits.

An unexpected result of this study is the discovery of elemental evidence of Ba^{2+} mobility and concentration in a Btg3 horizon. Because an enrichment of Ba/Sr ratio is commonly used as evidence for ancient paleosol surface horizons, the results of this study indicate that an enrichment may instead occur 70-100 cm below the surface in ancient acid sulfate soils and lower horizons of paleosols. Additionally, although it is commonly assumed that a Ba/Sr molecular ratio of 10 or more indicates strongly leached soils, the significant peak in the barite-bearing soil, and to a lesser extent in the pond profile, would give a false impression of enhanced leaching. Instead, the Ba peak more likely is fixed by Fe-oxides at depth near the base of the barite-bearing zone. Contrary to previous interpretations (e.g., Retallack and Kirby, 2007; Retallack and Huang, 2010) of paleohorizons in gypsic and baritic paleosols, related calcite nodules in barite-bearing soils occurs at a shallower depth than barite-bearing horizons. Barite-bearing horizons also occur relatively deeper than gypsum-bearing horizons associated with profiles lower on the landscape. Using the proposed relationship between mean annual precipitation (P, in millimeters) and depth to the By horizons for the pond profile (D, in centimeters) proposed by Retallack and Huang (2010) ($P=87.593e^{0.0209D}$), distinctly different values for mean annual precipitation are calculated for the two gypsum-bearing horizons (873 and 1075 mm). Compared to the actual mean annual precipitation (1008 mm) these

values fall well outside the suggested standard deviation, indicating that data from gypsum-bearing paleosols associated with barite-bearing paleosols may not be useful proxies for mean annual precipitation. These data should be used with caution, particularly in paleosols that developed in volcanically influenced systems (i.e., Retallack and others, 1999; Retallack and Kirby, 2007), and paleosols that contain jarosite and other sulfate minerals (e.g., Kraus, 1997; Kraus and Hasiotis, 2006).

One of the most important implications of barite-bearing paleosols and soils is the extended landscape stability that is necessary for their development. Contrary to past interpretations, this study documents that barite-bearing soils and gypsum-bearing soils occur in close proximity and develop coevally. The key to understanding and accurate interpretation of barite-bearing paleosols and modern soils is lateral, topofacies relationships, stable isotope geochemistry, and micromorphology. When studied in a well-documented paleogeographic context, barite-bearing soils are valuable to paleoclimate, paleoenvironmental, and paleohydrological studies. Combined with regional interfluvial paleosols, barite-bearing soils may document temporal changes in drainage, surface stability, and accommodation consistent with sequence boundaries and climate changes. Finally, this study serves as an example of how taphonomic uniformitarianism and a multianalytical approach can be used to solve more complex and difficult paleopedological problems.

APPENDIX

Outcrop Images

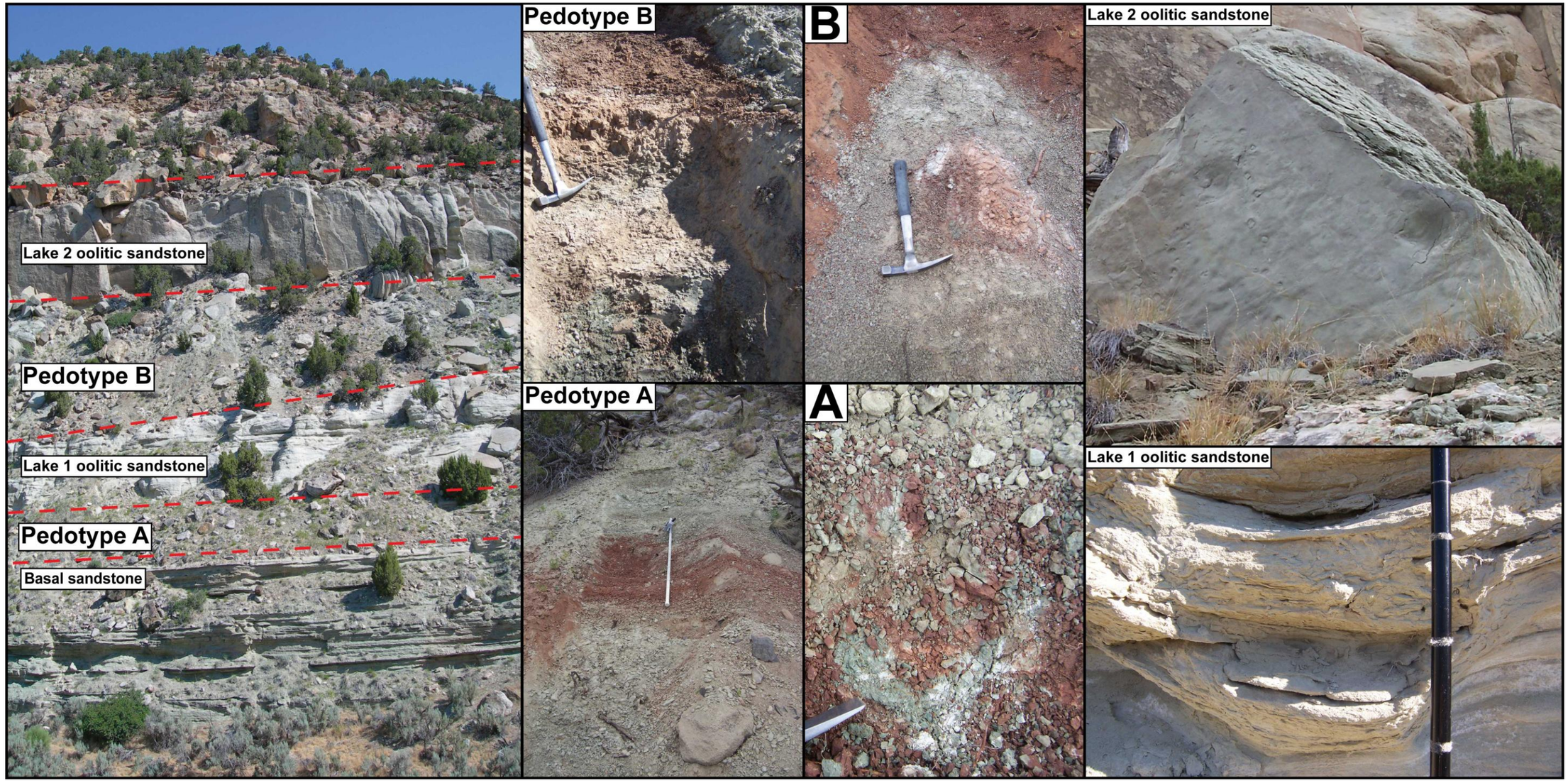

Outcrop images of Lake 1 and Lake 2 deposits with Pedotypes A and B, Section 6 are illustrated at the far left. Dashed lines on the first outcrop image delineate the boundaries between the lacustrine sequences and the associated well drained paleosols. Pedotype A and Pedotype B representative profiles are illustrated. Pedotype A tends to be very similar in appearance to Pedotype B. Gleyed mottles are present in both pedotypes (Image A). Krotovina are only documented in Pedotype B (Image B). Large dinosaur tracks are visible in cross section in Lake 1 oolitic sandstones (far right). Small theropod trackways are preserved in Lake 2 oolitic sandstones.

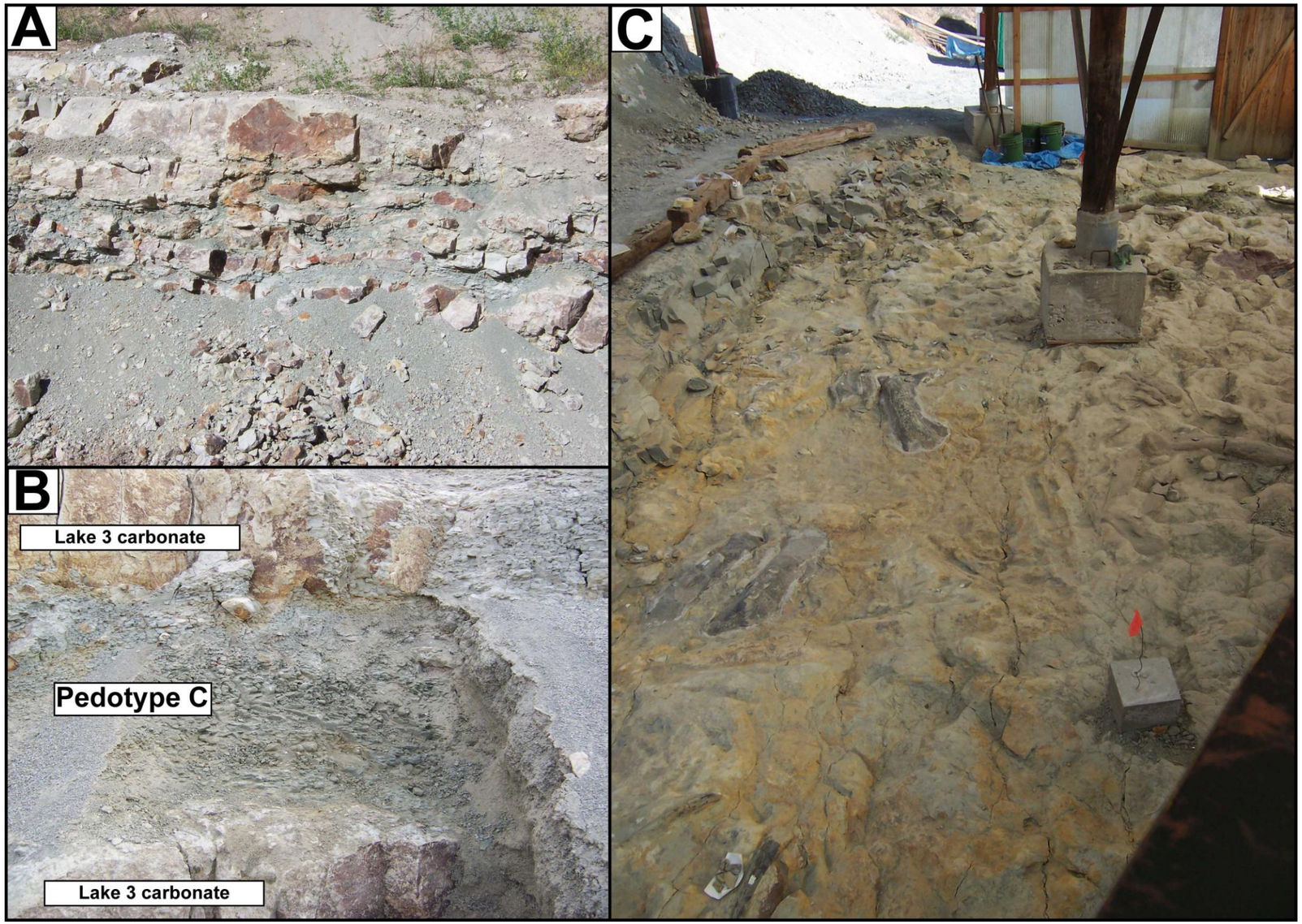

A) Interbedded limestone and mudstone characterizes this representative Lake 3 sequence. B) Pedotype C is bounded by trampled carbonate beds. C) A trampled surface and feeding site with dinosaur bones (brown elements) previously documented by Jennings and Hasiotis (2006).

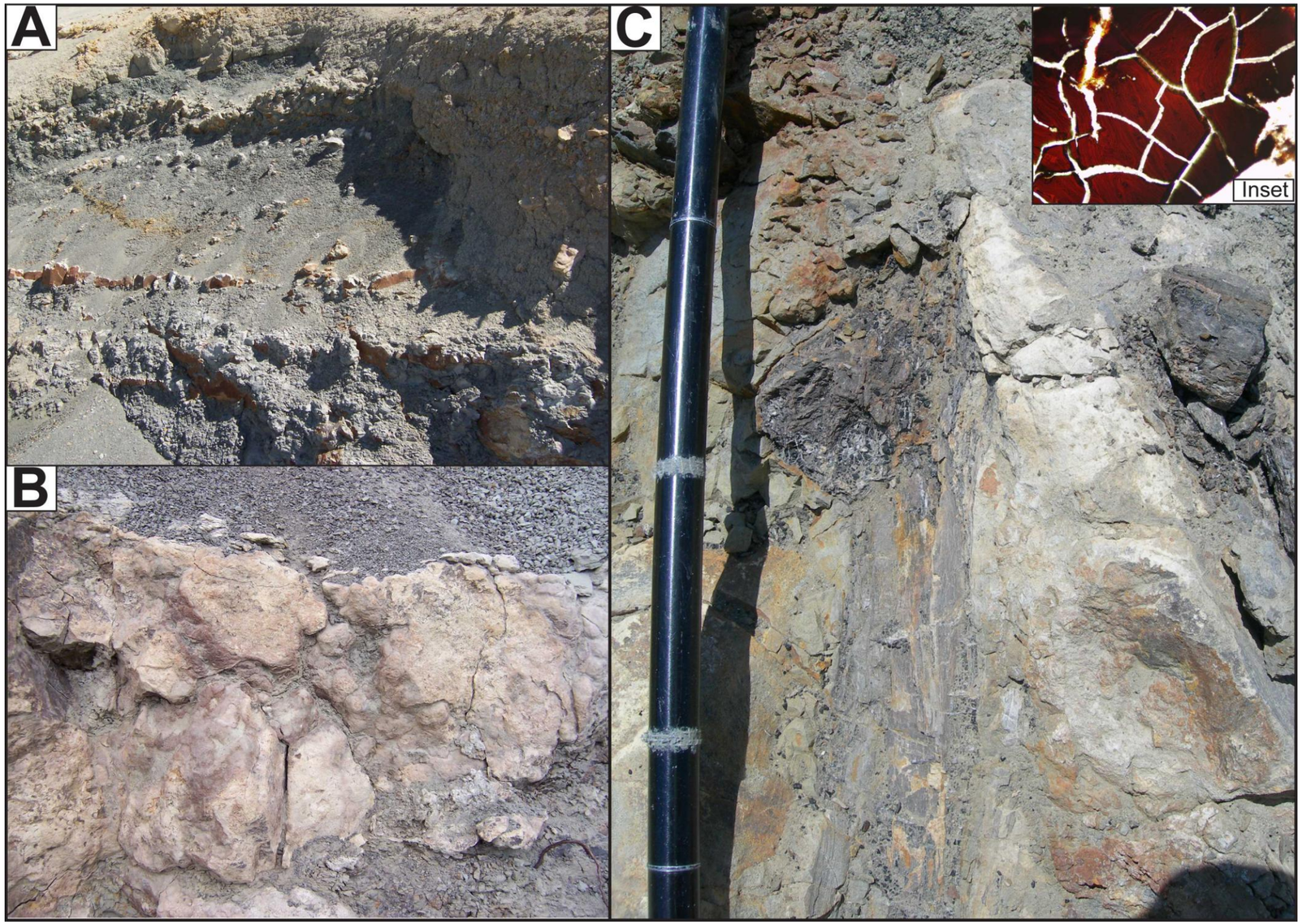

A) Pedotype D in outcrop. B) the parent material for Pedotype D is a bioturbated limestone. C) An example of a well-preserved log discovered at the base of Pedotype D (fossil now resides in the Wyoming Dinosaur Center museum, Thermopolis, Wyoming. The inset is a scan of an oversized thin section from this specimen. Fractures are an artifact of sample preparation.

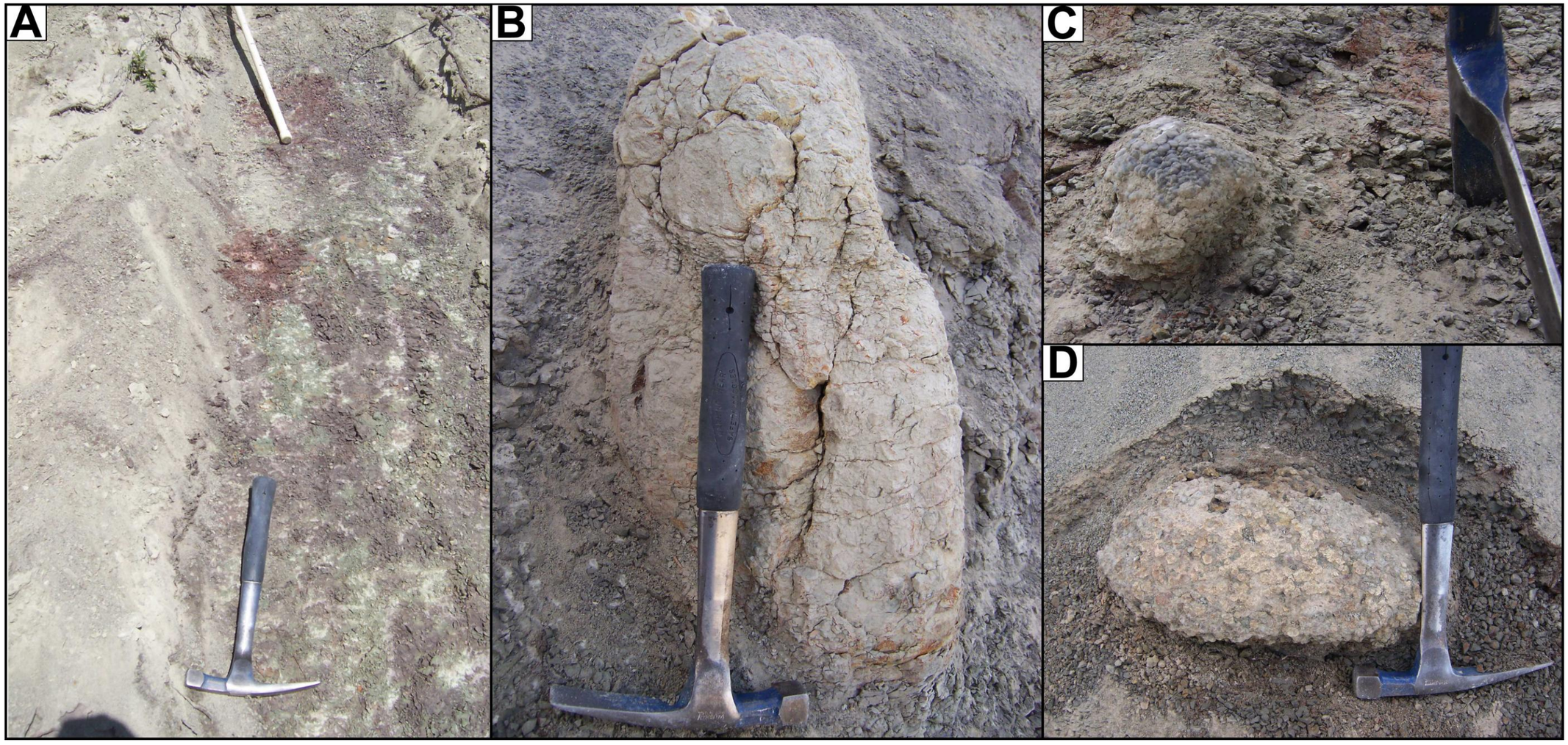

A) Representative profile of Pedotype E. B) Carbonate steinkerns occur at the top of Pedotype E have been interpreted as voids of trees and cycads left after a flooding event. C) An example of a barite nodule *in situ*. Barite nodules in this pedotype commonly are composed of clusters of cm-scale barite nodules. D) Above the barite-bearing horizon large clusters of cm-scale carbonate nodules are present. Clay is present between each nodule.

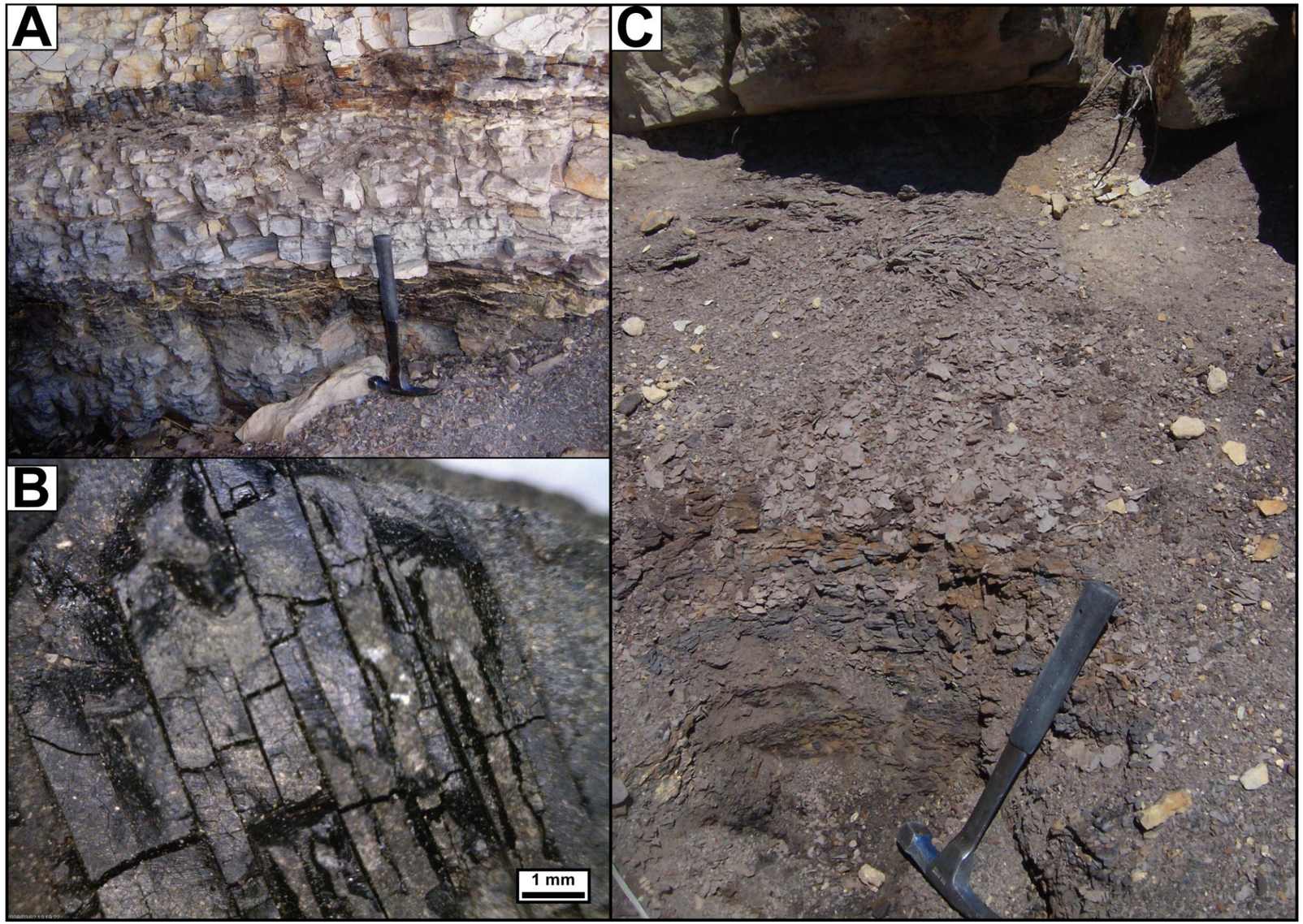

A) Laminated, organic-rich fen deposits of Pedotype H are illustrated in this image. B) Reflected light image of charcoal that was found in these deposits. C) The contact between the massive clay- and organic-rich Oa horizons that are present in the east and the shaly upper Oi horizon.

REFERENCES

Agbenin, J.O., 1997, Sulfate retention by kaolinitic Alfisols from Nigerian savannah: Soil Science Society of America Journal, v. 61, p. 53-57.

Ajwa, H.A., and Tabatabai, M.A., 1995, Metal-induced sulfate adsorption by soils: I. effect of pH and ionic strength: Soil Science, v. 159, no. 1, p. 32-42.

Alho, C.J.R., 2005, The Pantanal, *in* Fraser, L.H., and Keddy, P.A., eds., The World's Largest Wetlands: Ecology and Conservation: Cambridge, Cambridge University Press, p. 203-271.

Alonso-Zarza, A.M., 2003, Palaeoenvironmental significance of palustrine carbonates and calcretes in the geological record: Earth-Science Reviews, v. 60, p. 261-298.

Alonzo Zarza, A.M., Calvo, J.P., and Garcia del Cura, M.A., 1992, Palustrine sedimentation and associated features -- granification and pseudo-microkarst -- in the mIddle MIocene (Intermediate Unit) of the Madrid Basin, Spain: Sedimentary Geology, v. 76, p. 43-61.

Andreae, M.O., and Jaeschke, W.A., 1988, Exchange of sulphur between biosphere and atmosphere over temperate and tropical regions, *in* Howarth, R.W., Stewart, J.W.B., and Ivanov, M.V., eds., Sulphur Cycling on the Continents: Wetlands, Terrestrial Ecosystems and Associated Water Bodies: New York, John Wiley & Sons, p. 27-61.

Aoyagi, K., and Kazama, T., 1980, Transformational changes of clay minerals, zeolites, and silica during diagenesis: Sedimentology, v. 27, p. 179-188.

Armstrong, R.L., Taubeneck, W.H., and Hales, P.O., 1977, Rb-Sr and K-Ar geochronometry of Mesozoic granitic rocks and their Sr isotopic composition, Oregon, Washington, and Idaho: Geological Society of America Bulletin, v. 88, p. 397-411.

Ash, S.R., 1994, First occurrence of *Czekanowskia* (Gymnospermae, Czekanowskiales) in the United States: Review of Palaeobotany and Palynology, v. 81, p. 129-140.

Ashley, G.M., and Driese, S.G., 2000, Paleopedology and paleohydrology of a volcaniclastic paleosol interval: implications for early Pleistocene stratigraphy and paleoclimate record, Olduvai Gorge, Tanzania: Journal of Sedimentary Research, v. 7, no. 5, p. 1065-1080.

Aspler, L.B., Chiarenzelli, J.R., and Cousens, B.L., 2004, Fluvial, lacustrine and volcanic sedimentation in the Angikuni Sub-basin, and initiation of approximately 1.84-1.79 Ga Baker Lake Basin, western Churchill Province, Nunavut, Canada: Precambrian Research, v. 129, no. 3-4, p. 225-250.

Atun, G., and Bascetin, E., 2003, Adsorption of barium on kaolinite, illite, and montmorillonite at various ionic strengths: Radichimica Acta, v. 91, p. 223-228.

Baar, E.E., Yonovitz, M., Demko, T.M., Bodenbender, B.E., and Anonymous, 2005, Description of paleosols in the Upper Jurassic Morrison and Lower Cretaceous Cloverly Formations near a dinosaur site in the Bighorn Basin, WY: Abstracts with Programs - Geological Society of America, v. 37, no. 5, p. 33.

Beard, B.L., Johnson, C.M., Skulan, J.L., Nealson, K.H., Cox, L., and Sun, H., 2003, Application of Fe isotopes to tracing the geochemical and biological cycling of Fe: Chemical Geology, v. 195, no. 1-4, p. 87-117.

Beattie, J.A., and Haldane, A.D., 1984, The occurrence of palygorskite and barytes in certain parna soils of the Murrumbidgee region, New South Wales: Australian Journal of Science, v. 20, p. 274-275.

Behrensmeyer, A.K., Gordon, K.D., and Yanagi, G.T., 1989, Nonhuman bone modification in Miocene fossils from Pakistan, *in* Bonnichesen, R., and Sorg, M.H., eds., Bone Modification: Orono, Maine, Center for the Study of the First Americans, p. 99-120.

Biswas, H., Datta, S.P., and Singh, A.K., 2003, Adsorption and translocation of sulfur in some tropical acid soils: Journal of Plant Nutrition and Soil Science, v. 166, p. 519-520.

Bjoerlykke, K.O., and Griffin, W.L., 1973, Barium feldspars in Ordovician sediments, Oslo Region, Norway: Journal of Sedimentary Petrology, v. 43, no. 2, p. 461-465.

Blount, C.W., 1977, Barite solubilities and thermodynamic quantities up to 300 C and 1400 bars: American Mineralogist, v. 62, p. 942-957.

Blum, M.D., 1992, Modern depositional environments and recent alluvial history of the lower Colorado River, Gulf coastal plain, Texas: Austin, University of Texas at Austin, Dissertation, 304 p.

Boggs, J., Sam, 1995, Principles of Sedimentology and Stratigraphy: Englewood Cliffs, NJ, Prentice Hall, 774 p.

Bohacs, K.M., Carroll, A.R., Neal, J.E., and Mankiewicz, P.J., 2000, Lake-basin type, source potential, and hydrocarbon character: an integrated sequence-stratigraphic-geochemical framework, *in* Gierlowski-Kordesch, E.H., and Kelts, K.R., eds., Lake Basins Through Space and Time: Tulsa, American Association of Petroleum Geologists, p. 3-34.

Boixadera, J., Poch, R.M., Garcia-Gonzalez, M.T., and Vizcayno, C., 2003, Hydromorphic and clay-related processes in soils from the Llanos de Moxos (northern Bolivia): Catena, v. 54, p. 403-424.

Bonny, S.M., and Jones, B., 2008, Experimental precipitation of barite (BaSO4) among streamers of sulfur-oxidizing bacteria: Journal of Sedimentary Research, v. 78, p. 357-365.

Bowen, G.J., and Bloch, J., I., 2002, Petrography and geochemistry of floodplain limestones from the Clarks Fork Basin, Wyoming, U.S.A.: carbonate deposition and fossil accumulation on a Paleocene-Eocene Floodplain: Journal of Sedimentary Research, v. 72, no. 1, p. 46-58.

Brandt, D., Andreoli, M.A.G., and McCarthy, T.S., 2005, The late Mesozoic palaeosoils and Cenozoic fluvial deposits at Vaalputs, Namaqualand, South Africa: possible depositional mechanisms and their bearing on the evolution of the continental margin: South African Journal of Geology, v. 108, no. 2, p. 271-284.

Brantley, S.L., Goldhaber, M.B., and Ragnarsdottir, K.V., 2007, Crossing disciplines and scales to understand the Critical Zone: Elements, v. 3, p. 307-314.

Breheret, J.G., and Brumsack, H.J., 2000, Barite concretions as evidence of pauses in sedimentation in the Marnes Bleues Formation of the Vocontial Basin (SE France): Sedimentary Geology, v. 130, p. 205-228.

Brenner, R.L., and Peterson, J.A., 1994, Jurassic sedimentary history of the northern portion of the western interior seaway, USA, *in* Caputo, M.V., Peterson, J.A., and Franczyk, K.J., eds., Mesozoic systems of the Rocky Mountain region, p. 217-232.

Brock-Hon, A.L., Robins, C.R., and Buck, B.J., 2012, Micromorphological investigation of pedogenic barite in Mormon Mesa petrocalcic horizons, Nevada, USA: Implications for genesis: Geoderma, v. 179-180, p. 1-8.

Brock, A.L., and Buck, B.J., 2009, Polygenetic develpment of the Mormon Mesa, NV petrocalcic horizons: geomorphic and paleoenvironmental interpretations: Catena, v. 77, p. 65-75.

Buatois, L.A., and Mangano, M.G., 1998, Trace fossil analysis of lacustrine facies and basins: Palaeogeography, Palaeoclimatology, Palaeoecology, v. 140, p. 367-382.

Buck, B.J., Lawton, T.F., and Brock, A.L., 2010, Evaporitic paleosols in continental strata of the Carroza Formation, La Popa Basin, Mexico: record of Paleogene climate and salt tectonics: Geological Society of America Bulletin, v. 122, no. 7/8, p. 1011-1026.

Buck, B.J., and Van Hoesen, J.G., 2002, Snowball morphology and SEM analysis of pedogenic gypsum, southern New Mexico, U.S.A.: Journal of Arid Environments, v. 51, p. 469-487.

Bullock, P., Fedoroff, N., Jongerius, A., Stoops, G., Tursina, T., and Babel, U., 1985, Handbook for Soil Thin Section Description: Woverhampton, UK, Waine Research Publications, 152 p.

Burke, W.H., Denison, R.E., Hetherington, E.A., Koepnick, R.B., Nelson, H.F., and Otto, J.B., 1982, Variation of seawater $^{87}Sr/^{86}Sr$ throughout Phanerozoic time: Geology, v. 10, p. 516-519.

Calvo, J.P., Valleron, M.M., Rodriguez, J.P., Arandia, J.M., and Sanz, M.E., 1999, Authigenic clay minerals in continental evaporitic environments: Special Publications of the International Association of Sedimentologists, v. 27, p. 129-151.

Carroll, A.R., and Bohacs, K.M., 1999, Stratigraphic classification of ancient lakes: balancing tectonic and climatic controls: Geology, v. 27, no. 2, p. 99-102.

Carson, C.D., Fanning, D.S., and Dixon, C.J., 1982, Alfisols and Ultisols with acid sulfate weathering features in Texas, *in* Kittrick, J.A., ed., Acid Sulfate Weathering: Madison, WI, Soil Science Society of America, p. 127-146.

Carson, C.J., 1998, The structural and stratigraphic framework of the Warm Springs Ranch area, Hot Springs County, Wyoming, MS thesis: Oklahoma State University, 90 p.

Chadwick, O.A., and Chorover, J., 2001, The chemistry of pedogenic thresholds: Geoderma, v. 100, p. 321-353.

Chamley, H., 1989, Clay Sedimentology: New York, Springer-Verlag, 623 p.

Chervenka, G., 2002, Soil Survey of Brazos County, Texa, *in* United States Department of Agriculture, N.R.C.S.: College Station, United States Department of Agriculture, p. 268.

Childs, C.W., Searle, P.L., and Weatherhead, A.V., 1975, Note on occurrence of barite in B horizons of paleosols in loess, South Canterbury, New Zealand: New Zealand Journal of Science, v. 18, no. 2, p. 227-230.

Chowdhury, A.H., 2004, Hydraulic interaction between groundwater, Brazos River, and oxbow lakes: evidences from chemical and isotopic compositions, Brazos River Basin, Texas, *in* Groundwater Resources Division, T.W.D.B.: Austin, TX, p. 22.

Christiansen, E.H., Kowallis, B.J., and Barton, M.D., 1994, Temporal and spatial distribution of volcanic ash in Mesozoic rocks of the Western Interior: an alternative record of Mesozoic magmatism, *in* Caputo, M.V., Peterson, J.A., and Franczyk, K.J., eds., Mesozoic Systems of the Rocky Mountain Region, USA: Denver, Rocky Mountain Section SEPM, p. 73-94.

Chu, C., Lin, C., Wu, Y., Lu, W., and Long, J., 2006, Organic matter increases jarosite dissolution in acid sulfate soils under inundation conditions: Australian Journal of Soil Research, v. 44, no. 1, p. 11-16.

Church, T., 1970, Marine Barite: San Diego, University of California, 170 p.

Claypool, G.E., Holser, W.T., Kaplan, Y.R., SAkai, H., and Zak, I., 1980, The age of sulfur and oxygen isotopes in marine sulfate and their mutual interpretation: Chemical Geology, v. 28, p. 199-260.

Cohen, A.S., 2003, Paleolimnology: the history and evolution of lake systems: Oxford, Oxford University Press, Inc., 500 p.

Coleman, M.L., and Raiswell, R., 1981, Carbon, oxygen, and sulphur isotope variations in concretions from the Upper Lias of N.E. England: Geochemica et Cosmochimica Acta, v. 45, p. 329-340.

Collins, M.E., and Kuehl, R.J., 2001, Organic matter accumulation and organic soils, *in* Richardson, J.L., and Vepraskas, M.J., eds., Wetland Soils: genesis, hydrology, landscapes, and classification: New York, Lewis Publishers, p. 137-162.

Collinson, J.D., 1996, Alluvial sediments, *in* Reading, H.G., ed., Sedimentary Environments: processess, facies, and stratigraphy: London, Blackwell Science, p. 37-82.

Courchesne, F., Gobran, G.R., and Dufresne, A., 1995, The role of humic acid on sulfate retention and release in a podzol: Water, Air and Soil Pollution, v. 85, p. 1813-1818.

Craft, C.B., 2001, Biology of wetland soils, *in* Richardson, J.L., and Vepraskas, M.J., eds., Wetland Soils: genesis, hydrology, landscapes, and classification: New York, Lewis Publishers, p. 107-135.

Crum, J.R., and Franzmeier, D.P., 1980, Soil properties and chemical composition of tree leaves in southern Indiana: Soil Science Society of America Journal, v. 44, p. 1063-1069.

Cumba, A., and Imbellone, P., 2004, Micromorphology of paleosols at the continental border of the Buenos Aires province, Argentina: Revista Mexicana de Ciencias Geologicas, v. 21, no. 1, p. 18-29.

D'Angelo, E.M., and Reddy, K.R., 1999, Regulators of heterotrophic microbial potentials in wetland soils: Soil Biology and Biochemistry, v. 31, p. 815-830.

Dalai, T.K., Krishnaswamie, S., and Sarin, M.M., 2002, Barium in the Uamuna River system in the Himalaya: sources, fluxes, and its behavior during weathering and transport: Geochemistry, Geophysics, Geosystems, v. 3, no. 12, p. 1-23.

Darmoody, R.G., Harding, S.D., and Hassett, J.J., 1989, Barite authigenesis in surficial soils of mid-continental United States, *in* Miles, ed., Rock-Water Interaction: Rotterdam, p. 183-186.

DeCelles, P.G., 2004, Late Jurassic to Eocene evolution of the Cordilleran thrust belt and Foreland basin system, western U.S.A.: American Journal of Science, v. 304, p. 105-168.

Delmelle, P., and Bernard, A., 2000, Downstream composition changes of acidic volcanic waters discharged into the Banyupahit Stream, Ijen caldera, Indonesia: Journal of Volcanology and Geothermal Research, v. 97, no. 1-4, p. 55-75.

Demko, T.M., and Parrish, J.T., 1998, Paleoclimatic setting of the Upper Jurassic Morrison Formation: Modern Geology, v. 22, p. 283-296.

Dixon, J.B., 1991, Roles of clays in soils: Applied Clay Science, v. 5, p. 489-503.

Douglass, D.N., 1984, Stratigraphy and paleomagnetics of the Morrison and Cloverly Formations, Big Horn Basin, Wyoming: Hanover, New Hamshire, MS thesis: Dartmouth College.

Dowuona, G.N., Mermut, A.R., and Krouse, H.R., 1992, Stable isotopes of salts in some acid sulfate soils of North America: Soil Science Society of America Journal, v. 56, p. 1646-1653.

Drever, J.I., 1973, The preparation of oriented clay mineral specimens for X-ray diffraction analysis by a filter-membrane peel technique: American Mineralogist, v. 58, p. 553-554.

Drits, V.A., Sakharov, B.A., Lindgreen, H., and Salyn, A., 1997, Sequential structure transformation of illite-smectite-vermiculite during digenesis of Upper Jurassic shales from the North Sea and Denmark: Clay Mineralogy, v. 32, p. 351-371.

Dunagan, S.P., 2000, Lacustrine carbonates of the Morrison Formation (Upper Jurassic, Western Interior), East-central Colorado, U.S.A., *in* Gierlowski-Kordesch, E.H., and Kelts, K.R., eds., Lake Basins Through Space and Time: AAPG Studies in Geology, p. 181-188.

Dunagan, S.P., and Turner, C.E., 2004, Regional paleohydrologic and paleoclimatic setting of wetland/lacustrine depositional systems in the Morrison Formation (Upper Jurassic), Western Interior, USA: Sedimentary Geology, v. 167, p. 269-296.

Dunham, A.C., and Hanor, J.S., 1967, Controls on barite mineralization in the western United States: Economic Geology, v. 62, p. 82-94.

Dutton, A., Wilkinson, B.H., Welker, J.M., Bowen, G.J., and Lohmann, K.C., 2005, Spatial distribution and seasonal variation in 18O/16O of modern precipitation and river water across the conterminous USA: Hydrological Processes, v. 19, p. 4121-4146.

Eardley, A.J., and Gvosdetsky, V., 1960, Analysis of Peistocene core from Great Salt Lake, Utah: Geological Society of America Bulletin, v. 71, p. 1323-1344.

Eardley, A.J., Gvosdetsky, V., and Marsell, R.E., 1957, Hydrology of Lake Bonneville and sediments and soils of its basin: Geological Society of America Bulletin, v. 68, p. 1141-1201.

Elison, M.W., Speed, R.C., and Kistler, R.W., 1990, Geologic and isotopic constraints on the crustal structure of the northern Great Basin: Geological Society of America Bulletin, v. 102, p. 1077-1092.

Fallin, M.J., 2005, Carbon Isotope Stratigraphy of the Morrison and Cloverly Formations and Assessment of Vertical Color Change in the Morrison Formation, Coyote Basin, Wyoming: Boulder, University of Colorado, M.S. Thesis, 129 p.

Felmlee, J.K., and Cadigan, R.A., 1978, Spring-deposited radioactive barite in the Great Salt Lake area of Utah: U. S. Geological Survey Professional Paper, v. 38.

Fiedler, S., and Sommer, M., 2004, Water and redox conditions in wetland soils -- their influence on pedogenic oxides and morphology: Soil Science Society of America Journal, v. 68, p. 326-335.

Finlay, B.J., Hetherington, N.B., and Davison, W., 1983, Active biological participation in lacustrine barium chemistry: Geochemica et Cosmochimica Acta, v. 47, p. 1325-1329.

Fitzpatrick, E.A., 1993, Soil Microscopy and Micromorphology: New York, John Wiley, 304 p.

Freytet, P., and Verrecchia, E.P., 2002, Lacustrine and palustrine carbonate petrography: an overview: Journal of Paleolimnology, v. 27, no. 221-237.

Gambrell, R.P., 1994, Trace and toxic metals in wetlands -- a review: Journal of Environmental Quality, v. 23, p. 883-891.

Garces, B.L.V., and Aguilar, J.G., 1994, Permian saline lakes in the Aragon-Bearn Basin, western Pyrenees, Sedimentology and Geochemistry of Modern and Ancient Saline Lakes: SEPM, p. 267-290.

Goldstein, R.H., and Reynolds, T.J., 1994, Systematics of Fluid Inclusions in Diagenetic Minerals, SEPM Special publication, v. 31, 199 p.

Gonzalez-Munoz, M.T., Fernandez-Luque, B., Martinez-Ruiz, F., Chekroun, K.B., Arias, J.M., Rodriguez-Gallego, M., Martinez-Canamero, M., de Linares, C., and Paytan, A., 2003, Precipitation of barite by *Mycoccus xanthus*: possible implications for the biogeochemical cycle of barium: Applied and Environmental Microbiology, v. September, p. 5722-5725.

Gottardi, G., and Galli, E., 1985, Natural Zeolites: New York, Springer-Verlag, 409 p.

Gran, K.B., and Montgomery, D.R., 2005, Spatial and temporal patterns in fluvial recovery following volcanic eruptions: channel response to basin-wide sediment loading at Mount Pinatubo, Phillipines: Geological Society of America Bulletin, v. 117, no. 1-2, p. 195-211.

Gray, K.D., and Oldow, J.S., 2005, Contrasting structural histories of the Slamon River belt and Wallowa terrane: Implications for terrane accretion in northeastern Oregon and west-central Idaho: Geological Society of America Bulletin, v. 117, no. 5/6, p. 687-706.

Greb, S.F., DiMichele, W.A., and Gastaldo, R.A., 2006, Evolution and importance of wetlands in earth history, *in* Greb, S.F., and DiMichele, W.A., eds., Wetlands Through Time: Boulder, Geological Society of America p. 1-40.

Habicht, K.S., and Canfield, D.E., 2001, Isotope fractionation by sulfate-reducing natural populations and the isotopic composition of sulfide in marine sediments: Geology, v. 29, no. 6, p. 555-558.

Hanor, J.S., 2000, Barite-celestine geochemistry and environments of formation, *in* Alpers, C.N., Jambor, J.L., and Nordstrom, D.K., eds., Sulfate Minerals: crystallography, geochemistry, and environmental significance: Washington D.C., Mineralogical Society of America, p. 193-275.

Hasiotis, S.T., 2004, Reconnaissance of Upper Jurassic Morrison Formation ichnofossils, Rocky Mountain Region, USA: paleoenvironmental, stratigraphic, and paleoclimatic significance of terrestrial and freshwater ichnocoenoses: Sedimentary Geology, v. 167, p. 177-268.

Hay, R.L., 1970, Silicate reactions in three lithofacies of a semi-arid basin, Olduvai Gorge, Tanzania: Mineralogical Society of America Special Paper, v. 3, p. 237-255.

Hay, R.L., and Kyser, T.K., 2001, Chemical sedimentology and paleoenvironmental history of Lake Olduvai, a Pliocene lake in northern Tanzania: Geological Society of America Bulletin, v. 113, no. 12, p. 1505-1521.

Hillier, S., 1995, Erosion, sedimentation and sedimentary origin of clays, *in* Velde, B., ed., Origin and Mineralogy of Clays: New York, Springer-Verlag, p. 162-219.

Hocking, R., 2001, Remote Quadrio Lake; a new base metal frontier?: Prospect (Perth. 1992), v. 2001, no. March, p. 24-25.

Hocking, R.M., and Pirajno, F., 2000, Quadrio Lake; we've found the barite, where are the sulfides?: Record - Geological Survey of Western Australia, p. 25-27.

Hughes, R.E., Moore, D.M., and Reynolds, J., R.C., 1993, The nature, detection, occurrence, and origin of kaolinite/smectite, in Kaolin genesis and utilization: a collection of papers presented at the Keller '90 Kaolin Symposium, p. 291-323.

Hurt, G.W., and Carlisle, V.W., 2001, Delineating hydric soils, *in* Richardson, J.L., and Vepraskas, M.J., eds., Wetland Soils: genesis, hydrology, landscapes, and classification: New York, Lewis Publishers, p. 183-206.

Huston, D.L., and Logan, G.A., 2004, Barite, BIFs and bugs: evidence for the evolution of the Earth's early hydrosphere: Earth and Planetary Science Letters, v. 220, p. 41-55.

Hutchinson, K.J., Hesterberg, D., and Chou, J.W., 2001, Stability of reduced organic sulfur in humic acid as affected by aeration and pH: Soil Science Society of America Journal, v. 65, p. 704-709.

Ikejiri, T., Watkins, P., and Gray, D., 2006, Stratigraphy, sedimentology, and taphonomy of a sauropod quarry from the Upper Morrison Formation of Thermopolis, central Wyoming: Bulletin - New Mexico Museum of Natural History and Science, v. 36, p. 39-46.

Irving, W.N., Jopling, A.V., and Kritsch-Armstrong, I., 1989, Studies of bone technology and taphonomy, Old Crow Basin, Yukon Territory, *in* Bonnichesen, R., and Sorg, M.H., eds., Bone Modification: Orono, Maine, Center for the Study of the First Americans, p. 347-380.

Jackson, M.L., Lim, C.H., and Zelazny, W., 1986a, Oxides, hydroxides, and aluminosilicates, *in* Klute, A., ed., Methods of Soil Analysis, Part I -- Agronomy Monograph 9: (2nd ed.) Madison, Wisconsin, American Society of Agronomy, Inc., p. 101-142.

Jackson, M.L., Lim, C.H., and Zelazny, W., 1986b, Oxides, hydroxides, and aluminosilicates, *in* Klute, A., ed., Methods of Soil Analysis, Part 1 -- Agronomy Monograph 9: Madison, Wisconsin, American Society of Agronomy, Inc., p. 101-142.

Jacobs, P.M., West, L.T., and Shaw, J.N., 2002, Redoximorphic features as indicators of seasonal saturation, Lowndes County, Georgia: Soil Science Society of America Journal, v. 66, p. 315-323.

Jennings, D., Lovelace, D., and Driese, S.G., 2011, Differentiating paleowetland subenvironments using a multi-disciplinary approach: An example from the Morrison formation, South Central Wyoming, USA: Sedimentary Geology, v. 238, p. 23-47.

Jennings, D.S., 2004a, Identification of dinosaur tracks in palustrine-lacustrine deposits of the Morrison Formation; their significance to lacustrine sequence stratigraphy, Annual Meeting Expanded Abstracts - American Association of Petroleum Geologists: United States, American Association of Petroleum Geologists and Society for Sedimentary Geology : Tulsa, OK, United States, v. 13, p. 71.

Jennings, D.S., 2004b, A survey and assessment of lacustrine authigenic minerals from the Morrison Formation, Big Horn Basin, Wyoming, Abstracts with Programs - Geological Society of America: United States, Geological Society of America (GSA) : Boulder, CO, United States, v. 36, p. 472.

Jennings, D.S., 2005, A Paleoenvironmental Analysis of Morrison Formation Deposits, Big Horn Basin, Wyoming: a multivariate approach: Lawrence, University of Kansas, M.S., 110 p.

Jennings, D.S., and Driese, S.G., 2014, Understanding barite and gypsum precipitation in upland acid-sulfate soils: An example from a Lufkin Series toposequence, south-central Texas, USA: Sedimentary Geology, v. 299, p. 106-118.

Jennings, D.S., and Hasiotis, S.T., 2006a, Paleoenvironmental and stratigraphic implications of authigenic clay distributions in Morrison Formation deposits, Bighorn Basin, Wyoming: New Mexico Museum of Natural History Bulletin, v. 36, p. 25-34.

Jennings, D.S., and Hasiotis, S.T., 2006b, Taphonomic Analysis of a Dinosaur Feeding Site Using Geographic Information Systems (GIS), Morrison Formation, Southern Bighorn Basin, Wyoming, USA: Palaios, v. 21, p. In Press.

Jennings, D.S., Platt, B.F., and Hasiotis, S.T., 2006, Distribution of vertebrate trace fossils, Upper Jurassic Morrison Formation, Bighorn Basin, Wyoming, USA: Implications for differentiating paleoecological and preservational bias: New Mexico Museum of Natural History Bulletin, v. 36, p. 183-192.

Johnson, J.S., 1991, Stratigraphy, sedimentology, and depositional environments of the Upper Jurassic Morrison Formation, Colorado front range: Lincoln, Nebraska, Dissertation: University of Nebraska.

Jones, E., J.P., Nadeau, T.-L., Voytek, M.A., and Landa, E., R., 2006, Role of microbial iron reduction in the dissolution of iron hydroxysulfate minerals: Journal of Geophysical Research, v. 111, no. G01012, p. 1-8.

Jones, R.L., 1986, Barium in Illinois surface soils: Soil Science Society of America Journal, v. 50, no. 4, p. 1085-1087.

Jorgensen, R.R., 1983, The microbial sulphur cycle, *in* Krumbein, W.E., ed., Microbial Geochemistry: Oxford, Blackwell Science Ltd, p. 91-124.

Kabata-Pendias, A., 2001, Trace Elements in Soils and Plants (3rd ed.): New York, CRC Press, 432 p.

Kataoka, K., 2005, Distal fluvial-lacustrine volcaniclastic resedimentation in response to an explosive silicic eruption: the Pliocene Mushono tephra bed, central Japan: Geological Society of America Bulletin, v. 117, no. 1-2, p. 3-17.

Kelts, K., and Hsu, K.J., 1978, Freshwater carbonate sedimentation, *in* Lerman, A., ed., Lakes: Chemistry, geology, physics: New York, Springer-Verlag, p. 363.

Kirkland, J.I., 2006, Fruita paleontological area (Upper Jurassic, Morrison Formation), western Colorado; an example of terrestrial taphofacies analysis: Bulletin - New Mexico Museum of Natural History and Science, v. 36, p. 67-95.

Korte, C., Kozur, H.W., Bruchschen, P., and Veizer, J., 2003, Strontium isotope evolution of the Late Permian and Triassic seawater: Geochemica et Cosmochimica Acta, v. 67, no. 1, p. 47-62.

Kraus, M.J., 1997, Lower Eocene alluvial paleosols: pedogenic development, stratigraphic relationships, and paleosol/landscape associations: Palaeogeography, Palaeoclimatology, Palaeoecology, v. 129, p. 387-406.

Kraus, M.J., 1999a, Paleosols in clastic sedimentary rocks: their geologica applications: Earth-Science Reviews, v. 47, p. 41-70.

Kraus, M.J., 1999b, Paleosols in clastic sedimentary rocks: their geological applications: Earth-Science Reviews, v. 47, p. 41-70.

Kraus, M.J., and Gwinn, B., 1997, Facies and facies architecture of Paleogene floodplain deposits, Willwood Formation, Bighorn Basin, Wyoming, USA: Sedimentary Geology, no. 114, p. 33-54.

Kraus, M.J., and Hasiotis, S.T., 2006, Significance of different modes of rhizolith preservation to interpreting paleoenvironemtns and paleohydrological setting: examples from Paleogene paleosols, Bighorn Basin, Wyoming, U.S.A: Journal of Sedimentary Research, v. 76, p. 633-646.

Krouse, H.R., Stewart, J.W.B., and Grinenko, V.A., 1991, Pedosphere and Biosphere, *in* Krouse, H.R., and Grinenko, V.A., eds., Stable Isotopes in the Assessment of Natural and Anthropogenic Sulphur in the Environment: John Wiley & Sons, Ltd, p. 267-306.

Kuenzi, W.D., Horst, O.H., and McGehee, R.V., 1979, Effect of volcanic activity on fluvial-deltaic sedimentation in a modern arc-trench gap, southwestern Guatemala: Geological Society of America Bulletin, v. 90, no. Part 1, p. 827-838.

Kunze, G.W., and Oakes, H., 1957, Field laboratory studies of the Lufkin soil, a planosol: Soil Science Society of America Proceedings, v. 21, p. 330-335.

Kusakabe, M., Rafter, T.A., Stout, J.D., and Collie, T.W., 1976, Sulphur isotopic variations in nature: New Zealand Journal of Science, v. 19, p. 433-440.

LaMaskin, T.A., Vervoort, J.D., Dorsey, R.J., and Wright, J.E., 2011, Early Mesozoic paleogeography and tectonic evolution of the western United States: Insights from detrital zircon U=Pb geochronology, Blue Mountains Province, noretheastern Oregon: Geological Society of America Bulletin, v. 123, no. 9/10, p. 1939-1965.

Lawton, T., 1994a, Tectonic setting of Mesozoic sedimentary basins, Rocky Mountain region, United States, *in* Caputo, M.V., Peterson, J.A., and Franczyk, K.J., eds., Mesozoic System of the Rock Mountain Region, USA, p. 1-25.

Lawton, T.F., 1994b, Tectonic setting of Mesozoic sedimentary basins, Rocky Mountain region, United States, *in* Caputo, M.V., Peterson, J.A., and Franczyk, K.J., eds., Mesozoic Systems of the Rocky Mountain Region, USA: Rocky Mountain Section, Society of Economic Paleontolgists and Mineralogists, Special Publication, p. 1-25.

Liuqi, W., Zaixing, J., Yingchang, C., Wentao, H., and Jing, W., 1997, Lake sequence stratigraphy of the Shahejie Formation in the Zhanhua Hollow, Shandong Province: Acta Geologica Sinica, v. 71, no. 1, p. 104-114.

Liutkus, C.M., Wright, J.D., Ashley, G.M., and Sikes, N.E., 2005, Paleoenvironmental interpretation of lake-margin deposits using d13C and d18O results from early Pleistocene carbonate rhizoliths, Olduvai Gorge, Tanzania: Geology, v. 33, no. 5, p. 377-380.

Lo Forte, G.L., Orti, F., and Rosell, L., 2005, Isotopic characterization of Jurassic evaporites, Aconcagua-Neuquen Basin, Argentina: Geologica Acta, v. 3, no. 2, p. 155-161.

Lockley, M., 1986, The paleobiological and paleoenvironmental importance of dinosaur footprints: Palaios, v. 1, p. 37-47.

Lockley, M.G., Houck, K.J., and Prince, N.K., 1986, North America's largest dinosaur trackway site: implications for Morrison Formation paleoecology: Geological Society of America Bulletin, v. 97, no. 10, p. 1163-1176.

Lovelace, D., 2006, An Upper Jurassic Morrison Formation fire-induced debris flow: taphonomy and paleoenvironment of a sauropod (Sauropoda: *Supersaurus vivianae*) locality, East-Central Wyoming: New Mexico Museum of Natural History Bulletin, v. 36, p. 47-56.

Lovely, D.R., Coates, J.D., Blunt-Harris, E.L., Plhillips, E.J.P., and Woodward, J.C., 1998, Humic substances as electron acceptors for microbial respiration: Nature, v. 382, p. 445-448.

Lucas, S.G., and Kirkland, J.I., 1998, Preliminary report on conchostraca from the Upper Jurassic Morrison Formation, western United States: Modern Geology, v. 22, p. 415-422.

Luo, Z., and Wible, J.R., 2005, A Late Jurassic digging mammal and early mammalian diversification: Science, v. 308, p. 103-107.

Lynn, W.C., Tu, H.Y., and Franzmeier, D.P., 1971, Authigenic barite in soils: Soil Science Society of America Journal Proceedings, v. 35, p. 160-161.

Lyons, W.B., Hines, M.E., Last, W.M., and Lent, R.M., 1994, Sulfate reduction rates in microbial mat sediments of differing chemistries: implications for organic carbon preservation in saline lakes, Sedimentology and Geochemistry of Modern and Ancient Saline Lakes, SEPM Publication: SEPM (Society for Sedimentary Geology), p. 13-20.

Major, J.J., Pierson, T.C., and Costa, J.E., 2000, Sediment yield following severe volcanic disturbance--a two-decade perspective from Mount St. Helens: Geology, v. 28, no. 9, p. 819-822.

Martino, D.P., Grossman, E.L., Ulrich, G.A., Schlichenmeyer, J.L., Suflita, J.M., and Ammerman, J.W., 1998, Microbial abundance and activity in a low-conductivity aquifer system in east-central Texas: Microbial Ecology, v. 35, p. 224-234.

Mausbach, M.J., and Parker, W.B., 2001, Background and history of the concept of hydric soils, *in* Richardson, J.L., and Vepraskas, M.J., eds., Wetland Soils: genesis, hydrology, landscapes, and classification: New York, Lewis Publishers, p. 19-33.

May, S.R., Gray, G., G., Lumma, L.L., Stewart, N., R., Gehrels, G.E., and Pecha, M.E., 2013, Detrital zircon geochronology from the Bighorn Basin, Woming, USA: Implication for tectonostratigraphic evolution and paleogeography: Geological Society of America Bulletin, v. 125, no. 9/10, p. 1403-1422.

McCarthy, P.J., and Plint, A.G., 2003, Spatial variability of palaeosols across Cretaceous interfluves in the Dunvegan Formation, NE British Columbia, Canada: palaeohydrological, palaeogeomorphological and stratigraphic implications: Sedimentology, v. 50, p. 1187-1220.

Meunier, A., and Velde, B., 2004, Illite: origins, evolution, and metamorphism: New York, Springer-Verlag, 286 p.

Meyers, P.A., and Ishiwatari, R., 1993, Lacustrine organic geochemistry -- an overview of indicators of organic matter sources and diagenesis in lake sediments: Organic Geochemistry, v. 20, no. 7, p. 867-900.

Milroy, P.G., and Wright, V.P., 2000, A highstand oolitic sequence and associated facies from a Late Triassic lake basin, south-west England: Sedimentology, v. 47, p. 187-209.

Ming, D.W., and Dixon, J.B., 1988, Occurrence and weathering of zeolites in soil environments., *in* Kiado, A., ed., Occurrences, Properties, and Utilization of Natural Zeolites: Budapest, Hungary, p. 699-715.

Moore, D.M., and Reynolds, R.C., 1997, X-ray Diffraction and the Identification and Analysis of Clay Minerals: New York, Oxford University Press, 378 p.

NCDC, 2012, Climatography of the United States, No. 20, National Oceanic & Atmospheric Administration, v. 2011.

Nordt, L.C., and Driese, S.G., 2013, Application of the Critical Zone Concept to the Deep-Time sedimentary record: The Sedimentary Record, v. 11, no. 3, p. 4-9.

NRCS, 2010, NRCS Soils Website, http://soils.usda.gov/.

Owen, D.E., Turner-Peterson, C.E., and Fishman, N.S., 1989, X-ray Diffraction Studies of the <0.5-um Fraction from the Brushy Basin Member of the Upper Jurassic Morrison Formation, Colorado Plateau, *in* Interior, D.o.t., U.S. Geological Survey, v. 1808-G, p. G1-G25.

Parrish, J.T., Peterson, F., and Turner, C.E., 2004, Jurassic "savannah"--plant taphonomy and climate of the Morrison Formation (Upper Jurassic, Western USA): Sedimentary Geology, v. 167, p. 137-162.

Paz, J.D.S., and Rossetti, D.F., 2005, Linking lacustrine cycles with syn-sedimentary tectonic episodes: an example from the Codo Formation (late Aptian), northeastern Brazil: Geology Magazine, v. 142, no. 3, p. 269-285.

Pedons, V.A., 2002, Oxygen-isotope composition of Great Salt Lake, 1979 to 1996, *in* Richmond, M.W., Great Salt Lake: an overview of change: Salt Lake City, Special Publication - Utah Department of Natural Resources, p. 121-126.

Peterson, F., 1988, Pennsylvanian to Jurassic eolian transportation systems in the western United States: Sedimentary Geology, v. 56, p. 207-260.

Peterson, F., 1994, Sand dunes, sabkhas, streams, and shallow seas: Jurassic paleogeography in the southern part of the Western Interior basin, *in* Caputo, M.V., Peterson, J.A., and Franczyk, K.J., eds., Mesozoic systems of the Rocky Mountain region, USA, p. 233-272.

Peterson, R.C., Kyser, K., Pagano, R., and Klassen, K., 2003, Sulfur isotope analysis for the identification of sulfur sources: Mineralogical Record, v. 34, p. 171-175.

Pipujol, M.D., and Buurman, P., 1994, The distinction between ground-water gley and surface-water gley phenomena in Tertiary paleosols of Ebro basin, NE Spain: Palaeogeography, Palaeoclimatology, Palaeoecology, v. 110, p. 103-113.

Platt, S.G., Rainwater, T.R., and Brewer, S.W., 2004, Aspects of the burrowing ecology of nine-banded armadillos in northern Belize: Mammalian Biology, v. 69, no. 4, p. 217-224.

Plint, A.G., McCarthy, P.J., and Faccini, U.F., 2001, Nonmarine sequence stratigraphy: updip expression of sequence boundaries and systems tracts in a high-resolultion framework, Cenomanian Dunvegan Formation, Alberta forland basin, Canada: AAPG Bulletin, v. 85, p. 1967-2001.

Podwojewski, P., 1995, The occurrence and interpretation of carbonate and sulfate minerals in a sequence of Vertisols in New Caledonia: Geoderma, v. 65, no. 3-4, p. 223-248.

Pons, L.J., 1973, Outline of the genesis, characteristics, classification and improvement of acid sulphate soils, in Acid Sulphate Soils, Proceedings of the International Symposium, Wageningen, The Netherlands, International Land Reclamation Insititute, p. 3-27.

Rao, S.M., and Sridharan, A., 1984, Mechanism of sulfate adsorption by kaolinite: Clays and Clay Minerals, v. 32, no. 5, p. 414-418.

Renaut, R.W., 1993, Zeolitic diagenesis of late Quaternary fluvio-lacustrine sediments and associated calcrete formation in the Lake Borgoria Basin, Kenya Rift Valley: Sedimentology, v. 40, p. 271-301.

Retallack, G.J., Bestland, E.A., and Fremd, T.J., 1999, Eocene and Oligocene Paleosols of Central Oregon, Geological Society of America, Inc., v. Special Paper no. 344, 192 p.

Retallack, G.J., and Huang, C., 2010, Depth to gypsic horizon as a proxy for paleoprecipitation in paleosols of sedimentary environments: Geological Society of America Bulletin, v. 38, no. 5, p. 403-406.

Retallack, G.J., and Kirby, M.X., 2007, Middle Miocene global change and paleogeography of Panama: Palaios, v. 22, p. 667-679.

Richardson, J.L., Arndt, J.L., and Montgomery, J.A., 2001, Hydrology of wetland and related soils, *in* Richardson, J.L., and Vepraskas, M.J., eds., Wetland Soils: genesis, hydrology, landscapes and classification: New York, Lewis Publishers, p. 35-84.

Richardson, J.L., and Brinson, M.M., 2001, Wetland soils and hydrogeomorphic classification of wetlands, *in* Richardson, J.L., and Vepraskas, M.J., eds., Wetland Soils: genesis, hydrology, landscapes, and classification: New York, Lewis Publishers, p. 209-227.

Routh, J., McDonald, T.J., and Grossman, E.L., 1999, Sedimentary organic matter sources and depositional environment in the Yegua formation (Brazos County, Texas): Organic Geochemistry, v. 30, p. 1237-1453.

Sanchez-Pastor, N., Pina, C.M., and Fernandez-Diaz, L., 2006, Relationship between crystal morphology and composition in the (Ba, Sr)SO_4--H_2O solid solution -- aqueous solution system: Chemical Geology, v. 225, p. 266-277.

Santos, E.S., and Peterson, C.E., 1986, Tectonic setting of the San Juan Basin in the Jurassic, *in* Turner-Peterson, C.E., Santos, E.S., and Fishman, N.S., eds., A Basin Analysis Case Study: the Morrison Formation, Grants Uranium Region, New Mexico
American Association of Petroleum Geologists p. 27-33.

Scarciglia, F., Barca, D., De Rosa, R., and Pulice, I., 2009, Application of laser ablation ICP-MS and traditional micromorphological techniques to the study of an Alfisol (Sardinia, Italy) in thin sections: Insights into trace element distribution: Geoderma, v. 152, p. 113-126.

Scheiber, J., 2003, Simple gifts and buried treasures -- implications of finding bioturbation and erosion surfaces in black shales: The Sedimentary Record, v. 1, no. 2, p. 4-8.

Schmidt, D.R., 2009, Stable Isotope Geochemistry of Upper Cretaceous and Paleocene Strata in Big Bend National Park, Texas, Texas Tech University, 202 p.

Schnurrenberger, D., Russell, J., and Kelts, K., 2003, Classification of lacustrine sediments based on sedimentary components: Journal of Paleolimnology, v. 29, p. 141-154.

Schudack, M.E., Turner, C.E., and Peterson, F., 1998, Biostratigraphy, paleoecology, and biogeography of charophytes and ostracodes from the Upper Jurassic Morrison Formation, Western Interior, USA: Modern Geology, v. 22, p. 379-414.

Scott, A.C., 2000, The Pre-Quaternary history of fire: Palaeogeography, Palaeoclimatology, Palaeoecology, v. 164, p. 281-329.

Seal, I., Robert R., Alpers, C.N., and Rye, R.O., 2000, Stable isotope systematics of sulfate minerals, *in* Alpers, C.N., Jambor, J.L., and Nordstrom, D.K., eds., Sulfate minerals: crystallography, geochemistry, and environmental significance: Washington D.C., Mineralogical Society of America, p. 541-602.

Senkayi, A.L., Dixon, J.B., Hossner, L.R., Abder-Ruhman, M., and Fanning, D.S., 1984, Mineralogy and genetic relationships of tonstein, bentonite, and lignitic strata in the Eocene Yegua Formation of East-central Texas: Clays and Clay Minerals, v. 32, no. 4, p. 259-271.

Senko, J.M., Campbell, B.S., Henriksen, J.R., Elshahed, M.S., Dewers, T.A., and Krumholz, L.R., 2004, Barite deposition resulting from phototrophic sulfide-oxidizing bacterial activity: Geochemica et Cosmochimica Acta, v. 68, no. 4, p. 773-780.

Serrano, R.E., Arias, J.S., and Fernandez, P.G., 1999, Soil properties that affect sulphate adsorption by Palexerults in western and central Spain: Communications in Soil Science and Plant Analysis, v. 30, no. 9&10, p. 1521-1530.

Shanley, K.W., and McCabe, P.J., 1994, Perspectives on the sequence stratigraphy of continental strata: AAPG Bulletin, v. 78, no. 4, p. 544-568.

Sharpley, A.N., 1990, Kinetics of sulfate desorption from soil: Soil Science Society of America Journal, v. 54, p. 1571-1575.

Singer, A., 1984, The paleoclimatic interpretation of clay minerals in sediments -- a review: Earth-Science Reviews, v. 21, p. 251-293.

Smith, E., Hamilton-Taylor, J., Davison, W., Fullwood, N.J., and McGrath, M., 2004a, The effect of humic substances on barite precipitation-dissolution behaviour in natural and synthetic lake waters: Chemical Geology, v. 207, no. 1-2, p. 81-89.

Smith, E., Hamilton-Taylor, J., Davison, W., Fullwood, N.J., and McGrath, M., 2004b, The effect of humic substances on barite precipitation -- dissolution behaviour in natural and synthetic lake waters: Chemical Geology, v. 207, p. 81-89.

Smith, G.A., 1988, Sedimentology of proximal to distal volcaniclastics dispersed across an active foldbelt: Ellensburg Formation (late Miocene), central Washington: Sedimentology, v. 35, p. 953-977.

Smolders, A.J.P., Moonen, M., Zwaga, K., Lucassen, E.C.H.E.T., Lamers, L.P.M., and Roelofs, J.G.M., 2006, Changes in pore water chemistry of desiccating freshwater sediments with different sulphur contents: Geoderma, v. 132, p. 372-383.

Soils, N.T.C.H., 1987, Hydric Soils of the United States: Washington, DC, USDA Soil Conservation Service.

Stevenson, F.J., and Cole, M.A., 1999, Cycles of Soil: carbon, nitrogen, phosphorus, sulfur, micronutrients: New York, John Wiley & Sons, Inc., 427 p.

Stiles, C.A., Mora, C.I., and Driese, S.G., 2001, Pedogenic iron-manganese nodules in Vertisols: a new proxy for paleoprecipitation?: Geology, v. 29, no. 10, p. 943-946.

Stoffregen, R.E., Alpers, C.N., and Jambor, J.L., 2000, Alunite-jarosite crystallography, thermodynamics, and geochronology, *in* Alpers, C.N., Jambor, J.L., and Nordstrom, D.K., eds., Sulfate Minerals: Crysallography, Geochemistry, and Environmental Significance: Washington, DC, The Mineralogical Society of America, p. 453-479.

Stoops, G., and Poch, R.M., 1985, Micromorphological classification of gypsiferous soil materials, in IX International Working Meeting on Soil Micromorphology, Townsville, Australia, Developments in Soil Science, Elsevier, p. 327-332.

Stoops, G., and Poch, R.M., 1994, Micromorphological classification of gypsiferous soil materials, in IX International Working Meeting on Soil Micromorphology, Townsville, Australia, Developments in Soil Science, Elsevier, p. 327-332.

Stoops, G., and Zavaleta, A., 1978, Micromorphological evidence of barite neoformation in soils: Geoderma, v. 20, no. 1, p. 63-70.

Strauss, H., 1997, The isotopic composition of sedimentary sulfur through time: Palaeogeography, Palaeoclimatology, Palaeoecology, v. 132, p. 97-118.

Sullivan, L.A., and Koppi, A.J., 1993, Barite pseudomorphs after lenticular gypsum in a buried soil from Central Australia: Australian Journal of Soil Research, v. 31, p. 393-396.

Sullivan, L.A., and Koppi, A.J., 1995, Micromorphology of authigenic celestobarite in a duripan from central Australia: Geoderma, v. 64, no. 3-4, p. 357-361.

Surdam, R.C., and Eugster, H.P., 1976, Mineral reactions in the sedimentary deposits of the Lake Magadi region, Kenya: Geological Society of America Bulletin, v. 87, p. 1739-1752.

Suttner, L.J., 1969, Stratigraphic and petrographic analysis of Upper Jurassic-Lower Cretaceous Morrison and Kootenai formations, southwest Montana: American Association of Petroleum Geologists Bulletin, v. 53, no. 7, p. 1391-1410.

Swartz, J.J., Snoke, A.W., Cordey, F., Johnson, K., Frost, C.D., Barnes, C.G., LaMaskin, T.A., and Wooden, J.L., 2011, Late Jurassic magnatism, metamorphism, and deformation in the Blue Mountains Province, northeast Oregon: Geological Society of America Bulletin, v. 123, no. 9/10, p. 2083-2111.

Swirydczuk, K., and Wilkinson, B.H., 1979, The Pliocene Glenns Ferry oolite: lake-margin carbonate deposition in the southwestern Snake River Plain: Journal of Sedimentary Petrology, v. 49, no. 3, p. 995-1004.

Takehito, I., Watkins, P., and Gray, D., 2006, Stratigraphy, sedimentology, and taphonomy of a sauropod quarry from the Upper Morrison Formation of Thermopolis, Central Wyoming: New Mexico Museum of Natural History and Science Bulletin, v. 36, p. 39-46.

Tanner, W.F., 1968, Shallow lake deposits, lower part of Morrison Formation (late Jurassic), northern New Mexico: The Mountain Geologist, v. 5, no. 4, p. 187-195.

Taylor, M.W., and Surdam, R.C., 1981, Zeolite reactions in the tuffaceous sediments at Teels Marsh, Nevada: Clays and Clay Minerals, v. 25, no. 5, p. 341-352.

Tidwell, W.D., 1990, Preliminary report on the megafossil flora of the Upper Jurassic Morrison Formation: Hunteria, v. 2, no. 8, p. 12.

Tiercelin, J., Vincens, A., Barton, C.E., Carbonel, P., Casanova, J., Delibrias, G., Gasse, F., Grosdidier, E., Herbin, J., Huc, A.Y., Jardine, S., Le Fournier, J., Palacios, C., Paquet, H., Peniguel, G., Peypouquet, J., Raynaud, J., Renaut, R.W., de Reneville, P., Richert, J., Riff, R., Robert, P., Seyve, C., Vandenbroucke, M., and Vidal, G., 1987, Le demi-graben de Baringo-Bogoria Rift Gregory, Kenya. 30 000 ans d'histoire hydrologique et seddimentaire (The Baringo-Borgoria Half-graben, Gregory Rift, Kenya, 30,000 years of Hydrological and Sedimentaty History), Societe National Elf Aquitaine (Production), 540 p.

Tiner, R.W., 1999, Wetland Indicators: A Guide to Wetland Identification, Delineation, Classification, and Mapping: New York, Lewis Publishers.

Tiner, R.W., 2003, Geographically isolated wetlands of the United States: Wetlands, v. 23, no. 3, p. 494-516.

Triplehorn, D.M., Blake, B.M., and Anonymous, 2001, Authigenic barite precipitated in Paleosols below marine transgressions: Abstracts with Programs - Geological Society of America, v. 33, no. 6, p. 445.

Trujillo, K.C., 2003, Stratigraphy and Correlation of the Morrison Formation (Late Jurassic-?Early Cretaceous) Across the Western Interior, U.S.A., with special emphasis on southeastern Wyoming: Laramie, University of Wyoming, Dissertation, 192 p.

Trust, B.A., and Fry, B., 1992, Stable sulphur isotopes in plants: a review: Plant, Cell, and Environment, v. 15, p. 1105-1110.

Turchyn, A.V., Bruchert, V., Lyons, T.W., Engel, G.S., Balci, N., Schrag, D.P., and Brunner, B., 2010, Kinetic oxygen isotope effects during dissimilatory sulfate reduction: a combined theoretical and experimental approach: Geochimica et Cosmochimica Acta, v. 74, p. 2011-2024.

Turchyn, A.V., and Schrag, D.P., 2006, Cenozoic evolution of the sulfur cycle: insight from oxygen isotopes in marine sulfate: Earth and Planetary Science Letters, v. 241, p. 763-779.

Turner, C.E., and Fishman, N.S., 1991, Jurassic Lake T'oo'dichi': a large alkaline, saline lake, Morrison Formation, eastern Colorado Plateau: Geological Society of America Bulletin, v. 103, p. 538-558.

Turner, C.E., and Fishman, N.S., 1998, Late Jurassic Lacustrine Deposits and Implications for Paleohydrology: Deposition to Early Compaction, *in* Pitman, J.K., and Carroll, A.R., eds., Modern and Ancient Lake Systems: Utah Geological Association, p. 31-49.

Turner, C.E., and Peterson, F., 2004, Reconstruction of the Upper Jurassic Morrison Formation extinct ecosystem -- a synthesis: Sedimentary Geology, v. 167, p. 309-355.

Ulrich, G.A., Burger, K., Routh, J., Grossman, E.L., Ammerman, J.W., and Suflita, J.M., 1998, Sulfur cycling in terrestrial subsurface: commensal interactions, spatial scales, and microbial heterogeneity: Microbial Ecology, v. 36, p. 141-151.

Van Den Ende, J., 1991, Supersaturation of soil solutions with respect to gypsum: Plant and Soil, v. 133, p. 65-74.

Van Stempvoort, D.R., Reardon, E.J., and Fritz, P., 1990, Fractionation and sulfur and oxygen isotopes in sulfate soil by sulfate sorption: Geochimica et Cosmochimica Acta, v. 54, p. 2817-2826.

Vepraskas, M.J., 2001, Morphological features of seasonally reduced soils, *in* Richardson, J.L., and Vepraskas, M.J., eds., Wetland Soils: genesis, hydrology, landscapes, and classification: New York, Lewis Publishers, p. 163-182.

Vepraskas, M.J., and Faulkner, S.P., 2001, Redox chemistry of hydric soils, *in* Richardson, J.L., and Vepraskas, M.J., eds., Wetland Soils: genesis, hydrology, landscapes, and classification: New York, Lewis Publishers, p. 85-105.

Vepraskas, M.J., Wilding, L.P., and Drees, L.R., 1992, Aquic conditions for Soil Taxonomy: concepts, soil morphology and micromorphology, in IX International Working Meeting on Soil Micromorphology, Townsville, Australia, Elsevier, p. 117-131.

Walker, R.G., and Cant, D.J., 19984, Sandy fluvial systems, *in* Walker, R.G., ed., Facies Models: (2nd ed.) Newfoundland, Canada, Geological Association of Canada, p. 71-89.

Warner, B.G., and Rubec, C.D.A., eds., 1997, The Canadian Wetland Classification System (2nd ed.): Waterloo, Ontario, National Wetlands Working Group, 7 p.

White, P.D., and Schiebout, J., 2008, Paleogene paleosols and changes in pedogenesis during the initial Eocene thermal maximum: Big Bend National Park, Texas, USA: Geological Society of America Bulletin, v. 120, p. 1347-1361.

Wood, J.R., Worthy, T.H., Rawlence, N.J., Holdaway, R.N., and Reed, S.E., 2008, A deposition mechanism for Holocene miring bone deposits, South Island, New Zealand: Journal of Taphonomy, v. 6, no. 1, p. 1-20.

Wright, V.P., Marriott, S.B., and Vanstone, S.D., 1991, A 'reg' palaeosol from the Lower Triassic of south Devon: stratigraphic and palaeoclimatic implications: Geological Magazine, v. 128, no. 3, p. 517-523.

Zang, P.-C., Brady, P.V., Arthur, S.E., Zhou, W.-Q., Sawyer, D., and Hesterberg, D., 2001, Adsorption of barium (II) on montmorillonite: an EXAFS study: Colloids and Surfaces A: Physicochemical and Engineering Aspects, v. 190, p. 239-249.